Comparative analysis of the molecular pathways involved in spinal cord injury in axolotls vs. mammals

A DISSERTATION SUBMITED TO THE FACULTY OF THE GRADUATE SCHOOL OF THE UNIVERSITY OF MINNESOTA BY

Juan Felipe Diaz Quiroz

IN PARTIAL FULFILLMENT OF THE REQUIREMENTS FOR THE DEGREE OF DOCTOR IN PHILOSOPHY

Advisor, Karen Echeverri, Ph.D.

April 2015

Acknowledgments

I would like to thank my mentor Karen Echeverri, for her guidance, her patience, for not giving up on me and always believing in me, though I often didn't believe in myself.

I thank my fellow grad students form the Echeverri Lab Jami Erickson and Keith Sabin, for making the lab such a great environment to work in, and for being friends more than co-workers.

I want to thank former members of the Echeverri lab, Tina Sehm, Jackie Essig and Susan Lehmann, and current members Drew Honson and John Hartzheim for their help at different points during my Ph.D.

I also want to thank my friends in Dresden Ana Zarsoza, Marija Poldoski, Julieta Aprea, Benedetta Artegani, Miki Nonaka, Jonathan Rodenfelds, Tiago Ferreira, Nikos Kyritsis, Erdinc Sezgin, and Norman Gerstner; and my friends in Minneapolis Joe Belanto, Ana Gabilondo, Felix Scholz, Michelle Smith, Marino Eccher, Anna Rockne, Luke Manlove, Charlie Perkins and Judd Hultquist for being my family away from home.

I thank my previous mentors Marta Fontanilla, Enrico Nasi and Maria del Pilar Gomez for planting in me the seed of scientific curiosity.

I would like to thank my friends from Colombia Sandra Ruiz, Tatiana Sanchez, Edgar Escobar, Paul Gis, Paula Arevalo, Gabriela Ospina, Catalina Botello, Maria Antonieta Plata, Diego Pierotty, Diana Florez, Jesus Acuña, Yamile Celis, Ximena Perez, Edward Suesca, Lady Espinosa, Julio Rios, Lily Cohen, Hector Montaño, Ketty Valoyes, Gloria Cubillos, Luis Cordoba, Eliana Valencia, Milena Ordoñez for their support.

I would like to thank my sisters Natalia and Catherina Diaz Quiroz, my brothers Juan Carlos Diaz Ibarra, Andres and Camilo Diaz Quiroz, and my parents Portolatino Diaz Murillo and Maria Yolanda Quirós Boada for all their support and encouragement.

I like to thank the University of Minnesota and the Department of Genetics, Cell Biology and Development, in particular Sue Knoblauch and Kathleen Conklin for their help when I started at the UMN.

I want to thank the Ervasti Lab, the Asakura Lab for sharing reagents and the Kikyo Lab for their input in this project during lab meetings.

Lastly I want to thank my committee members Lihsia Chen, Thomas Hays, David Odde and Walter Low for their constant support.

Dedication

This dissertation is dedicated to my mother Maria Yoalnda Quirós Boada.

Esta tesis está dedicada a mi madre, Maria Yoalnda Quirós Boada.

Abstract

Spinal cord injuries (SCI) in mammals are major causes of physical disabilities. In contrast the Mexican salamander (axolotl) possesses amazing regenerative capabilities and can regenerate a fully functional spinal cord after injury. We have attempted to identify the molecular determinants underlying this evolutionary divergence by undertaking a detailed comparative analysis of a regenerative model, the axolotl spinal cord, and a corresponding non-regenerative system, rat spinal cord after injury. This approach identified a small number of highly conserved microRNAs that are differentially regulated in axolotl versus. Detailed *in vivo* studies of one of these microRNAs, miR-125b that is highly expressed in axolotl but low in rat has identified it as a key regulator of the regenerative response in axolotl. We also found that upregulation of miR-125b after injury improves SC repair in rats. In addition, we have identified SEMA4D as a target gene regulated by this microRNA after SCI in both axolotl and rat. We also studied how this miRNA is regulated in the axolotl to promote regeneration after SCI. We found that in the absence of injury, actin cytoskeleton de-polymerization induced by Cytochalasin D (Cyto D) induced a decrease in miR-125b expression similar to the decrease induced by injury in axolotl. Analyses of the regulatory region of the miR-125b axolotl gene revealed predicted binding sites for c-Fos. When we performed SCI in axolotls, we observed an increase in the expression of c-Fos 1 day after injury. As expected, we found that in the absence of injury, treatment with Cyto D induced similar changes in c-Fos expression similar to injury. Lastly, we proposed the development of a 3D *in vitro* co-culture model system to study at the cellular and molecular level how miR-125b SCI regulates the response to injury in rats and whether miR-125b expression is regulated by biomechanical activation of the Rho-c-Fos pathway. The proposed model will allow better imaging, better spatial and temporal control over modulating microRNA and gene expression in different cells at different time points. Our overall data suggest that dynamic changes in the actin cytoskeleton after injury induces changes in miR-125b expression, possibly through activation of cFos in the RhoA pathway, to create a permissive environment for regeneration in axolotls.

Table of content

List of Figures

List of tables

Chapter 1: Introduction

Spinal Cord Injury in mammals

(Adapted from the review Spinal cord regeneration: where fish, frogs and salamanders lead the way, can we follow? (Diaz Quiroz and Echeverri, 2013))

Traumatic spinal cord injury in mammals is the cause of major physical disabilities such a loss of motor and sensory function, defects in body temperature, heart beat and breathing control, and even bowel and sexual dysfunction. The spinal cord, as the rest of the mammalian central nervous system (CNS) has very poor regenerative capabilities. Understanding the biological and molecular processes that govern the response to injury is an essential step in the search for therapies that can help reverse or ameliorate the adverse outcomes of traumatic spinal cord injury in humans.

Glia Scar

The glial scar is a major hallmark of injury in the mammalian CNS. After injury to nerve cells, myelin sheaths insulating the axons begin to degenerate, while astrocytes, oligodendrocyte precursors and immune cells all migrate to the injury site (Figure 1). More specifically, injury to the CNS initiates the process of reactive gliosis (Norton et al., 1992; Sofroniew, 2009), characterized by the presence of hypertrophic proliferating astrocytes, also known as reactive astrocytes, which upregulate expression of intermediate filaments such as glial fibrillary acidic protein (GFAP), vimentin and nestin. The glial scar is often referred to both as a physical and chemical barrier to axon regeneration. Although the glia scar is often thought to be mainly composed of reactive astrocytes, other cell types such as microglia, macrophages and oligodendrocyte precursor cells (OPCs) may also be involved in its formation. (Gwak et al., 2012), (Busch et al., 2010; Norton et al., 1992; Silver and Miller, 2004). Interestingly, while microglia activation may be beneficial for injury repair (Streit et al., 1999), macrophage invasion increases axonal retraction after injury (Horn et al., 2008) and inhibits axonal regeneration (Wu et al., 2012). Moreover, *in vivo* and *in vitro* work has shown that precursor cells expressing nestin, vimentin and NG2 (a marker for OPCs) prevent macrophage-induced axonal retraction and promote axonal growth across inhibitory environment of the glia scar (Busch et al., 2010).

Even though the association of dystrophic axons with reactive astrocytes led to the idea that the glia scar is inhibitory for axonal regeneration, it has been shown that

reactive gliosis may in fact be somewhat beneficial (Silver and Miller, 2004). For example, one study showed that, when reactive astrocytes where selectively ablated in rats after a stub or crush injury, axonal degeneration and demyelination were both increased and recovery of motor function was reduced. This suggests that, rather than inhibiting axonal growth, the role of the glia scar is to conceal the damage caused by the injury and promote tissue repair (Faulkner et al., 2004; Menet et al., 2003).

Beyond the cells involved, another important component of the glia scar is the extracellular matrix (ECM) surrounding them. After spinal cord injury, the levels of many ECM components are markedly increased. These components include Collagen IV, α-Laminin, γ-Laminin, Laminin-1 (Liesi and Kauppila, 2002), Keratan Sulfate Proteoglycans (KSPGs) (Krautstrunk et al., 2002) and Chondroitin Sulfate Proteoglycans (CSPGs) (Jones et al., 2003). In view of the enrichment of these components at the injury site, it has been widely thought that the components of the ECM act as inhibitory cues to axonal growth at the injury site. Interestingly, removal of the CSPG glycosaminoglycan chains attenuates the inhibitory activity of CSPG and resulted in functional regrowth of both ascending and descending axons in an *in vivo* model of spinal cord injury (Alilain et al., 2011; Bradbury et al., 2002). However, some evidence suggests that not all neuronal cell types respond in the same way to ECM-rich environments. A study using showed that nociceptive, sensory and rubrospinal axons were able to grow into the graft across a CSPGs-rich environment in association with the CSPG NG2 (Jones et al., 2003). Moreover, in NG2 knock out mice cortico-spinal track (CST) axons did not improve regeneration after spinal cord transection, suggesting that NG2 might not be involved in axonal inhibition *in vivo* (Hossain-Ibrahim et al., 2007) or that the different CSPGs up-regulated after injury (NG2, Brevican, Nuerocan and Versican) might have redundant roles in inhibiting axonal growth (Fisher et al., 2011).

Together, these studies point to an overall model of glial scar functionality defined primarily by its important early role in response to injury, assuring the structural stabilization of the lesion site and thereby preventing further tissue damage. This then carries the unfortunate drawback that this natural “bracing system” in itself, at least partly because of the key proteins expressed in building it, happens to be inhibitory to axonal regeneration through the lesion site. Thus, according to this model, evolution of the mammalian CNS repair system has carried a difficult trade-off resulting in the flawed

outcome we know all-to-well, i.e. restoration of structural integrity being favored at the expense of functional recovery.

Myelin Axon growth Inhibitors

In the mammalian CNS, oligodendrocytes produce myelin sheaths that surround and insulate the axons, playing a key role in enabling their fast, saltatory transmission of excitatory signals. In the CNS myelin contribute strong inhibitors of axonal outgrowth after injury. The group of Martin Schwab was the first to identify the inhibitory effect of myelin and showed that this effect could be attenuated by treatment with proteases (Caroni and Schwab, 1988). Since this major breakthrough, the inhibitory components of myelin, Nogo, myelin associated glycoprotein (MAG) and oligodendrocyte-myelin glycoprotein (OMgp), have been discovered and their role in axon inhibition has been broadly studied.

Nogo encodes at least 3 major splice variants, Nogo-A, B, C. Nogo A is highly expressed in oligodendrocytes and is the only Nogo isoform to inhibit neurite outgrowth *in vitro* and *in vivo* (Chen et al., 2000; Dimou et al., 2006; Schwab, 2004). While the lack of expression of Nogo-A in the Peripheral Nervous System (PNS) suggested that the B and C variants were not inhibitory for axon regeneration (Chen et al., 2000), it was also shown that the conserved lumenal/extracellular domain of the Nogo variants (Nogo-66) was sufficient to induce growth cone collapse (GrandPré et al., 2000). Studies using a dorsal hemi-section injury in rats treated with an antibody against Nogo-A (Merkler et al., 2001), or a peptide to block the Nogo-66 receptor (GrandPré et al., 2002) or mutant mice lacking Nogo-A/B (Kim et al., 2003) showed a modest but significant improvement, as compared to untreated controls.

MAG is an adhesion molecule expressed both by oligodendrocytes in the CNS. Although recombinant MAG induces growth cone collapse in embryonic mouse hippocampal neurons and cerebellar granule neurons (CGNs) *in vitro* (Li et al., 1996), in MAG deficient mice only a few axons were detected caudal to the injury site (Bartsch et al., 1995; Li et al., 1996). These results suggest that MAG might not play as strong an inhibitory role after injury as Nogo. A study showed that in MAG null mice neuronal degeneration increased in comparison to wild type mice, correlated with decreased motor function behavior (Nguyen et al., 2009). Moreover, treatment of Dorsal Root Ganglia (DRG) with soluble MAG reduced vincristine-induced axonal die back *in vitro*.

Moreover MAG-null mice myelin induced growth cone collapse and inhibition of neurite outgrowth *in vitro* (Lee et al., 2010d; Li et al., 1996), further supporting the notion that MAG may not be involved in axonal inhibition after SCI.

Omgp is a membrane protein expressed in oligodendrocytes and in some neurons. It has been shown that both soluble and immobilized Omgp inhibit neurite outgrowth of E13 chick DRGs *in vitro,* comparable to Nogo-66 inhibition (Wang et al., 2002). Also, Omgp null mice showed improvement in motor function recovery after complete transection, in comparison to wild type mice (Ji et al., 2008). A study showed that myelin extracted from triple null mice for Nogo, MAG and Omgp did not inhibit neurite outgrowth *in vitro* and improvement in recovery of motor function, suggesting that Nogo, Omgp, and MAG synergize after spinal cord injury (Cafferty et al., 2010). Though another study performed using triple null mice for Nogo, MAG and Omgp showed no regeneration transection injuries or dorsal hemi-sections, (Lee et al., 2010a) the discrepancy between studies may be at least partly attributable to differences in the genetic background of the mice employed and the types of injury performed. Interestingly, both studies showed that in MAG single mutants (Lee et al., 2010a) or Omgp/MAG double mutants (Cafferty et al., 2010) motor function recovery and CST axons regeneration were not improved and could even be worsened. This further supports the notion that MAG might play a protective role after spinal cord injury.

The overall data suggest that the *in vivo* role of myelin derived proteins after spinal cord injury remains only partially understood. Further progress in this area will require increased clarity with respect to such contributing factors as genetic background, types of injury and neuronal susceptibility.

Semaphorins

Myelin-derived inhibitory proteins are not the sole inhibitors of axonal growth at the injury site. Indeed, many studies in recent years have also documented such a role for classical axon guidance proteins such as semaphorins. Semaphorins (Sema) were first described as a family of secreted and transmembrane guidance molecules in *Drosophila* (Kolodkin et al., 1993). Up to date around 30 different semaphorins have been described, grouped in 8 classes. Semaphorins classes 1 and 2 are found in invertebrates, classes 3 to 7 are found in vertebrates though one class 5 semaphorin is also expressed in invertebrates, and class 8 correspond to a viral semaphorins (Fig. 1-

2). Semaphorins from the class 2, 3 and are secreted while semaphorins from the others classes are membrane associated (Kruger et al., 2005; O'Malley et al., 2014). The receptors for semaphorins are called plexins and are grouped in 4 classes, A through D. While in invertebrates there only one class A and one class B plexins, in vertebrates there are 4 class A, 3 class B one class C and one class D (Kruger et al., 2005; O'Malley et al., 2014).

Since their discovery in the early 90s semaphorins and plexins have been described to play an important role in growth cone guidance during development (Kruger et al., 2005; O'Malley et al., 2014), as well as endothelial cell guidance during vasculogenesis and even during the pro-inflammatory response of the immune system (Kruger et al., 2005). Due to its role in axon guidance during development, it is not surprising that semaphorins have been described to be involved in the response to injury to the CNS and in particular in spinal cord. Semaphorins from the class 3 (De Winter et al., 2002; Niclou et al., 2003; Shifman and Selzer, 2007; Zhang et al., 2014b) the class 4 (Moreau-Fauvarque et al., 2003; Shifman and Selzer, 2007; Zhang et al., 2014a) class 6 (Shim et al., 2012) and 7 (Kopp et al., 2010) have been described to inhibit the growth of axons across the glia scar after spinal cord injury. (De Winter et al., 2002; Lee et al., 2010a; Moreau-Fauvarque et al., 2003; Niclou et al., 2003; Sandvig et al., 2004; Shim et al., 2012). *In vitro* studies have shown that semaphorins and plexins inhibit axonal regeneration by promoting growth cone collapse through the Rho GTPases signaling pathway (Kruger et al., 2005; Pasterkamp and Verhaagen, 2006). The widespread expression of semaphorins in the CNS in neurons, astrocytes oligodendrocytes and microglia, and the promiscuity between semaphorins with plexin receptors, makes the study of the role of semaphorins in spinal cord regeneration specially challenging.

Axonal dieback and Wallerian Degeneration

As described above, axon regeneration is inhibited by extrinsic factors in the tissue environment, but also by intrinsic changes within the axon itself and also by an age-dependent decline in regenerative ability (Moore et al., 2009). For an axon to regenerate after injury, it must first seal off its membrane and reorganize its cytoskeleton to form a growth cone (Bradke et al., 2012). The growth cone is a specialized, highly motile structure located at the growing tip of a neurite, its center being dominated by microtubules (MTs) while its peripheral domains are more enriched in actin bundles

(Bradke et al., 2012). Axons in the CNS fail to regenerate, they do not form a growth cone in response to injury, and instead form what is referred to as a “dystrophic end bulb” originally described by Ramón y Cajal (Ramón y Cajal, 1928). Dystrophic end bulbs vary in size and shape but typically involve a massive disorganization of the tightly packed and uniformly oriented microtubule array post-injury, as well as an accumulation of vesicles causing a notable swelling of the tip of the axon (Ertürk et al., 2007). While this may seem like a dead end situation, some pioneering work has shown that, in fact, dystrophic end bulbs retain the inherent ability to regenerate if placed in an appropriately permissive environment. It has been shown that CNS axons can regenerate into an implanted peripheral nerve graft even after four weeks in a non-permissive environment (Houle, 1991).

While these observations relate to the portion of the axon that is still connected to the neuronal cell body, the other portion that is left on the other side of the injury typically undergoes rapid “Wallerian” degeneration (Fig. 1-1)(Kerschensteiner et al., 2005). Initially there is an acute degeneration phase that actually affects both the proximal and distal parts of the severed axon and has been shown to be mediated via an influx of calcium and activation of the Ca^{2+}-dependent protease calpain (Fig. 1-1) into the cut ends of the axon (George et al., 1995). This is followed by a latency period that can last for 24-48hrs during which the distal part of the axon remains morphologically intact and is still electrically excitable for a short period (Tsao et al., 1994). This is followed by a rapid degeneration phase during which the cytoskeletal components of the axon disassemble and macrophages invade the site, presumably to remove axonal debris (Griffin et al., 1992; Lubińska, 1982).

A type of signaling well known to be activated after axonal injury is the Jun kinase pathway. Chemical inhibition of JNK kinase has been shown to result in axon protection for up to 48hrs post axotomy (Miller et al., 2009). Loss of DLK, mitogen activated kinase family or inhibition of GSK3 give a similar effect. However it remains unknown how these kinases are activated and the neuronal protection effect is only observed if the pathways are inhibited within the first 3hrs post axotomy suggesting that these kinases act as an early injury sensor (Miller et al., 2009).

Another key component of the axon that is targeted in axonal protection strategies is the cytoskeleton. Degeneration of the axon results in rapid depolymerization of the microtubules that are the core structural component of the axon (Bradke et al.,

2012). In normal axons, the proteasome is responsible for regulating the normal turnover of microtubule-associated proteins (MAPs) that assure both the highly structured microtubule architecture and bidirectional transport processes that it supports (Ehlers, 2004). Inhibition of the proteasome complex in injured axons has been shown to prevent the turnover of such MAPs as tau and MAP1, which results in increased stabilization of the MTs, leading to protection of the axon from degeneration (Zhai et al., 2003). In more recent studies, the Bradke lab have shown that application of Taxol, a drug that stabilizes MTs, reduces scarring and promotes axonal regeneration after injury in rats (Hellal et al., 2011). Taxol not only stabilized MTs in the axons but also led to reduced production of the glial scar proteins laminin, fibronectin and collagen IV, suggesting that a more permissive environment was created to allow axonal regeneration. Taxol appears to work by preventing the trafficking of kinesin 1 and dynamin, therefore preventing smad2 from activating TGF-B signaling, which is known to activate genes involved in glial scar formation (Hellal et al., 2011). This approach offers new and exciting potential for drug-based therapies that target more than one cellular process. While the full mechanism by which taxol promotes axon regeneration is still unclear, previous work from the same lab has shown that low doses of taxol can induce axon formation *in vitro* (Witte et al., 2008).

Spinal Cord Regeneration

(Adapted from the review Spinal cord regeneration: where fish, frogs and salamanders lead the way, can we follow? (Diaz Quiroz and Echeverri, 2013))

The wondrous ability of certain fortunate animals to fully regenerate entire appendages following major injuries has fascinated their human observers as far back as Aristotle's time (Aristotle, 1910). By 1714, the French naturalist Réaumur published the first experimental evidence showing that crayfish can replace appendages after amputation (Reaumur). Over the centuries, the regeneration models of choice have varied widely, with different scientists favoring a wide array of species including worms, lizards, lampreys and salamanders. This rich body of work, primarily comprising detailed characterizations and experimentation based on classical developmental and cytological approaches, has yielded a wealth of invaluable insights into regenerative abilities throughout the animal kingdom (Goss and Russell, 1969).

Epimorphic Regeneration

Regeneration is the natural ability to replace missed or damage cellular structures, tissues, organs and body structures, for new ones that have the same properties and function as the lost ones. In nature exist different levels of regeneration (Fig. 1-3). Adult humans, for example are able to regenerate certain tissues such as epidermis and skeletal muscle, however we lack the capacity to regenerate more complex structures. While some organisms like the zebra fish can regenerate organs such as the heart, other animals such like the axolotl are able to regenerate an entire limb. The maximum expression of regeneration is the ability exhibit by certain species of *Planarian* and starfish to regenerate complete bodies starting from a body part (Bely and Nyberg, 2010). When regeneration is achieved through the formation of a mass of proliferative undifferentiated cells, called blastema, is known as epimorphic regeneration.

Epimorphic regeneration has been described to take through a series of sequential events (Stewart et al., 2007; Stoick-Cooper et al., 2007). The first one is the formation of the wound epithelia. Epidermal cells surrounding the injury site migrate over injury to close the wound and form the wound epithelium. It has been demonstrated that the formation of the wound epithelium is necessary for regeneration to occur and it is thought that chemical cues coming for the wound epithelia signal the underlying tissue to

induce the regenerative response (Poss, 2010; Stoick-Cooper et al., 2007). The second step is the formation of the blastema. The blastema is a mass of proliferative undifferentiated cells that eventually will give rise to the new tissues. The source of the cells that conform the blastema is still debated. Though some evidence suggest that blastema cells come form resident stem cells that are activated upon injury, there has been evidence that cells from the injured tissue can dedifferentiate and form part of the blastema (Poss, 2010). The last step of epimorphic regeneration is differentiation. Cells in the blastema proliferate to increase the cellular population and start to differentiate in a proximal to distal manner(Mariani, 2010). Interestingly, the new structure has the same size as the one that was lost. Although there is some evidence showing that chemical gradients such as of retinoic acid (Brockes, 1997; Maden, 1982) give positional information to the new tissues being formed, how exactly the cells know how much tissue needs to be replaced is still unknown.

Humans and mammals in general are able to achieve great degree of regeneration during fetal development and early in childhood; however such capacity diminishes with time until is lost in adults (Seifert and Voss, 2012). Studying the cellular and molecular mechanisms that govern epimorphic regeneration it is widely thought to be promising way to generate alternative therapies to improve the repair of lost or damage tissues and structures in human bodies, such as the spinal cord.

Spinal cord regeneration after injury in salamanders

Tailed amphibians, such as salamanders, have long been considered the champions of regeneration, having the remarkable ability to regenerate a wide range of body parts throughout life (Brockes and Kumar, 2008; Tanaka and Ferretti, 2009). While the Mexican “axolotl” salamander naturally remains aquatic and retains juvenile characteristics throughout life, when forced to become terrestrial like newts, it still maintains its ability to regenerate (Ehrlich and Mark, 1977; Seifert et al., 2012). In recent years, spurred on by a surge of interest in regenerative medicine, these model systems have come to the fore, favored for this extensive regenerative capacity, as well as exquisite cytology and key advances in molecular and transgenic tools.

To date, much of the work carried out on spinal cord regeneration in salamanders has been in the context of tail regeneration following amputation, although many older studies have also documented their regenerative repair of more discrete

spinal cord lesions. As early as 1965, Butler and Ward first described the regeneration and functional recovery after a lesion in the spinal cord of the newt (Butler and Ward, 1965; Butler and Ward, 1967). Their work described a process in which the two ends of the spinal cord are sealed over and migrate towards one another, and over time, axons then regrow through the lesion site (Butler and Ward, 1965). Retrograde labeling of axons has shown a strong correlation between coordinated swimming and regrowth of the descending supraspinal axons (Clarke et al., 1988). More recent work in newt has shown that putative meningeal and glial cells create a regeneration-permissive environment after spinal cord injury (Zukor et al., 2011). Interestingly the meningeal fibroblasts and glial cells migrate into the injury site along with endothelial cells and create a substrate on which the axons can regrow. In their model, although sensory neurons do not appear to regenerate, the animals appear to regain full motor control (Zukor et al., 2011). The authors suggest that in the newt, the meningeal cells, glial cells and neuronal axons all move as a coordinated unit to fill the injury gap. This would be in stark opposition to what is observed following mammalian spinal cord injury, where meningeal fibroblasts and astrocytes together form a glial scar that actually inhibits axonal regrowth through the lesion site (Silver and Miller, 2004).

Beyond these observations from discrete lesions, the ability of the salamander spinal cord and surrounding tail to fully regenerate following a full amputation has also been thoroughly documented in various species over the years (Butler and Ward, 1965; Butler and Ward, 1967; Egar and Singer, 1972; Géraudie et al., 1988; Howard, 1951; Singer et al., 1979; Sybil, 1956). Early papers already established the necessity of the spinal cord for tail regeneration to proceed successfully. Work from Nordlander and Singer already postulated, based on ultrastructural observations, that descending axons regenerate by moving along channels present in regenerating ependymal glial cells (Egar and Singer, 1972; Singer et al., 1979). Early in the field, work from the Bryant lab carefully documented five distinct stages of tail regeneration in the newt and showed that the length of tail regenerated is proportional to the amount originally removed (Iten and Bryant, 1976a; Iten and Bryant, 1976b).

More recent work on understanding spinal cord regeneration has also focused on the context of tail amputations. Cell lineage tracing and transplantation studies have shown that in both *Pleurodeles* and *Ambystoma*, radial ependymal cells give rise to the new glial cells in the regenerating spinal cord and can also differentiate to produce new

neurons, suggesting that these have properties similar to neural stem cells (Echeverri and Tanaka, 2003; Zhang et al., 2003). This observation has triggered the key question of whether these cells retain such pluripotency throughout development from the embryonic state, or whether this capacity is newly induced in response to injury. While recent work has shown that adult axolotl spinal cord cells indeed retain expression of certain embryonic development genes such as Pax7, Pax6 and shh, these are not associated with stemness or pluripotency per se, but rather, encode key dorsoventral positioning cues, consistent with the maintenance by most spinal cord cells of their dorsoventral identity during regeneration (McHedlishvili et al., 2007; McHedlishvili et al., 2012; Schnapp et al., 2005). Furthermore, Pax7 has been shown to be downregulated in the zone just proximal to the amputation plane from where cells migrate out to form the regenerate, suggesting that these cells may indeed revert to a more stem cell-like state as a result of injury (Sehm et al., 2009). In fact, there have been no published reports to date of stem cell or pluripotency markers being expressed in the adult axolotl spinal cord or surrounding tail tissues outside of the injury context. Such a marker, namely fgf2, has been shown in newts to be upregulated in radial glial cells after injury in a zone adjacent to the injury site (Zhang et al., 2000). The implied role in regulating proliferation and differentiation of these cells (Moftah et al., 2008; Zhang et al., 2000) therefore adds further support to the hypothesis that they are reverting to a more neural stem cell-like, or pluripotent, state as a response to injury. Data from several groups have also confirmed the upregulation of not only fgf signaling molecules, but also Hox, Wnt and BMP pathways components during the early stages of axolotl spinal cord regeneration (Carlson et al., 2001; Caubit et al., 1997; Monaghan et al., 2007; Sehm et al., 2009; Zhang et al., 2000). The consistency of these findings with observations from zebrafish and *xenopus* further supports the emerging view that these signaling pathways represent key, conserved requirements underlying natural regenerative capacities in many, if not most, of these organisms.

Early lineage tracing experiments in the axolotl using overexpression of GFP driven by a glial-specific promoter has shown that radial glial cells divide and migrate in response to tail amputation, essentially acting as a neural stem cell population as they give rise to new glial cells and neurons (Echeverri and Tanaka, 2002). These experiments also suggested that these cells are capable, at a low frequency, of giving rise to cells of the mesodermal lineage. This is also potentially supported by

observations that cells exit out of the regenerating spinal cord via the terminal vesicle and enter surrounding tissues, although the exact fate of these cells remains as yet undetermined (Echeverri and Tanaka, 2002; McHedlishvili et al., 2007; McHedlishvili et al., 2012).

There are remarkable similarities observed between species in their response to injury. In both anurans, urodeles and mammals glial cells are seen to migrate and divide in response to injury and signaling pathways like Notch, BMP and Wnts are activated, however the question remains as to why mammals favor structural repair over functional regeneration. Although much progress has been made in understanding where cells come from and what their potential is during axolotl and newt spinal cord regeneration, much work has yet to done to understand the signals that drive cells to divide, migrate and differentiate at the correct times and locations after injury and this may help us to promote functional regeneration versus basic repair in mammals

Spinal Cord Regeneration in Zebrafish

In recent years, the zebrafish has grown in popularity as a model system for studying regenerative processes due to its genetic tractability and similarity to higher vertebrate architecture in many organs and tissues (Becker and Becker, 2008). Although the basic cytology of the zebrafish spinal cord is relatively similar to that of a mammalian spinal cord, their respective cellular responses to injury appear quite different, resulting in functional injury repair only in the zebrafish (Becker and Becker, 2008; Hui et al., 2010).

Recent work has shown that in response to spinal cord injury, glial cells in the adult zebrafish are capable of amplifying and migrating to repair the lesion (Hui et al., 2010) (Goldshmit et al., 2012). Work from the Currie lab has shown that the glial cells adjacent to the injury initially proliferate and migrate 3-5 days post injury. Cells migrating into the lesion site are found to downregulate GFAP, upregulate nestin and undergo a significant morphological change to become bipolar. (Goldshmit et al., 2012). These newly born glial cells then undergo a distinct differentiation process that includes upregulation of GFAP, maintenance of nestin expression and further elongation to span the width of the lesion site along the AP axis, effectively creating a “glial bridge” upon which axons can grow across the lesion site. Formation of the glial bridge is an Fgf dependent process and has been shown to be essential for locomotive recovery in the

zebrafish (Goldshmit et al., 2012). While the same study also suggested that functional recovery is driven by this axonogenesis across the glial bridge from a mixture of newly-formed and mature neurons, other reports have pointed to the presence of inherent cell populations, such as olig2+ependymal radial glial cells, that give rise to new motor neurons in a notch-regulated process (Dias et al., 2012). Interestingly in mammals those neural progenitor cells are also present in the adult mammalian spinal cord (Barnabé-Heider et al., 2010; Johansson et al., 1999; Meletis et al., 2008).

These findings illustrate how the zebrafish system is indeed providing valuable insights into the basic cellular processes and molecular cues responsible for spinal cord regeneration in this organism.

Spinal cord regeneration in Frog Tadpoles

Tailless amphibians, such as frogs, are of particular interest in the present context since these organisms live through multiple developmental life stages, only some of which carry regenerative capacities (Beattie et al., 1990; Gibbs et al., 2011). Indeed, while most of the larval stages have the ability to regenerate limbs and tails including a fully innervated spinal cord, metamorphosis to later stages typically results in a complete loss of these regenerative abilities. As such, these models offer the unique possibility of conducting comparative studies between regenerative and non-regenerative repair processes within the same organism, including attempts to promote regeneration at the larval refractory stages.

Among these organisms, *Xenopus laevis* displays, in addition to its other, well-documented experimental advantages, and a refractory period during larval development that has also been used as a system for studying regeneration. One of the first descriptions of frog larval tail regeneration was that of Harrison in 1898, where he recorded the regeneration of the larval tail after various types of amputations and wounding, noting that “the regenerated appendage never becomes exactly like the original”. Interestingly, Harrison already posed key questions about the effect of the position of “the regenerating center” with regard to the whole stump and went on to carry out some of the first transplantation studies in *xenopus* embryos,(Harrison, 1898) which ultimately led to some to the first successful tissue culture experiments (Rose, 1907). More recently, elegant studies using transplantation of specific structures or tissue regions, such as somites or neural folds, from GFP-positive embryos into wild type

embryos have been used to trace the lineage of cells in the regenerate. These studies have revealed that spinal cord and notochord arise from the corresponding mature cells in the stump, while new muscle is formed from satellite cells that migrate from the mature muscle adjacent to the injury site (Gargioli and Slack, 2004).

Of note in this context, *xenopus* have recently been shown to harbor Sox2-positive cells, a putative neural stem cell population within the spinal cord, which proliferates and migrates in response to injury to the spinal cord alone and after transection of the tail (Gaete et al., 2012). Downregulation of Sox2 expression correlates with the loss of regenerative capacity as the *xenopus* undergoes metamorphosis. These findings also suggest that, in the context of spinal cord transections, these cells migrate and form a substrate for supporting axonal regeneration (Gibbs and Szaro, 2006), which is crucially missing in mammals. Although neural stem cells exist in mammals and can proliferate in response to injury (Barnabé-Heider et al., 2010; Johansson et al., 1999; Meletis et al., 2008), their response to injury is does not promote a regeneration competent environment.(Fawcett and Asher, 1999).

Axonal regeneration after injury in *C. elegans*

In contrast to mammals, in species that do regenerate their central nervous system we see vary degrees of axonal regeneration. In the zebrafish both axonal degeneration and regeneration is observed, while in salamanders it is unclear what exactly happens of the axons on the caudal side of the injury (Table 1-1). One of the most interesting and novels systems for studying axonal regeneration in recent years is the invertebrate model *C.elegans*. By thereby accessing some of the most elegant genome-scale screening methodologies available in any model, researchers have been able to undertake molecular-level dissections of those regenerative processes that are also observable in these systems, particularly, as it happens, in the neural context (Chen et al., 2011; Chiu et al., 2011)

C. elegans has a relatively simple, highly invariant and uniquely well characterized nervous system consisting of 302 neurons, each of which offers a fully documented developmental lineage, morphology and synaptic connectivity (White et al., 1986). The first study of axon regeneration in *C. elegans* used femtolaser surgery to perform careful axotomies and showed how these axons can in fact regenerate (Yanik et al., 2004). This seminal study has effectively launched a new field that has lead to more

precise molecular and cell biology descriptions of the factors necessary to promote axonal regeneration, enabling very interesting and even broader cross-species comparisons than ever before.

How axons regenerate in *C. elegans* depends largely on the type of axon that is injured (Yanik et al., 2006). Interestingly, mechanosensory axons regenerate via fusion of the proximal and distal ends of the cut axon (Neumann et al., 2011). Ultrastructural studies have shown that reconnection occurs via fusion of the two pieces, both membrane and cytoplasm becoming continuous as a result (Ghosh-Roy et al., 2010; Neumann et al., 2011). Intriguingly in mammals there have also been reports of axonal regeneration via fusion of severed ends(Britt et al., 2010; Lore et al., 1999). In most *C. elegans* neurons that get severed, however, the distal portion of the axon, i.e. the one that is no longer connected to the cell body, degenerates in a fashion that is at last superficially reminiscent of the so-called Wallerian degeneration observed in mammals (Neumann et al., 2011; Yanik et al., 2006). These findings illustrate to what extent the *C. elegans* system offers a powerful opportunity for studying the molecular and cellular aspects of axonal regeneration per se.

microRNAs

microRNAs (miRNAs) are about 21 base pair (bp) long non-coding RNAs. They were first described as key regulators of developmental timing in *C. elegans* (Lee et al., 1993). Since then, they have been found to be a highly conserved mechanism of gene regulation in many cellular processes such as cell differentiation, apoptosis, cancer, axonal growth, dendrite arborization, myelination, transcription and injury (Bartel, 2009; Kosik, 2006; Krol et al., 2010). Due to the capacity of one miRNA to regulate different genes, miRNAs are regarded as master regulators of biological processes (Bartel, 2009). Conversely, multiple RNAs can regulate a single gene; therefore, understanding what regulates miRNA transcription might be a key step in understanding how they regulate gene expression in different biological processes.

microRNA biogenesis

miRNAs can be encoded within intronic regions of a protein-coding gene (host gene) or on a gene by its own, and are transcribed in its majority by Polymerase II. The transcribed RNA, forms a hairpin precursor microRNA (pri-miRNA). The Pri-miRNA is processed in the nucleus by a protein complex formed by the endonuclease Drosha and a double stranded binding protein called Prasha in *Drosophila* and DGCR8 in mammals (Bartel, 2004; Kosik, 2006). The processed miRNA, known as pre-miRNA, exists the nucleus and is further processed in the cytoplasm by the endonuclease Dicer and its partner TRBP leaving as a result double stranded RNA (dsRNA) of approximately 21 bp long and with 2 nucleotides overhangs at the 3' ends. The double stranded RNA is then assembled into a protein complex known as miRISC (miRNA Induced Silencing complex) where the two strands are separated and one of them, the mature miRNA, is used as guide sequence while the other strand is degraded. The most important component of the miRISC complex is a protein member of the Argonaut (AGO) family. There are 4 AGO proteins in mammals, from which the most studied is AGO2 (Filipowicz et al., 2008; Krol et al., 2010; Winter et al., 2009). The ribonucleoproetin complex form by the mature miRNA and miRISC is the machinery in charge of repressing mRNA translation and/or degradation of target genes (Fig. 1-4) (Winter et al., 2009). Interestingly, it has been suggested that translational repression by miRNA in some

cases might work as a way to prevent mRNA degradation, in particular during mRNA transportation along the axons or dendritic spines in neurons(Kosik, 2006).

Though the general miRNA biosynthesis process is understood up to certain extent, transcriptional regulation of miRNAs is still largely unknown. The transcription of miRNAs that are encoded within introns is regulated by the transcription factors that regulate the expression of its host gene. It has been shown that intronic miRNAs generally regulate the same cellular processes related to their host genes, by either targeting its host gene or functioning synergistically in a feed-forward fashion (Davis and Hata, 2009; Small and Olson, 2011).

On the other hand, though some studies have already started to shed light on the mechanisms that regulate transcription of miRNAs in independent genes, the matter remain largely unknown. Bioinformatic analysis of genomic sequences have predicted that the known transcription factors that regulate the expression of coding RNA can potentially regulate transcription of miRNAs since similar recognition sequences have been found in the regulatory region of miRNAs (Schanen and Li, 2011; Xiao et al., 2013). Functional experiments have shown that the expression of miR-124 is inhibited by the RE1 silencing transcription factor (REST) in non-neuronal cells during neuronal development in mice (Visvanathan et al., 2007). It has also been described that the Serum response factor (SRF) directly regulates transcription of miR-1 during cardiogenesis in mouse (Olson and Nordheim, 2010; Zhao et al., 2005). Moreover, Myc has been shown to regulate the expression of a wide range of miRNAs in human and mouse models of B-cell lymphomas(Chang et al., 2007), and miR-18a in human mammary malignant epithelial cells (Mouw et al., 2014). Due to the wide spread of processes in which miRNA regulation is a key player, it is important to better understand how the transcription of microRNAs is regulated in response to stimuli.

microRNA regulation mechanisms

Posttranscriptional regulation of gene expression by microRNAs is a process that is highly conserved across species. There have been described different mechanisms by which miRNAs can regulate gene expression by interacting with the mRNA of a target gene. One of them is promoting mRNA cleavage upon fully complementary binding of the miRNA to the coding region on the mRNA, similar to what has been described for interference RNA (iRNA or RNAi) (Bartel, 2004). Though this mechanism is very

frequent in plants, in metazoans is seen rarely and only occurs when AGO2 is part of the miRSC complex but not the other AGO family members. The most common miRNA regulation mechanism in animal cells is the repression of mRNA translation (Filipowicz et al., 2008). In this mechanism, the mature miRNA pairs imperfectly to the mRNA 3' untranslated region (UTR) except for 8 nucleotides known as the seed sequence. Upon biding, the miRISC complex interacts with protein complexes required for translation. These interactions can block translation initiation, block translation elongation, induce proteolysis of nascent proteins or induce deadenylation of the mRNA. Up to the date, the best understood interactions are the ones that lead to block of translation initiation and deadenylation (Filipowicz et al., 2008).

Translation is a process that is initiated by the binding of the eukaryotic translation initiation factor (eIF) to the 5' m^7G cap. The recognition of the 5' cap by eIF is dependent on the eIF4E subunit. Upon binding, the eIF3 subunit recruits the 40s ribosomal subunit to the start codon, generally AUG, for subsequently start translation after binding of the 60s ribosomal subunit (Filipowicz et al., 2008; Krol et al., 2010). The recruitment of the 40s subunit by eIF3 is dependent of the interaction of the eIF with the 3' poly adenosine tail (PolyA) mediated by the PolyA biding protein 1 (PABP1). While the AGO proteins from the miRISC complex seem to compete with the eIF4E for the biding to the 5' cap thus blocking translation initiation, another protein of the miRISC complex, GW182, interacts with PABP1 preventing its association with eIF and the recruitment of the 40s ribosomal subunit (Filipowicz et al., 2008). Interaction of GW182 with PABP1 also induces the recruitment of deadenyliting proteins CCR4 and CAF1 and subsequent degradation of the mRNA. This suggest that translation blocking would be coupled with mRNA deadenylation and degradation, however, miRNA-induced translation blocking have been shown in miRNAs lacking the polyA tail; therefore translation blocking and deadenylation are thought to be two separated mechanisms of miRNA regulation (Filipowicz et al., 2008; Krol et al., 2010).

The function of microRNA in biological process is generally thought to be restricted to downregulation of gene expression by mRNA translation repression and/or degradation, however, there is evidence that show that miRNA might have other functions as well. For example, in mouse embryonic cortical neurons, the translation repression of the Postsynaptic Density protein 95 (PSD-95) by miR-125a can be reversed by stimulation of Glutamate receptors in dendrites (Muddashetty et al., 2011).

Similar conditional reversion of miRNA-mediated repression has been described for LIMK1 by miR-134 in the dendrites of rat neurons (Filipowicz et al., 2008; Kosik, 2006). The fact that in both studies translation repression could be reversed locally at the dendrite, suggests that miRNAs could serve as a mean to protect mRNA from degradation while is transported to the dendrites where it can be locally translated for a fast response to a external stimuli. miRNAs also seem to be able to induce translation instead of repressing it. In HEK cells, serum starvation induces activation of Tumor necrosis factor alpha (TNFα) in an AGO2 dependent manner. AGO2 binding to AU rich elements (ARE) in the TNFα mRNA is necessary for starvation induced translation and is dependent on miR-369-3 for ARE recognition (Filipowicz et al., 2008). These results show that miRNA regulation is a more complex and dynamic process than when it was first described. A better understanding of miRNA regulation will help elucidate its role in different cellular process such as regeneration or response to spinal cord injury.

Actin and Microtubule cytoskeleton

The cytoskeleton is the system of polymer-based scaffolds that provides the cell with structural support, shape, intracellular space organization, and ability to move and divide (Fletcher and Mullins, 2010). The cytoskeleton is composed mainly by three types of polymers, microtubules, intermediate filaments (e.g Vimentin, nestin, GFAP, neurofilament.) and actin. The different components of the cytoskeleton perform different functions. Actin filaments function mainly in cell shape and motility, microtubule in internal transport and the intermediate filaments provide structural and mechanical stability (Fletcher and Mullins, 2010; Huber et al., 2013; Mofrad, 2009). Aside for cell shape, structure and motility, the cytoskeleton is a highly dynamic structure that also functions as a bridge between the intracellular and the extracellular environment. Increasing evidence point towards the importance of the cell cytoskeleton in transducing external stimuli, in particular mechanical signals (Janmey and Miller, 2011). Therefore, making sense of the molecular and physical mechanisms through which the cell cytoskeleton regulates gene expression could represent a key step for understanding cellular behavior in response to injury.

Actin cytoskeleton

The actin cytoskeleton is composed of actin filaments (F-actin) that are polymers of globular actin (G-actin). G-actin polymerizes in an ATP dependent manner to form a polarized actin filament with two defined ends, known as the barbed and the pointed ends. Actin filaments are dynamic in a constant equilibrium between polymerization and depolymerization. The addition of new G-actin units occurs at the barbed ends of the filament while depolymerization occurs preferentially at the pointed end of the filament (Schmidt and Hall, 1998). The growth and organization of the actin cytoskeleton is mainly regulated by actin binding proteins (ABPs) that can bind to G-Actin, F-actin or both. Different ABPs regulate different structural changes in the actin cytoskeleton such as bundling, branching, crosslinking, and depolymerization (Fig. 1-5a) (Schmidt and Hall, 1998). For example the actin related protein Arp2/3 complex induces F-actin branching, Fascin and α-Actinin induce formation of actin bundles by cross-linking actin filaments, Spectrin links F-actin to molecules located in the cell membrane, Formin and Profilin

induce polymerization while Cofilin and Gelsolin induce depolymerization (Dent et al., 2011; Pak et al., 2008). The activity of the ABPs to induce changes in actin cytoskeleton formation is dependent on the cellular localization and is regulated by the Rho family of small GTPases. How the small GTPases regulate actin dynamics will be discussed later.

One of the most important ABPs is non-muscle myosin II (NM II). NM II is a motor protein expressed in all cells, including muscle, and plays a key role in cell motility, actin bundling and actin-microtubule cross talk (Even-Ram et al., 2007; Vicente-Manzanares et al., 2009). Structurally, NM II is composed by two sets of subunits, two myosin heavy chains and four light chains (MHCs and MLCs respectively). Each MHC has three domains, the head domain that binds both actin and ATP, required for its motor function, the neck domain that binds the MLCs subunits, and the tail domain that wraps around the tail domain of the other MHC forming a coiled-coil rod that hold the two MCHs together. Two MLCs, named regulatory (RLC) and essential (ELC) light chains, bind to the neck of each MHC. While phosphorylation of the RLCs regulates NM II function, the ELCs stabilize the MHCs. NM II can form non-polar filaments by self-association of coiled-coil tail domains (Fig. 1-5b) (Vicente-Manzanares et al., 2009). These filaments induce bundling of actin filaments and, together with α-Actinin, the formation of stress fibers. Stress fibers work as the main contractile unit needed for cell migration (Tojkander et al., 2012). Stress fibers contraction is regulated by the phosphorylation of the RLCs through the RhoA small GTPase pathway.

Another important component of the actin cytoskeleton and stress fibers in particular are the focal adhesions. Focal adhesions are protein complexes that bind actin filaments and stress fibers to the cell membrane and the extracellular matrix through binding to integrins (Geiger et al., 2009; Tojkander et al., 2012). Focal adhesions have been described to play an important role in cell migration, mechanotransduction and actin-microtubule crosstalk. Components of the focal adhesions include proteins such as Vinculin, Talin, and Paxilin that physically attach the actin filaments to the integrins and the cell membrane, and the Focal adhesion kinase (FAK) that regulates the formation of the focal adhesion as well as the formation and contraction of the stress fibers (Etienne-Manneville, 2004; Provenzano and Keely, 2011). The regulatory role of FAK is still largely not understood, however it is known that mutual regulation of FAK and RhoA activity is required for the formation and function of stress fibers in both cell motility and mechano-transduction(Provenzano and Keely, 2011). Due to their role in regulating actin

structure and function, it is important to understand the interactions between actin NM II and FAK when studying the mechano-transduction pathways where actin dynamics are involved.

Rho family of small GTPases

The Rho GTPases is a family of small G proteins whose activity is regulated by their capacity to hydrolyze GTP. Though around 22 members of the family have been described, the most studied are RhoA, Rac1 and Cdc42. The activation of Rho GTPases is regulated by guanine nucleotide exchange factors (GEFs) that allow the Rho GTPs to switch form a GDP-bound inactive state to a GTP-bound active state (Sit and Manser, 2011; Spiering and Hodgson, 2011). On the other hand, GTPase activating proteins (GAPs) facilitate the hydrolysis of the bound GTP into GDP, thus inactivating the GTPase. The activation of RhoA, Rac1 and Cdc42 leads to the activation of signaling cascades, composed mainly by kinases that eventually induce changes in gene expression as well as the organization of the actin cytoskeleton (Schmidt and Hall, 1998; Spiering and Hodgson, 2011). Each one of these three Rho GTPases has been associated to have a particular role in actin dynamics (Fig. 1-6). While Rac1 and Cdc41 regulate actin dynamics mainly in lamelipodia and fillipodia during cell migration and in the neuronal growth cone, RhoA regulates stress fibers and focal adhesion formation and contraction (Dickson, 2001; Schmidt and Hall, 1998).

The regulation of stress fibers formation and contraction by RhoA is still largely not well understood. Nonetheless, it has been shown that RhoA can induce fiber formation by the activation of two downstream effectors, the Rho-associated kinase 1/2 (ROCK) and the formin mammalian diaphanous (mDia). While ROCK promotes actin polymerization by blocking cofilin-mediated F-actin depolymerization, mDia directly promotes actin polymerization (Provenzano and Keely, 2011). Furthermore, MLC phosphorylation by ROCK induces the formation of NM II filaments, necessary for stress fiber formation. The activation of Rho signaling pathway to form stress fibers is induce as a response to the extracellular mechanical environment. Cell adhesion to the extracellular environment through integrins will induce the formation of focal adhesions, which will lead to the activation of FAK (Provenzano and Keely, 2011). Activation of FAK will in turn lead to the activation of RhoA and ROCK through the GEFs p115RhoGEF, LARG and p190RhoGEF. The increase in ROCK-mediated NM II contraction will

positively feedback into the focal adhesion, promoting its growth and further activation of FAK (Provenzano and Keely, 2011). This feed back loop could lead into changes in the expression of genes that are regulated by RhoA. Therefore, the close interaction between focal adhesions and RhoA signaling could be and important mechanism to regulate gene expression in response to external mechanical stimuli.

Microtubule-actin cytoskeleton crosstalk

Microtubules are hollow tubes formed by the self-assembly of fibers, known as protofilaments that are in turn polymers of α and β-tubulin heterodimers. Microtubules are usually composed of 11 to 13 protofilaments and have a (+) and (-) polarity. Microtubule formation begins at the nucleation center were a ring of γ-tubulin caps the (-) end; while polymerization of GTP-bound alpha-beta tubulin heterodimers occurs at the (+) end. In addition to actin filaments, microtubules are highly dynamic structures, under going constant polymerization and depolymerization at the (+) end. Microtubules play important roles during cell division as well as growth cone guidance and cell motility (Akhmanova and Steinmetz, 2008). In the later two, microtubules crosstalk with the actin cytoskeleton to elicit coordinated movement (Rodriguez et al., 2003).

Crosstalk between microtubules and actin cytoskeleton can be at the regulatory level, through signaling cascades, or at the structural level, through direct protein interactions (Rodriguez et al., 2003). At the regulatory level it has been shown that RhoA can play a role in actin-microtubule crosstalk, in particular in the regulation of focal adhesion and stress fibers formation and function (Fig. 1-7)(Etienne-Manneville, 2004). It has been shown that depolymerization of microtubules can induce further positive feedback into the focal adhesion and stress fibers contractility via RhoA. It is thought that the GEF-H1 that binds to microtubules, is freed during microtubules depolymerization, inducing RhoA to change from a GDP to a GTP bound state and becoming active to induce focal adhesion and stress fiber formation as discussed before (Krendel et al., 2002; Palazzo and Gundersen, 2002). On the other hand, microtubule polymerization seems to favor dissolution of focal adhesions through a structural interaction via the microtubule associated motor protein kinesin-1, though the exact mechanism is still not fully understood (Krylyshkina et al., 2002). Though many other microtubule-associated proteins (MAPs) have been described to interact with the actin cytoskeleton in cellular processes such as cell division and migration (Rodriguez et al., 2003), how the

regulatory or structural interaction between actin and microtubules induces changes in gene expression in response to external mechanical stimuli is still a field open for exploration.

Cytoskeleton and injury

The effect of injury in in the cellular cytoskeleton has been mainly focused on studying the changes in microtubules in the context of axon transection. While axonal microtubules are normally kept in a stable steady state in the axon, upon injury, these undergo significant changes to form a dynamic growth cone that may involve growth of microtubule ends and/or formation of new microtubule nucleating centers (Bradke et al., 2012). Recent work has shown that in injured mechanosensory neurons in *C. elegans*, microtubules increase at the injury site at the same time as the depolymerizing kinesin KLP-7 is downregulated (Ghosh-Roy et al., 2012). A second phase of axonal outgrowth requires post-translational modifications of alpha tubulin units by the cytosolic carboxypeptidase CCPP-6. Interestingly both of these phases of axon outgrowth were shown to be mediated by the DLK-1 Map kinase pathway (Ghosh-Roy et al., 2012). This work sheds important new insight into the dynamic process of how a transected axon rearranges its cytoskeleton to form a new growth cone and regenerate the axon.

Changes in actin cytoskeleton have also been studied in the context of axon transection. As discussed previously, axotomy induces increases in intracellular calcium that eventually lead to actin depolymerization as well as calpain-dependent actin-spectrin cleavage. For the new growth cone to form after axon transection, actin depolymerization is necessary (Bradke et al., 2012). Treatment of neuronal cultures of the sea slug *Aplysia californica* with jasplakinoline, a drug known to stabilize F-actin, to prevent depolymeriaztion of the actin cytoskeleton in response to axotomy, prevented the formation of a functional growth cone. Interestingly, though depolymerization and rearrangement of microtubules and actin cytoskeleton after axotomy are not interdependent, the dynamic changes of both structures are needed for the formation of a functional growth cone (Spira et al., 2003). In contrast to these results, single cell injury experiments performed in *Xenopus* showed that the proper formation of an acto-myosin contractile ring to close the wound is dependent on the flow of microtubules to the injury site (Mandato and Bement, 2003). Moreover, microtubules seem to migrate to the injury site by structural interaction with actin, which also flows towards the injury site. This

suggests that the response of the actin and microtubule cytoskeleton to injury, which is governed by regulatory and/or structural interactions could be dependent of the type of cell, the type of injury and the type of structure that needs to be rebuilt.

Other single cell injury assays performed in Drosophila embryos showed that aside from the formation of the acto-myosin contractile ring and microtubule flow to the injury site, co-localization of Rho-GTPases at ring is necessary for the proper closure of the wound (Abreu-Blanco et al., 2014). The coordinated activities of RhoA, Rac and Cdc42 are needed for the proper localization and function of the contractile acto-myosin ring. Interestingly, the authors found that in this context, RhoA regulates acto-myosin function through the effectors ROCK and Dia, the same effectors that seem to be involved in stress fiber-related mechanotransduction. Furthermore, while the proper formation of the acto-myosin was dependent of Rho-GTPases crosstalk, the localization of the GTPases was also dependent on the acto-myosin dynamics (Abreu-Blanco et al., 2014). This would suggest that response to injury could in part be regulated through similar pathways that control the transduction of external mechanical stimuli, as discussed before.

3D *in vitro* mammalian tissue models

In vitro cultures have been shown to be a powerful tool to dissect the molecular pathways that govern cellular behavior. Primary cultures and cell lines have become standard model systems to study cell division, migration, signaling pathways, growth cone guidance, response to injury, cytotoxicity and cancer among many others. However, the better we understand cellular behavior, the more clear it becomes the role that the physicochemical extracellular environment plays in modulating such behavior (Baker and Chen, 2012; Provenzano and Keely, 2011; Santos et al., 2012). In particular, it has been widely shown that the extracellular matrix can regulate the gene expression in response to external stimuli. The effort to create a more physiologically relevant environment for cells has lead to the creation of a wide variety of 3D *in vitro* model systems (Subramanian et al., 2009). Though most advances in creating 3D *in vitro* culture system have been done in the context of Tissue Engineering to replace damaged or lost tissue in humans, the same basic principles can be used for the development of 3D *in vitro* model system for molecular, cellular and developmental biology.

3D scaffolds and biopolymers for *in vitro* tissue model

Across nature, different cells are immersed in different extracellular environments that vary in chemical composition as well as in mechanical properties (Santos et al., 2012). To provide cells with an environment that better mimics their *in vivo* context, the selection of an appropriate material that provides both the chemical and mechanical milieu needed is a key step in the development of 3D *in vitro* systems. The materials used in 3D cultures can be classified in 2 main categories, synthetic and natural. Among the most common synthetic polymers used are polyethylene glycol (PEG) polyglycolic acid (PGA) polylactic acid (PLA) and combination of them, as well as poly-ε-caprolactone (PCL) and polyhydroxy butyrate (PHB) (Ma, 2004). Due to its hydrophilic nature PGA is widely used in the elaboration of hydrogels, while the more hydrophobic character of PLA makes it more appealing in applications where slow degradation is desired. Although PCL also has a slow rate of degradation, due to its physical properties and malleability has become a main material for 3D applications especially in nervous tissue (Subramanian et al., 2009).

The most commonly used natural macromolecules for cellular scaffolds are collagen, chitosan, alginate, agarose and sodium hyalunorate (Ma, 2004; Subramanian et al., 2009). Collagen is one of the components of the extracellular matrix of most tissues, therefore if the preferred natural material for the development of 3D systems (Ma, 2004). Other components of the extracellular matrix such as Fibronectin and Laminin are rather used as surface modifiers to improve the cell adhesion to scaffolds elaborated with either synthetic polymers or natural materials (Subramanian et al., 2009). Though biomaterials offer a chemical environment more similar to *in vivo* conditions, their mechanical properties and the difficulty to perform chemical modifications to improve them, have favored the use of synthetic materials for applications where the mechanical environment could have a stronger influence that the chemical environment. Therefore, it is also common to prepare scaffolds made of mixtures of synthetic and natural materials, to provide both the desired mechanical and chemical properties(Subramanian et al., 2009).

Aside from the material to be used, during the development of a scaffold for 3D *in vitro* culture, parameters such as pore size, porosity, superficial area, biodegradability, biocompatibility, mechanical integrity and stiffness should be taken into account, since each one of them can affect cell adhesion, motility proliferation and survival (Ma, 2004). Changes in these parameters can be achieved by chemical modifications or variations in the technique used to obtain the 3D scaffold. For example, to increase the mechanical integrity of collagen scaffolds, UV or glutaraldehyde mediated crosslinking is often used (Chevallay and Herbage, 1999; Hanson Shepherd et al., 2011; Ma, 2004; Subramanian et al., 2009). Furthermore, an elegant system to easily induce changes in mechanical properties by controlling the nanostructure of the materials has been developed. Through a process known as electrospinning, in which perfusing a solution of the biomaterial through a magnetic field forms nanofibers, the pore size, porosity and stiffness of the scaffold can be modulated by changes in the concentration of the biomaterial solution, the strength of the magnetic field and the amount of nanofibers deposited (Kumbar et al., 2008). Further advances in the material sciences will lead to the fabrication of 3D scaffolds that would provided the cells in vitro a mechanical and chemical environment that fully recapitulates their *in vivo* context.

In vitro spinal cord models

In the context of the nervous system, advancement in 3D cultures has been focused in the creation of scaffolds that allow the regrowth of axons across the injury site in the peripheral nervous system (PNS) (Bellamkonda, 2006; Kumbar et al., 2008) and the spinal cord after injury (Madigan et al., 2009; Norman et al., 2009). The most common material used to promote PNS regeneration is collagen alone or in combination with fibronectin, fibronectin and laminin or PCL (Gu et al., 2014). Though there are differences in the composition and internal structure of the scaffolds used, all of them seemed to improve the growth of axons across the injury site. Though this would suggest that in the context of PNS regeneration, the sole presence of a guidance scaffold is sufficient to promote regeneration regardless of the chemical composition of the mechanical properties, the development of an optimal scaffold or engineered tissue is still to be achieved (Bellamkonda, 2006; Gu et al., 2014).

In the context of the spinal cord numerous studies have been carried using both natural (Table 1-2) and synthetic materials (Table 1-3) (Madigan et al., 2009; Norman et al., 2009). Among the natural materials the used are agarose (Stokols et al., 2006; Stokols and Tuszynski, 2004) collagen and fibronectin. Inclusion of growth factors such as the brain derived neurotrophic factor (BDNF) and functional molecules as blocking antibodies against the epidermal growth factor receptor (EGFR) seem to greatly improve the effects of the use of 3D scaffolds to promote axonal regeneration in spinal cord (Han et al., 2010; Han et al., 2009; Han et al., 2015) as well as the inclusion of mesenchymal stem cells (Liu et al., 2013). In spite of the advances in the material sciences to produce engineered scaffolds to promote spinal cord regeneration, the use of similar approaches to create model system to study the cellular and molecular pathways that govern the response to spinal cord injury has not been so well developed. Some examples of such approach are the use of PLA nanofibers to study of axon myelination by oligodendrocytes (Lee et al., 2012), collagen hydrogels to study Schwann cells spreading and guidance behavior (Rosner et al., 2005) and collagen gel to study reactive gliosis (East et al., 2009).

The development of relevant 3D cultures to better understand the development of the glia scar and how the engineered tissues tested so far have improved spinal cord regeneration should be a priority in order to modify the current available therapeutic approaches to better elicit spinal cord recovery in mammals and ultimately in humans.

Figures

Figure 1-1. Schematic diagram of spinal cord injury in mammals.

After injury to the mammalian spinal cord cells migrate to the injury site. Macrophages engulf dying cells, while astrocytes, fibroblasts and endothelial cells fill the cavity created by the injury. Some of these cells express and secrete proteins that inhibit axonal growth. On the caudal side of the injury axons that have been disconnected from their cell body begin to undergo a process called Wallerian degeneration, which ultimately results in death of the axon. Adapted from Diaz Quiroz & Echeverri, 2013 (Diaz Quiroz and Echeverri, 2013).

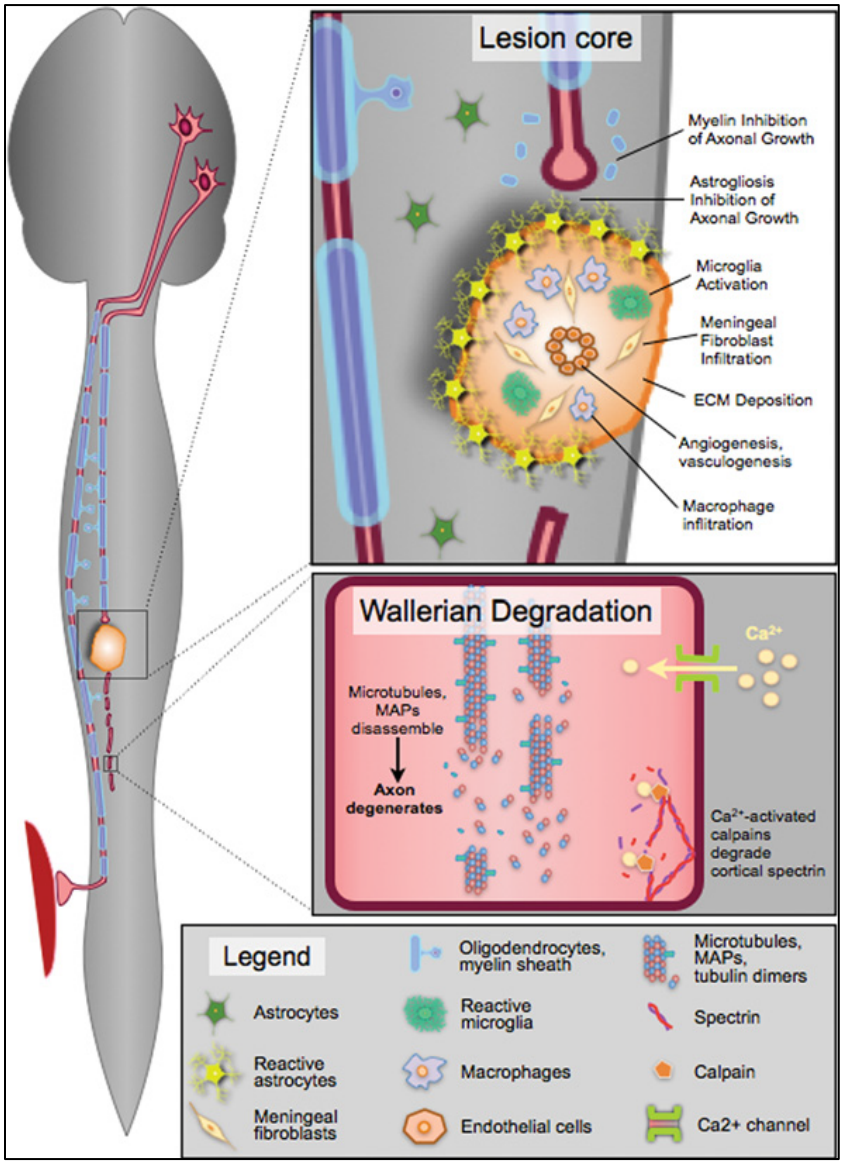

Figure 1-2. Classes of semaphorins and plexins.

Classes 1 and 2 are found in invertebrates, 3 to 7 in vertebrates and 8 is known as viral semaphoring. There are 4 classes of plexins A to D. Semaphorin and plexins share a Sema domain. One semaphorin can bind to different plexins and one plexin can recognize different semaphorins. Adapted from Kruger et.al., 2005 (Kruger et al., 2005).

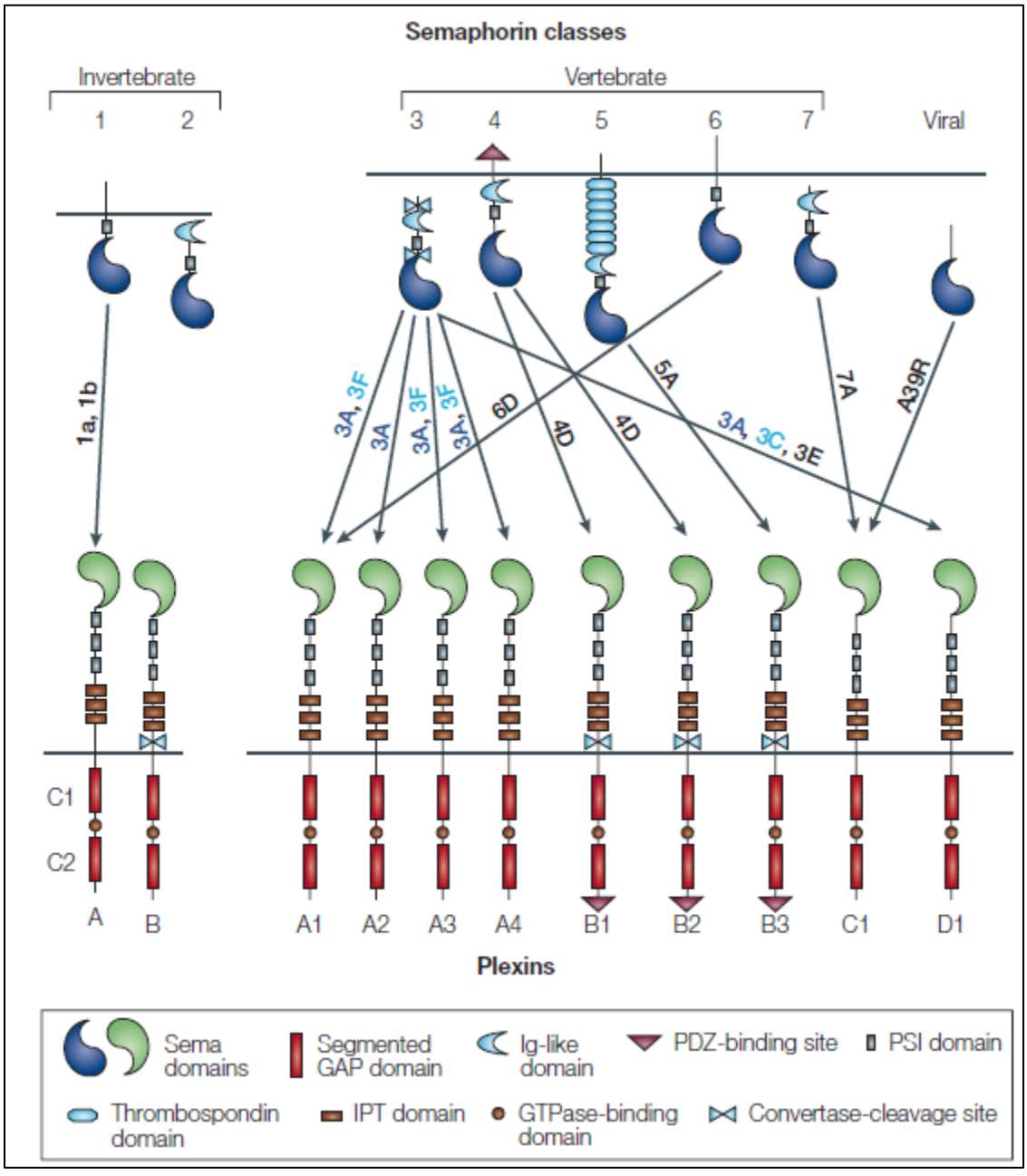

Figure 1-3. Regeneration across levels of biological complexity.

In nature regeneration can be achieved at different levels, while planarian are able to regenerate a whole body, other organisms with more restricted regenerative capabilities can only regenerate tissues. Adapted from Bely, & Nyberg, 2010 (Bely and Nyberg, 2010).

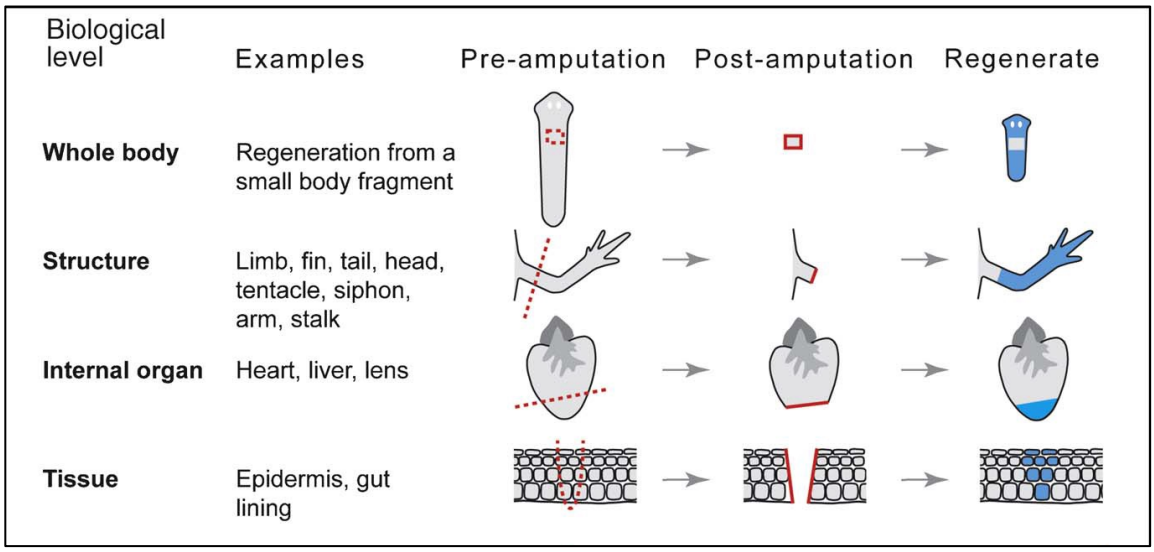

Figure 1-4. Biogenesis of and function of microRNAs.

After transcription by Pol II precursor miRNA (pri-miRNA) is cleaved by Drosha/DGCR8. The processed miRNA (pre-miRNA) is exported to the cytoplasm and cleaved by Dicer/TRBP. Double stranded miRNA assembles the RNA induced silencing complex, whose main component is the protein Argonaut 2 (AGO2). The mature miRNA binds to the RISC complex while the complementary strand is degraded. The ribonucleoprotein complex regulates gene expression by cleaving, blocking translation and inducing deadenylation of the target gene mRNA. Adapted from Winter et al., 2009 (Winter et al., 2009).

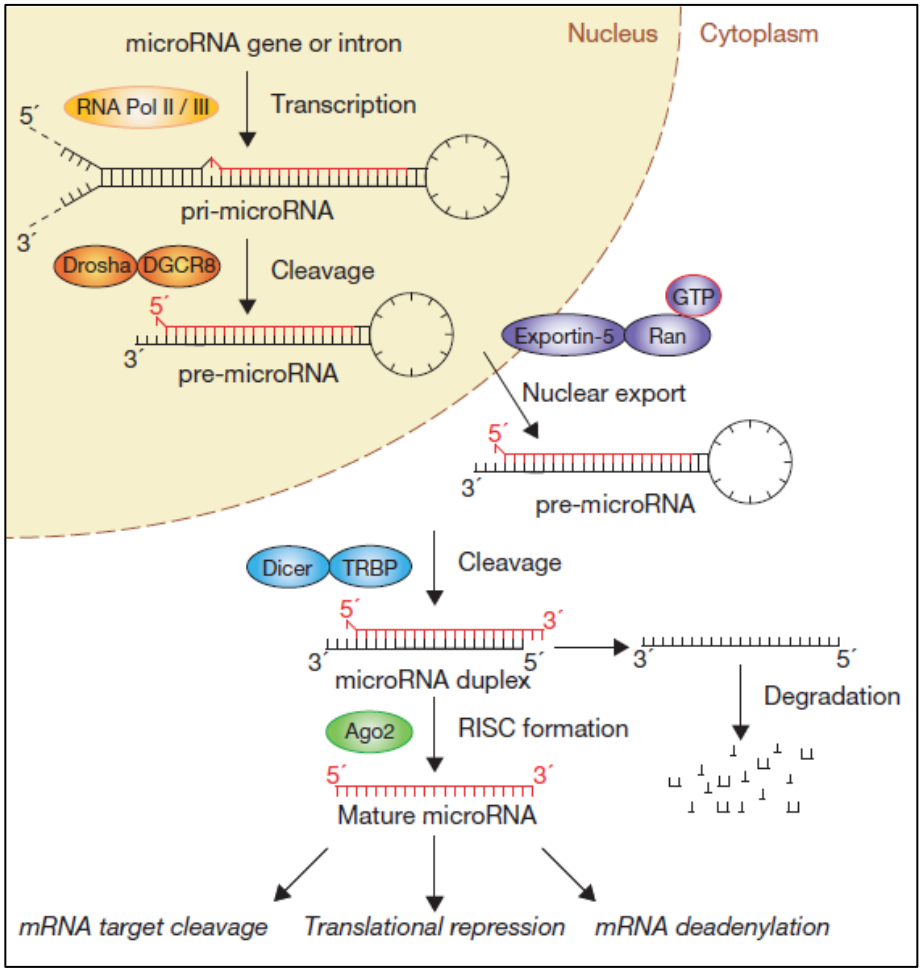

Figure 1-5. Actin and myosin filaments.

(A) Actin structure is regulated by the activity of different actin binding proteins. Adapted from http://greatcourse.cnu.edu.cn. (B). Self assembly of non muscle myosin through the tail domain forms myosin filaments that bind to F-actin and promote stress fiber formation. Adapted from Vicente-Manzanares et al., 2009 (Vicente-Manzanares et al., 2009).

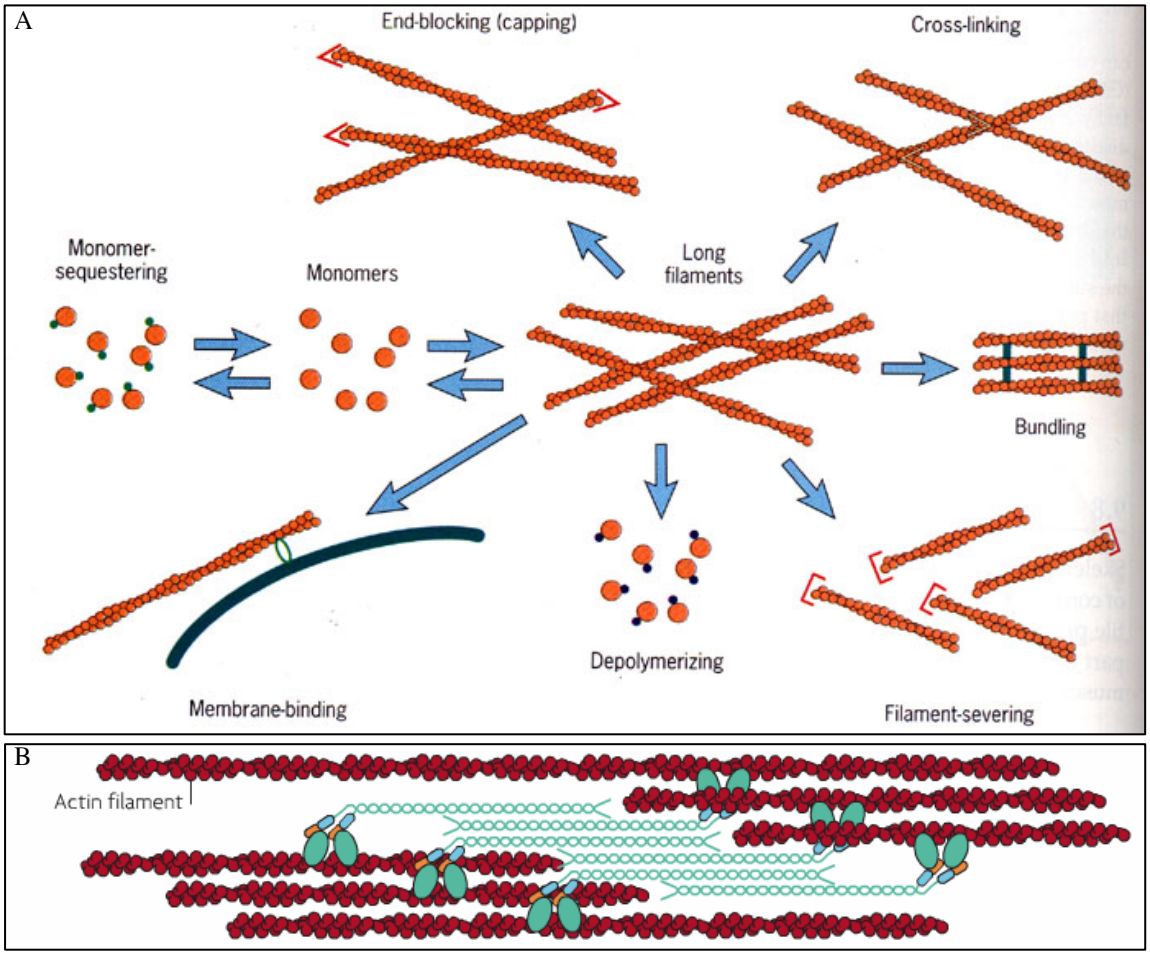

Figure 1-6. Rho family of small GTPases.

Activation of small GTPases activates signaling cascades that induce changes in gene expression and actin organization. RhoA, Rac1 and Cdc42 have different roles in regulating actin organization Adapted from Schmidt & Hall, 2009 (Schmidt and Hall, 1998).

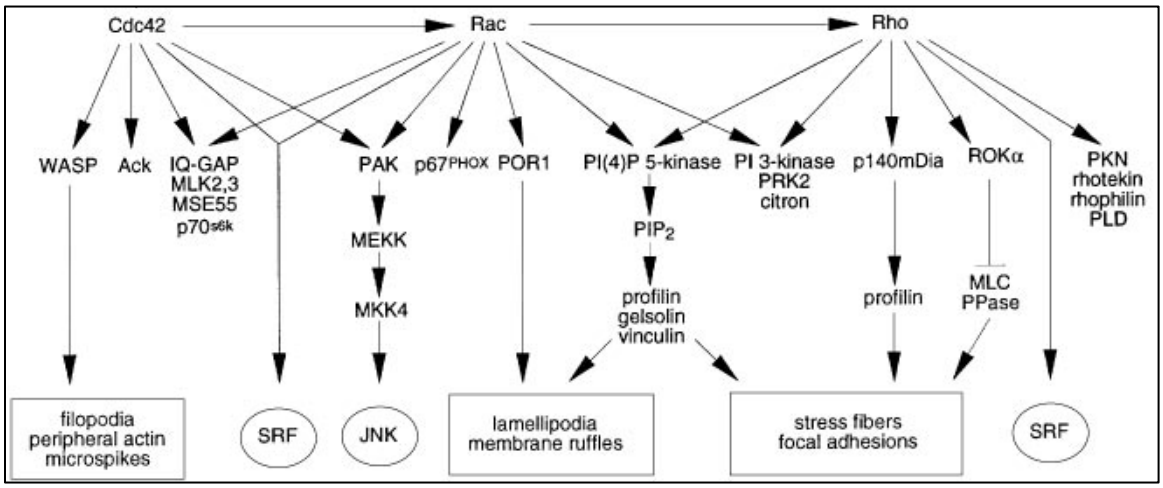

Figure 1-7. Actin, microtubule and Rho crosstalk.

Cell adhesion activates RhoA, which lead to the formation of focal adhesions an actin stress fibers. Contraction of stress fibers further strengths the focal adhesion and the activation of Rho. Microtubule polymerization negatively regulates Rho activity and focal adhesion stability. Adapted from Etienne-Manneville, 2004 (Etienne-Manneville, 2004).

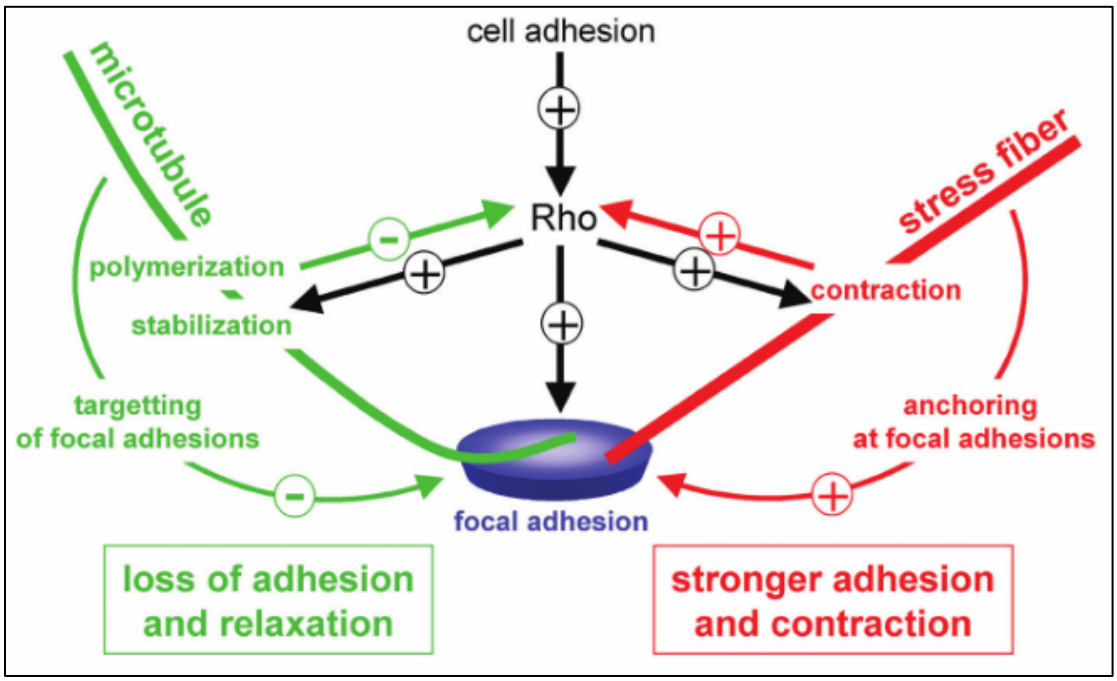

Tables

Table 1-1. Overview of regeneration in different species.

Adapted from Diaz Quiroz & Echeverri, 2013 (Diaz Quiroz and Echeverri, 2013).

n.a., not applicable.

Process	Worms	Fish	Frogs	Axolotls and newts	Mammals
Glial response	n.a.	Proliferation Migration Bridge formation [4–7]	Proliferation Migration New tube formation [19,29]	Proliferation Migration New tube formation [43,46,51,54,56,61,64,80]	Proliferation Migration Up-regulation of scar proteins [8–11,62,63,65–67,71]
Glial scar	n.a.	No [4–6]	Not in larvae, unknown in non-regenerative adult [15,16]	No [41,64]	Yes [42,73–75,82]
Axon degeneration	Yes [139]	Some [14]	In adults [16]	Unknown	Yes [122–129]
Axon regrowth	Yes [137–140]	Yes [12–14]	Yes, in larvae, not in adults [15,16,27,30]	Yes [38–41,44,50]	No (limited regeneration can be promoted) [66,69,71,76–78,115,117–121,130,144,146]
Functional recovery	Yes [135,137]	Partial [12–14]	Yes, in larvae, not in adults [15,29,30]	Yes [38,39,41]	No (limited recovery can be promoted) [69,71,72,76–78,130,153,154]

Table 1-2. Overview of natural material used for tissue engineering in the spinal cord.

Adapted from Mandigan et al., 2009 (Madigan et al., 2009).

Natural polymers	Structure	Examples of applications for spinal cord repair
Natural hydrogels		
Collagen, type I	Glycine-X-Y polypeptide fibrils	Collagen gels as extracelluar support growth matrix. (Marchand et al., 1993; Ma et al., 2004) Collagen gels with embedded neurotrophic factors [NT-3, BDNF] (Houweling et al., 1998) Collagen filament bridges as growth substrates (Yoshii et al., 2004; Pfister et al., 2006) Linear ordered collagen scaffolds with collagen binding BDNF (Han et al., 2009) Schwann cell delivery (Dewitt et al., 2009) Electrospun nanofibres and stem cell differentiation (Xie et al., 2009) Gels for drug delivery [EGF and FGF-2] (Jimenez Hamann et al., 2005) Growth factor infused matrix for synthetic polymer channels (Tsai et al., 2006) Collagen coating of PLGA for gene delivery (De Laporte et al., 2009) Guidance gradients with incorporated laminin (Yao et al., 2009)
Agarose/alginate	Linear polysaccharide, β-D-mannuronic acid and α-L-guluronic acid	Agarose gels as growth matrix (Bellamkonda et al., 1995; Balgude et al., 2001) Microencapsulation of neurotrophic factors (Maysinger et al., 1996) Agarose gels with neurotrophic gradients (Cao and Shoichet, 2001). Freeze dried alginate sponges as neurite growth substrate (Kataoka et al., 2004) Cell encapsulation into alginate hydrogel (Novikova et al., 2006) Linear guidance pore scaffolds (freeze dried agarose) (Stokols and Tuszynski, 2006) Uniaxial multichannel scaffolds with BDNF-secreting MSCs (Stokols et al., 2006) Scaffolds with neurotrophin integration (Jain et al., 2006; Stokols and Tuszynski, 2006) Guidance gradients with incorporated laminin (Dodla and Bellamkonda, 2006) Steroid delivery with agarose embedded PLGA nanoparticles (Chvatal et al., 2008)
Hyaluronic acid	Dissacharide units of glucuronic acid and *N*-acetylglucosamine	Intrathecal drug and growth factor delivery with as a methylcellulose composite gel. (Gupta et al., 2006; Shoichet et al., 2007; Kang et al., 2009)
Chitosan	Co-polymer of *N*-acetylglucosamine and *N*-glucosamine	Chitosan scaffolds supporting cell adhesion and growth (Freier et al., 2005; Freier et al., 2005) Schwann cell encapsulation (Yuan et al., 2004) Neural stem cell differentiation (Zahir et al., 2008) Protein elution (Kim et al., 2008) Extra and intramedullary tissue bridge conduits with neural stem cell differentiation (Nomura et al., 2008)
Fibronectin	Plasma glycoprotein dimer	Fibronectin mats for oriented axonal growth (King et al., 2003) Neurotrophin and drug delivery (Phillips et al., 2004)
Fibrin	Fibrillar glycoprotein polymer	Neurotrophin elution from heparin complexes (Taylor et al., 2006) Embryonic stem cell differentiation (Willerth et al., 2007) Gliosis inhibition (Johnson et al., 2009)

Table 1-3. Overview of synthetic materials used for tissue engineering in the spinal cord.

Adapted from Mandigan et al., 2009 (Madigan et al., 2009).

Synthetic Polymers	Structure	Examples of Applications for Spinal Cord Repair
Biodegradable		
PLA	Poly(D,L lactic acid)	Single and multichannel scaffolds seeded with Schwann cells.
PGA	Poly(glycolic acid)	PLA: single channel (Oudega et al., 2001)
PLGA	Poly(lactic-co-glycolic acid)	Freeze dried macroporous foam scaffold with incorporated BDNF (Patist et al., 2004) Freeze dried macroporous scaffold with BDNF-secreting Schwann cells (Hurtado et al., 2006) PLGA: multichannel scaffolds seeded with Schwann cells (Moore et al., 2006) Multichannel scaffolds seeded with neural stem cells (Teng et al., 2002) Neurotrophin-eluting micro and nanospheres within scaffolds (Yang et al., 2005; Wang et al., 2008) Protein release from chitosan scaffolds (Kim et al., 2008)
PCL	Poly-ε-caprolactone	Nanofibre spinning for axonal growth orientation (Schnell et al., 2007)
PCLF	Poly-ε-caprolactone fumarate	Multichannel scaffolds (Wang et al., 2009)
Hydrogels		
PEG	Polyethylene glycol	Intravenous solution (Laverty et al., 2004) Immunoprotective sealant gel (Borgens et al., 2002; Duerstock and Borgens, 2002) Injectable gel with PLA for NT-3 delivery (Piantino et al., 2006) and BDNF (Soderquist et al., 2008) Three-dimensional neurite growth matrix (Namba et al., 2009) Intravenous PEG with Magnesium Sulfate (Ditor et al., 2007; Kwon et al., 2009)
Non-biodegrabable hydrogels		
pHEMA	Poly(2-hydroxyethyl methacrylate)	pHEMA sponges (Giannetti et al., 2001) Guidance channels (Tsai et al., 2004) Fibre templated scaffolds (Flynn et al., 2003) Cell adhension gradients (Yu and Shoichet, 2005) Neurotrophic gradients (Moore et al., 2006) Co-polymer with chitosan including cell adhesion peptides (Yu et al., 2007) Coil (Nomura et al., 2006) or multilayered pHEMA (Carone and Hasenwinkel, 2006) scaffold reinforcement Surface charge modification for cell adhesion (Lesny et al., 2006) and axonal growth (Hejcl et al., 2008)
pHEMA-MMA	pHEMA-co-methyl methacrylate	NGF-release from PGLA microspheres and pHEMA-NGF polymer bilayer (Piotrowicz and Shoichet, 2006) Matrix filled channels for acidic fibroblast growth factor (FGF-1) and NT-3 delivery (Tsai et al., 2006)
pHPMA	Poly[*N*-(2hydroxypropyl) methacrylamide]	pHPMA colloid gel (Woerly et al., 1998) Colloid gel with cell adhesion peptides (Woerly et al., 2001) (Neurogel™) Colloid gel with CNTF and BDNF (Loh et al., 2001)
PAN/PVC	Poly(acrylonitrile-co-vinylchloride)	Schwann cell seeded scaffolds with BNDF & NT-3 cord infusion(Bamber et al., 2001) Schwann cell seeded scaffolds with GDNF Matrigel™(Iannotti et al., 2003)

Chapter 2: Comparative analysis of microRNA expression after spinal cord injury in the regeneration competent axolotl vs regeneration incompetent rat.

(Adapted from the paper “Precise control of miR-125b levels is required to create a regeneration-permissive environment after spinal cord injury: a cross-species comparison between salamander and rat) (Diaz Quiroz et al., 2014)

Summary

Our starting hypothesis is that the differences in response to SCI between mammals and the axolotl is due to differences in gene regulation, and in particular, differences in post-transcriptional regulation at the microRNA level. To answer this question we carried out a comparative analysis of miRNA expression after SCI in axolotls and rats. The analysis showed that after SCI only a small group of miRNAs showed significant difference between the two species. Out of this miRNAs, miR-125b was identified to be involved in regulating the response to injury in both axolotls and rat. *In vivo* modulation of miR-125b expression in axolotl impaired spinal cord regeneration after injury, while upregulation of miR-125b in rats improved recovery after spinal cord injury. In particular, we showed that miR-125b regulates the expression of the repellant axonal guidance cue Semaphorin 4D (Sema4D) after injury in both rat and axolotl. While in the axolotl miR-125b maintains the expression of Sema4D at the proper levels and the proper location to allow axonal growth across the injury, in the rat the low expression levels of the miRNA allows for overexpression of Sema4D, thus impairing axonal growth in mammals after injury. Microarray analyses from tissue samples from rats treated with miR-125b mimic after injury to increase the levels, suggest that miR-125b works in a complex regulatory network to provide a permissive environment for regeneration.

Introduction

In mammals, axonal regrowth following spinal cord injury is inhibited by the formation of a glial scar consisting primarily of reactive astrocytes and proteoglycans that seem to play important protective roles in stabilizing the delicate central nervous system (CNS) tissue (Sandvig et al., 2004; Silver and Miller, 2004). Injured axons on the rostral or cell-body side of the injury site retract in a process referred to as dieback, and dystrophic end bulbs that retain the ability to generate new growth cones if given the right environment (Busch et al., 2010). On the caudal side of the injury, the severed axons that are disconnected from their neuronal cell bodies undergo Wallerian degeneration within 24-48 hours, which results in the loss of all motor and sensory function caudal to the injury site (Kerschensteiner et al., 2005; Lubińska, 1982; Wang et al., 2012).

Some vertebrates have maintained a remarkable ability to regenerate a fully functional spinal cord after tail amputation or injury (Butler and Ward, 1965; Butler and Ward, 1967; Goss, 1969; Sanchez Alvarado and Tsonis, 2006; Slack et al., 2008; Tanaka and Ferretti, 2009). In the Mexican axolotl salamander, this process involves the formation of terminal vesicle-like structures on both the rostral and caudal ends of the injured neural tube. Cells within ~500 μm of the injury site begin to divide and migrate to replace the missing or damaged portion of the neural tube (Butler and Ward, 1965; Butler and Ward, 1967; Egar and Singer, 1972; Géraudie et al., 1988; Holtzer, 1951; Holtzer, 1952; Holtzer, 1956; Singer et al., 1979). Various genes have been identified that are up- or downregulated in the glial cells at the injured ends of the spinal cord; these cells then proliferate and repair the lesion (Beck et al., 2003; Chernoff et al., 2003; Chevallier et al., 2004; Dawley et al., 2012; Ferretti et al., 2003; Hui et al., 2013; McHedlishvili et al., 2012; Moftah et al., 2008; Monaghan et al., 2007; Schnapp et al., 2005; Tanaka and Ferretti, 2009; Walder et al., 2003). No evidence of glial-scar formation is detectable in axolotl salamanders, as assessed by pre- and post-injury levels of GFAP, vimentin, chondroitin sulfate proteoglycans (CSPGs) or collagens. Axons regrow across the original lesion site, leading to restored motor and sensory functions caudal to the injury (Clarke et al., 1988; Clarke and Ferretti, 1998). It is still unclear how functional recovery occurs in axolotls. It is unclear whether severed axons

regrow and reconnect to the same targets, or whether new neurons are born, establishing new neuronal connections.

Many of the glial-scar components that inhibit mammalian axonal regrowth have been identified, and the process of Wallerian degeneration is well understood at the molecular level. However, attempts to promote regeneration after spinal cord injury in mammals are still largely unsuccessful. We have taken a novel approach to understand the molecular cues that regulate gene expression after injury in the regeneration-competent axolotl salamander (Ambystoma mexicanum), versus the regeneration incompetent rat. We focused on the environment of the injury site because the intrinsic differences that occur at the injury site could provide novel insights into how salamanders create a regeneration permissive environment after injury.

Results

Comparative array assay

(Experiments were carried out in collaboration with Matthew Coyle and Eve Tsai from the Ottawa Hospital research Institute, Canada)

To investigate the molecular basis for the cross-species differences in spinal cord injury repair systems, we focused on microRNAs (miRNAs), which function as high-level pathway regulators and offer convenient entry points for these studies (Hagen and Lai, 2008). Our previous work revealed 93% conservation in miRNAs between axolotl and other vertebrates (Sehm et al., 2009). We initiated the present studies by carrying out a comparative miRNA profiling analysis at different time points following spinal cord transections in axolotl and rat (Fig. 2-1A). The arrays used covered all known miRNAs from rat, human and mouse at the time of the experiment. Microarray-based miRNA profiles were generated using spinal cord extracts from the rostral and caudal sides of the injury that were collected 1 and 7 days after complete transection of the spinal cord. These time points were chosen so that early changes in miRNA expression could be detected along with those changes that occur later in regeneration when, in axolotl, radial glial cells are dividing and migrating to replace lost tissue and axons are regrowing (Butler and Ward, 1965; Butler and Ward, 1967; Chernoff et al., 2003; Egar and Singer, 1972; Géraudie et al., 1988; Holtzer, 1951; Holtzer, 1956; Monaghan et al., 2007; Singer et al., 1979; Tanaka and Ferretti, 2009) whereas, in rats, a glial scar is taking the place of the lost tissue (Hossain-Ibrahim et al., 2007; Silver and Miller, 2004). We identified miRNAs that exhibited reproducibly significant changes in abundance during the days following the injury, determined whether these changes were specific to only one or both sides of the injury site, and assessed differences within these patterns between the two species (Fig. 2-1A). The array's probe collection was designed to cover ~3400 known miRNA sequences from human, mouse, rat and other vertebrate species. Our data identified 27 miRNAs that showed differential regulation at the different time points between the two sides of the injury in rat alone, whereas 36 were significantly differentially changed in axolotl alone. Fourteen miRNAs were identified that showed significant differences after injury in rat versus axolotl (Fig. 2-1A). This low number of differentially regulated miRNAs suggests that these miRNAs very specifically regulate

genes involved in the response to injury in neural tissue. The observed differential regulation of miR-126 suggests that the tissue samples also contained large amounts of vasculature, because expression of this miRNA is well characterized in endothelial cells of zebrafish, mouse and human (Anand and Cheresh, 2011; Fish et al., 2008). When this miRNA is downregulated in zebrafish, it leads to blood-vessel collapse. Because it is downregulated in axolotls after injury, this suggests that quick closure of blood vessels might prevent some inhibitory molecules from arriving at the injury site.

We identified miR-125b as an interesting candidate for further study because it showed marked differences between axolotl and rat, and it has been implicated previously in normal development and in cancer and stem-cell differentiation (Lee et al., 2009; Xia et al., 2009; Zhang et al., 2011). Under pre-injury conditions in axolotl, we found that miR-125b expression in the spinal cord was concentrated primarily in radial glial cells (Fig. 2-1C). Axolotl glial cells have a large nucleus that occupies much of the cytoplasm; therefore, the staining appears at the apical side of the cell adjacent to the central canal. However, the levels in the rat spinal cord were below the detection level of in situ hybridization, so qRT-PCR was used to identify the cells that express miR-125b in the adult rat spinal cord. Astrocytes had the highest level of miR-125b expression in rat (Fig. 2-1D).

In the normal homeostatic condition, miR-125b showed eightfold higher levels in axolotl compared with that in rat (Fig. 2-1B). By 1 day after spinal cord transection, the rostral side of the injury site showed a rapid ~40% reduction of the initially high miR-125b levels in axolotl, whereas the corresponding levels decreased by less than 1% in rat (Fig. 2-1B). At the same time point, the caudal side showed a more modest (~20-30%) decrease in miR-125b levels in axolotl, whereas the corresponding levels did not change dramatically in rat. By contrast, the levels of miR-125b in rat displayed marked decreases from day 1 to 7 on both sides of the injury, which coincided with the emergence of a glial scar (Fig. 2-1B). These data suggest that the earlier and more pronounced decrease in abundance of miR-125b in axolotl compared with rat could be an important and active regulatory process required for regeneration in this species, presumably by triggering the upregulation of one or more gene(s) targeted by miR-125b.

In vivo modulation of miR-125b levels in Axolotls

To test this hypothesis, we studied the effects of modulating miR-125b levels *in vivo* on spinal cord injury repair following complete transection in both axolotl and rat. For the axolotl studies, ablation injuries were performed and the levels of miR-125b were modulated by microinjection of a synthetic inhibitor: an RNA hairpin that binds owing to its complementary sequence to the mature miRNA, sequestering the miRNA and inhibiting the miRNA from functioning. To increase the levels of miR-125b, a commercially available chemically synthesized mature form of the miRNA (mimic) was injected after injury (Diaz Quiroz and Echeverri, 2012). We previously showed that this technique resulted in functionally relevant modulation of miRNA levels during regeneration in axolotls (Sehm et al., 2009). Modulators were microinjected among the glial cells within 500 μm rostral or caudal to the injury because in situ hybridization studies showed that these were the main cells expressing miR-125b (Fig. 2-1C). The optical transparency of the axolotl allows us to clearly identify where the lumen of the spinal cord is and to therefore specifically inject into the central canal or into groups of glial cells. Electroporation was used to aid uptake of the mimics or inhibitors (Diaz Quiroz and Echeverri, 2012). The efficiency of modulation of the levels of miR-125b was quantified by qRTPCR, and was effective for both mimic and inhibitor (Fig. 2-2E,F). The mimic induced increased levels of miR-125b, resulted in aberrant sprouting of the axons on both the rostral and caudal sides, and reduced the growth of axons through the lesion site by 7 days post-injury (Fig. 2-2B), at which time the control animals showed full regeneration (Fig. 2-2A). Histological examination of the underlying neural tube revealed that the reconnection process remained incomplete despite clear regrowth from both sides, and resulted in a failure to restore an open lumen, compared with control animals, which showed full reconnection (Fig. 2-2C,D). The aberrant axon sprouting was observed at exactly the point where the rostral and caudal sides of the neural tube failed to reconnect, consistent with the possibility that either the re-growing axons use the neural tube as a directional guide or that reconnection of the tube might require correctly oriented axons.

Microinjection of a miR-125b inhibitor in axolotl to reduce miR-125b to levels similar to those observed in rats resulted in strong inhibition of axonal regeneration (Fig. 2-3A,C) and a degeneration of axons caudal to the injury site (Fig. 2-3B,D). Regeneration of the neural tube was complete in this case, including full reconnection and restoration of the open lumen, although with a notable deposition of fibrin identified

by staining with acid fuchsin orange G (AFOG) (Fig. 2-3E,F). This result is reminiscent of the glial scar observed in non-regenerative organisms. These data indicate that precise control of miR-125b expression is required for correct regeneration of the axolotl spinal cord following complete-transection injuries. The phenotypic observations from the inhibition of miR-125b and from increasing the levels of mature miR-125b after spinal cord injury suggest that a precise regulation of that miRNA is necessary to achieve functional regeneration in axolotl.

Role of Semaphorin 4D in spinal cord injury

We used bioinformatics analyses to identify downstream proteincoding transcripts regulated by miR-125b. These studies identified the well-known class of Semaphorin genes, in particular Sema4D, as a predicted target of this miRNA. Sema4D has been described previously as a transmembrane axonal repulsion cue whose expression is upregulated in mice at the site of injury following spinal cord injury (Moreau-Fauvarque et al., 2003). In uninjured axolotl, Sema4D protein was not detectable by immunofluorescence in glial cells, whereas it was observed in rat GFAP+ astrocytes (Fig. 2-4A,B). To test whether this pathway is conserved in axolotl, we cloned the axolotl homolog of Sema4D and found that it contained an 8-mer seed sequence for miR-125b in its 3' UTR (Fig. 2-4C). We confirmed that the 3' UTR of axolotl and rat Sema4D could confer downregulation of a reporter luciferase gene expressed in cells in culture (Fig. 2-4D).

Sema4D expression in cells on the outside of the neural tube was transiently upregulated in axolotl at 3 days post-injury. This suggests a possible role in guidance of the re-growing axons through the lesion site (Fig. 2-3G). This role for Sema4D in axolotl, and its regulatory link to miR-125b, were both corroborated by results showing that inhibition of miR-125b causes upregulation of *Sema4D* in cells at the injury site (Fig. 2-3H; Fig. 2-5A), whereas decreased levels of *Sema4D* were observed in mimic treated animals (Fig. 2-5B). On the basis of these results, we hypothesize that the requirement for precisely controlled levels of miR-125b early during axolotl spinal cord regeneration underlies an equally precise and rapid increase in expression of *Sema4D* that is essential for faithful and functional regeneration. In support of this model, overexpression of either axolotl or human Sema4D in cells at the injury site was

sufficient to inhibit axonal regeneration in axolotl, and generates a similar phenotype as that resulting from treatment with the miR-125b inhibitor (Fig. 2-5A).

We investigated how these results might translate to the mammalian model by modulating the levels of miR-125b *in vitro* in rat primary neural cells. Initial cell-culture experiments showed that astrocytes had the highest levels of both miR-125b and Sema4D (Fig. 2-1D; Fig. 2-4B). *In vitro* assays confirmed that a reduction in miR-125b levels in astrocytes leads to an increase in Sema4D levels (Fig. 2-6B). We then examined the effects of decreased levels of Sema4D in astrocytes on the neuronal response to scratch-induced injury. When neurons were grown on astrocytes under normal *in vitro* conditions, the axons retracted and did not grow into the injury site (Fig. 2-7A,C). Depletion of Sema4D protein in astrocytes by RNAi created a more permissive environment, and the injured neurons projected axons into the scratched area (Fig. 2-7B,D). Using this cell-culture injury model, we observed that *in vitro* inhibition of miR-125b in astrocytes led to increased levels of Sema4D (Fig. 2-6A,B). These results confirm that this regulatory pathway is conserved in axolotl and rat.

In vivo modulation of miR-125b levels in rats

(Surgeries in rats, function recovery assays and immunohistological analysis were carried out by Matthew Coyle and Eve Tsai from the Ottawa Hospital research Institute, Canada)

We tested the effect of modulating the levels of miR-125b *in vivo* in rat following spinal cord injury. After spinal cord injury in rat, miR-125b levels were significantly decreased by 7 days post-injury and *Sema4D* levels increased (Fig. 2-8A). A synthetic mimic of the mature form of rat miR-125b, which is identical to human, mouse and axolotl miR-125b, was mixed into pluronic gel, an inert biodegradable gel that facilitates the localized delivery of siRNAs *in vivo* to the spinal cord (Cronin et al., 2006). The miR-125b in pluronic gel was injected into the lesion site immediately after injury. At 7 days post-injury, tissue samples showed a significant increase in miR-125b levels on the rostral site of the injury compared with that of control (Fig. 2-8B), and had decreased levels of *Sema4D* (Fig. 2-8C). These results support the proposed miR-125b–*Sema4D* regulatory pathway.

Animals were assessed weekly for detectable changes in locomotive abilities using the Basso, Beattie and Bresnahan (BBB) scoring method (Koopmans et al., 2005;

Martinez et al., 2009). These tests demonstrated significant improvements in the miR-125b-treated animals compared with controls. This included BBB scores ranging from 4-5 for the majority of miR-125b-mimic-treated animals. Some animals achieved scores of 6-8, accounting for the sizeable standard deviation from the mean at 4 weeks post-treatment, which represents remarkable recoveries from complete spinal cord transection (Fig. 2-9A). Effects on bladder control were also assessed; however, no significant differences were observed. At 8 weeks, the animals were euthanized and effects on glial-scar formation and axonal outgrowth were examined. Mimic-treated animals with BBB scores of 4-8 showed clear decreases in the levels of GFAP expression, and overall decreases in the size of the GFAP+ scar tissue (Fig. 2-8D; supplementary material Fig. S6). In the miR-125b-treated animals, the number and length of axons projecting into the scar tissue increased (Fig. 2-9B). However, *in vivo* antero- and retrograde tracing of axons in control- and mimic-treated animals showed no clear evidence of regeneration of long-tract axons in miR-125b-mimic-treated animals. This suggests that the axons in the injury site observed by histological staining are possibly regrowth of local interneurons.

Because miRNAs can target hundreds of genes, it is unlikely that the phenotypic effects resulting from the mimics are due to modulation of *Sema4D* alone. Therefore, microarrays were performed using RNA samples harvested one week post-treatment of control- and miR-125b-mimic-treated animals. The arrays revealed ~1500 genes that were differentially regulated in the mimic-treated animals; 53 of these were predicted to have seed sequences for miR-125b in the 3' UTR, and 23 of the 53 were significantly decreased on the rostral side of the injury (Table 2-1). Genes involved in glial-scar formation were affected, as observed in the significantly diminished levels of *GFAP*, *CSPG4* and *Col6A1* (Fig. 2-9C) in mimic-treated versus control samples. The arrays identified significantly higher levels of genes involved in microtubule stabilization, neurite outgrowth and axon guidance in mimic-treated rats (Fig. 2-9C). These data suggest that the mimic treatment improves the preservation of severed axons on the rostral side of the injury and promotes an environment that is more favorable to post-injury neurite outgrowth by inhibiting the expression of some glial-scar proteins (Fig. 2-9C; Fig. 2-10).

Discussion

This study shows that regulators of gene expression are conserved among vertebrates, but can exhibit very different responses to injury. miR-125b is expressed in similar cell types in axolotl and rat, but the expression levels are very different in uninjured and injured tissues. It is unknown what regulates the miRNA response after injury, and regulation might occur at many different levels because the response of cells to injury is extremely complex.

We used established methods for modulating gene expression levels *in vivo* in axolotl, and showed that inhibition of miR-125b leads to defective axonal regeneration due to upregulation of the axon-repulsion gene *Sema4D*. Maintaining high levels of miR-125b after injury also leads to defective axonal regeneration because the axons sprout randomly around the injury site and are not directed through the lesion site. Our data show that miR-125b and its target *Sema4D* need to be regulated in the right cells at the right time to guide axons through the lesion site (Fig. 2-11A,B). This suggests that miR-125b plays a role in fine-tuning gene expression during regeneration (Fig. 2-11B). We do not rule out that miR-125b could target other genes that might be involved in the glial-scar response. The inhibitor-treated cells did show an increase in fibrin deposition, which is indicative of scarring. In previous studies we also used transcriptional profiling to identify miRNAs involved in the early stages of tail regeneration; interestingly, in that study, increased levels of miR-125b were seen at 3 days post-amputation (Sehm et al., 2009). This could suggest that miR-125b plays a different role depending on the regeneration paradigm and will be interesting to determine in the future.

We then examined the role of miR-125b in rat. The initial comparative array analysis showed that miR-125b is expressed at ~eightfold lower levels in rat than in axolotl. After injury, only a slight decrease in miR-125b was initially observed, but its levels were significantly reduced at 7 days post-injury, when the predicted target gene, *Sema4D* levels are increased. *In vitro* analysis in primary astrocytes showed that inhibition of miR-125b leads to increased levels of the Sema4D protein, and reduction of Sema4D by RNAi creates a more permissive environment for neural outgrowth after scratch-induced injury (Fig. 2-7). These data gave us a rationale to modulate miR-125b levels *in vivo* in rat after spinal cord injury. This was achieved by mixing the chemically synthesized mature form of the miRNA into a biodegradable gel and directly injecting it

into the injury site. Previous work showed that cells internalize the gel via endocytosis, and thereby take up the gel contents. This strategy worked for performing RNAi *in vivo* (Cronin et al., 2008; Cronin et al., 2006) and for delivery of the miRNA in the current study. The qRT-PCR analysis showed that the method was successful for delivering the mimic, resulting in a decrease in the predicted target gene on the rostral side of the injury, but no effect was observed on the caudal side of the injury. This might be because the gel was not taken up by those cells, or because it was displaced from that area, or because, by the time of analysis, those cells might have died. Despite this, we observed a clear improvement in the locomotive abilities of the mimic-treated animals compared with that in control treated animals after complete transection. Histological analysis showed a decrease in GFAP expression in the scar area and an increase in axons growing into the scar tissue, which suggests a more regeneration-permissive environment. Although anterograde and retrograde tracing of axons was attempted, the results were inconclusive owing to the high background in the samples in the scar-tissue area. This leaves an open question as to whether the improved locomotive ability is due to regeneration of long-tract cortical axons, prevention of dieback of the severed axons, or to a more local regeneration of inter-neurons. Behavioral analyses conducted in *Sema4D*-knockout mice showed increased motor activity when subjected to the open-field locomotive test compared with that of control mice, suggesting that a lack of *Sema4D* might promote more neurogenesis (Yukawa et al., 2009). This observation in the knockout mice corresponds with the locomotive recovery observed in the miR-125b-treated rats.

The array analysis of the animals shows that a single dose of miR-125b targets multiple pathways that improve functional recovery after complete transection of the spinal cord. In the future it will be interesting to follow up on the role of several of these target genes; for example, *SLC16A6*, which encodes a monocarboxylate transporter, is a predicted target of miR-125b and its expression levels were significantly decreased in miR-125b-mimic-treated rats after injury. Previous work in Xenopus limb and tail regeneration has linked other monocarboxylate transporters, such as *SLC5A8*, to regeneration-induced epigenetic modifications. It will be interesting to determine whether modification of these transporters can play a similar role in spinal cord injury repair in mammals (Tseng et al., 2010; Tseng and Levin, 2012). This result opens many new avenues for locally targeted treatment of spinal cord injury using a method that does not

cross the blood-brain boundary. In the future, it will be essential to test whether multiple treatments with miRNA alone increase the functional recovery, or whether combinations of modulators of miRNAs are more effective.

Our data define the first miRNA-regulated pathway involved in axolotl spinal cord injury repair, and elucidate key functional components of this pathway. This comparative study offers the first substantial translation of new molecular insights aimed at defining a new biological understanding of major mammalian pathways and new avenues for the development of innovative treatments for human spinal cord injuries.

Figures

Figure 2-1. Conserved miRNAs are differentially expressed in rat versus axolotl after spinal cord injury.

(A) Heat map shows differentially expressed miRNAs at 1 and 7 days after injury, compared with those in uninjured samples. Only miRs with a P>0.01 were considered. (B) Quantitative RT-PCR confirms that miR-125b has ~eightfold higher expression in axolotl than in rat in uninjured tissue. It is significantly less abundant in axolotl at 1 day post-injury compared with controls (P<0.001), and shows the greatest reduction in levels at 7 days post-injury in rat (P<0.001). (C) In situ hybridization localizes miR-125b to radial glial cells in the axolotl spinal cord, as indicated by the arrows. (D) Quantitative RT-PCR of miR-125b from individual cultures of primary rat neural cells. OPCs, oligodendrocyte precursor cells. *P<0.05, **P<0.01 and ***P<0.001.

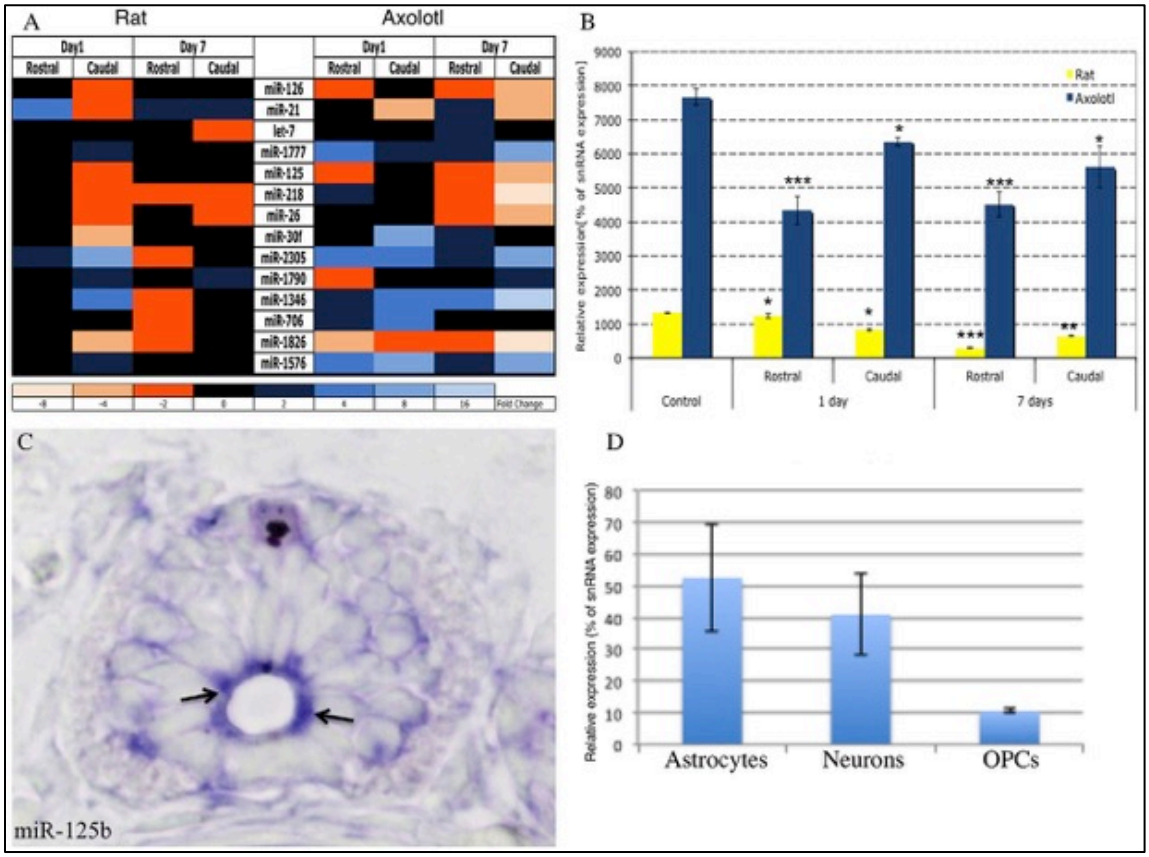

Figure 2-2. Increased levels of miR-125b in vivo in axolotl after injury leads to defects in regeneration.

(A,B) Whole-mount anti-β-IIItubulin staining in control axolotls (A, n=42) versus miR-125b-mimic-injected axolotls (B, n=40). Injected axolotls show defects in the regrowth of axons through the lesion site (asterisk); axons appear to sprout in random directions (arrows) but do not grow through the lesion site. (C,D) Longitudinal sections through spinal cord stained with AFOG show a failure of the lumen to reconnect in miR-125b-mimictreated animals (D, n=16) versus controls (C, n=20), in which full reconnection of the lumen occurs by 7 days post-injury (arrows). (E,F) Quantitative RT-PCR shows how levels of miR-125b are significantly altered after injection of the mature miR-125b mimic (***P<0.001) (E) or after injecting an inhibitor of miR-125b (**P<0.01) (F). Scale bar: 100 μm.

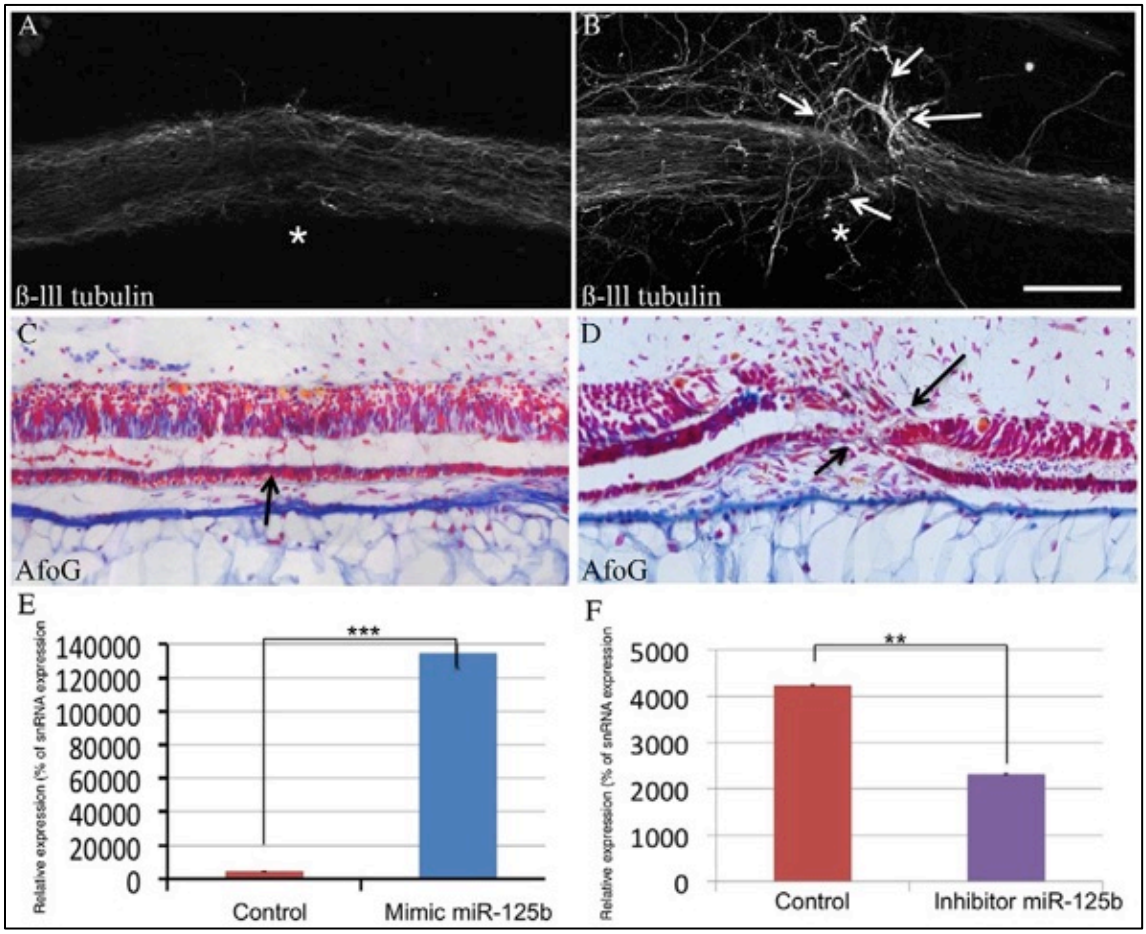

Figure 2-3. Inhibition of miR-125b in axolotl after injury causes defects in regeneration.
(A-D) Whole-mount anti-β-III-tubulin staining of control (A,B) (n=48) and miR-125b-inhibitor-treated (C,D) (n=51) axolotls. Upon inhibitor treatment, axons fail to cross the injury site (yellow box and arrow in C), and degeneration of dorsal-root ganglion axons is observed on the caudal side of the injury (arrows D), whereas this is never observed in controls (A,B). Yellow box marks the injury site. Arrows in B indicate normal dorsal-root ganglion cell bodies and axons. (E,F) AFOG histological staining of sections. In control-injected animals, rostral and caudal sides of the neural tube are reconnected (arrow, E) (n=10). In miR-125b-inhibitor-injected animals, fibrin deposition, an indicator of scar tissue, is observed in the neural tube (arrows and asterisk in F) (n=15). (G,H) Sema4D, a predicted target gene of miR-125b, is normally found in cells on the outside of the neural tube during axonal regeneration (G) (n=12); by contrast, in animals treated with miR-125b inhibitor, Sema4D protein is found in many more cells throughout the injury site (H) (n=15). Green: anti-β-IIItubulin; red: anti-Sema4D; blue: DAPI.

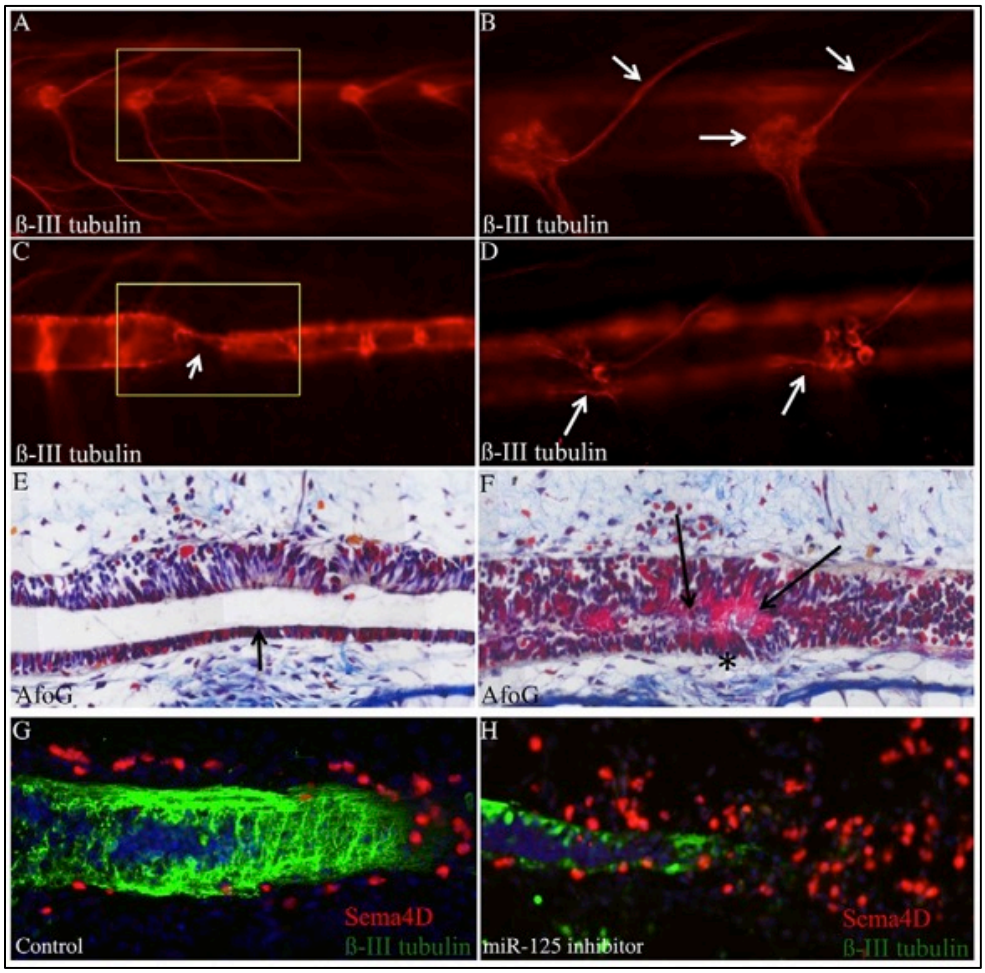

Figure 2-4. Sema4D regulation by miR-125b is conserved between axolotl and rat.

(A) No Sema4D protein is detected by immunofluorescence in the uninjured axolotl spinal cord. (B) In uninjured rat spinal cord, Sema4D protein is detected in GFAP- positive cells. (C) The seed sequence for miR-125b is highly conserved among species, and is identical in rat and axolotl. (D) Luciferase assay shows functional targeting of miR-125b to the 3'UTR of rat and axolotl Sema4D ($P<0.05$).

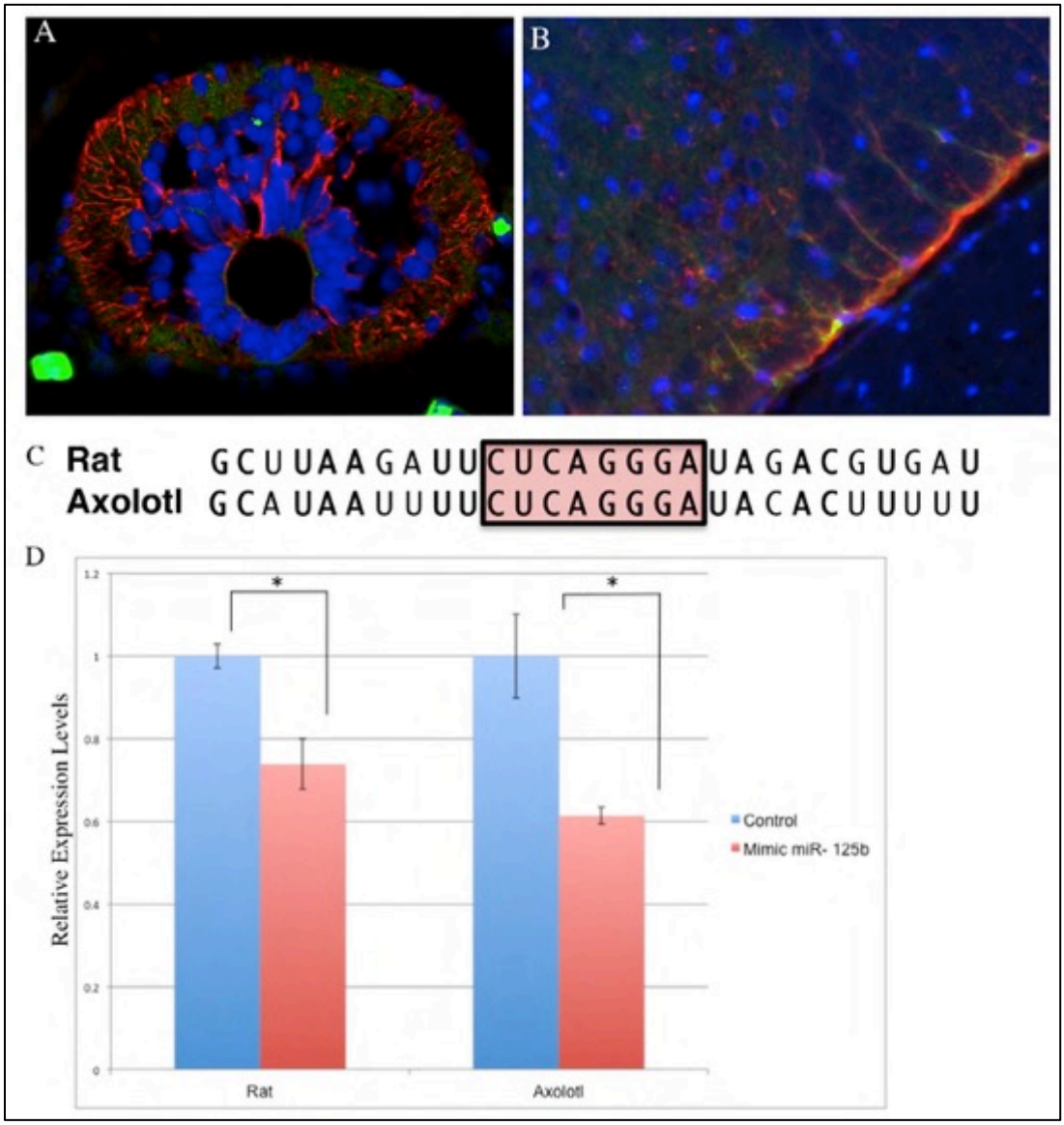

Figure 2-5. Sema4D overexpression inhibits axonal regeneration after injury in the axolotl. (A) Wholemount anti-β-III staining on axons 7 days post injury in animals injected with a plasmid driving expression ofSema4D in cells at the injury site in axolotl after injury suffices to inhibit axonal regeneration. (B) Quantitative RT-PCR of Sema4D levels in axolotl after treatment with miR-125b mimic or inhibitor. In mimic-treated animals, Sema4D levels decrease ($P<0.01$); inmiR-125b inhibitor-treated animals, the levels of Sema4D increase ($P<0.001$).

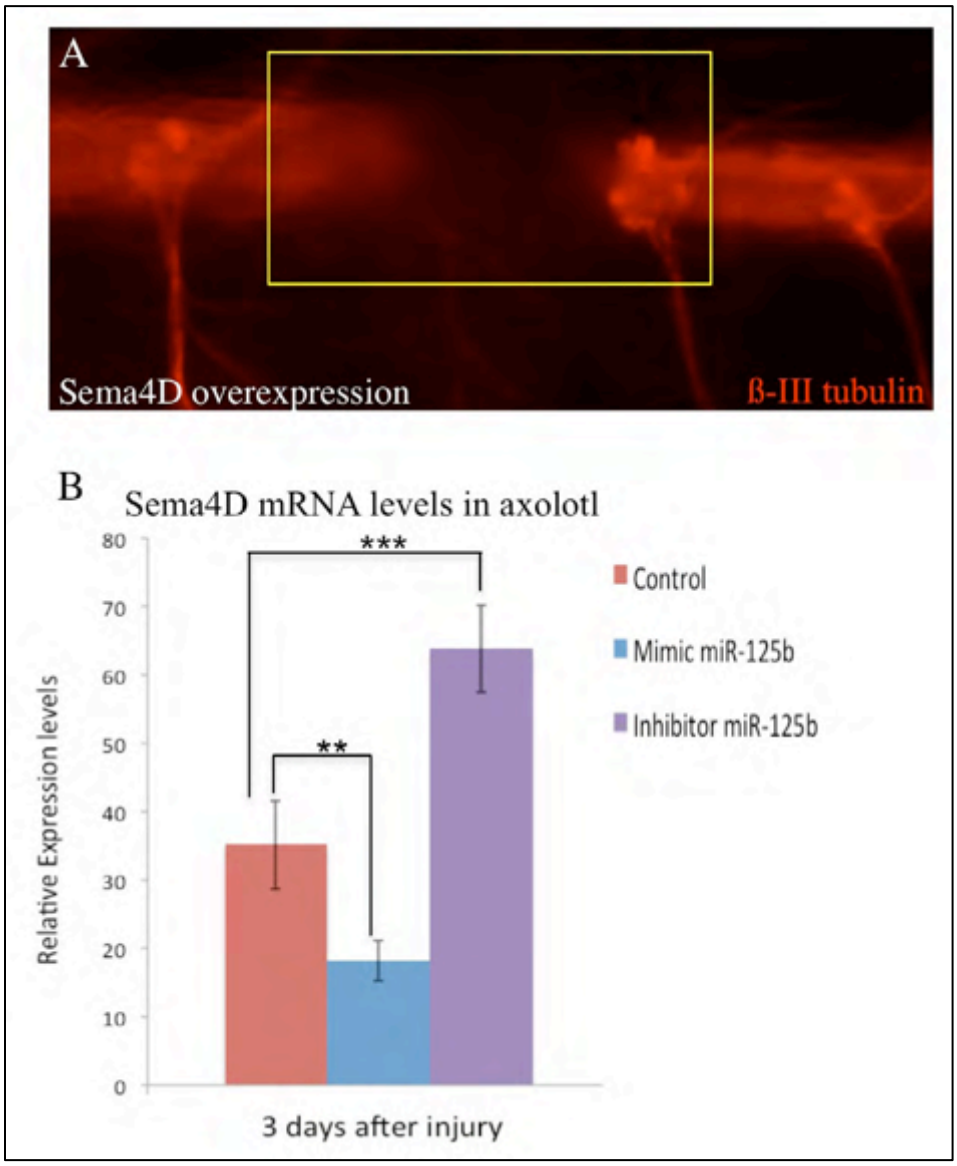

Figure 2-6. miR-125b inhibition induces Sema4D expression *in vitro*.

(A) Quantitative RT-PCR of miR-125b in primary astrocytes after treatment with miR-125b inhibitor. (B) Sema4D levels increase in miR-125b inhibitor-treated astrocytes, P<0.01.

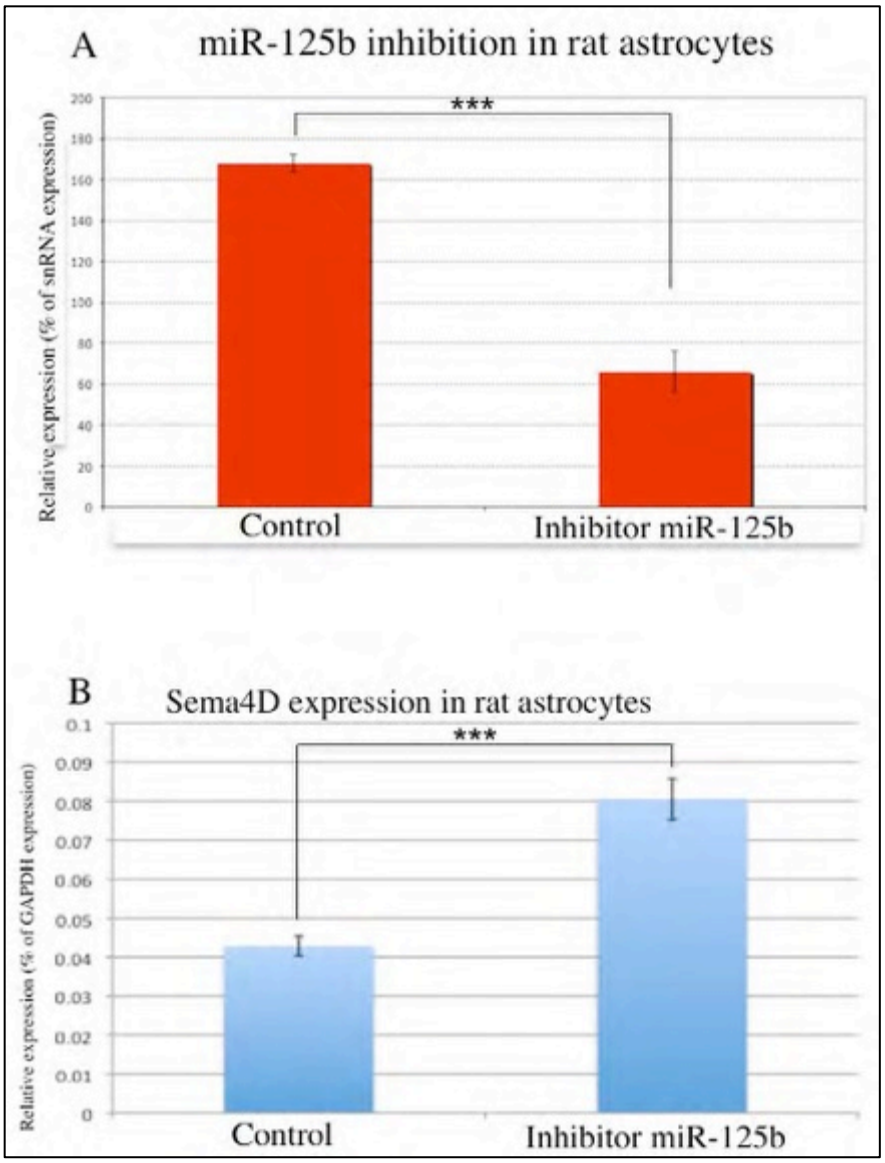

Fig 2-7. Sem4D downregulation promotes axonal growth *in vitro*.

Co-culture assay of primary rat astrocytes and neurons, neurons are stained with anti-β-III tubulin (A,B). In control samples after a scratch assay is performed neurons fail to regrow axons into the injury area (A). Levels of Sema4D are decreased in astrocytes using siRNA-mediated silencing, which creates a more permissive environment for neurons to extend axons into the injury site after a scratch assay (B). (C,D) Quantitation of the angle of projection of axons after injury in control versus Sema4D siRNA conditions. The angle distribution was plotted using the Rosetta histogram tool from Matlab, and the statistical significance of the data was analyzed using a one-way Anova ($P < 0.001$).

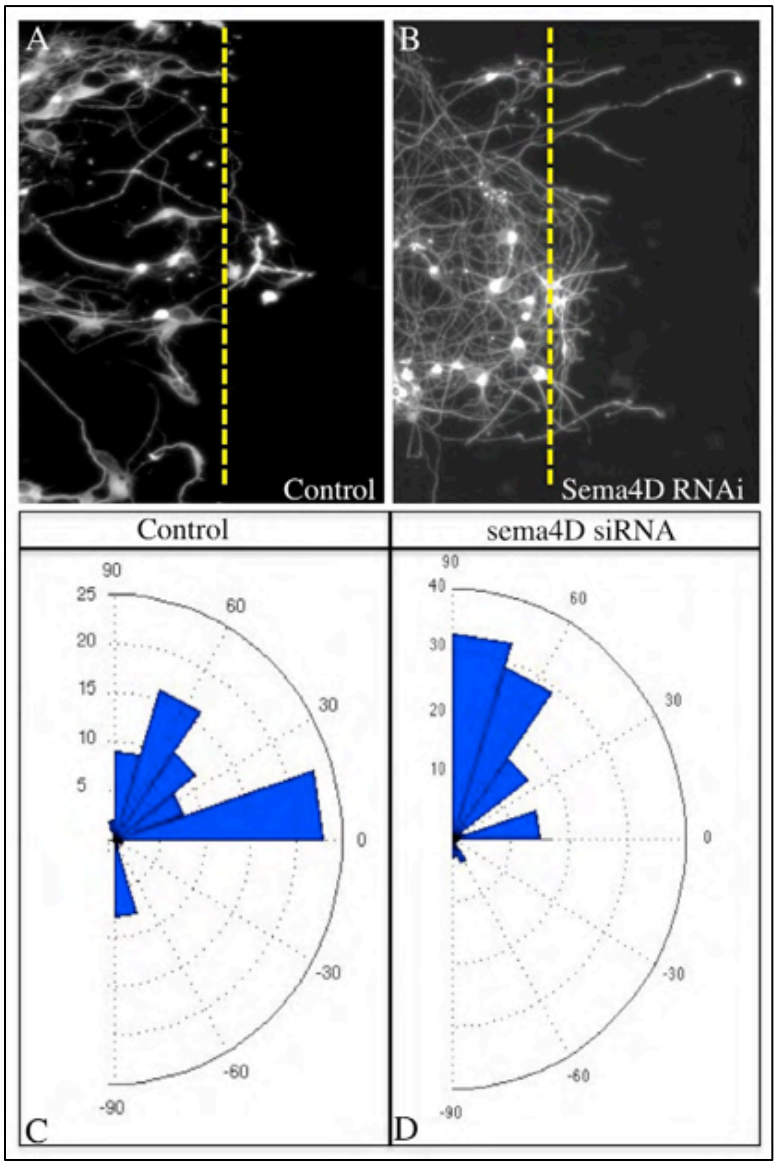

Figure 2.8 Mimic treatments to increase miR-125b levels in vivo following spinal cord injury in rat lead to decreased levels of the target gene Sema4D.

(A) Untreated animals show a decrease in abundance of miR-125b (blue bars) in vivo by 7 days post-injury, whereas endogenous levels of Sema4D (green bars) are increased by 7 days post-injection. (B,C) Local post-injury treatment with a synthetic mimic of miR-125b leads to a significant increase in miR-125b on the rostral side of the injury (B), whereas reduced levels of Sema4D are observed (C). (D) Post-injury modulation of miR-125b causes a significant decrease in the size of the GFAP-positive glial scar tissue. *P<0.05, **P<0.01 and ***P<0.001.

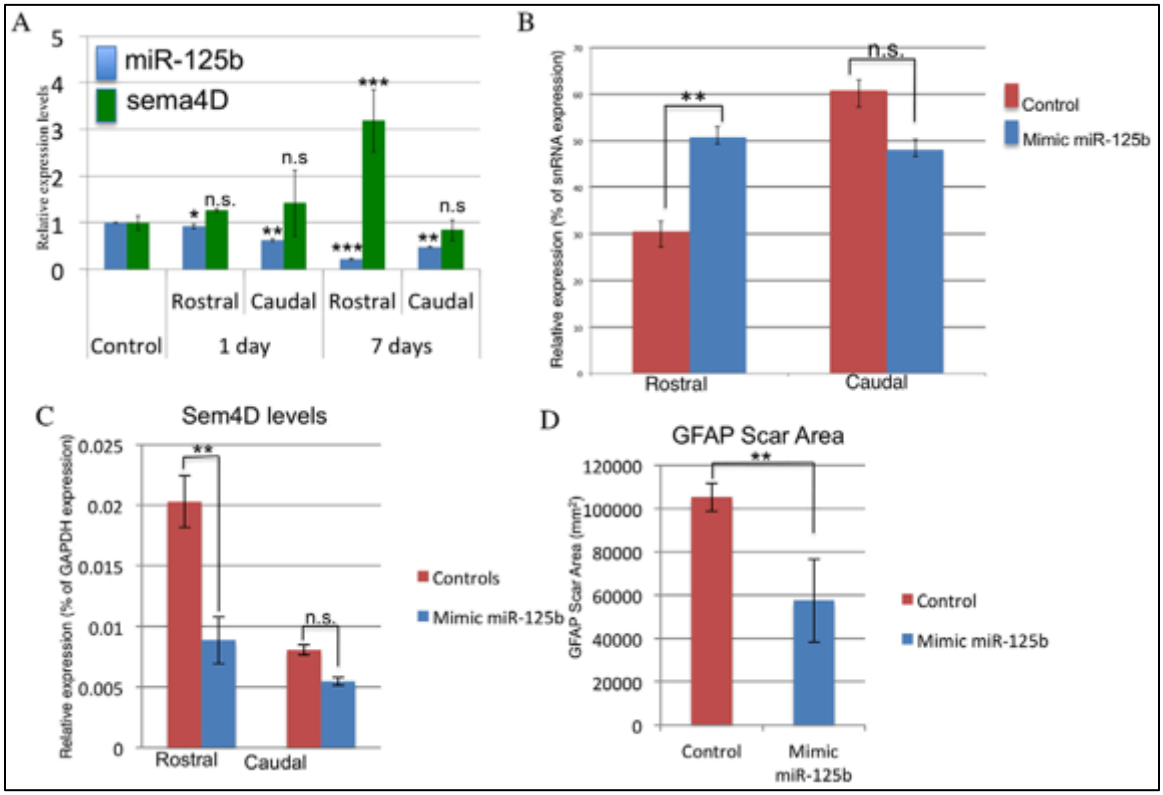

Figure 2-9. Mimic treatment to increase miR-125b levels in vivo in rat following complete spinal cord transection improves functional recovery.

(A) Results from open-field locomotion experiments (cohort size of n=13) revealed significant improvements in BBB scores, ranging up to 8, in animals treated with the miR-125b mimic (***P<0.001). (B) Axons grew further into the scar tissue area in miR-125b-mimic-treated animals compared with controls (**P<0.01). (C) Array analysis of miR-125b-mimictreated animals showed that glial-scar genes, neurogenesis genes and axon protective genes displayed the most notable differential regulation after treatment. Blue text indicates genes that were upregulated in miR-125b-mimictreated rats; yellow text indicates genes that were downregulated in miR-125b mimic-treated rats.

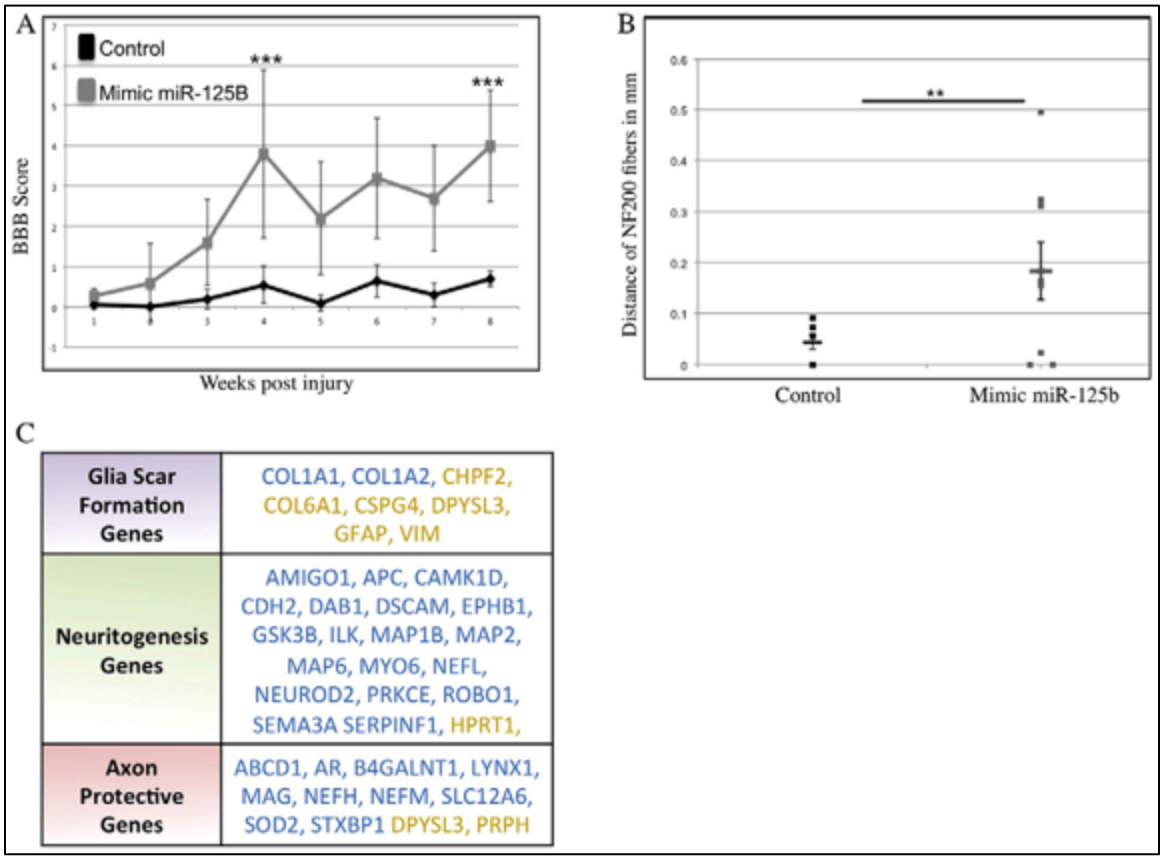

Glia Scar Formation Genes	COL1A1, COL1A2, CHPF2, COL6A1, CSPG4, DPYSL3, GFAP, VIM
Neuritogenesis Genes	AMIGO1, APC, CAMK1D, CDH2, DAB1, DSCAM, EPHB1, GSK3B, ILK, MAP1B, MAP2, MAP6, MYO6, NEFL, NEUROD2, PRKCE, ROBO1, SEMA3A SERPINF1, HPRT1,
Axon Protective Genes	ABCD1, AR, B4GALNT1, LYNX1, MAG, NEFH, NEFM, SLC12A6, SOD2, STXBP1 DPYSL3, PRPH

Figure 2-10. Model of how miR-125b promotes a regeneration-permissive environment in rat.

Array analysis identified differential regulation of multiple targets of miR-125b in the mimic-treated rat samples. The phenotype observed is due to modulation of several pathways, possibly due to reducing production of several glial-scar genes, creating a less hostile tissue for axons to regrow on. Significant regulation of genes involved in stabilizing microtubules was also observed, suggesting that more axons might be preserved at the injury site in miR-125b-treated animals.

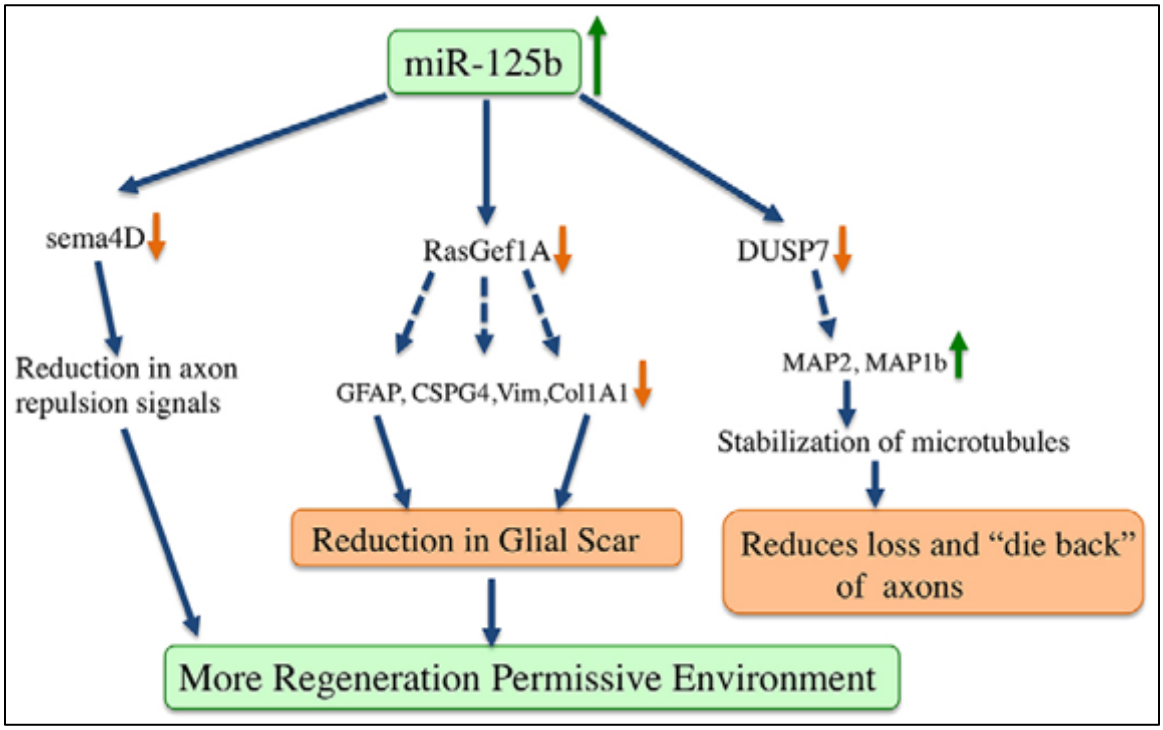

Figure 2-11. Model of miR-125b and Sema4D regulation of axonal regeneration in axolotl after injury.

(A) Schematic diagram of the axolotl spinal cord undergoing regeneration. Peach ovals represent the radial glial cell, red lines are the axons and the green circles represent cells that express Sema4D protein after injury. miR-125b levels are reduced after injury, whereas Sema4D is more abundant in a discrete set of cells (green circles) and functions to repel axons (red lines) and thereby guide them to grow through the lesion site (green dots) along the ependymal tube formed by radial glial cells (peach ovals). (B) The in vivo axolotl experiments show that, if miR-125b levels are too high or too low, it leads to defective axonal regeneration. This suggests that a balance of miRNA and target gene expression is necessary for perfect regeneration.

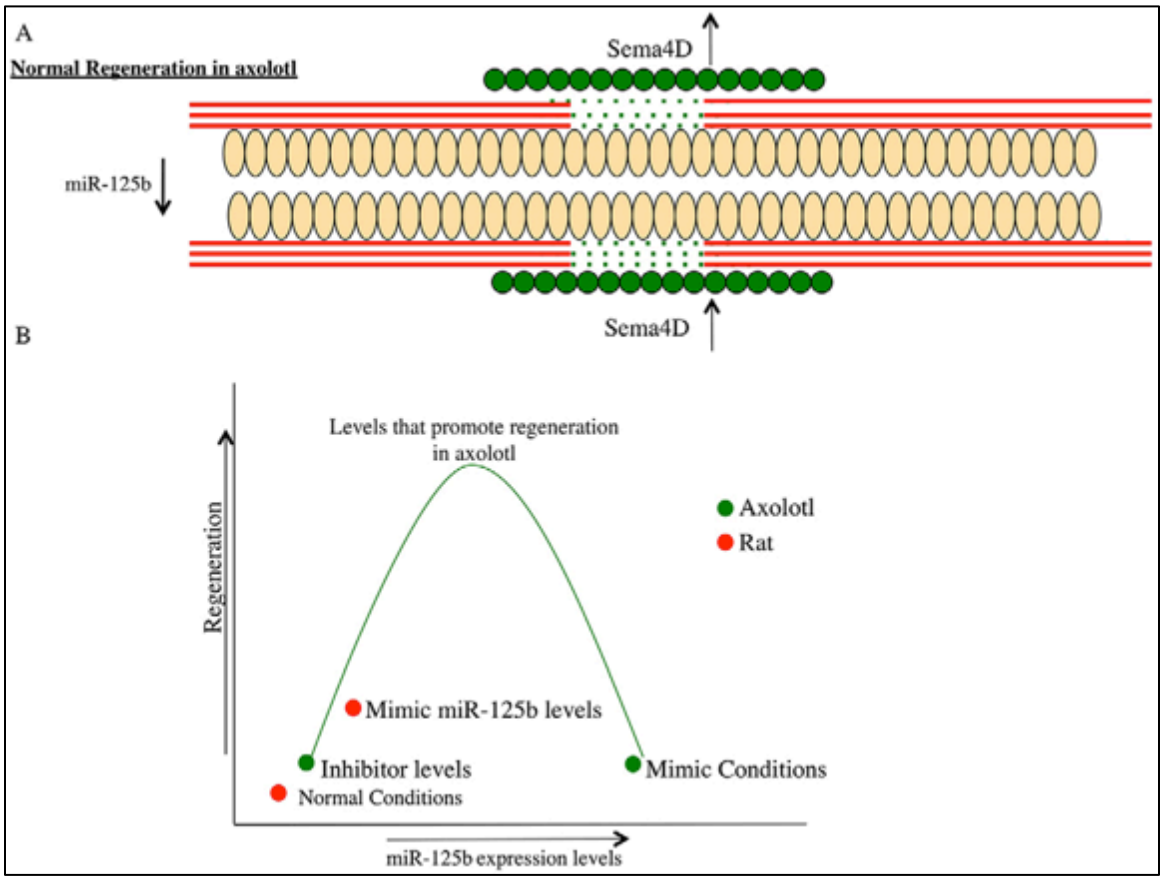

Tables

Table 2-1. Downregulated genes that contain seed sequences for miR-125b in their 3'UTR from the array on mimic-treated rats.

Gene	Location	Family
ADAMTS4	Extracellular Space	Peptidase
ATOH8	Unknown	Other
AZI2	Cytoplasm	Other
BRCC3	Nucleus	Enzyme
DUSP7	Cytoplasm	Phosphatase
EDC3 (includes EG:315708)	Cytoplasm	Other
ESRRA	Nucleus	Ligand-dependent nuclear receptor
HOXD9	Nucleus	Transcription regulator
LETM1	Cytoplasm	Other
LRPAP1	Plasma Membrane	Transmembrane receptor
MGAT4A	Cytoplasm	Enzyme
PPP2R1B	Unknown	Phosphatase
PROS1	Extracellular Space	Other
RALGPS2	Unknown	Other
RASGEF1A	Unknown	Other
SBNO1	Unknown	Enzyme
SESTD1	Extracellular Space	Other
SLC16A6	Plasma Membrane	Transporter
SLC44A2	Extracellular Space	Transporter
SNX33	Cytoplasm	Other
TBX4	Nucleus	Transcription regulator
TSPAN8	Plasma Membrane	Other
USP46	Unknown	Peptidase

Chapter 3: Biomechanical regulation of miR-125b expression in response to spinal cord injury

Summary

Spinal cord regeneration in salamanders has been studied as early as 1965. Since then, some information has been gained about the cellular and molecular mechanisms that govern spinal cord regeneration in salamanders. However still little is known about the cues that trigger the regenerative programs after SCI. Knowing that miR-125b plays a major role in spinal cord repair after injury, we decided to investigate the early cues that trigger changes in the expression of this miRNA in response to injury. *In vivo* experiments with drugs that affect actin and microtubule cytoskeleton suggest that the depolymerization of the actin cytoskeleton after injury induces changes in the expression of miR-125b.

To better understand how miR-125b expression could be regulated, we performed bioinformatic analyses of the regulatory region of miR-125b. These analyses indicated that the expression of this microRNA could be under the regulation of the transcription factor c-Fos. *In vivo* injury experiments showed that c-Fos is activated in response to injury in the spinal cord.

The overall data suggest that in response to injury, actin cytoskeleton depolymerization triggers changes in the expression of miR-125b through the RhoA/c-Fos pathway.

Introduction

Since they were first described in the early 1990s, microRNAs have emerged as important regulators of posttranscriptional gene expression. A great deal of knowledge has been gain in understanding the mechanisms of gene regulation by microRNAs and their biosynthesis (Ambros, 2004; Filipowicz et al., 2008; He and Hannon, 2004; Winter et al., 2009). However little is known about the mechanisms that regulate miRNA transcription itself (Krol et al., 2010). Studies using a combination of bioinformatics, genome wide ChiP-seq and ChIP-ChiP data have identify conserved transcription factors (Pou5f1, Sox2, Nanog, Tcf3 and FoxA1 e.g.) that could modulate miRNA expression, mainly in human skeletal muscle and embryonic stem cells (Schanen and Li, 2011; Xiao et al., 2013). In particular, cMyc has been found to be a main regulator of microRNA expression in breast (Mouw et al., 2014) lymphoma (Chang et al., 2007) cancer. However, the regulation of miRNA expression in other biological processes such as injury is still unknown.

Many regulatory pathways of gene expression are activated in response to traumatic spinal cord injury. For example, it has been shown that Wnt signaling is activated after injury in rats (Miyashita et al., 2009) while FGF is activated in radio glial cells response to spinal cord injury in newts (Zhang et al., 2000). However it is unknown how these pathways are activated. The disruption of the cell membrane induces important chemical and physical changes in the cell such a change in the membrane potential (Adams et al., 2007), increase in the concentration of intracellular calcium and depolymerization of the actin and microtubule cytoskeleton(Bradke et al., 2012). These physicochemical changes could be the early cues that induce the activation of regulatory gene pathways. For example, spinal cord injury induces strong activation of the Rho signaling pathway in glial cells and neurons as early as 1.5 hrs after injury (Dubreuil et al., 2003). Due to its known role in regulating actin and microtubule dynamics(Etienne-Manneville, 2004), activation of Rho signaling after spinal cord injury could be responding to the early changes in the cell cytoskeleton. Many studies have shown that modulation of Rho signaling seems to promote axonal growth after spinal cord injury (Boomkamp et al., 2012; Dergham et al., 2002; Dubreuil et al., 2003); therefore it is important to understand how early physicochemical cues activate regulatory pathways

that can lead to creating a permissive or a non-permissive environment for spinal cord repair after injury.

These studies showed that Rho activation is caused by the presence of inhibitory molecules such as Chondroitin Sulfate Proteoglycans (Forgione and Fehlings, 2013) Myelin Associated Glycoprotein, myelin (Dergham et al., 2002) and Nogo (Madura et al., 2004) after spinal cord injury. Since the presence of these molecules is detected 1 day after injury (Dubreuil et al., 2003) and some of them, such as CSPG peak one week later when macrophages and oligodendroyte precursor cells infiltrate the injury (Jones et al., 2002), the early activation of Rho signaling at 1.5 hrs after injury observed in rats (Dubreuil et al., 2003) suggests that earlier events could also trigger Rho activation. Moreover, for Rho to respond to these inhibitory molecules it is necessary the establishment of a newly formed growth cone with a full operational actin and microtubule cytoskeleton that are dependent on Rho activation (Bradke et al., 2012). Therefore Rho is likely to be activated by mechanical signals rather than chemical ones at early time points. Though our understanding of how chemical cues regulate gene expression, in the context of spinal cord injury it is likely that mechanical cues could play as an important role, especially at early time points.

Biomechanical regulation of gene expression has been shown to play an important role in different cellular processes including stem cell differentiation (Costa et al., 2012; Spiering and Hodgson, 2011), cell proliferation (Provenzano and Keely, 2011) and cell migration (Ng et al., 2012). Interestingly, it has been suggested that in malignant mammary epithelial cells Myc can regulate the expression of miR-18 in response to mechanical cues such as the stiffness of the extracellular environment (Mouw et al., 2014). Since spinal cord injury is caused by a mechanical stress, we decided to study whether biomechanical cues activated in response to spinal cord injury in axolotls could regulate the expression of miR-125b to create a permissive environment for regeneration.

Results

Actin dynamics affect miR-125b expression in the spinal cord of axolotl

From our microarray analysis we know that miR-125b expression decreases 1 day after injury on both the caudal and the rostral side of the injury in axolotls. We also know that the expression levels of the microRNA are sustained seven days after injury (Fig. 2-1) and, that such changes create a permissive environment for regeneration. We were interested to know what triggers the change in miR-125b expression. To answer this question, we decided to look at the role of early mechanical cues such as microtubule and actin cytoskeleton depolymerization in regulating miR-125b expression after injury.

To study the role of the actin cytoskeleton depolymerization after injury, we decided to inject axolotls in the presence and in the absence of injury with cytochalasin D (Cyto D) a drug known to depolymerize actin filaments. Treatment with Cyto D in the absence of injury induced changes in miR-125b expression levels that mimics the changes observed after injury (Fig. 3-1A). When animals where injured after treatment with Cyto D there was not a further decreased in the expression levels of miR-125b, suggesting that chances in miR-125b after injury are mainly dependent on actin depolymerization. To confirm that the changes in miR-125b levels were due to changes in transcription and not mature miRNA stability, we also look at the levels of the precursor microRNA (pre-miR-125b, Fig. 3-1B). As observed for the mature miR-125b, after injury and treatment with Cyto D the levels of miR-125b decreased, indicating that injury and actin depolymerization induce changes in the transcription of miR-125b.

Since depolymerization of actin filaments caused changes in miR-125b, we wanted to know what if actin filaments stabilization after injury could affect miR-125b expression. When animals were injected with Jasplakinoline (Jasp) in the absence or the presence of injury, the levels of miR-125b increased, opposite to the effect caused by injury (Fig. 3-1C). This suggests that stabilization of actin filaments with Jasp prevents changes in the miR-125b levels. When we looked at pre-miR-125b we observed that treatment with Jasp decreased the levels of miR-125b in comparison to uninjured animals (Fig. 3-1D). These results suggest that rather than actin depolymerization, changes in actin dynamics influence miR-125b. The results also suggest that Jasp might

stabilize the mature form of miR-125b, therefor the levels of miR-125b did not decreased after injury.

Since microtubule depolymerization is another early mechanical cue in response to injury, we decided to also look whether changes in microtubule cytoskeleton could modulate miR-125b expression. We used Nocodazole to induce microtubule cytoskeleton depolymerization, and Taxol to induce its stabilization. None of the drug treatments induced changes in the expression levels of the mature microRNA in the absence of injury (Fig. 3-1E), suggesting that changes in miR-125b expression in response to injury are independent of microtubule dynamics. However the expression levels of miR-125b remained unchanged when animals were injured after treatment with Nocodazole or Taxol, suggesting that dynamic microtubules are needed for the proper change in miR-125b expression after injury. The expression levels of the pre-miRNA were equal to what was observed for the mature miRNA (Fig. 3-1F) suggesting that unlike what treatments with Nocodazole and Taxol can influence miR-125b rather than its stability, as observed for animals treated with Jasp. The fact that treatment with Taxol and Nocodazole did not induce changes in miR-125b transcription even after injury, confirms the need of dynamic microtubules to induce changes in miR-125b transcription in response to injury due to depolymerization in actin cytoskeleton.

To confirm that the changes in miR-125b expression observed were not due to off-target effect of the different drugs used, we quantified the expression levels of another microRNA that we know is expressed in the axolotl but it expression did not showed significant changes after injury in our microRNA array analysis (Fig. 2-1A). As expected, after injury the expression levels of miR-29 did not change significantly in comparison to uninjured conditions. Treatment with Cyto D, Jasp, Nocodazole or Taxol in the absence of injury did not induced significant changes in miR-29 expression either (Fig. 3-1G-J) suggesting that the changes observed for miR-125b were a specific response to injury or actin cytoskeleton depolymerization. Interestingly injury after treatment with Jasp or Taxol did induced changes in the levels of the mature miR-29. These results suggest that the dynamic state of the actin or microtubule cytoskeleton can alter the normal response to external stimuli such as injury.

Injury induces changes in actin cytoskeleton in axolotls

To confirm that injury induced changes in actin cytoskeleton, we collected tissue samples from injured animals and stained them with rhodamine tagged phalloidin, a mycotic toxin that binds specifically actin filaments. We collected tissue samples 1 min, 10 min, 30 min, 1 hour and 4 hours after spinal cord injury. At 1 min (Fig. 3-2B) and 10 hours (Fig. 3-2C) post injury, phalloidin staining on the apical surface of the glial cells was reduced in comparison to uninjured controls (Fig. 3-2A). After 30 min (Fig. 3-2D) phalloidin staining was visible again at the apical cortex of ependymal cells. Phalloidin staining was then sustained 1 hour (Fig. 3-2E) and 4 hours (Fig. 3-2F). These results suggest that changes in actin cytoskeleton in response to injury it's a rather fast process that occurs at early time points after the mechanical insult.

We also performed phalloidin staining in animals treated with Cyto D and Jasp to confirm the effectiveness of these drugs in the axolotl spinal cord. As expected, treatment with Cyto D (Fig. 3-3B) reduced phalloidin stain, both in the apical surface and the projections of the radio glial cells towards the basal membrane of the spinal cord (endfeet processes), in comparison to uninjured tissue (Fig. 3-3A). In contrast treatment with Jasp did not affected actin filaments localization at apical surface or the endfeet processes (Fig. 3-3C) in comparison to untreated animals.

Due to the necessity of dynamic microtubule cytoskeleton to induce a proper change in miR-125b expression in response to actin depolymerization after injury, we decided to look at phalloidin stain after treatment with Nocodazole and Taxol. Treatment with Nocodazole (Fig. 3-3D) did not seem to affect actin at the apical surface or endfeet processes of radio glial cells. Treatment with Taxol didn't seem to affect apical actin either, however phalloidin stain decreased at the endfeet processes (Fig. 3-3F). These results are in agreement to previous reports that suggest that actin and microtubule cytoskeleton regulate each other (Rodriguez et al., 2003). As result of this cross talk, microtubule depolymerization induces actin filament stabilization, suggesting that microtubule stabilization could induce actin depolymerization as observed for the animals treated with Taxol. To confirm the effect of the drugs on microtubule cytoskeleton we stained tissue sections against alpha tubulin. Treatment with Nocodazole clearly induced depolymerization of microtubules at both the apical surface and the endfeet (Fig. 3-3G) processes while treatment Taxol did not affected microtubule cytoskeleton (Fig. 3-3H) in comparison to untreated animals (Fig. 3-3F).

To have a better understanding of actin dynamics after injury we injected the animals with a construct that expresses a mCherry-tagged peptide (lifeact) that bind specifically to actin filaments and does not interferes with actin cytoskeleton physiology (Riedl et al., 2008). Taking advantage of the fact that axolotls are optically clear we tried to do *in vivo* imaging using an epifluorescence microscope. Images taken of uninjured animals showed that the construct worked and we could observe mainly cortical actin delimiting the cell shape (Fig. 3-4A, B). Differential interference contrast (DIC) images showed that the expression of lifeact was specific in the spinal cord (Fig. 3-4A', B'). After injury it was difficult to get the same cellular resolution obtained before (Fig.3-4C). Though changes in fluorescence could be measured over time (Fig. 3-4D), due to the low resolution it was not possible to tell if those changes were caused by changes in actin dynamics or artifacts of the imaging process.

To improve the resolution we tried to do the *in vivo* imaging using a 2-photon microscope. With the 2-photon microscope we were able to obtain images with cellular resolution (Fig. 3-5A-A''). A technical disadvantage of this set up is that it does not allow taking DIC images; therefore it is not possible to determine that lifeact expression is restricted to the spinal cord. Nonetheless the cell morphology greatly resembles neurons; therefore we can assume that we were at the spinal cord. Unlike using the epifluorescence scope, the resolution was not lost after injury (Fig. 3-5B). Time-lapse images show how injury induced changes in the cortical actin of the indicated cells (Fig. 3-5C). Quantification of the fluorescence showed that in both cells that for both cells the fluorescence intensity diminished over time, until the cells were no longer visible 13 and 17 min after starting the time lapse. This suggests that actin is being constantly depolymerizing in response to injury. However the decline in fluorescence could be due to the cells dying. The increase in auto-fluorescent background noise (Fig 3-5C) over time is an indication of tissue damage that could be inflicted by the imaging process. Also, the process of setting up the samples before and after injury was time consuming, depending on the sample it could take over an hour. Such time delay could have induce further stress in the animals and we were possibly missing the early changes in actin dynamics.

We then decided to test whether the use of organotypic cultures of spinal cords of axolotls expressing lifeact could be use as a model to study in actin cytoskeleton after injury. Using a vibratome, 50 μm sections were obtained (Fig. 3-6) from tail samples

embedded in low melting point agarose. Using an epifluorescence scope it was easy to detect in the sections radial glial cells expressing the lifeact construct in the spinal cord (Fig. 3-6A,B). Radial glial cells can be easily identified by the typical morphology. They have a cuboid shaped cytoplasm, membrane contacts to the lumen of the ependymal tube and projections towards the basal lamina of the spinal cord (Fig. 3-6A,B). After injury, changes in the in cell morphology, and therefore in actin cytoskeleton are evident (Fig. 3-6C,D). However, optimal conditions for the maintenance of the organotypic cultures had not been established, therefore the changes observed in cell morphology and actin cytoskeleton could have been caused by cell death. Though organotypic cultures look promising, major technical issues need to be solved before it can be use in a reproducible manner to obtain significant results. A major technical drawback was that the agarose wouldn't hold the tissue in place causing the tissue to brake or fall out of the tissue holder once the blade made contact with it. Therefore only in one out of ten tissue samples tested were decent tissue samples obtained. For this strategy to be useful to study rearrangements of actin cytoskeleton in response to injury in the axolotl it is necessary to establish optimal sectioning and culture conditions.

The overall data suggest that injury seems to be able to induce changes in actin cytoskeleton in the spinal cord injury of axolotls. However the lack *in vivo* of data at cellular resolution does not allow us to clearly establish the dynamics of such changes and how can they be related to changes in the expression of miR-125b.

Actin cytoskeleton changes induced by injury induces in rat astrocytes

Since miR-125b plays an important role in regulating the response to injury in both the axolotl and rats, we wanted to know if regulation of miR-125b expression in response to injury by changes in actin cytoskeleton was a conserved mechanism between the species.

From our study on the role of miR-125b in spinal cord repair we know that this microRNA is mainly expressed in astrocytes, therefor we used confluent primary cultures of rat cortical astrocytes injured by scratching with a P10 pipette tip as mammalian model. The cultures were then fixed at different time points after injury and stained with rodhamine-tagged phalloidin and beta-catenin (to delimit the cell membrane) (Fig. 3-7). When cell were fixed 10 min after the scratch, in some cells at the wound edge there is a visible reduction in phalloidin staining (Fig. 3-7B) in comparison to unscratched cells

(Fig. 3-7A). A similar phenotype was observed in cells acutely treated for 30 min with Cyto D (Fig. 3-7C). Interestingly, cells treated with Jasp did not showed reduction of phalloidin staining after injury. This data suggest that, as observed in axolotls, injury could induce actin depolymerization in response to injury; similar at the depolymerization induced by treatment with Cyto D.

We also stained against alpha tubulin to see if actin depolymerization induced by injury could induce changes in microtubule cytoskeleton. In a few cells at the injury site a lack of staining was noticed (Fig. 3-7B'). However the shape of the nucleus stain with DAPI suggest that the cell is dying hence the lack of tubulin staining. When cells where treated with Cyto D (Fig. 3-7C') there was difference in the microtubule cytoskeleton structure or organization in comparison to control cultures (Fig. 3-7A'). Though cell membrane looks widely affected after treatment with Cyto D, the microtubule cytoskeleton seems normal. When the cells were scratched after treatment with Jasp we observe the same phenotype of the cells scratched (Fig. 3-7D'). In a few cells at the wound edge there was a lack of tubulin staining. Again the DAPI staining suggests that the cells are dying. This suggest that in astrocytes, injury induced depolymerization of actin cytoskeleton did not seem to affect microtubule cytoskeleton.

We then wanted to see if altering the microtubule cytoskeleton could affect the actin cytoskeleton. After acute treatment with Nocodazole for 30 min, we did not observed an effect on phalloidin staining (Fig. 3-7E) in comparison to control cells (Fig. 3-7A). Alpha-tubulin staining confirmed that the drug effectively affected microtubule cytoskeleton (Fig. 3-7E'). Interestingly, treatment with Taxol did affect the actin cytoskeleton (Fig. 3-7F). Acute treatment with Taxol (30 min) induced retraction of actin filaments from the cells membrane (Fig.3-7E), similar to the phenotype observed in injured cells or cells treated with Cyto D. As expected, treatment with Taxol stabilized microtubule cytoskeleton as evidence by a denser microtubule network in comparison to untreated cells (Fig. 3-7A').

An important component of actin cytoskeleton dynamics is myosin II. We use Blebbastatin (Blebb) to inhibit the contractile activity of myosin II. Acute treatment with Blebb did not induce changes in actin cytoskeleton as evidenced by the phalloidin staining (Fig. 3-7G). Blebb treatment did not affect microtubule cytoskeleton either (Fig. 3-7G'). To confirm that the phenotype observed in scratched cultures was due to cytoskeleton depolymerization, we decided to treat the cells with Latrinculin B (Lat B),

another drug that also depolymerizes the actin cytoskeleton. As expected, after treatment with Lat B cells lacked phalloidin staining (Fig. 3-7H) resembling the phenotype of cells treated with Cyto D or scratched. Microtubule cytoskeleton was not affected by Lat B treatment (Fig. 3-7H').

These results suggest that injury of astrocytes *in vitro* may induce actin cytoskeleton depolymerization similar to treatment with Cyto D or Lat B. These results also confirm the importance of dynamic microtubules in the maintenance of a proper actin cytoskeleton. As it was observed for the axolotls, when the dynamism of microtubules were affected by stabilization with Taxol, the actin cytoskeleton depolymerized.

Multiple factors affect miR-125b expression in astrocytes *in vitro*

Since injury seems to affect actin dynamics in astrocytes, we wanted to know if those changes would also affect the expression of miR-125b in astrocytes *in vitro*. Quantification of expression levels of microRNA at different time points after injury showed and increased in the levels of mir-125b within minutes after injury (Fig. 3-8A). The levels miR-125b remained significantly higher six hours after injury but return to normal levels 12 hours after injury (Fig. 3-8A). 24 hrs after injury the expression levels are again significantly higher in comparison to unscratched controls (Fig. 3-8A). The increase in the expression levels of miR-125b after injury contradicts the results we found for *in vivo* injury in rats. One day after spinal cord injury in rats the expression levels of miR-125b decrease in comparison to uninjured controls (Fig. 2-1B). The difference between the *in vivo* and *in vitro* response could be due to the miR-125b expression quantified from RNA extracted from spinal cord injury includes the changes in expression of other cell types, not only astrocytes as in an in pure *in vitro* culture. It is possible that expression levels of miR-125b *in vivo* in astrocytes increase as observed *in vitro*, but on the other cell types (neurons, oligodendrocytes, microglia, meningeal fibroblast and infiltrating macrophages) miR-125b was strongly downregulated, therefore when looking as the tissue as a whole the total levels of miR-125b decreased. It is also important to take into account the artificial environment in which the astrocytes are grown *in vitro*. In contrast to the *in vitro* culture, *in vivo* astrocytes are in contact with other cell types such as neurons and oligodendrocytes as well as components of the

extracellular matrix. All this interactions may influence the gene expression of astrocytes *in vivo* and how the cells response *in vivo vs in vitro* to external stimuli such as injury.

We decided to take a closer look at the upregulation observed 24 hrs after injury. When the experiment was repeated, we observed that even between groups there were differences in the expression levels of miR-125b response to injury. This time, contrary to what was observed during the determination of miR-125b dynamics in one of the groups the expression levels of miR-125b decreased 24 hrs after injury while in the other two groups there was no significant change in comparison to unscratched controls (Fig. 3-8B). This discrepancy in results suggested that in astrocytes *in vitro* injury might not be regulating the change in expression of miR-125b as we observed in the axolotls. To confirm that the injury did not induced reproducible changes in miR-125b transcription after scratch, we decided to quantify the expression levels of the precursor microRNA in the same samples. In the three groups studied we observed an increase in pre-miR-125b 24 hrs after injury in comparison to unscratched cultures (Fig. 3-8C) confirming our first results. The difference between the results obtained for miR-125b and pre-miR-125b suggest that the changes in expression of the mature microRNA are due to the stability of the mature microRNA and is not related to change in gene expression in response to a external stimuli.

We then wanted to know if the changes in pre-miR-125b in response to injure were related to the changes in actin cytoskeleton. When we treated the cells with Cyto D to induce actin filament depolymerization we observed that miR-125b levels increased similar to scratched cultures (Fig. 3-8D). This suggests that as observed in the axolotl, actin depolymerization in response to injury could be inducing changes in miR-125b expression. Treatment with Jasp in the presence or absence of injury did no induced changes in miR-125b (Fig. 3-8D). This suggests that actin depolymerization after injury is needed to induce changes in miR-125b in response to injury. Treatment with Nocodazole, Lat B and Blebb in the presence of absence of injury led to a decrease in the expression levels of miR-125b (Fig. 3-8D). Since Nocodazole did not induce visible changes in actin cytoskeleton changes in miR-125b expression in comparison to unscratched cells were not expected. Microtubule depolymerization can induce actin filament and stress fibers formation; therefore we were expecting similar results as to Jasp. The fact that Nocodazole was able to block normal change of miR-125b after scratch suggest once again that dynamic microtubules might be necessary for proper

response to injury induce actin depolymerization. Lat B induces actin depolymerization by binding to free globular actin monomers (G-actin) while Cyto D induces actin depolymerization by biding to the actin filaments and inducing it's fragmentation and subsequent depolymerization. The difference in the action mechanism between these two drugs that induce actin depolymerization could be the cause of the difference in the expression of miR-125b in response to the treatments. Cyto D treatment induces actin filaments fragmentation, which in turns induces contraction of the fragmented filaments (Kolega et al., 1991). Blocking myosin II contraction with Blebb could have prevented the normal change in miR-125b expression induced by actin depolymerization after injury. Injury induced actin depolymerization requires dynamic microtubules and contraction to induce increase in miR-125b expression.

Do to the variability in the results in miR-125b observed before we decided to quantify the expression levels of the precursor microRNA after treatment with Cyto D and Jasp to confirm that the changes observed were due to changes in miRNA transcription and nor stability. However changes in the expression of miR-125b (Fig. 3-8E) and pre-miR-125b (Fig. 3-8F) were not consistent between the groups. Although the variability in between groups was previously only noticed in the expression levels of miR-125b, in the experiments with Cyto D and Jasp there was also variation in the levels of pre-miR-125b.

The dynamics of miR-125b after injury showed that the levels of miR-125b rose quickly, then decreased 12 hrs after injury, and then rise up again at 24 hrs (Fig. 3-7A). It is possible that culture conditions, such as days in culture before performing the assay (Table 6-1) could induce changes in miR-125b expression independently or in conjunction with injury, specially at late time points. However, the rise in miR-125b expression at early time points should show a similar trend among different experimental groups if the changes are mainly dependent on actin cytoskeleton depolymerization induced by injury. We decided then to look at the expression of miR-125b at 10 min and 4 hours after injury or acute treatment with Cyto D (Fig. 3-9). At both time points, the changes in miR-125b expression in response to injury or Cyto D were not consistent between the groups (Fig. 3-9A-C). To discard the possibility that difference in day in culture could cause differences between groups even at early time points, we decided to perform injuries and treatments with Cyto D and Jasp at the same time in the three experimental groups. Also, to discard the possibility that the serum in the media added

after injury or drug treatment (15% Fetal bovine serum) could be inducing changes in miR-125b independently of injury, we decided to reduce the serum concentration after injury or drug treatment (2% FBS). Once more, the changes in expression of miR-125b or pre-miR-125b are not consistent between groups.

The overall data suggest that the expression and/or stability of miR-125b in rat primary cortical astrocytes *in vitro* could be influenced by different external factors besides injury. Although we studied the influence of the few factors enumerated on table 6-1, we were unable to determine the main factor that was causing the variability among the experimental groups. One factor that has to be taken into account but cannot be modified is the intrinsic variability of primary cultures (Mather and Roberts, 1998). Also, the lack of a realistic environment (cell-cell, cell-ECM interaction) could influence the response of astrocytes to injury *in vitro.* For the scratch assay and drug treatment of primary astrocytes to work as a relevant and reproducible model system it is necessary to study carefully and thoroughly all the factors that could influence gene expression.

c-Fos expression is activated in response to injury in the axolotl

(c-Fos immunostaining and microarray data analysis was carried out by Jacklyn Essig)

In the axolotl, actin depolymerization after injury seems to regulate miR-125b expression. Therefore we wanted to know which transcription factors could be regulating the expression of miR-125b in response to injury. To answer this question, we decided to clone a portion of the regulatory region upstream the miR-125b gene in the axolotl. We ran a bioinformatics analysis to determine what transcription factors were predicted to bind to the cloned region in the axolotl and across different species. Out of the predicted transcription factors (Fig. 3-10F), we looked for those that have been described in the literature to be related to changes in actin cytoskeleton. One of the transcription factors predicted to bind to the cloned regulatory region of miR-125b that has been previously been described to be regulated by changes in actin cytoskeleton was c-Fos (Zambetti et al., 1991). c-Fos is predicted to bind to two overlapping segments in the cloned region (Fig. 3-10G). c-Fos is a transcription factor from the Fos family that forms heterodimers with members of the Jun family of transcription factors. The heterodimers formed by the Fos and Jun family members are known as the AP-1 transcription factor family (Zenz et al., 2008). In the cloned upstream region of miR-125b

there are also predicted biding sites for cJun and AP-1 factors (Fig. 3-10G). The c-Jun predicted biding site overlaps with the c-Fos predicted biding sites and one of the AP-1 predicted biding sites. This suggests that miR-125b expression might be regulated by AP-1 transcription factor.

To confirm that injury-induced changes in the actin cytoskeleton could induce changes in c-Fos expression we stained spinal cord sections with an antibody against c-Fos before and after injury. We observed that one day after injury, there was an increase in c-Fos expression, specifically in radio glia cells within 500μm to the injury site (Fig. 3-10B) in comparison to uninjured animals (Fig. 3-10A). These results confirmed our previous microarray data where c-Fos was up-regulated one day after injury and it's expression decayed at 3 days post injury (Fig. 3-10C). We also found that the expression of c-Fos in response to injury was seen mainly in radio glial cells (Fig. 3-10D). Interestingly this are the cells were miR-125b is expressed (Fig. 2-1C) and the cells were we observed the changes in actin cytoskeleton in response to injury (Fig. 3-2).

To test whether the change in c-Fos expression was affected by changes in actin cytoskeleton in response to injury we quantified c-Fos expression after treatment with the drugs that alter actin or microtubule cytoskeleton dynamics (Fig. 3-10E). As expected c-Fos expression was significantly higer one day after injury in comparison to uninjured controls. Animals that were treated with Cyto D, in the presence or absence of injury, also showed a higher expression of c-Fos, suggesting that actin cytoskeleton depolymerization after injury can induce changes in c-Fos expression. Treatment with Jasp did not induced significant changes in the expression of c-Fos in the presence of absence of injury in comparison to uninjured controls. Treatment with Nocodazole did not induced changes in the expression of c-Fos in the absence of injury; however, when animals were injured after treatment with Nocodazole there was a significant increase in c-Fos expression. This suggest that possibly injury can override the block in expression of c-Fos done by Nocodazole, however this override it's not enough to induce miR-125b expression. On the other hand treatment with Taxol alone did induced changes in cFos expression while injury after Taxol treatment did not showed significant changes in c-Fos expression in comparison to uninjured controls. Since Taxol and Nocodazole have opposite effects on microtubule stability it was not unexpected to see that they had opposite effects on c-Fos expression. However such opposite effect of the drugs was not observed in miR-125b expression levels. This suggests that microtubule dynamics could

have a strong effect on c-Fos expression while the effect on miR-125b is dependent on the actin dynamics. It is also possible that the changes observed in c-Fos mRNA levels after the different treatments might no reflect changes in c-Fos protein levels that would in turn regulate miR-125b expression.

To determine whether c-Fos and/or cJun can regulate the expression of miR-125b by direct binding to the regulatory region of the microRNA gene in the axolotl we decided to perform a Chromatine Immuno Precipitation (ChIP) assay. Due to the lack of antibodies specific for axolotl, the ChIP assay was carried out different antibodies for c-Fos (Fig. 3-11). PCR amplification in immuno-precipitated chromatin using the c-Fos antibody previously used for immunostaining (Fig. 3-10A-B) or an antibody against c-Jun showed amplification for the regulatory region of miR-125b (arrows in Fig. 3-11A). As expected similar products were observed in positive control samples using an antibody against Polymerase II (Pol-II) and in the input sample and there was no product amplification using a normal mouse IgG (mIgG) antibody. However an unexpected product was observed in the mock sample (no antibody) and unspecific amplifications were observed in all the samples positive for miR-125b. Repetition of the PCR with a different set of primers did not yield product for Poll II, c-Fos or c-Jun precipitated DNA, and instead yield product for the mock and the mIgG samples. A western blot using protein extract from one day post injury spinal cords showed that the mIgG antibody binds non-specifically to axolotl proteins while the c-Fos and the Pol-II did not recognized the axolotl proteins. Since c-Jun antibody recognized the axolotl protein we decided to keep using this antibody for future precipitation. New ChIP assays were carried out with two different c-Fos antibodies (Fig. 3-11B,C) Histone 3 (H3) antibody as positive control and normal rabbit IgG (rIgG) as negative control. Though the positive and the negative controls as well as the mock control gave the expected results, no PCR product was obtained from the DNA precipitated using c-Fos or c-Jun antibodies. Of the two c-Fos antibodies tested only one seemed to recognize the axolotl protein on western blot (Fig. 3-11C). The overall data suggest that neither c-Fos nor c-Jun bind to the regulatory region of miR-125b to regulate the expression of the microRNA in response to injury. However, it is possible that the antibodies used might not work specifically for ChIP assays in the axolotl. Another way to study the interaction of c-Fos and c-Jun with the regulatory region of miR-125b is using a luciferase assay. If the regulatory region for miR-125b is inserted in a reporter construct cloned upstream of a luciferase gene,

changes in luciferase expression after co-expressing c-Fos and/or c-Jun would indicate whether these transcription factors bind to the regulatory region of miR-125b

miR-125b changes in expression are dependent on the RhoA/c-Fos pathway

We then wanted to know if c-Fos activation in response to injury was conserved in rat as observed in the axolotl (Fig. 3-10). To answer this question we stained astrocyte primary cultures with an antibody against phospho-c-Fos (p-c-Fos, active form of c-Fos) after injury or treatment with cytochalasin D (Fig. 3-12A-F'). Cultures fixed ten minutes after injury or acute treatment with Cyto D did not showed expression of p-c-Fos, similar to the unscratched controls (Fig. 3-12A-C'). However, nuclear localization of p-c-Fos was observed in cultures fixed 4 hours after scratch (Fig. 3-12E,E') or Cyto D treatment (Fig.3-12F, F'). Although in the unscathed cells p-c-Fos nuclear localization was also observed at this time point, the percentage of p-c-fos positive cells in scratch and Cyto D treated cultures was significantly higher in comparison to unscratched controls (Fig. 3-12K). These data suggest that the observed activation of c-Fos was due mainly to actin depolymerization in response to injury and not to as a response to the presence of serum in the media.

It has been widely studied that c-Fos expression can be regulated by the small GTPase (Marinissen et al., 2004) RhoA. Since RhoA can regulate and be regulated by actin cytoskeleton dynamics (Banerjee and Wedegaertner, 2004; Ren et al., 1999; Tojkander et al., 2012), we decided to study whether RhoA has a role in regulating c-Fos in response to depolymerization of actin after injury. We decided to inhibit RhoA activity by using the toxin C3 transferase. C3 is known to specifically inhibit Rho activity by transferring an ADP-ribose moiety close to or into the switch-1 region of Rho GTPases (Aktories et al., 2004). In astrocyte primary cultures treated with C3 after scratch or treatment with Cyto D we observed the absence of p-c-Fos in the nuclei 4 hrs after treatment, similar to untreated controls (Fig. 3-12G-J'). This indicates that c-Fos activation in response to actin depolymerization after injury is dependent on Rho activity.

To test whether changes in response to miR-125b in response to injury are induced by RhoA-dependent c-Fos activation, we decided to quantify the expression of the microRNA after treatment with C3 (Fig. 3-13). In normal conditions we found that miR-125b expression levels are significantly higher at 10 min and 4 hrs after scratch in comparison to unscratched cultures. Treatment with C3 abolished the increase in miR-

125b levels at 10 min but not at 4 hrs after injury. This difference between the two time points can be explained by the short life-time of C3 in culture (approximately 4 hrs in culture). Therefore it is possible that in our culture conditions C3 was not longer active at 4hrs to prevent the increase of miR-125b in response to injury. This suggests that increase of miR-125b in response to injury is dependent on Rho activity, at least at early time points. Though in normal conditions nuclear p-c-Fos is not detected 10 minutes after injury, C3 treatment affected the levels of miR-125b. Conversely, C3 treatment prevented p-c-Fos nuclear localization at 4 hrs after injury but not the increase in miR-125b expression. The discrepancy between p-c-Fos immunostaining and miR-125b expression levels at this time points can be explained in part by the timely sencitivity of both techniques. Protein to be detected by immunostaing is dependent on the accumulation of that protein. Therefore, it is possible that c-Fos is already activated 10 min after scratch or 4 hrs after treatment with C3, but the accumulation of the protein was not enough for it to be detected by immunostaining. However, the activation of c-Fos 10 min after scratch or 4 hrs after treatment with C3 could be enough to induce changes in miR-125b.

Discussion

Through a pharmacological, study we found that the polymerization state of actin cytoskeleton and its interaction with microtubule cytoskeleton can regulate the expression of miR-125b in the spinal cord in the axolotl. We observed that actin depolymerization in the absence of injury induces changes in miR-125b transcription. On the other hand, stabilization of actin filaments not only induced changes in miR-125b transcription but also seemed to stabilize the mature form of the microRNA. Though the role of actin, and in particular of monomeric actin (G-actin) in gene transcription has been studied to certain depth (Pederson and Aebi, 2002; Rando et al., 2000) only until recently the correlation between actin dynamics and gene transcription has started to be studied in more detail (Olson and Nordheim, 2010). Interestingly, though the suggestion that actin dynamics can regulate microRNA transcription has been previously proposed for miR-1, miR-133 miR-143 and miR-145 in cardiac and skeletal muscle (Olson and Nordheim, 2010), no functional data showing a direct correlation has been produced yet. In that regard, our work would be the first to describe a link between changes in actin cytoskeleton and changes in the transcription of a particular microRNA.

Interestingly, most biomechanical studies focus solely on the role of actin cytoskeleton, without taking into account the possible role of microtubule cytoskeleton. Though the interaction between actin and microtubule cytoskeleton has been shown to play an important role in regulating several cellular functions such as cell adhesion, cell migration, cell division and wound healing (Etienne-Manneville, 2004; Rodriguez et al., 2003) little has been described about the role of such interaction in regulation of gene expression. Our data suggest that regulation of miR-125b expression after injury by actin cytoskeleton is dependent on microtubule dynamics. Though modulation of microtubule cytoskeleton in the absence of injury did not induced changes in miR-125b expression, modulation of microtubule dynamics interfered with the normal change in miR-125b in response to injury-induced actin depolymerization. Furthermore, the interaction of actin-microtubule cytoskeleton was visible in phalloidin staining in both axolotl and primary astrocytes. Stabilization of microtubules in of axolotls or astrocytes with Taxol, caused depolymerization of the actin cytoskeleton, similar to the observed in axolotls or astrocytes treated with Cyto D. Again, this is the first report of actin-microtubule interaction regulating microRNA expression.

To better understand how actin depolymerization in response to injury regulates miR-125b expression, it was necessary to take a closer look to the changes in actin dynamics. It has been previously described that gene regulation by actin is dependent on the available cytoplasmic free G-actin (Olson and Nordheim, 2010; Pederson and Aebi, 2002). Cytoplasmic G-actin can translocate to the nucleus to form protein complexes with Polymerases I and II (Percipalle et al., 2003; Percipalle et al., 2002; Philimonenko et al., 2004) and chromatin re-arrangement (Chen and Shen, 2007)to regulate gene expression. As well, cytoplasmic G-actin has been described to bind to co-transcription factors, preventing their translocation to the nucleus to induce transcription of Serum Response Factor (SRF) target genes (Miralles et al., 2003; Olson and Nordheim, 2010). The amount of cytoplasmic G-actin is regulated by the steady-state equilibrium between G-actin and actin in cytoskeletal filaments (F-actin). Studying whether injury could induce changes in the G-actin F-actin would shed light into the molecular mechanism through which actin cytoskeleton is regulating changes in miR-125b expression.

To study actin dynamics we stained for phalloidin tissue fixed at different time points after injury. Though with this technic it is possible to get cellular resolution of the actin cytoskeleton, it is hard to get a true sense of the actin dynamics. Since each time point observed is just a snapshot of a dynamic process is hard to tell whether we are observing actin depolymerization or repolymerization. Reorganization of actin cytoskeleton in response to external stimuli is a rather fast process. In a drosophila embryo single cell injury model, reorganization of cortical actin to form a contractile ring around the wound is observed within the first 60 seconds after injury (Abreu-Blanco et al., 2014); therefore a more proper way to study actin dynamics in response to injury would be to use *in vivo* imaging. When we tried doing *in vivo* imaging using the lifeact construct and different strategies (epifluoresnce microscopy, two photon microscopy and organotypic cultures) we encounter technical difficulties related to resolution, time limitations and sample preparation that didn't allow us to draw significant conclusions regarding the actin dynamics in response to injury. The use of lifeact seems a promising tool to study actin dynamics in response to injury; however the proper conditions for each strategy need to be optimized in order to obtain reproducible and significant results.

Since miR-125b showed to play a key role in spinal cord injury repair in both rats and axolotls, we wanted to study whether regulation of miR-125b by actin depolymerization in response to injury was a mechanism conserved between the two species. When we performed phalloidin or alpha tubulin staining in rat primary cortical astrocytes, we observed that injury induced changes in actin cytoskeleton that resembled the changes observed after treating the cells with Cyto D, suggesting that actin depolymerization after injury is conserved between rat and axolotl. However, due to inconsistent results, we were not able to determine whether injury induced-actin depolymerization could modulate the expression of miR-125b in astrocytes *in vitro.* Though *in vitro* cultures are often reliable simple model systems, there are many factors that can greatly influence the response of the system to a particular stimulus. Such factors could be intrinsic variability of primary cells, batch to batch variability in the primary cells and the serum used as supplement, the stability of the culture media, the rigor in the maintenance of the cultures, cell density and age of the cultures (Mather and Roberts, 1998). It is also important to take into account that, due to oversimplification, *in vitro* cultures may yield non-biologically relevant results. Therefore, it is necessary to develop better *in vitro* models, such as 3D co-cultures, in which the cells are in a more natural environment and the response to stimuli (e.i. injury) would be more reliable and hopefully less variable.

To determine how changes in actin cytoskeleton could be driving changes in miR-125b expression after injury, we decided to clone the regulatory region of the axolotl gene for miR-125b and look within this region, in the axolotl gene and across different species, for predicted transcription factors. Around 150 predicted biding sites were found within this region for multiple transcription factors. Out of these factors only Sox2 has been previously proposed to regulate microRNA expression in human embryonic stem cells (Marson et al., 2008). Other transcription factors that have been described to regulate microRNA expression such as SRF for miR-1 in cardiomyocytes and skeletal muscle (Zhao et al., 2005) cMyc for miR-18a in mouse malignant mammary epithelial cells (Mouw et al., 2014) and Microphthalmia-associated transcription factor for different microRNAs including miR-125b-2 in melanoma cells (Ozsolak et al., 2008) were not predicted to bind to miR-125b in our analysis. Though MITF has been described to bind to the promoter region of miR-125b-2 through an accessible chromatin analysis, functional binding has yet to be shown (Ozsolak et al., 2008). Though miR-125b-1 and 2

have the same seed sequence, since their precursor sequence and genomic loci differs, there could be differences in the predicted transcription factors that could bind to each gene. Since the genome of the axolotl has not been sequence, we don't know how many miR-125b genes exist. For that reason in our analysis we used the sequences of both miR-125b-1 and miR-125b-2 in the species where both miRNAs have been reported.

Within the predicted transcription factors for miR-125b, we look for those that have been described previously to be regulated by actin dynamics. An early work trying demonstrate that "the nucleus can respond to signals related to the structural organization of the cytoskeleton" (Zambetti et al., 1991) showed upregulation of c-Fos in HeLa cells treated with Cyto D. Furthermore, since RhoA can regulate c-Fos expression (Chihara et al., 1997; Marinissen et al., 2004; Whitmarsh and Davis, 1996) and actin dynamics (Tojkander et al., 2012) as well as being regulated by actin dynamics (Banerjee and Wedegaertner, 2004; Ren et al., 1999) we decided to study whether c-Fos could have a role in regulating the expression of miR-125b after depolymerization of the actin cytoskeleton in response to injury. We found that both protein and mRNA levels of c-Fos increase in response to injury. We also found that activation of c-Fos in response to injury is transient, peaking 1 day after injury and decresing 3 days after injury. The same transient expression of c-fos was in found in HeLa cells treated Cyto D (Zambetti et al., 1991) suggesting that actin depolymerization after injury induces the rapid activation of c-Fos to regulate early genes needed for regeneration. Consistent with these results, we found and increase in c-Fos expression 1 day after treatment with Cyto D but not with Jasp or Nocodazole. Interestingly treatment with Taxol did activate c-Fos expression. Since we observed that Taxol could induce certain level of actin depolymerization, it is possible that that level of depolymerization is sufficient to activate c-Fos expression without affecting miR-125b. However Taxol treatment together with spinal cord injury did not induce a significant increase in c-Fos expression, which could explain why in the same conditions no change of miR-125b expression was observed. Unexpectedly, Nocodazole treatment together with injury also increased c-Fos expression. These results suggest that c-Fos expression it's not sufficient to induce changes in miR-125b, and that and extra step between c-Fos expression and miR-125b transcription, probably c-Fos activation by phosphorylation could be also dependent on actin dynamics.

Increase in c-Fos expression in response to actin depolymerization after injury seems to be a conserved mechanism across species. An early work looking at the timely expression of early genes, cytokines and neutrophins, showed a transient expression of c-Fos peaking within 1 and 3 hours after injury (Hayashi et al., 2000). In rat primary cortical fibroblast we detected the upregulation of c-Fos in response to scratch and treatment with Cyto D. As for the axolotl, the changes in c-Fos after injury or treatment with Cyto D correlate with changes in miR-125b. Interestingly, the effect of c-Fos in miR-125b transcription is the opposite between the systems. This difference in the regulation of miR-125b by c-Fos could explain the difference observed in miR-125b expression after injury between the rat and the axolotl. However, the lack of consistency in the miR-125b data obtained in vitro makes it difficult to draw definitive conclusions; therefore the need to develop a system that can faithfully mimic in vivo behavior of mammalian spinal cord and reduce variability in the results.

Nonetheless, our current system allowed us to determine that the activation of c-Fos in response to injury and actin depolymerization is dependent on the activity of the small GTPase RhoA. Inhibition of RhoA activity by the exosyme C3 transferase prevented c-Fos activation in response to injury or treatment with Cyto D. These results suggest that actin depolymerization induces RhoA-dependent c-Fos activation. Interestingly, in a single cell injury model it was shown that the coordinated activity of Rho family GTPAses is needed for the proper reorganization of the acto-myosin cortical cytoskeleton for wound closure (Abreu-Blanco et al., 2014). The pathways through which the small GTPases Rho, Rac and Cdc42 regulate the actin cytoskeleton in response to external stimuli mainly in cell migration are well understood (Spiering and Hodgson, 2011). However little is known on how the actin cytoskeleton signals or feeds back into the small GTAPses pathways to regulate their activity. A key player in modulating the interaction between the actin cytoskeleton and the small GTPases seems to be the Focal Adhesion Kinase (FAK). Focal adhesions are protein complexes that link the actin cytoskeleton to the integrins in the cell membrane that attach the cell to the extracellular matrix (Geiger et al., 2009; Provenzano and Keely, 2011). Focal adhesions serve as nucleation centers for acto-myosin bundles, known as stress fibers, and can also anchor microtubules (Etienne-Manneville, 2004; Geiger et al., 2009). Focal adhesion assembly and disassembly is regulated by RhoA and FAK crosstalk. Tissue contraction, induced by actin depolymerization after injury (Kolega et al., 1991), could activate FAK which in

turn would activate RhoA to induce actin re-polymerization (Provenzano and Keely, 2011) and c-Fos activation. To test this hypothesis experiments blocking FAK activity as well as myosin II are needed to have a better understanding of the mechanotransduction cascade in the context of spinal cord injury injury.

Though, demonstrating that c-Fos or c-Jun can bind to the regulatory region of axolotl miR-125b by ChIP assay was unsuccessful, this does not rule out that c-Fos or c-Jun regulates miR-125b expression. The success of ChIP assays is highly dependent on the ability of the antibodies to recognize the protein in the assay conditions; therefore in a still unexplored model system like the axolotl, it is possible that the antibodies didn't recognize the protein form of c-fos. An alternative strategy to determine whether c-Fos regulates miR-125b is to do a luciferase assay. By subcloning the regulatory region of miR-125b upstream the luciferase gene in a reporter vector, we can quantify *in vitro* whether co-transfection with an axolotl c-Fos-GFP and/or c-Jun-dsRed expression vectors alters luciferase expression in comparison GFP empty vector co-transfected controls. Moreover, the c-Fos-GFP and c-Jun-dsRed expression vectors can be used to overexpress this factors in vivo and measured changes in miR-125b expression after transfection. Lastly, these vectors can also be used to perform another ChIP assay, this time using an antibody against GFP, to precipitate DNA in animals that have been transfected with c-Fos-GFP and c-Jun-GFP expression vectors. Hopefully, one of this alternatives would gives the answer whether c-Fos or the AP-1 transcription factor can regulate the expression of miR-125b in response to actin depolymerization induced by spinal cord injury.

With the overall data we propose the following model for how spinal cord injury induces changes in miR-125b expression in axolotls (Fig. 3-14). The mechanical disruption of axons and glial cells induces tissue contraction and actin depolymerization. Glial cells in the ependymal tube within 500μm from the injury re-arrange their actin and microtubule cytoskeleton and seal the open ends of the ependymal tube. In these glial cells c-Fos is transiently activated 1 day after injury, probably through FAK-RhoA signaling pathway. Activated c-Fos is predicted to binds the regulatory region of miR-125b to inhibit its transcription. Downregulation of miR-125b creates a permissive environment for spinal cord regeneration.

Figures

Figure 3-1. Actin dynamics affect miR-125b expression in the spinal cord of axolotl.
(A-F) Expression levels of miR-125b (A,C,E) or pre-miR-125b (B, D, F) after injury or treatment with Cyto D (A,B) Jasp (C, D) Nocodazol or Taxol (E,F). (G-J) Expression levels of miR-29 after injury or treatment with Cyto D (G) Jasp (H) Nocodazole (I) or Taxol (J). * P< 0.05; ** P< 0.05; ***P<0.001 n.s. not significant.

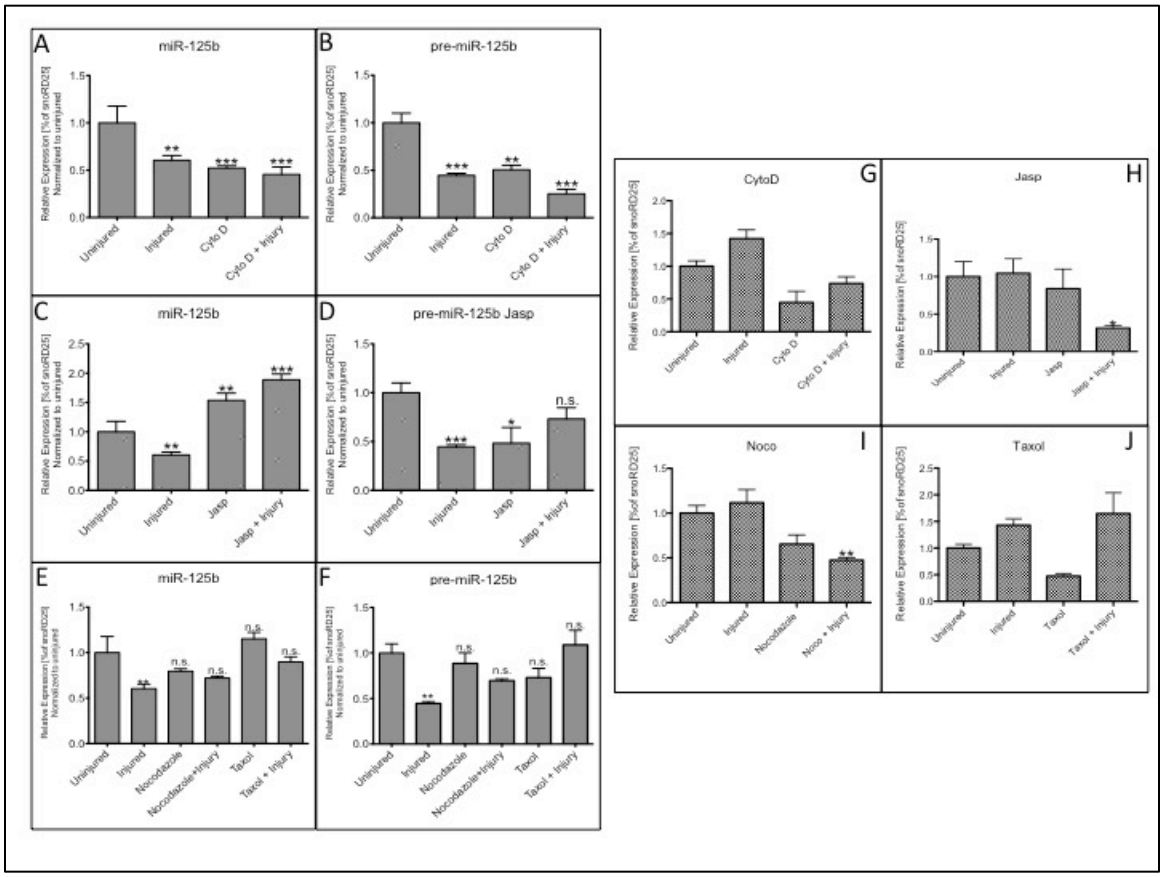

Figure 3-2. Injury induces changes in actin cytoskeleton.

(A-F) Phalloidin staining of longitudinal sections of uninjured spinal cord (A) or 1 min (B) 10 min (C) 30 min (D) 1 hr (E) or 4hrs (F) after injury. (A'-F') DAPI staining of longitudinal sections of uninjured or injured spinal cord. (A''-F'') Merged images. Arrows in B and C indicate cells without phalloidin staining. Arrows in C, D, E indicate cells with apical phalloidin staining.

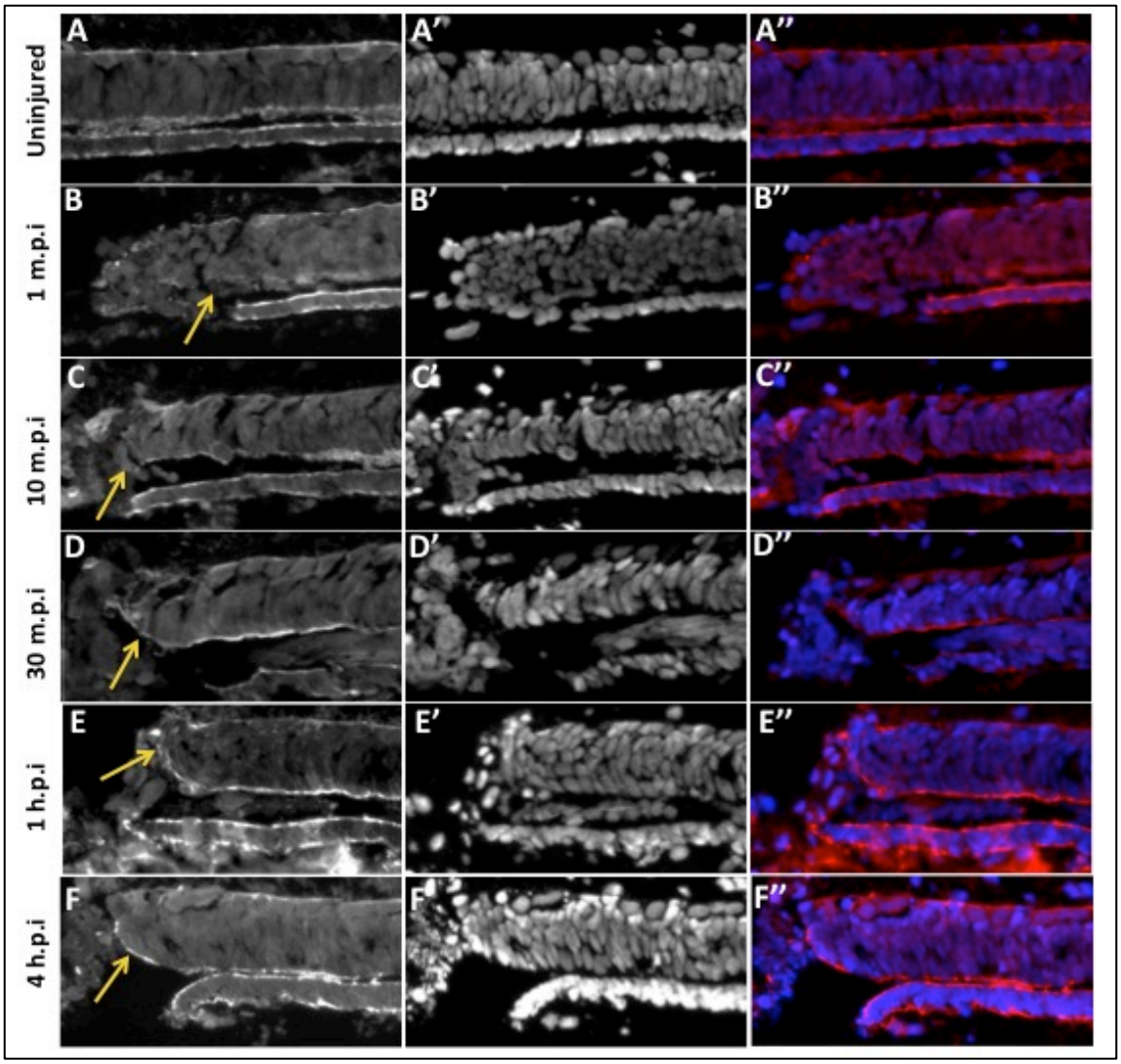

Figure 3-3. Pharmacological treatment of spinal cords in axolotl.

(A-E) Phalloidin staining of longitudinal sections of uninjured spinal cord (A) or after Cyto D (B) Jasp (C) Nocodazole (D) or Taxol (E) treatment. (A'-E') DAPI staining of longitudinal sections of uninjured or or drug treated spinal cords. (A''-F'') Merged images. (F-H) α-Tubulin staining of longitudinal sections of uninjured spinal cord (F) or after Nocodazole (G) or Taxol (H) treatment. (F'-H') DAPI staining of longitudinal sections of uninjured or or drug treated spinal cords. (F''-H'') Merged images. Arrows in B and E indicate cells without phalloidin in the glial cell processes reaching the basal surface. Arrow in C indicates increment in apical phalloidin staining. Arrow in D shows glial cell process reaching spinal cord's basal membrane. Arrows in G indicate cells without tubulin in the glial cell processes. Arrow in H shows glial cell process reaching spinal cord's basal membrane.

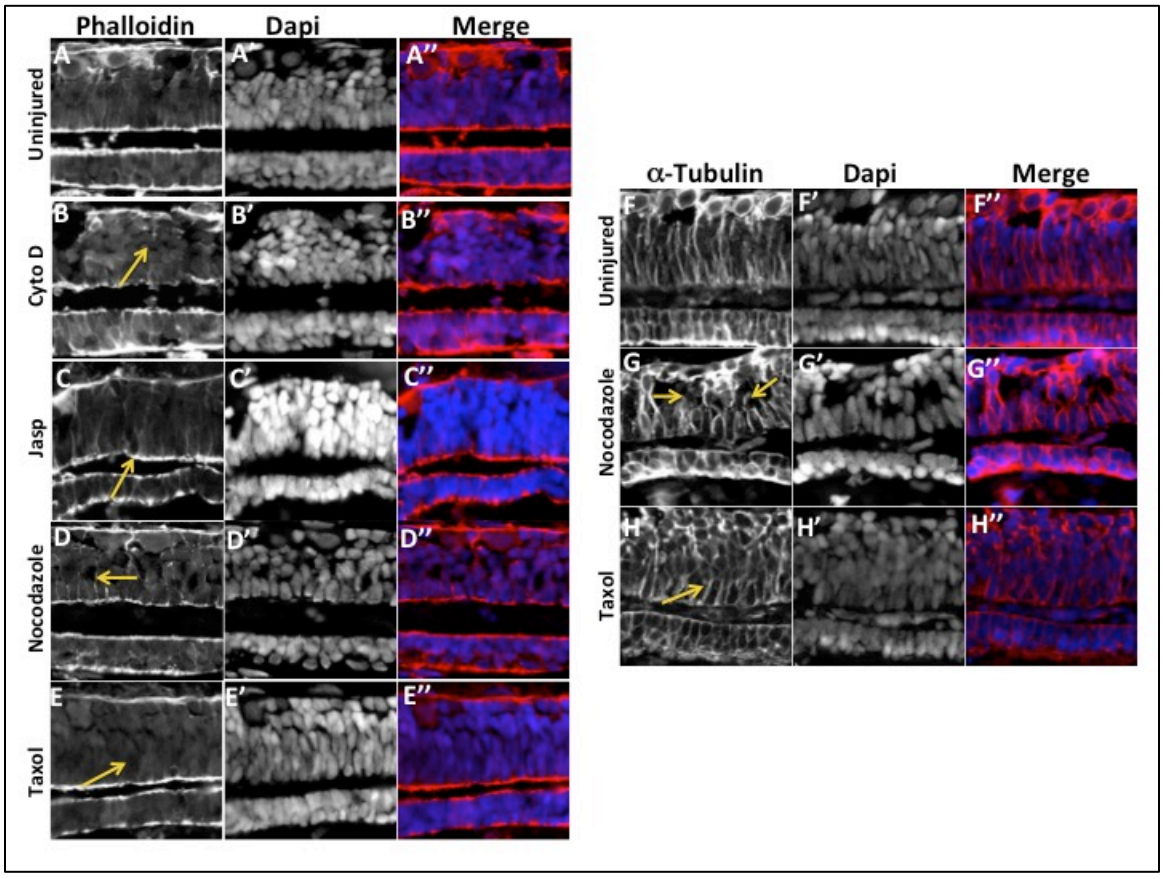

Figure 3-4. Lifeact imaging in epifluorescence microscope.

(A) Uninjured spinal cord with cells expressing the lifeact. (B) Higher magnification of the region boxed in A. (A') DIC image of the spinal cord in (A) showing that lifeact expression is restricted to the spinal cord. (B') Higher magnification of the boxed area in A'. (C) Spinal cord after injury showing 3 cells expressing lifeact near the injury site, denoted by the dotted white line. (C') DIC image of the injured spinal cord shown in C. (D) Fluorescence intensity over time of the three cells in C. The color of each curve corresponds to the color of the arrows in C. Blue dotted line in A' B' and C' marks the spinal cord.

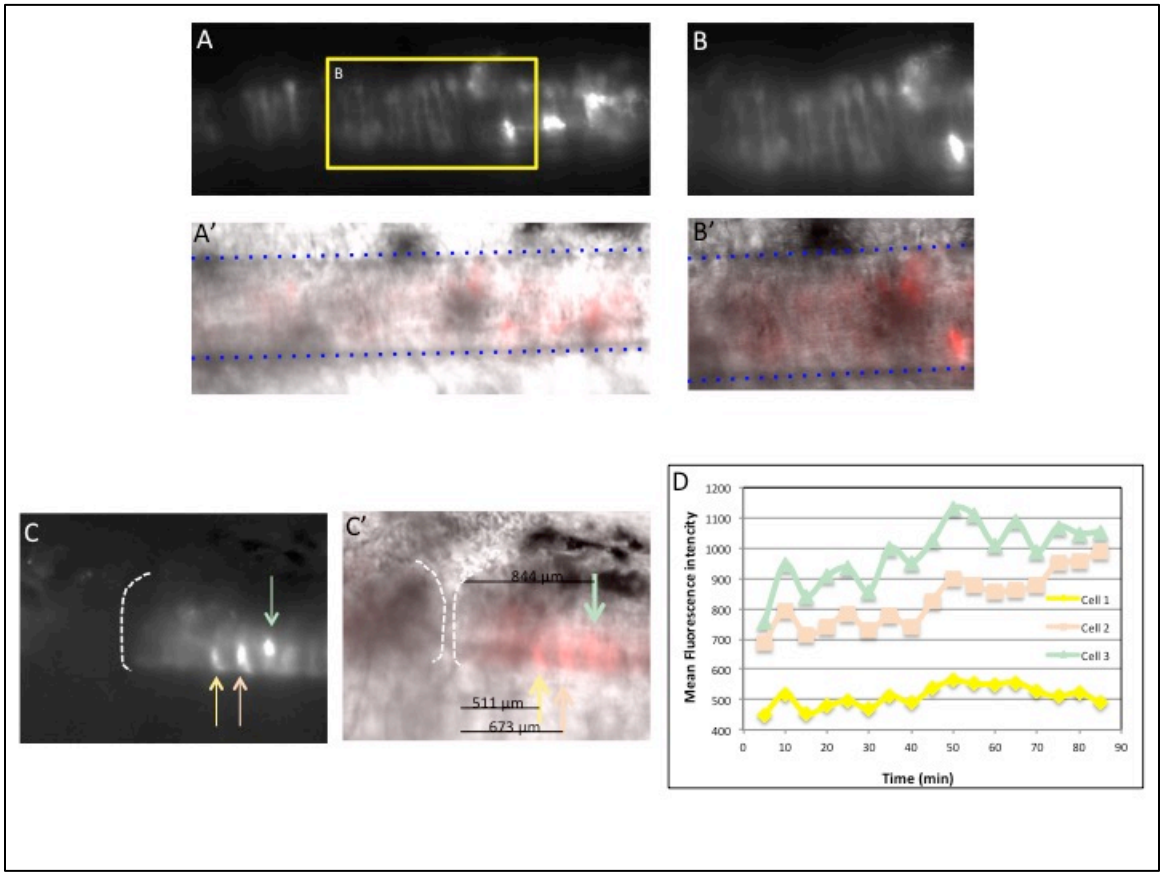

Figure 3-5. Lifeact imaging in 2-photon microscope.

(A) Uninjured spinal cord with cells expressing the lifeact. (A', A'') Higher magnification of the regions boxed in A. (B) Spinal cord after injury showing two cells (arrows) expressing lifeact near the injury site, denoted by the dotted white line. (C) Snapshots of a time lapse following the changes in actin in the cells marked by the arrows. (D) Fluorescence intensity over time of the two cells in C. The color of each curve corresponds to the color of the arrows in C.

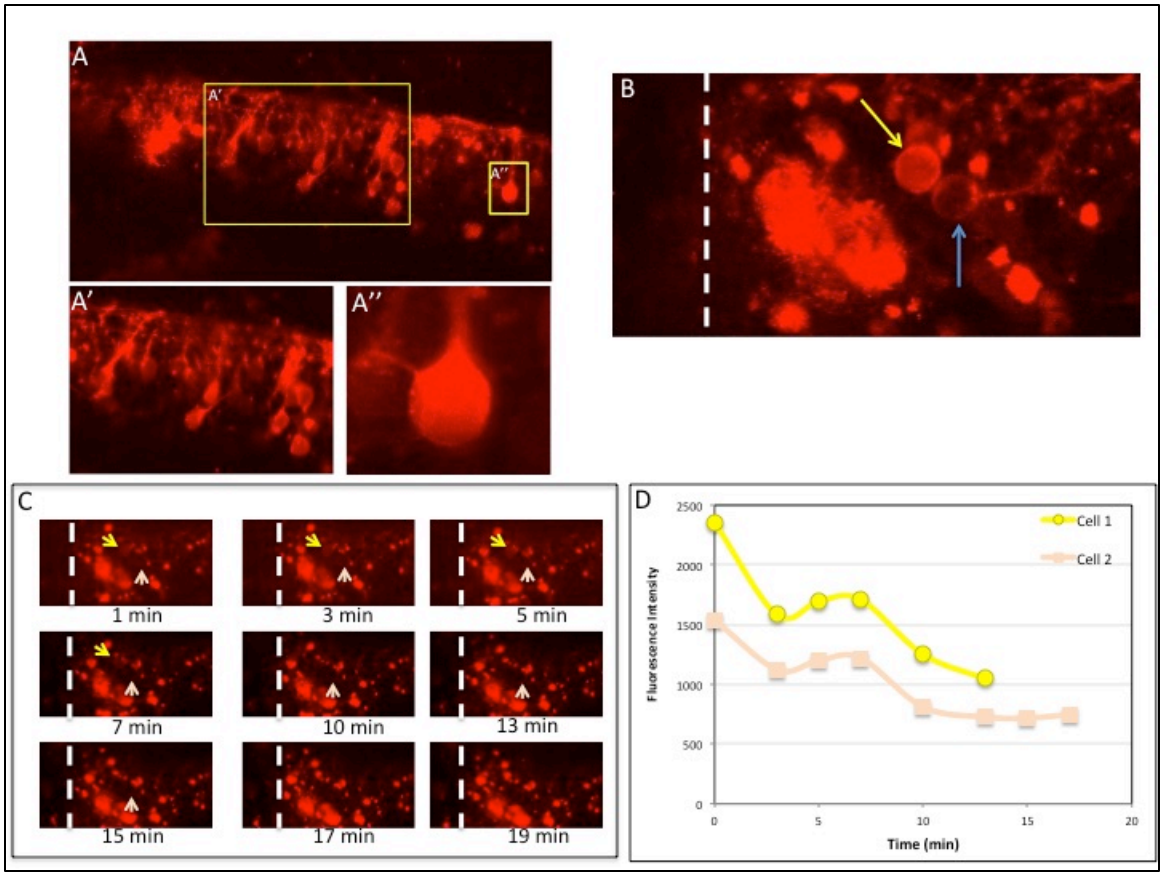

Figure 3-6. Lifeact imaging in organotypic cultures.

(A) Uninjured spinal cord section with cells expressing the lifeact. (B) Higher magnification of the region boxed in A. (A') DIC image of the spinal cord in (A) showing that lifeact expression is restricted to the spinal cord. (B') Higher magnification of the boxed area in A. (C) Spinal cord after injury showing two cells expressing lifeact near the injury site, denoted by the dotted white. (C') DIC image of the injured spinal cord shown in B and C. (D) Spinal cord two hrs after injury showing the cell marked by the arrow in C. Blue dotted line in A' B' marks the spinal cord.

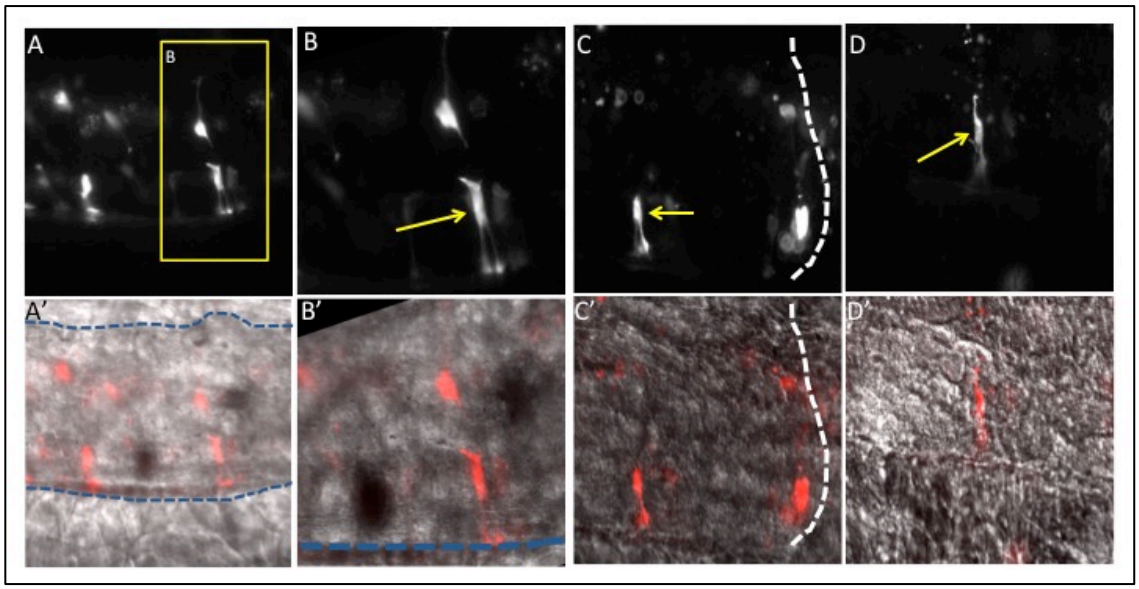

Figure 3-7. Injury induces changes in actin cytoskeleton in astrocytes *in vitro*.

(A-D) Phalloidin staining (green) of unscratched astrocytes (A) or after scratch (B) Cyto D (C) or Jasp treatment. (A'-D') α-Tubulin (green) staining of unscratched astrocytes (A') or after scratch (B') Cyto D (C') or Jasp (D') treatment. (E-G) Phalloidin (green) staining of astrocytes after Nocodazole (E) Taxol (F) or Lat B (G) or Blebb (H) treatment. (E'-G') α-Tubulin (green) staining of astrocytes after Nocodazole (E') Taxol (F') or Lat B (G') or Blebb (H') treatment. In all images the nuclei are marked with DAPI (blue) and the cell membranes are stained with β-catenin (red). Arrows in B, C and F indicate cells without phalloidin staining or retracting filaments. Arrow in B' indicates a cell at the injury site without tubulin staining. Arrows in D shows astrocytes at the wound edge with stable actin filaments. Red dotted line in B and C delimits the cell marked by the arrows. White Dotted line in B, B', D and D' marks the scratch.

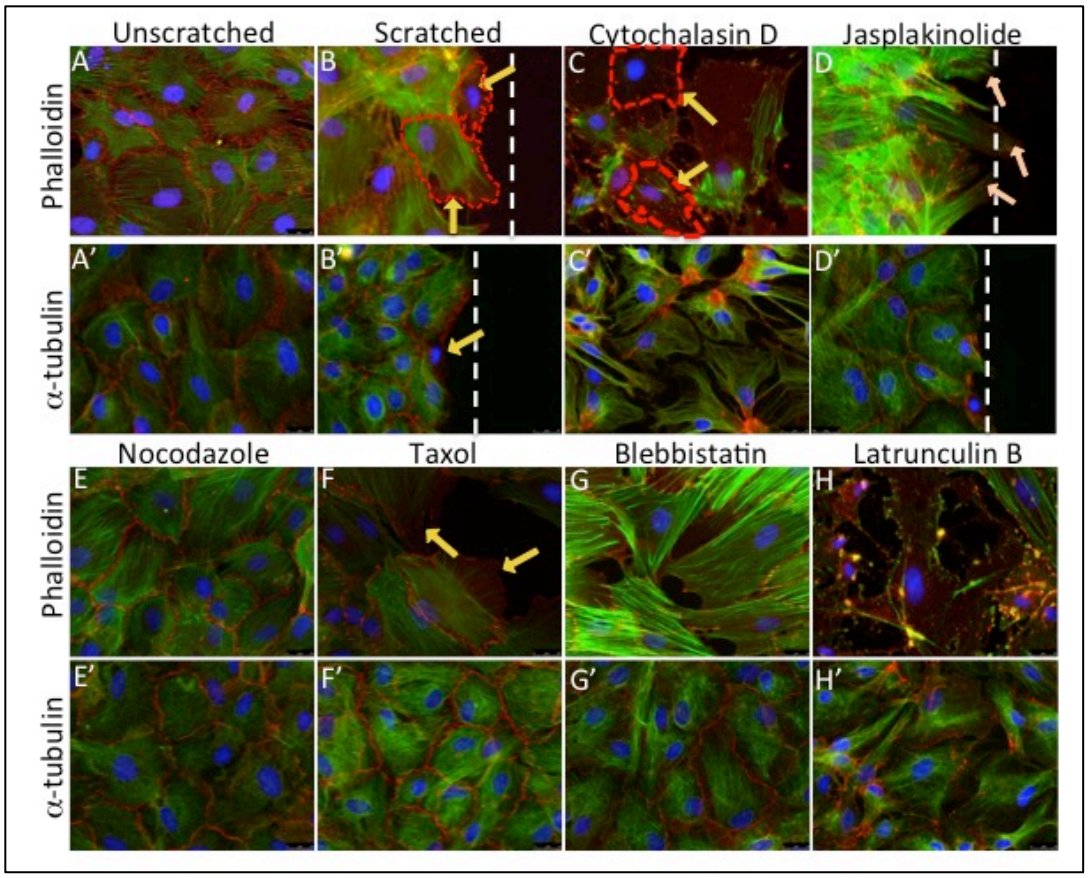

Figure 3-8. Multiple factors affect miR-125b expression in astrocytes *in vitro*.

(A) Dynamics of miR-125b expression after injury. (B) Expression levels of miR-125b 24 hrs after scratch in three independent samples. (C) Expression levels of pre-miR-125b 24 hrs after scratch in the samples from B (D) Expression levels of miR-125b 24 hrs after scratch or treatment with Cyto D, Jasp, Nocodazol, Taxol, Lat B or Blebb in the presence or absence of injury. (E) Expression levels of miR-125b 24 hrs after scratch or treatment with Cyto D or Jasp in the presence or absence of injury in three independent samples. (F) Expression levels of pre-miR-125b 24 hrs after scratch or treatment with Cyto D or Jasp in the presence or absence of injury in the samples from E. * P< 0.05; ** P< 0.05; *** P<0.001 n.s. not significant.

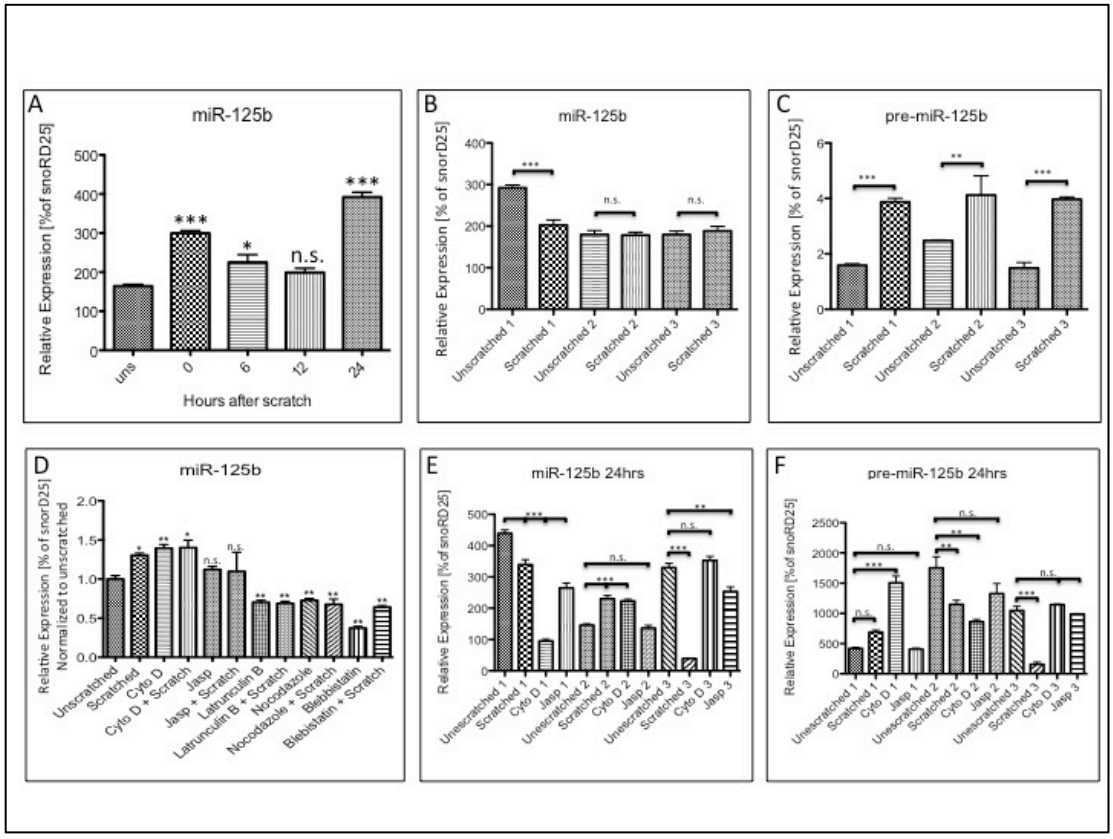

Figure 3-9. Multiple factors affect miR-125b expression in astrocytes *in vitro*.

(A-C) Expression levels of miR-125b 10 min or 4hrs after scratch or treatment with Cyto D in three independent samples. (D,E) Expression levels of miR-125b (D) or pre-miR-125b (E) 4 hrs after scratch treatment with Cyto D in low serum conditions (2%FBS) in three independent samples. * P< 0.05; ** P< 0.05; *** P<0.001 n.s. not significant.

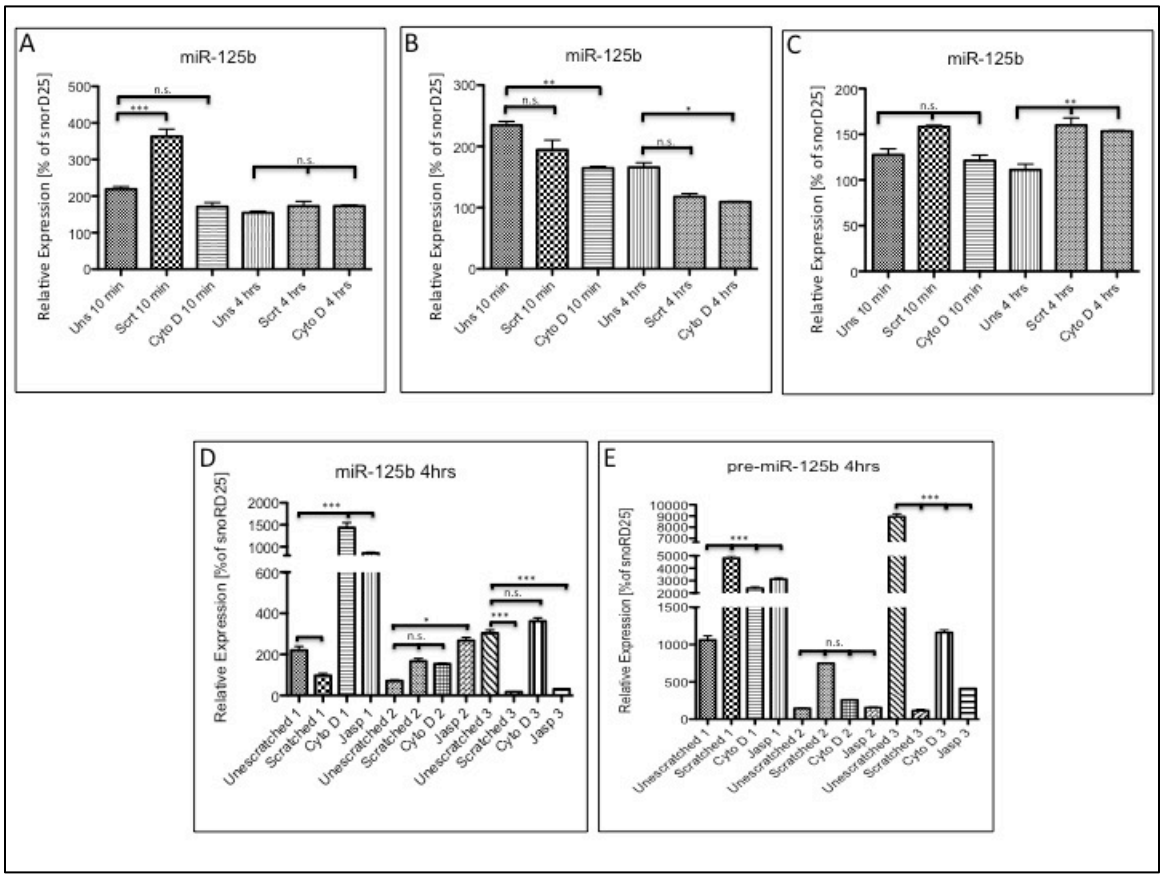

Figure 3-10. Spinal cord injury induces c-Fos expression in axolotls.

(A,B) c-Fos staining in uninjured (A) or 1 day post injury (B) spinal cords. (A'-B'') DAPI staining and merge images of spinal cords in A and B. (C) Microarray data for c-Fos showing a sharp induction of c-Fos 1 day after injury and a decrease to normal levels 3 and 7 days after injury. (D) Quantfication of c-fos positive glial cells 1, 3, 7 and 10 days post injury. (E) Expression levels of c-Fos 1 day after injury or treatment with Cyto D, Jasp, Nocodazol, or Taxol in the presence or absence of injury. (F) Transcription Factors predicted to bind to the regulatory region of miR-125b across species. Asterisks mark predicted AP-1 family members. (G) Sequence of the regulatory region of miR-125b gene in axolotl showing the predicted biding sites for c-Fos, c-Jun and Ap-1 in red. * P< 0.05; ** P< 0.05; *** P<0.001.

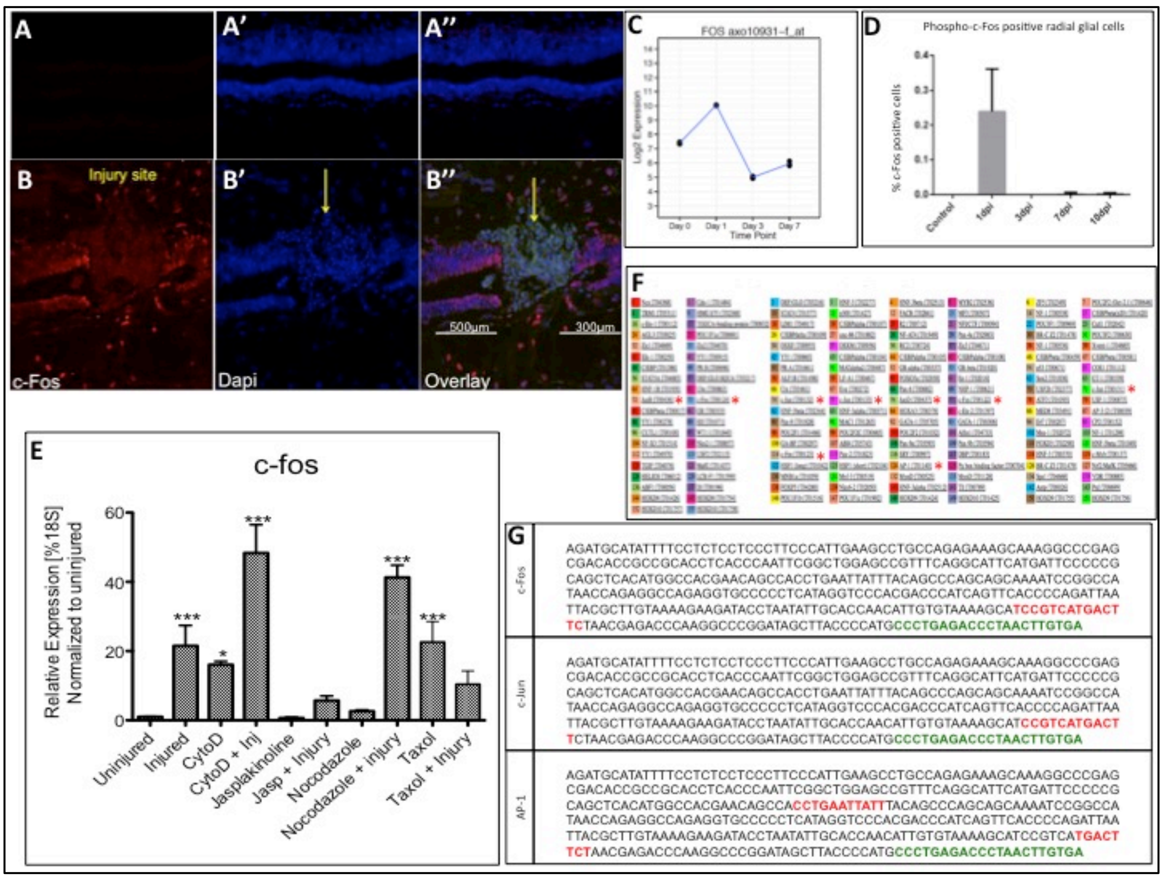

Figure 3-11. ChiP assay in axolotls.

(A-C) PCR amplification of miR-125b regulatory region in immunoprecipitated DNA. Arrows in A mark the product of the expected size (aprox 500 bp). Pol II is Polymerase II , mIgG is normal mouse IgG, rIgG is normal rabbit IgG, H3 is Histone 3, c-Fos-1 is Santa Cruz antibody, c-Fos-2 is Cell Signaling antibody, c-Fos-3 is Millipore antibody. (A'-B') Western Blots testing the antibodies used in the immunoprecipitations in A, B and respectively. (C') Western Blot testing the c-Fos antibody used in the immunoprecipitations in C in protein extracts from uninjured and 1 day post injury spinal cords.

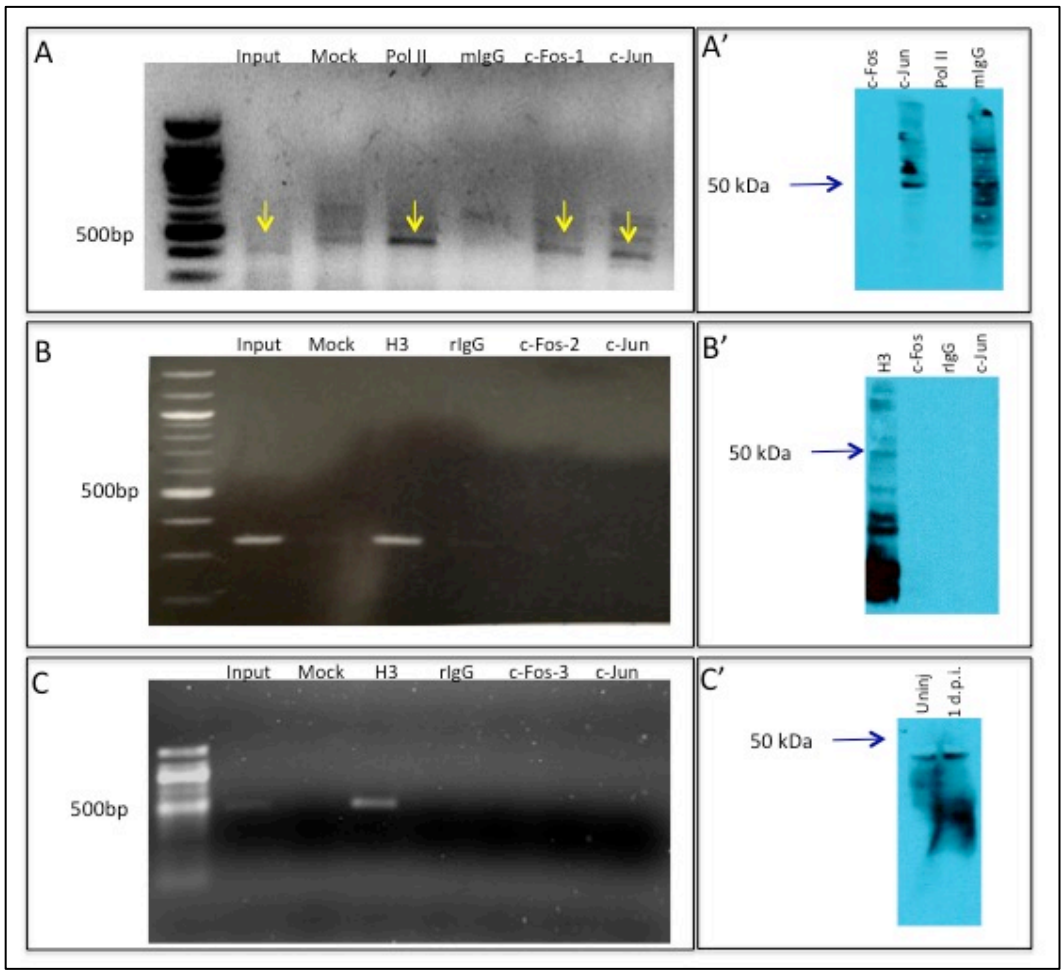

Figure 3-12. c-Fos activation after injury is Rho dependent in astrocytes *in vitro*.

(A-C) Phospho-c-Fos staining in unscratched astrocytes (A) or 10 min after scratch (B) or Cyto D (C) treatment. (D-F) Phosphor-c-Fos staining in unscratched astrocytes (D) or 4 hrs after scratch (E) or Cyto D (F) treatment. (G-J) Phosphor-c-Fos staining in unscratched astrocytes (G) or 4 hrs after treatment with C3 (H) or scratch (I) or Cyto D (J). (A'-J') DAPI staining of the astrocytes in A-J. (K) Percentage of phosphor-c-Fos positive unscratched astrocytes or 4 hrs after scratch or Cyto D treatment. White dotted lines in B, B', E, E' I and I' denote the scratch. * P< 0.05; ** P< 0.05; *** P<0.001.

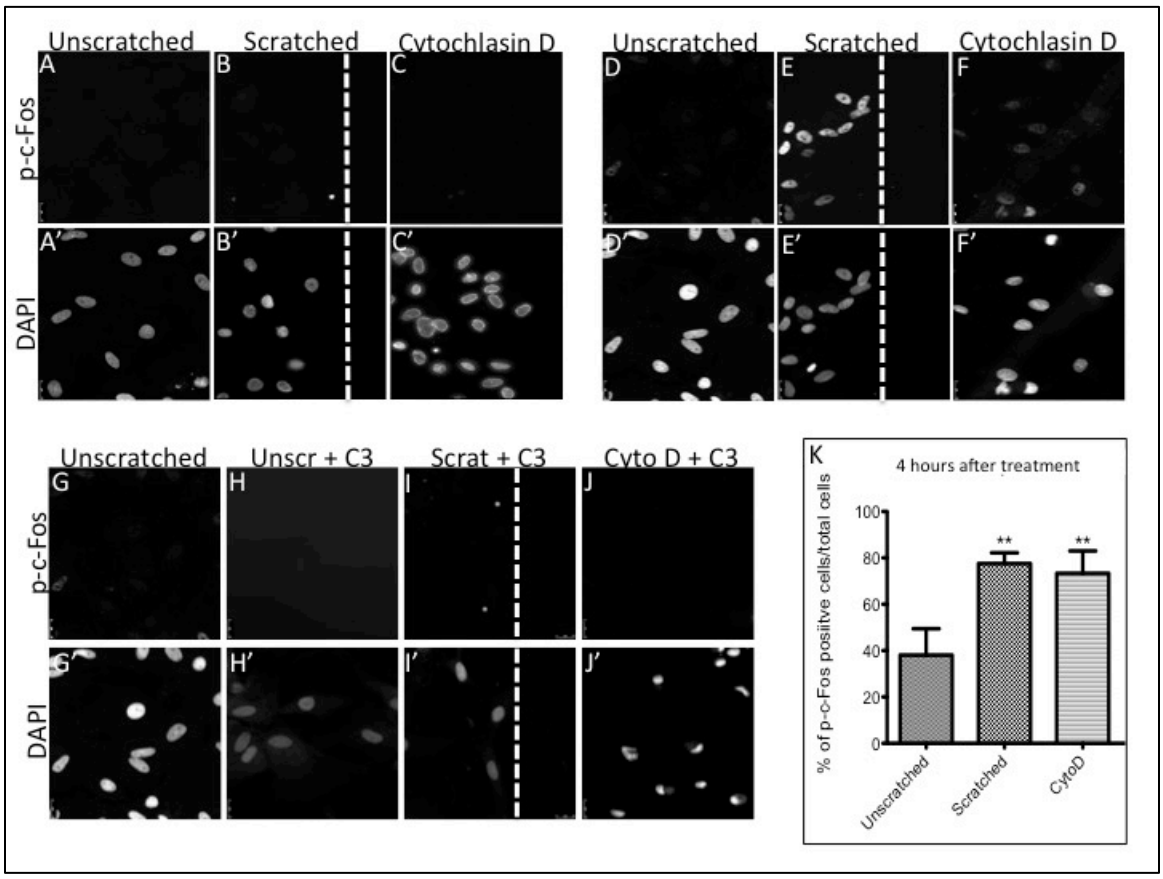

Figure 3-13. Changes in miR-125b expression after injury is Rho dependent in astrocytes *in vitro*.

Expression levels of miR-125b 10 min, 4 hrs or 24 hrs after treatment with C3, scratch or scratch and treatment with C3. * P< 0.05; ** P< 0.05; *** P<0.001 n.s. not significant.

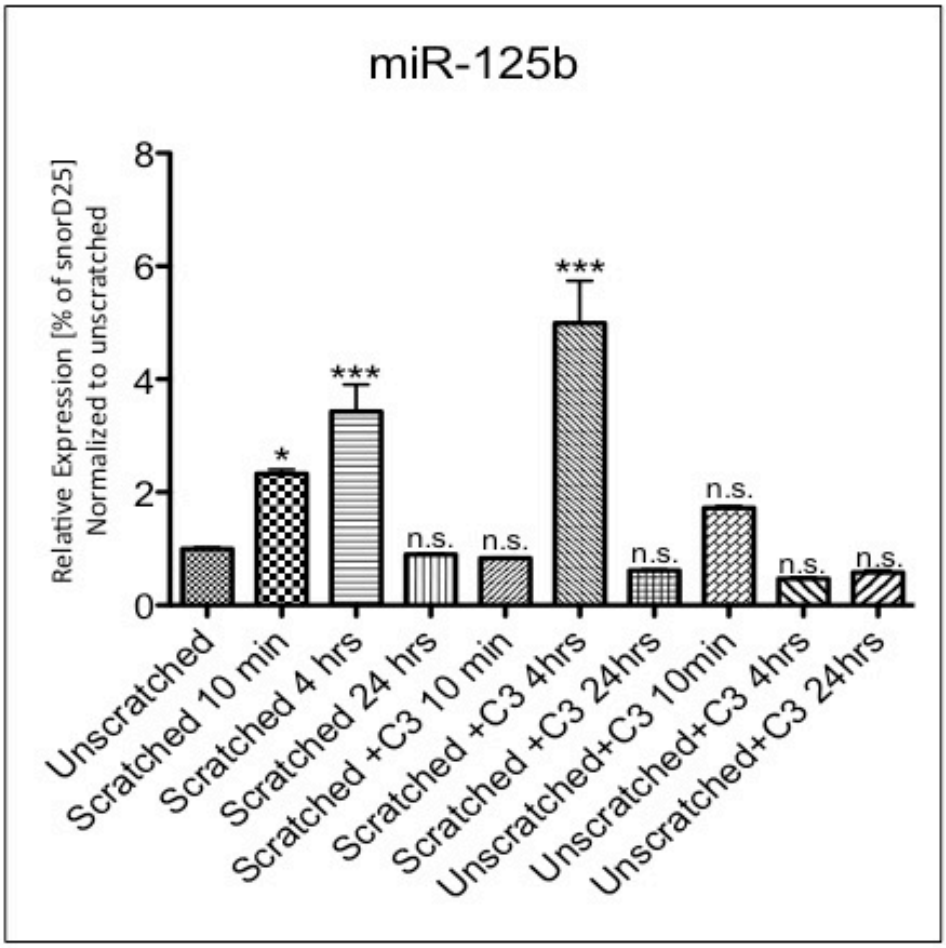

Figure 3-14. Proposed model of miR-125b regulation after spinal cord injury in axolotl.
In axolotls, the mechanical disruption of axons and glial cells induces a tissue contraction. Glial cells in the ependymal tube re-arrange their cytoskeleton in response to injury and seal the open ends of the ependymal tube. In these glial cells c-Fos is transiently activated, probably through RhoA pathway. We propose that activated c-Fos binds to the regulatory region of miR-125b to inhibit its transcription. Downregulation of miR-125b creates a permissive environment for spinal cord regeneration.

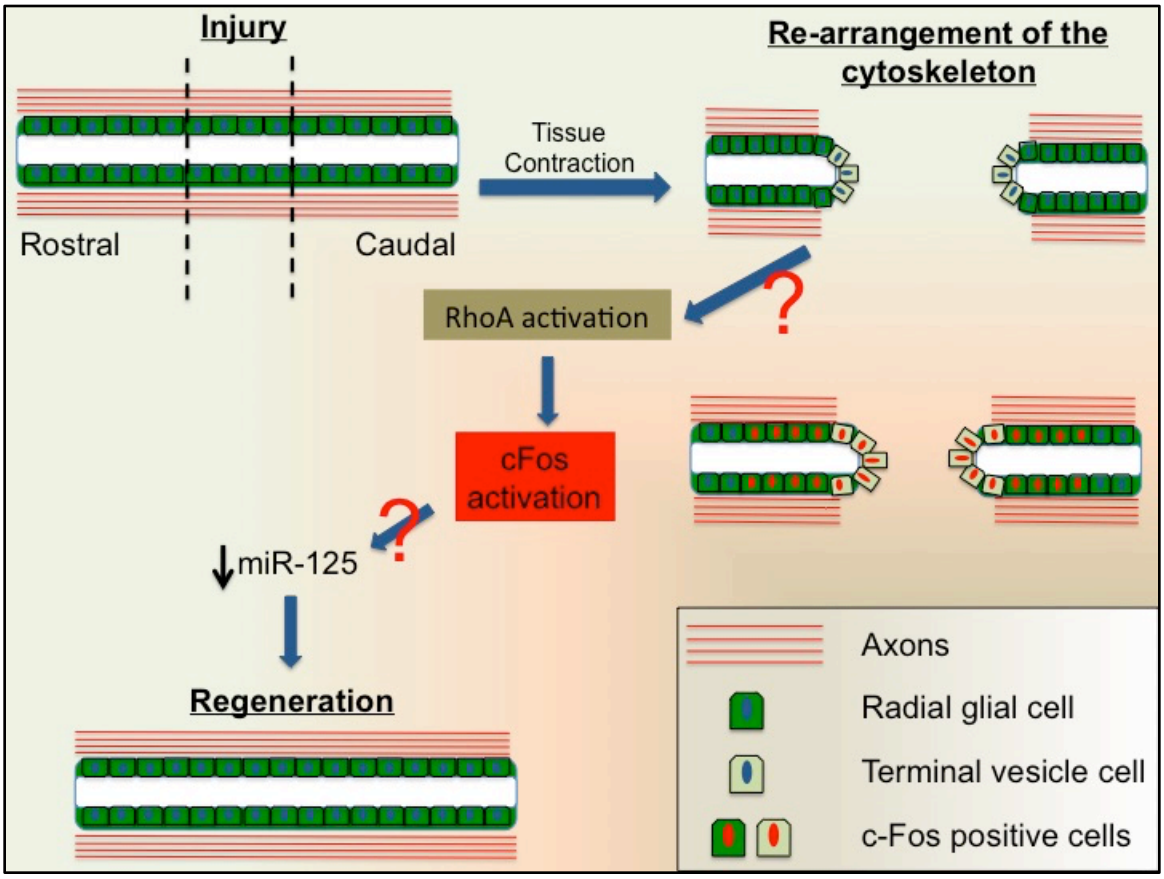

Chapter 4: Development of a 3D *in vitro* Mammalian Spinal Cord Model

Summary

SCI in mammals is a multifactorial, complex process. Although current mammalian models for SCI (primarily rat and mice) have provided a great deal of information about the events that govern SCI in mammals, the complexity of the systems and the difficulty to follow *in vivo* the particular response of each cell type to injury, have limited our understanding of SCI at the cellular and molecular level. On the other hand, *in vitro* models provide many useful tools to probe the molecular and cellular mechanisms that govern SCI; however, the over-simplification and artificial conditions of *in vitro* cultures raise questions about the biological relevance of the results.

We proposed to develop a 3D, *in vitro* model of the mammalian spinal cord, in which the complexity of the *in vivo* environment could be retained, but at the same time the advantages of *in vitro* manipulation could be achieved. For our model, multiple materials for the 3D scaffold were tested (Agarose, poly-ε–caprolactone and type I collagen). We decided to start with co-cultures of astrocytes and neurons as this two cell types play a major role in SCI. We used primary rat cortical astrocytes and a neuroblastoma derived cell line that can be induced to differentiate into neurons (B35 cells). We found that co-cultures of astrocytes and B35 cells grow better on collagen type I scaffolds coated with fibronectin and laminin. The conditions to improve axonal growth and cell survival from the neurons are still to be determined. Preliminary experiments performing a compression injury on these scaffolds seeded with astrocytes showed that these cells seem to respond in an *in vivo* like manner to injury. We could observe proliferation of the astrocytes as well as overexpression of GFAP and extracellular matrix components such as Collagen IV.

Once culture conditions that allow for co-culture, axon growth, and cell survival, as well as an *in vivo* like response to injury, have been determined, this model will be a powerful tool to study how upregulation of miR-125b in mammals could create a permissive environment for spinal cord repair.

Introduction

In the past few decades *in vitro* culture systems have become an attractive alternative for the study of cell biology. The simplicity of *in vitro* systems allows for more detailed studies at the cellular and subcellular levels using methods that are technically challenging in *in vivo* systems (e.g. real time imaging). On the other hand, the oversimplification of complex biological systems could neglect important interactions of the cell with other cells and with the environment that in turn influence the cell response to particular stimuli. For example, the growth cones of *Xenopus* retinal neurons cultured *in vitro* are attracted by netrin, however the same cue repels the growth cones when the substrate is coated with laminin-1(Höpker et al., 1999; Ravi et al., 2015).

Although a great deal of information has been obtained from 2D cultures, it has become more and more clear that in these systems important input from the environment, in particular interactions between different cell types and with the proteins of the extracellular matrix (ECM), is being ignored. Interestingly, it has been shown that aside from cell-cell and cell-ECM proteins interactions, the topography and the stiffness of the tissue itself can affect cellular behavior response to external stimuli. For example, mesenchymal stems cells can be induced into an adipogenic fate when cultured on stiff substrates, and to an osteogenic fate lineage when cultured on softer substrates (Costa et al., 2012). 3D *in vitro* co-culture systems have emerged as way introduce the input from cell ECM and topography interactions to create models that better mimic *in vivo* conditions, without compromising the advantages of having a simpler system.

Different 3D model systems had been developed to study different cellular process within the CNS. For example, DRG neurons have been seeded into collagen scaffolds to study growth cone migration (Dubey et al., 1999), OPCs have been seeded on polystyrene nanofibers to study myelination (Lee et al., 2012), and even the establishment of co-culture of neurons and Schwann cells on poly-ε–caprolactone (PCL) fibers has been attempted (Daud et al., 2012). Although a great deal of effort has been put into designing 3D systems to improve recovery after spinal cord regeneration, no 3D models have been developed to study spinal cord injury itself.

There are two primary, existent spinal cord injury models, both of which have limitations. The first, organotypic cultures, require the extraction of the spinal cord from

the animals, an injury in and of itself that could trigger cellular repair processes and alter experimental results. The second, 2D *in vitro* co-cultures, is more easily manipulated, but the interactions of different cell types with the extracellular matrix composition and topography are missing. Therefore, there is a necessity for a 3D system designed specifically to study the response of astrocytes and neurons to traumatic injury in an *in vivo* like environment. We decided to develop a 3D *in vitro* model of the mammalian spinal cord by co-culturing primary astrocytes and neurons on tube shaped scaffolds of different materials. Our objective was to determine the materials and culture conditions that will allow not only for cell survival but also for an *in vivo* like response to injury.

Results

Cell growth on agarose gels

The first material we tested was agarose. Agarose has been previously described to support growth and neurite extension from chick dorsal root ganglia (DRG) neurons (Balgude et al., 2001; Bellamkonda et al., 1995) Using silicon based polymer (Polydimethylsiloxane PDMS) cast, we constructed 1% agarose tubed-shaped scaffolds. The tubes obtained were 15 mm long with an external diameter of 5mm and lumen diameter of 1.2mm (Fig. 4-1A). To further promote cell adhesion and neurite extension the agarose tubes were coated with P poly-L-lysine (PLL) and Collagen. We tested the growth of a neuroblastoma derived cell line (B35 cells) that can be induced to differentiate into neurons (Schubert et al., 1974). Undifferentiated B35 cells were able to attach and grow in both the external surface and the luminal surface (Fig. 4-1 B-D) of the coated tubes. B35 cell-seeded tubes were cultured in low serum media containing Dibutyryl-cAMP (Db-cAMP) to induce differentiation into neurons. Immunostaining against b-III-tubulin showed evident neurite outgrowth along the surface of the tube (Fig. 4-1 E-G). These results indicate that 1% agarose scaffolds support B35 cells growth and differentiation into neurons.

We then tested whether agarose could support the growth of astrocytes, another key component of the CNS and a major player in the response to spinal cord injury. Opposite to what was observed for the B35 cells, astrocytes showed poor attachment and growth on the agarose surface, even after coating the tubes with PLL and collagen (Fig. 4-1 H-J). Since agarose could not support the growth of astrocytes we decided to discard agarose as candidate material for the development of the *in vitro* 3D model.

Cell growth on polycaprolactone tubes

The second material tested was poly-ε–caprolactone (PCL). PCL tubes were obtained from the Nanofiber Solutios Company. The PCL tubes provided were 15 mm long with an external diameter of raging between 1.2 and 1.7mm and a lumen diameter of 1mm (Fig. 4-2A,B). The differences in the external diameter were due to differences in the wall thickness of the tubes. Tubes with three different wall thicknesses (200, 400 and 700µm) were used for experiments.

Since astrocytes showed poor attachment to agarose tubes, we first tested the adhesion and growth of astrocytes to the PCL tubes. Immunostaining of the tubes with GFAP showed that astrocytes were able to grow and attached all over the surface of the tube (Fig. 4-2C-E). Therefore, in terms of supporting astrocyte adhesion and growth, PCL seems to be a superior material in comparison to agarose.

One of the qualities we hoped to obtain in the 3D system is the capacity to be able to follow the response to injury in real-time, which cannot be done by immunostaining. Therefore, we decided to transfect B35 cells with a GFP-tubulin construct to facilitate the visualization of the cells without fixing the cultures for immunostain (Fig. 4-2F-H). To improve B35 cell attachment and neurite extension we coated the tubes with either fibronectin or PLL. B35 cells were able to attach to the surface of the tubes coated with fibronectin or PLL (Fig. 4-2I-N). However, after inducing differentiation, the cells growing on fibronectin-coated tubes extended longer neurites (Fig. 4-3I-K) in comparison to cells growing on PLL-coated tubes (Fig. 4-2L-N, Tables 4-1,4-2). We also observed that the cells survival was higher in fibronectin-coated tubes in comparison to PLL-coated ones (Table 4-1). We did not observe a significant difference in the length of neurites among different wall thicknesses in fibronectin-coated tubes (Table 4-1, 4-3). However, we did observe a decrease in cell survival when increasing the wall thickness (Table 4-1). Therefore, we picked fibronectin coating of 400μm wall thickness tubes as the optimal culture conditions.

After confirming that astrocytes and B35 cells can grow on PCL tubes, we decided to test whether co-cultures could be done on these scaffolds. To facilitate astrocyte visualization, we transfected the cells with an RFP-Histone (RFP-his) construct (Fig. 4-3A-C). To establish co-cultures, 400μm wall thickness tubes were coated with fibronectin and seeded with RFP-his astrocytes. Twenty-four hours after astrocyte seeding, GFP-tub B35 cells were seeded on top of the astrocytes. We observed that one day after seeding, both B35 cells and astrocytes survived the co-culture conditions (Fig. 4-3D). Interestingly, we observed that some B35 cells were already extending neurites, indicating that the presence of astrocytes was inducing B35 cell differentiation. To further push differentiation, we serum starved the co-cultures. Serum starvation (less than 1% serum in the media) induces differentiation in B35 cells with less toxicity than the previously used Db-cAMP. However, four days after serum starvation, cell survival was close to 0 for both cell types (Fig. 4-3E). Thus, although PCL can better support the

growth of both astrocytes and B35 cells than agarose, it could not support survival in B35 differentiation conditions, making PCL an undesirable material for the development of our 3D spinal cord model.

Cell growth on collagen scaffolds

(Production of Collagen I hydrogels and sheets was carried out by Yuping Li from the Aparicio lab in the Dentistry Department, UMN)

We next decided to test a material that would better resemble the extracellular environment of the spinal cord, collagen type I. Collagen type I is one of the most common materials used for the fabrication of 3D scaffolds for cell culture. We decided to first test the ability of B35 cells to grow and differentiate in collagen hydrogels. B35 cells survived after seeding on to Fibronectin-Laminin (Fb/Lm) coated gels, although their morphology was altered (Fig. 4-4A,B). Cells were not bipolar and looked more round than normal. When cells were serum starved to induce differentiation, no neurite extension was observed (Fig. 4-4C,D). These results likely indicate that B35 cells require a harder surface to differentiate and extend neurites. Therefore, we decided to test neurites extension in collagen sheets that have the same collagen concentration as the hydrogels, but wherein the water has been removed via lyophilization (Figure 4-7A). Undifferentiated B35 cells seeded on the collagen sheets showed a more characteristic morphology (Fig. 4-4E,F). When B35 cells were induced to differentiate, neurite outgrowth was observed (Fig. 4-4G,H). These results further support the notion that the stiffness of the substrate in which the cells are growing can greatly impact the cells response to external stimuli; furthermore, and, in this particular case, their response to serum starvation.

We then tested the capacity of collagen sheets to support astrocyte attachment and growth. We observed that astrocytes were also able to grow on Fb/Lm coated collagen sheets. Untransfected astrocytes showed normal morphology and normal expression of GFAP (Fig. 4-5A,B). Since collagen seems to be the appropriate material for supporting astrocytes and B35 cells survival and B35 cells differentiation, we decided to keep using collagen as scaffolding material for further experiments.

In vitro injury model

To test whether collagen scaffolds could induce an *in vivo* like response in astrocytes, we decided to use a compression injury model. Astrocytes seeded collagen sheets were compressed by holding them tightly with forceps. The compression injuries were done along the diameter of the sheet. After injury, the cultures were put back into fresh media and incubated for 48 hours. Immunostaining showed increased expression of GFAP in astrocytes close to the injury site (Fig. 4-5C,D) in comparison to uninjured cultures (Fig. 4-5A,B). Increased expression of GFAP is one of the main markers of reactive gliosis, which is the response of the astrocytes to spinal cord injury *in vivo* (Pekny and Nilsson, 2005). Thus, collagen seems to elicit an *in vivo* like response of the astrocytes to injury.

Another marker of reactive gliosis in response to spinal cord injury is astrocyte proliferation. A commonly used method to evaluate cell proliferation is by quantification of 5-ethynyl-2′-deoxyuridine (EdU) incorporation. EdU is a synthetic nucleoside that is incorporated specifically into the DNA of actively dividing cells. We evaluated EdU incorporation after injury, as a marker of injury-induced proliferation. We observed that EdU incorporation was higher in cells close to the injury site (Fig. 4-5G,H) in comparison to uninjured cultures (Fig. 4-5E,F). Increased GFAP expression and cell proliferation are both indicators that astrocytes are behaving in an *in vivo* like manner in response to injury in our *in vitro* model.

To further confirm the induction of reactive gliosis in response to injury *in vitro*, we decided to look at other markers of reactive gliosis and glia scar formation. Another intermediate filament that is overexpressed in response to injury besides GFAP is Vimentin (Pekny and Nilsson, 2005). Immunostaining showed a clear upregulation of Vimentin expression in cells close to the injury site (Fig. 4-6E) in comparison to uninjured cultures were Vimentin expression is not detected (Fig. 4-6B). Interestingly, the observed Vimetin expression is restricted to the cells that are also overexpressing GFAP in the injured cultures (Fig. 4-D,E) while in the uninjured cultures no Vimetin expression was observed even in the regions with higher GFAP expression (Fig. 4-6A,B).

Some of the components of the extracellular matrix that form the glia scar are Collagen IV (Hermanns et al., 2001; Klapka and Müller, 2006; Liesi and Kauppila, 2002) and CSPGs (Klapka and Müller, 2006; Sandvig et al., 2004; Sharma et al., 2012). A clear deposition of Collagen IV was observed at the injury boundary in injured cultures (Fig. 4-6H), while in the uninjured cultures such a specific deposition of collagen was not

observed (Fig. 4-6G). Similarly, specific CSPG deposition that was not detected in uninjured cultures (Fig. 4-6I) was observed at the injury border in compressed cultures (Fig. 4-6J).

The overall data indicates that astrocytes grown on Fb/Lm coated Collagen I sheets proliferate, upregulate GFAP and Vimentin, and deposit components of the ECM (Collagen IV and CSPG) in response to injury, thus mimicking the *in vivo* response of astrocytes after SCI. Therefore, this *in vitro* system could be potentially used for studying the role of miR-125b in reactive astrocytes and how modulation of this microRNA could lead to a more permissive environment for regeneration.

Co-cultures on collagen scaffolds

(Production of Collagen I tubes was carried out by Yuping Li from the Aparicio lab in the Dentistry Department, UMN)

To have a better *in vitro* model of the mammalian spinal cord, we decided to try to establish co-cultures of Astrocytes and differentiated B35 cells in collagen scaffolds with a more *in vivo* like architecture. In collaboration we the Aparicio lab, we obtained 5-7mm long tube shaped scaffolds with a luminal diameter of 1.2-1.5mm (Fig. 4-7B,C). Similar to what we observed for the PCL tubes, Fb/Lm coated collagen I tubes supported the survival of astrocytes and B35 after seeding (Fig. 4-7D). Also, as observed for PCL tubes, on the collagen scaffolds some B35 cells started to extend neurites 24 hours after being seeded onto the astrocyte-seeded tubes (Fig. 4-7D). In contrast to PCL tubes, induction of B35 cell differentiation did not induce massive cell death. We were able to maintain the co-cultures in differentiation conditions for at least one week (Fig. 4-7E). After one week in culture, we observed that B35 cells extended neurites (Fig. 4-7E). However we also observed that the amount of cells in the 1-week cultures diminished in comparison to 1-day cultures (Fig. 4-7D,E). This indicates that, although collagen scaffolds offer a better environment for neurite extension and survival than PCL tubes, better culture conditions still need to be established to achieve a fully functional and operational system.

Discussion

In the development of a 3D culture system, a determining step is the selection of an appropriate scaffolding material. The selection of the scaffolding material will depend mainly on: 1) the type of tissue that will be modeled and, 2) the desired mechanical properties for the scaffold. The mechanical properties ideal for our scaffold, besides supporting cell growth, include the abilities to be shaped into a tube, allow for real time imaging, and retain structural integrity after a mechanical injury. Different types of materials, both synthetic and natural, have been used for the growth of CNS derived cells and we decided to test several for the properties discussed above, including agarose, PCL, and collagen type I networks.

Agarose is a polysaccharide obtained mainly from seaweed. It is an attractive agent to use as it is a natural polymer, optically clear, and its stiffness can be readily adjusted by changing the concentration of the gel. Agarose scaffolds have been previously used to grow chick DRG (Balgude et al., 2001; Bellamkonda et al., 1995) and the neuroblastic cell line PC12 (Bellamkonda et al., 1995; Lin et al., 2005). In accordance to the previous findings, we found that agarose supports the growth of our neuronal cell line, B35. Also, in agreement with what has been observed for chick DRG cells, an agarose gel with a concentration of 1% is permissive for the extension of neurites. However, agarose gels don't seem to support the growth of CNS non-neuronal cells such as astrocytes. This result was surprising due to the fact that astrocytes are known to easily adhere to culture dishes. It is possible that a 1% agarose gel might have the stiffness necessary to promote neuronal growth, but lack the sturdiness required for glial cell growth. While increasing the concentration of agarose in the gels could have been an alternative to improve astrocyte growth, at concentrations of 1.25% the average neurite elongation rate of chick DRG cells is reduced (Balgude et al., 2001). Therefore, a trade off between astrocyte growth and neurite elongation would have come into consideration. Since we wanted both astrocyte growth and neurite extension, it seemed more logical to look for another material.

Poly-ε–caprolactone (PCL) is synthetic polyester that has a wide variety of uses in biomedical sciences. The FDA has approved the use of PCL for suture, controlled drug release devices and adhesion barriers. Due to its biodegradable quality, PCL is a common synthetic polymer used in 3D *in vitro* nerve culture systems (Daud et al., 2012;

Gee et al., 2012; Madigan et al., 2009; Ribeiro-Resende et al., 2009). Nanofiber Solutions™ (NS) is an Ohio based company that has specialized in the elaboration of PCL based 3D scaffolds for clinical applications as well as for life sciences research. NS uses electrospinning for the fabrication of PCL nanofibers that can be shaped into different configurations (Han et al., 2011; Johnson et al., 2009). They have successfully shown that they can grow human glioma cell lines (Agudelo-Garcia et al., 2011), mouse embryonic stem cells (Nam et al., 2011), neonatal rat ventricular cardiomyocytes (Kim et al., 2010), and rat primary chondrocytes (Nam et al., 2009). Due to the expertise of NS in the fabrication of costume 3D scaffolds we decided to contact them to obtain tube-shaped PCL scaffolds.

Growth of primary astrocytes was greatly improved in the PCL scaffolds in comparison to agarose gels. This further suggests that astrocytes require a harder surface to attach and grow. Experiments carried out using Poly-acrylamide (PA) gels with different ratios of bis-acrylamide/acrylamide to change the gel stiffness showed that rat primary astrocytes adhere better to hard gels in comparison to soft PA gels (Georges et al., 2006). Furthermore, the number of astrocytes adhered to the soft gel decreased significantly within 24 hours, suggesting that overtime astrocytes detached form soft surfaces (Georges et al., 2006).

As well as astrocytes, B35 cells adhered and grew on the PCL tubes. Upon serum starvation, B35 cells were able to extend neurites as was previously obserbed in agarose scaffolds treated with DbcAMP. However, we observed that the neurite length was dependent on the tube coating. In PCL tubes coated with fibronectin, B35 cells extended longer neurites than in tubes coated with Poly-L-Lysine. These results suggest that not only the mechanical properties of the scaffold but also the chemical composition of it is determinant in guiding cell behavior, specially considering we did not observed differences in neurite length among the wall thicknesses tested (200, 400 and 700µm).

Although both Fibronectin and PLL are natural macromolecules, Fibronectin is a normal component of the extracellular matrix of the CNS, while PLL is obtained by bacterial fermentation. Studies have been carried out comparing the performance of both macromolecules in different *in vitro* neuronal models (Chen et al., 2013; Evans et al., 2007; García-Parra et al., 2013). Similar to our results, mice primary hippocampal neurons (Chen et al., 2013) extended longer neurites when seeded on fibronectin or laminin coated PDMS or glass substrates in comparison to PLL coated ones.

Interestingly, neurons extended longer neurites when grew on glass in comparison to softer substrates made of PDMS. In contrast to our results, ear spiral ganglion neurons (Evans et al., 2007) seemed to extent neurites preferentially on PLL coated culture plates in comparison to fibronectin. However, this preference seemed to be dependent on the fibronectin concentration. At lower fibronectin coating concentrations the neurites showed no marked preference for PLL or fibronectin. These results suggest that a balance between substrate stiffness as well as ECM composition and concentration must be achieved to induce proper neurite outgrowth. It could also suggest different types of neurons respond differently to different substrates, hence the importance of testing different substrate conditions when developing a 3D *in vitro* model for a particular use.

Fibronectin coated PCL tubes seemed a fitting scaffold for the development of or 3D in vitro model, since it supported the growth of both astrocytes and neurons, and neurite extension could be induced in B35 cells. When we seeded B35 cells on top of astrocytes growing on Fb coated PCL tubes, some B35 cells were able to extend neurites without induction of neurite outgrowth by serum starvation, suggesting that astrocytes have an inductive effect on the B35 neurite outgrowth. It has been reported for primary spinal motor neurons of rat that neurite extension is improved when the cells are culture on top of cortical astrocytes or Schwann cells (Ragancokova et al., 2009) in comparison to glass. This study further supports the idea that astrocytes could have a neurite-inductive effect on neurons.

However when we serum starved the co-cultures to further induce neurite growth, both astrocytes and B35 cells died. In contrast to our results, several studies have suggested that astrocytes play a neuro-protective role *in vivo* and *in vitro*. In particular it has been shown that in astrocytes-neurons *in vitro* co-cultures, neuronal survival is improved after exposure to different neurotoxins such as Kainic acid (Ragancokova et al., 2009), Methylmercury (Yin et al., 2009) and Ammonia (Rao et al., 2005). Nonetheless, it has also been reported that the response of astrocytes to stress, in particular production of reactive oxygen species (Abramov et al., 2004; Nagai et al., 2007) and nitric oxide (Hu et al., 1997), can induce neuronal death *in vitro* . Yet, serum starvation not been reported to induce astrocytic death *in vitro (Chou and Langan, 2003)*. Furthermore, in preliminary experiments, we did not observed neuronal or astrocytic death when 2D co-cultures were serum starved to induce neurite outgrowth.

Therefore, it could be that the PCL scaffold in which the astrocytes grow can influence their response to serum starvation, thus inducing neuronal and astrocytic cell death. Though PCL tubes supported the monoculture of astrocytes and B35 cells, it did not support the survival of co-cultures in the conditions needed for the B35 cells to extent neurites. Therefore, we decided to look for another biomaterial for the 3D *in vitro* model.

Collagen type I is the most abundant collagen protein in the human body and it is therefore the most common material for 3D *in vitro* culture systems (Madigan et al., 2009; Mouw et al., 2014). Collagen is very versatile, can be use as hydrogel or can be electrospun into nanofibers. The mechanical properties of collagen scaffolds can be easily adjusted by varying collagen concentration and crosslinking (Gee et al., 2012) Collagen type I scaffolds have been used for the construction of artificial tissue for different systems such as skin, oral mucosa, bone, cartilage, bladder among others (Abou Neel et al., 2013; Yannas et al., 2010).

Within the nervous system, collagen scaffolds have been mainly studied to improve peripheral nerve regeneration *in vivo* (Archibald et al., 1991; Bozkurt et al., 2007; Ceballos et al., 1999; Kemp et al., 2009; Stang et al., 2005). More recently collagen has been used to improve axonal regeneration after spinal cord injury in in vivo models. It has been shown that the use of collagen scaffolds as a delivery system for Neuronal Progenitor Cells (NPCs) and a Endothelial Grow Factor Receptor (EGFR) neutralizing antibody in rats improves axonal regeneration *in vivo* (Li et al., 2013), while delivery of Chondroitinase ABS and Neurotrophin-3 improves axonal growth from embryonic rat DRGs *in vitro* (Liu et al., 2012). Han *et al.* showed that linear ordered collagen scaffolds with immobilized Brain Derived Neurotrophic Factor (BDNF) improved axonal regeneration after SCI (Han et al., 2009) and that co-immobilization of EGFR neutralizing antibody further improves axonal regeneration and reduces glia scar (Han et al., 2010). A recent study from the same group showed that the linear ordered collagen scaffolds with BDNF could also improve axonal regeneration and improve functional recovery in an *in vivo* canine model (Han et al., 2015).

Though the use of collagen scaffolds has yielded some modest but promising results in spinal cord injury recovery in mammals, the cellular and molecular mechanism by which the different cell types interact within each other and with the extracellular matrix to improve axonal regeneration is largely unknown. In order to develop therapeutic alternatives that can promote full SCI recovery in mammals, it is necessary

to understand the interactions among cells and with their environment in a model that can faithfully mimic the *in vivo* behavior of cells. Due to the success of collagen scaffolds to support axonal growth and cell survival both in vitro and in vivo, we decided to test collagen type I as material for our 3D *in vitro* model of the mammalian spinal cord.

The group of Conrado Aparicio from the Dentistry Department of the University of Minnesota has successfully used collagen type I for the fabrication of bone grafts (Li and Aparicio, 2013; Li et al., 2012) and dental implants (Marín-Pareja et al., 2014). In collaboration with the Aparicio lab we decided to test collagen hydrogels as possible substrates for our 3D in vitro model. When B35 cells were seeded onto Fb/Lm coated 3mg/ml collagen type I hydrogels, we immediately notice that the morphology of the undifferentiated cells, changed from being biopolar into round cells. Moreover, after induction of neurite outgrowth by serum starvation we did not observe differentiation of B35 cells or change in their morphology. However, when we cultured the B35 cells on Fb/Lm lyophilized collagen scaffolds sheets with the same concentration as the hydrogels, the cells recovered their biopolar morphology and extended neurites upon serum starvation. These results highlight once more the influence of the mechanical properties, aside of the chemical properties, of the scaffold on cell behavior. It has been previously reported than 0.5 mg/ml collagen hydrogels supported neurite outgrowth of primary embryonic rat cortical neurons (O'Connor et al., 2001); however, the B35 cells could not extend neurites in our hydrogels. This could be due to intrinsic differences between the cell types or the process of gel fabrication. As expected, collagen sheets coated with fibronectin and laminin also supported the growth of astrocytes that showed a normal morphology and expression of GFAP.

Astrocytes are major players in the response to SCI; they become hypertrophic, up-regulate the expression of GFP, proliferate and deposit components of the extracellular matrix, in particular collagen type IV and CSPG (Burda and Sofroniew, 2014). A common cause of spinal cord injury is the compression of the spine, usually as consequence of car crash (Boido et al., 2011). However, one of the most common models to study astrocyte response to injury is scratch assay in 2D *in vitro* monocultures. This injury model presents little relevance to how actual injuries occur *in vivo*. In scratch assays, proliferation of astrocytes and migration towards the injury is observed; however, GFAP up regulation or deposition of components of the extracellular matrix is very poor (Környei et al., 2000; Yang et al., 2009; Zhu et al., 2007). When we

performed compression injuries on collagen scaffolds we observed that astrocytes started to proliferate, revealed by the incorporation of EdU, but also showed other markers of reactive gliosis, such as GFAP and Vimentin upregulation, as well as collagen type IV and CSPGs deposition. As observed for the B35 cells, these results indicate that the substrate has a deep impact in astrocytes behavior in response to injury. Since the response to injury in our 3D culture system seems to mimic the response observed in mammals in vivo, the Fb/Lm coated collagen scaffolds seem to be a proper substrate to study the molecular and cellular mechanisms that govern spinal cord injury in mammals.

Although monocultures of astrocytes fail to evoke the proper response to injury, 2D co-cultures of rat astrocytes with a rat spinal cord-derived cell suspension seem to mimic some of the *in vivo* response to injury such as GFAP up-regulation, and CSPG deposition (Boomkamp et al., 2012). Although in this system the interaction of the cells with the extracellular matrix is neglected, it highlights the importance of cell-cell interaction in the recapitulation of proper *in vivo* response to injury. Though we observed an *in vivo* like response to injury in astrocytes cultures on collagen scaffolds, it was necessary to include other cell types involved in the response to SCI to obtain a more faithful model. Contrary to our previous results with PCL scaffolds, astrocyte-B35 co-cultures survived up to seven days, even in serum starving conditions, when cultured on Fb/Lm coated collagen type I tubes.

This result confirmed to us that it is possible to build our 3D system in a modular manner, allowing us to modulate gene expression in each different cell type at different time points to better understand the individual role of each cell in response to SCI. In the system proposed by Boomkamp et al. (Boomkamp et al., 2014; Boomkamp et al., 2012), they observed a bulk effect after drug treatment, but drew conclusions based only on neuronal behavior neglecting the effect of on the rest of the cells in their system. For example, Rho inhibition not only has an effect on neurite extension from neurons, but could be also altering expression of microRNAs in astrocytes as shown in the previous chapter of this thesis. Another disadvantage of the Boomkamp system is the inability of real time imaging. As shown for the PCL tubes we can independently transfect cells to express fluorescently tagged proteins before seeding them on the scaffolds and performing real time imaging. Therefore, a successful *in vitro* model should not only elicit

the proper *in vivo* response to stimuli, but it should also be dynamic and allow for manipulations that are not technically feasible *in vivo*.

The overall data suggest that the fibronectin-laminin coated tubes are a viable option for the development of the mammalian spinal cord injury *in vitro* model. Nonetheless, it is necessary to test whether the astrocytes-B35 cells' co-cultures will elicit the proper response to injury. It would be interesting to see whether the inclusion on B35 cells in the model affects the response to injury that we observed in the astrocytes cultures. Also, it is necessary to test other culture conditions during the differentiation stage of the B35 cells, such as the addition of neuronal supplements (BDNF, B27, N2 e.g.) that could help maintain cell viability over time. Lastly, for the *in vitro* model to better mimic *in vivo* conditions, it would be desirable to include other cell types that also play an important role in the response to SCI such as oligodendrocytes precursor cells (OPCs) or microglia (Burda and Sofroniew, 2014).

In conclusion, we showed that in the development of a 3D *in vitro* system that can properly recapitulate cell behavior in response to injury, the composition, architecture, chemical and mechanical properties of the material used for the scaffold are critical parameters. Such parameters can have a profound influence in cell-cell interactions and the response of cells to external stimuli; therefore, affecting the relevance of the *in vitro* model. We also showed that a 3D system composed by collagen type I scaffolds coated with fibronectin and laminin and seeded with primary rat astrocytes and B35 neuronal cells, it's a promising start to develop a functional *in vitro* mammalian spinal cord where the molecular and cellular mechanisms of repair after spinal cord injury can be studied.

Figures

Figure 4-1. Cell growth on agarose scaffolds.

(A) Tube shaped 1% agarose scaffold. (B-D) B35 cells grew in the luminal surface of the agarose tube marked by the asterisk in the DIC image (B) DAPI counter stain (C) and merge image (D). (E-G) B35 cells stained against anti-β-III-tubulin (E) and counter stained with DAPI (F) after treatment with DbcAMP to induce neurite outgrowth (arrows) (G) Merged image. (H-J) Primary rat cortical astrocytes failed to grow on 1% agarose scaffolds. (H) DIC image (I) DAPI counter stain (J) and merge image.

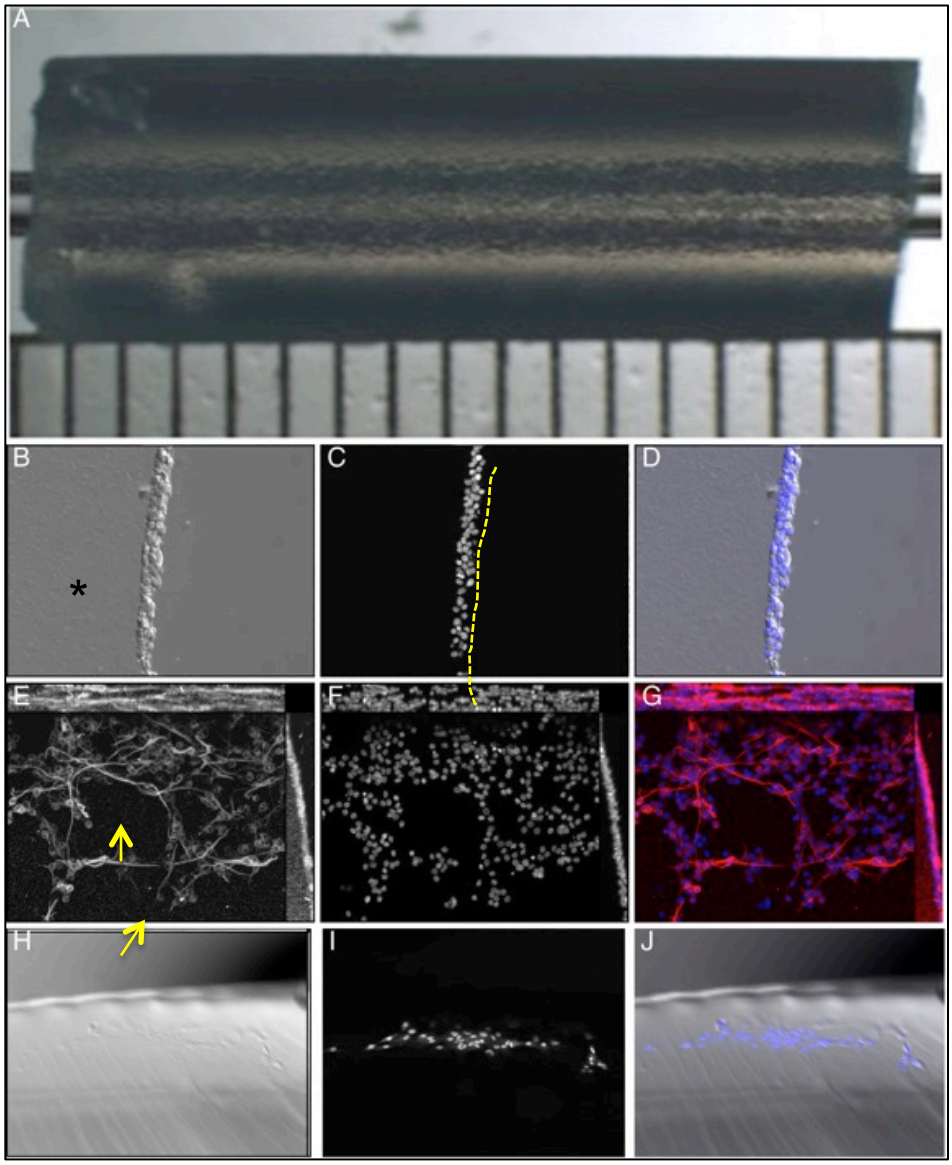

Figure 4-2. Cell growth on PCL scaffolds.

(A,B) PCL nanofibers tube (C-E) Primary rat cortical astrocytes immunostained for GFAP (red) and counter stained with DAPI (blue) Astrocytes could be imaged at 10X (C) 20X (D) and 40X(E). (F-H) B35 cells transfected with GFP-Tubulin (F). (G) DIC image and (H) merged image. (I-N) B35 cells extended neurites on fibronectin (I-K) or PLL (L-N) coated PCL tubes with a wall thickness of 200μm (I,L) 400μm (J, M) and 700μm (K,N).

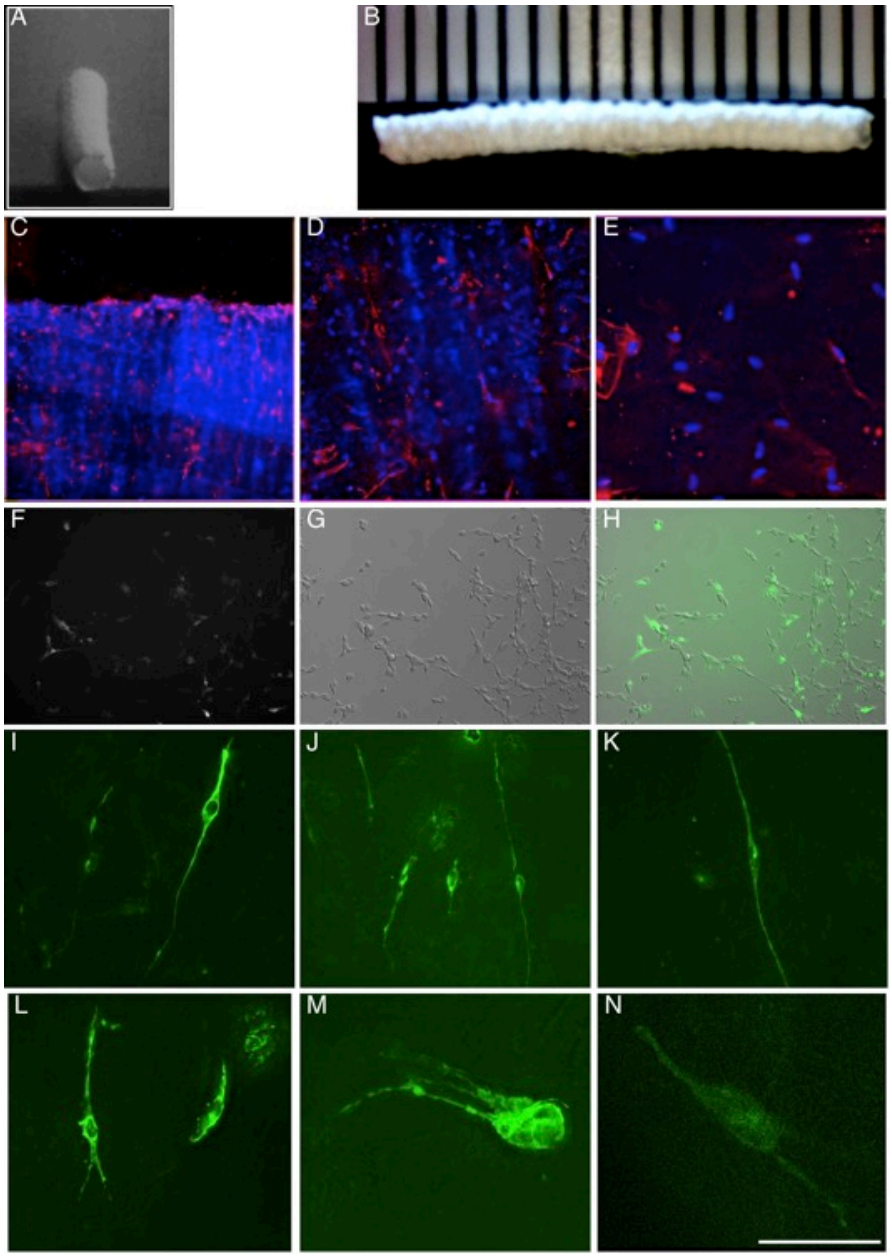

Figure 4-3. Co-cultures on PCL scaffolds.

(A-C) Primary rat astrocytes transfected with RFP-Histone2B. (A) RFP signal (B) DIC image and (C) merged image. (D) GFP-Tubulin transfect B35 cells grew neurites 1 day after seeding on RFP-Histone2B transfected astrocytes on PCL tubes. (E) Both GFP-Tubulin transfected B35 cells and RFP-Histone2B transfected astrocytes died after 4 days of serum starvation to further induce the differentiation of the B35 cells.

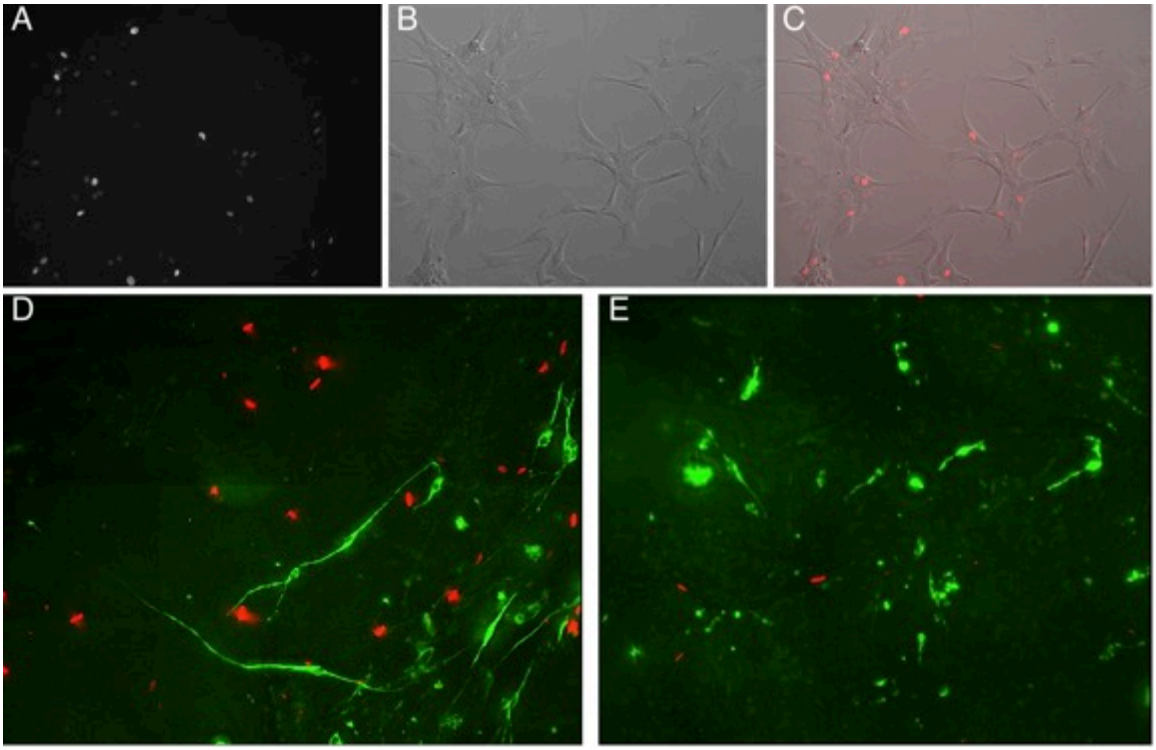

Figure 4-4. Cell growth on collagen scaffolds.

(A-D) GFP-tubulin transfected B35 cells seeded on collagen hydrogels (A,B) 1 day after seeding or (C,D) 6 days after serum starvation . (E-H) GFP-tubulin transfected B35 cells seeded on lyophilized collagen scaffolds (E,F) 1 day after seeding or (G,H). (A,C,G,E) GFP signal and (B,D,F,I) DIC image.

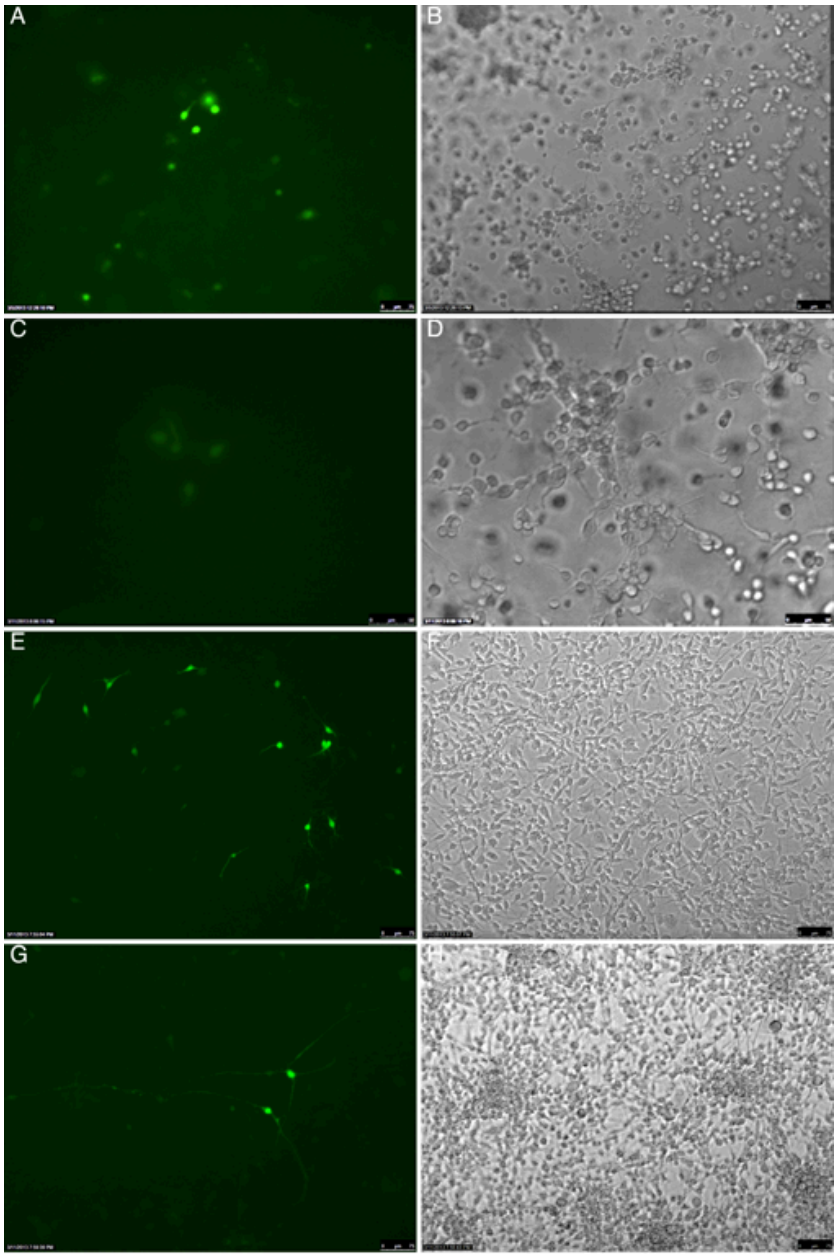

Figure 4-5. Astrocytes response to injury on collagen scaffolds.

(A-D) Astrocytes stained for GFAP (B,D) and counter stained with DAPI (A,C) before (A,B) and after injury (C,D). Arrows indicate group of cells up-regulating GFAP expression. Astrocytes stained for EdU (F,I) and counter stained with DAPI (E,G) before (E,F) and after injury (G,I). Doted line shows the injury site in (C,D,G,H)

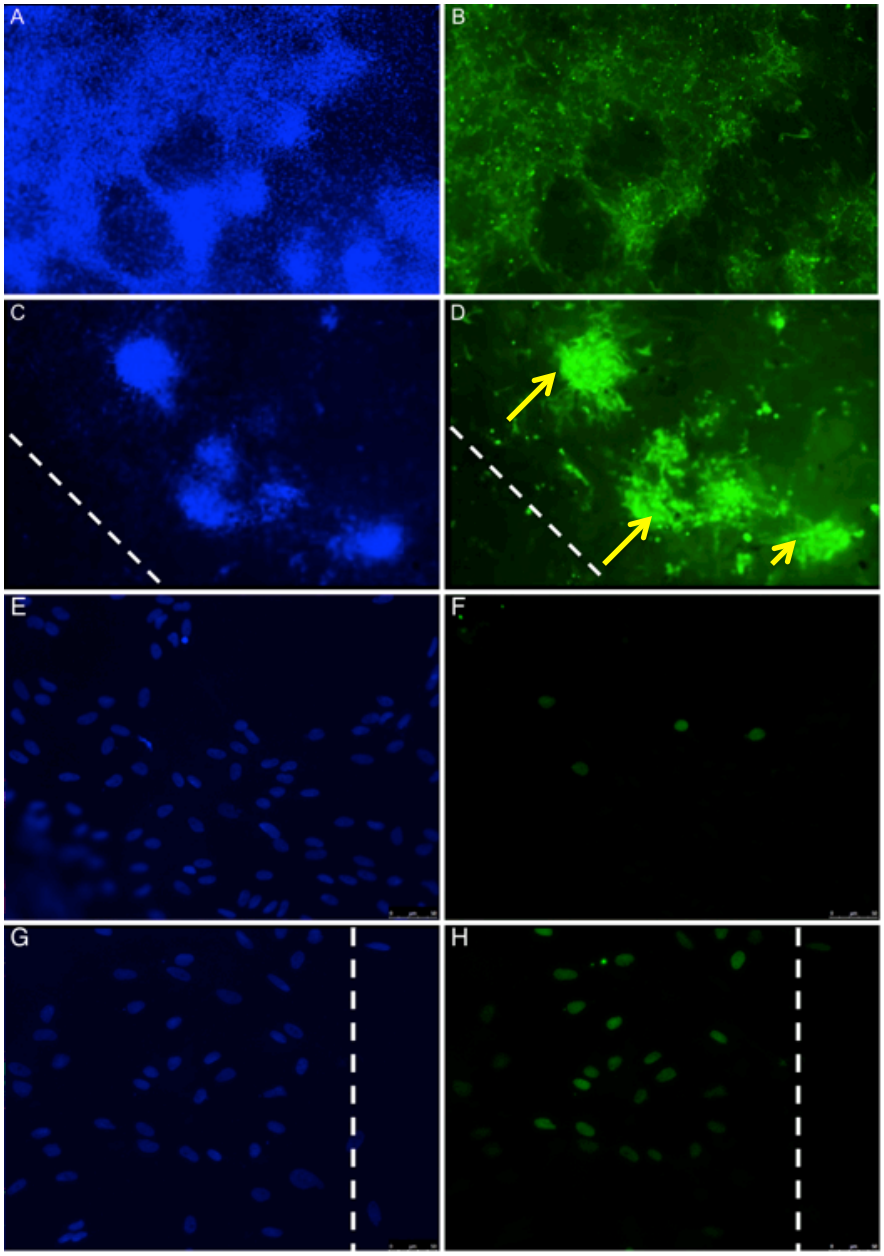

Figure 4-6. Astrocytes response to injury on collagen scaffolds.

(A-F) Astrocytes stained for GFAP (A,D) Vimentin (B,E) before (A-C) and after injury (D-F) and counter stained with DAPI. (C,F) Merged images. Astrocytes stained for Collagen IV (G,H) or CSPG (I,J) in red, GFAP in green and counter stained with DAPI before (G,I) and after injury (H,J). Arrows in (H) indicate collagen IV deposition at the injury border. Doted line shows the injury site in (D-F,H,J).

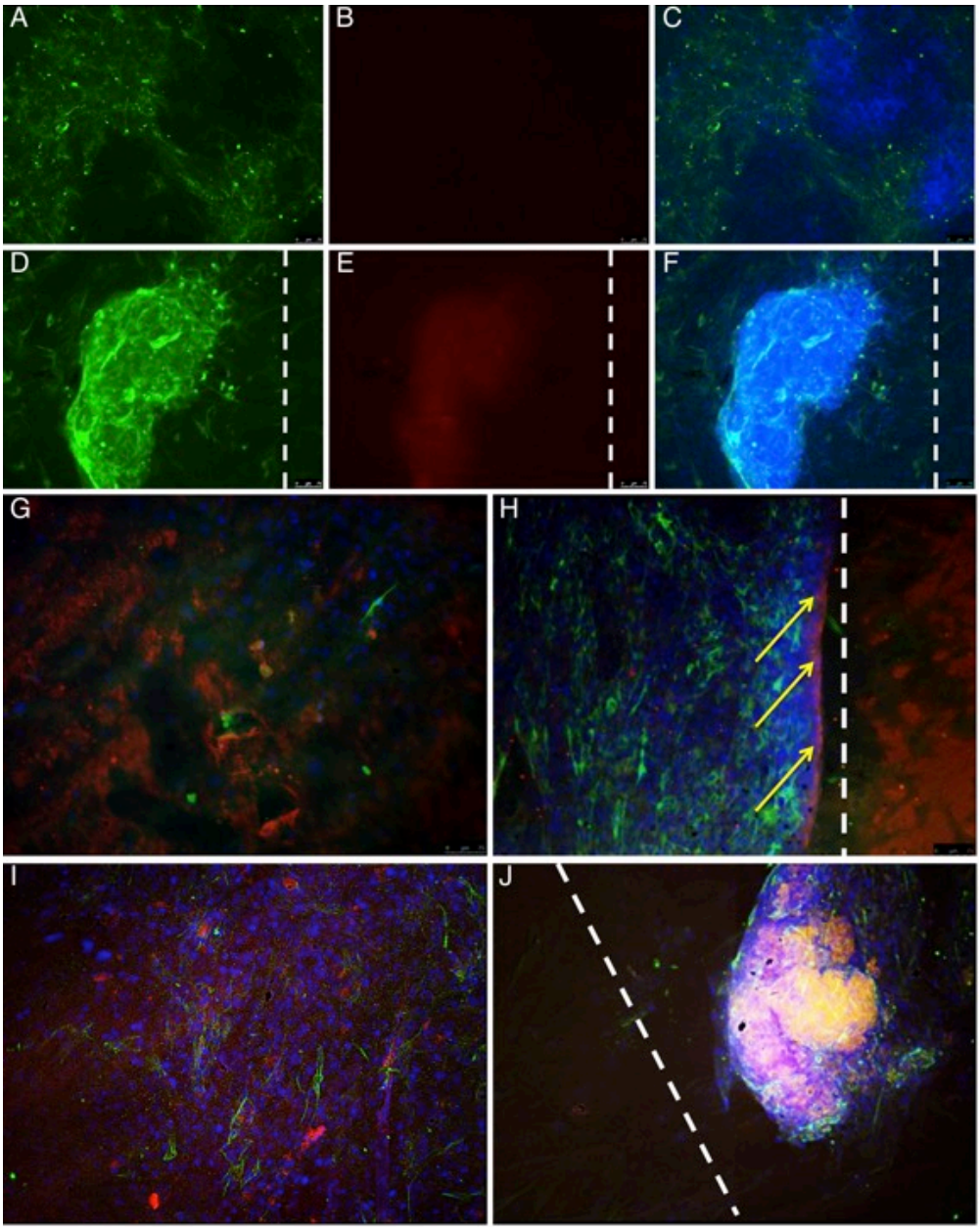

Figure 4-7. Co-cultures on collagen scaffolds.

(A-C) Collagen scaffolds in the shape of sheets (A) or tubes (B,C). (D,E) B35 cells stain for b-III-tubulin in green, grew neurites on astrocytes stained for GFAP in red 1 day after seeding (arrows in D) and keep on growing neurites six days after serum starvation (arrows in E).

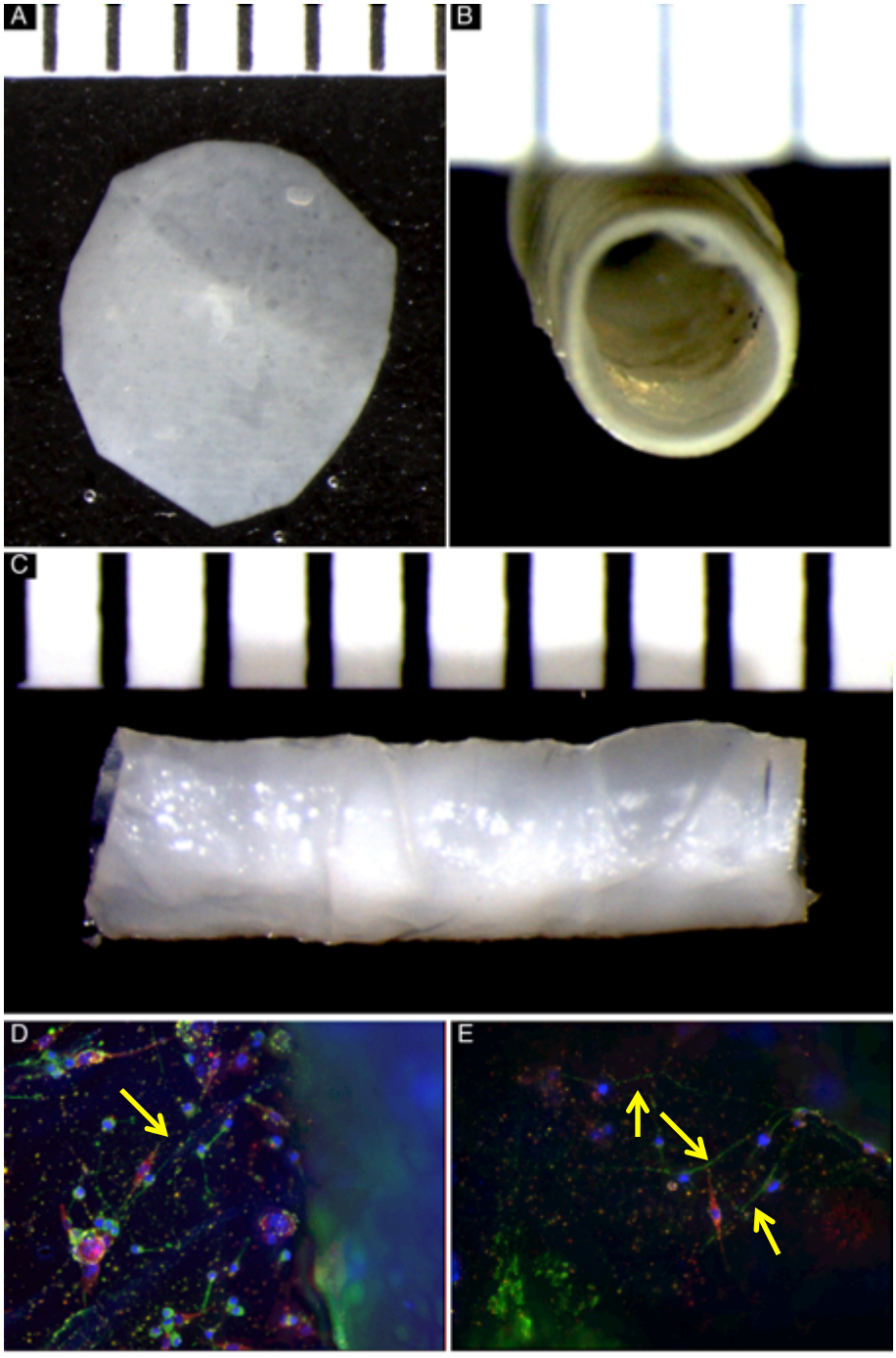

Tables

Table 4-1. Comparison of neurite length for B35 cells growing on Fibronectin or PLL coated PCL tubes with 200, 400 or 700µm wall thicknesses.

	Fibronectin			Poly-L-Lysine		
	200 µm	**400 µm**	**700 µm**	**200 µm**	**400 µm**	**700 µm**
Count	34	21	16	18	3	4
Mean	86.00567	93.16445	88.25221	45.63383	64.5848	63.30023
Minimum	8.1236	21.6976	26.3376	13.1095	50.3523	36.3526
Maximum	214.1338	223.7147	226.7253	110.7908	81.3689	101.0895

Table 4-2. ANOVA analysis of neurite length differences for B35 cells growing on Fibronectin or PLL coated PCL.

Source of Variation	SS	df	MS	F	p-level	F crit
Between Groups	11,604.80168	1	11,604.80168	4.96218	0.02908	5.66451
Within Groups	166,043.99361	71	2,338.6478			
Total	177,648.79529	72				

Table 4-3. ANOVA analysis of neurite length differences for B35 cells growing on Fibronectin coated PCL with 200, 400 or 700μm wall thicknesses.

Source of Variation	SS	df	MS	F	p-level	F crit
Between Groups	2,955.12128	2	1,477.56064	0.51284	0.60174	4.21553
Within Groups	152,701.13907	53	2,881.15357			
Total	155,656.26036	55				

Chapter 5: Conclusions

The present work focused on trying to understand the molecular pathways that regulate the cellular response to spinal cord injury. To this end we decided to take a comparative analysis approach, by looking at the differences and conserved mechanisms in the response to spinal cord injury between the axolotl, as model for regeneration competent species, and the rat, as model for regeneration incompetent mammals. In both model systems we studied how changes in post-transcriptional regulation at the microRNA level seem to play key role in directing the cellular response after spinal cord injury to create a permissive or non-permissive environment for regeneration. Those changes in post-transcriptional regulation appear to be triggered by alterations of the cellular cytoskeleton caused by mechanical stress both in rat and in the axolotl. We also attempted to develop a 3D *in vitro* model for the mammalian spinal cord, in which we could get a better understanding of the afore mentioned cellular processes by using experimental approaches that in an *in vivo* model could be technically challenging, time consuming and expensive.

Due to its prevalence and various debilitating outcomes in humans, a lot of effort has been invested into finding therapies to improve spinal cord repair after injury. To the date our understanding of the cellular and molecular mechanisms that govern the response to injury in mammals has been obtained mostly from *in vivo* models such as rat and mouse. Thanks to this body of work we know that the major impediment for axonal regeneration in mammals after injury is the formation of the glial scar. Though many of the inhibitory components of the glia scar have been identified, a therapy for complete functional regeneration is yet to be developed. On the other hand, studies carried out in animal models that have the natural capacity to regenerate such a salamanders, zebrafish and frog-tadpoles, have offered new insights into the phenomenology of spinal cord injury in mammals. However this work is the first study in which both regeneration competent and non-competent models are compared side by side to find whether conserved molecular mechanism that induce regeneration in the axolotl can be modulated to improve spinal cord regeneration in mammals.

This comparative approach allowed us to identify miR-125b as a key regulator of the response to spinal cord injury in both mammals and axolotls. Though we demonstrated that miR-125b after injury regulates the expression of the repellent axon guidance cue Sema4D, we propose that miR-125b works in a complex regulatory network to modulate the expression of glia scar and axonal growth related genes to

create a permissive environment for regeneration in axolotls or in rats in which miR-125b was overexpressed after injury. It would be interesting to study the role of the other microRNAs found in our study during spinal cord regeneration in the axolotl to understand whether the ability to regenerate spinal cord is due to the combined effect of the regulation of different pathways by different microRNAs. It would be also interesting to study the effect on rats of microRNAs that we found to be exclusively expressed in the axolotl and dissect whether the capacity of regeneration is due to the presence of this set of exclusive miRNAs in the axolotl or the rather by misregulation of conserved miRNAs in rats. Continuing to use this comparative approach could be a streamline strategy to understand conserved and non-conserved biological processes that govern the response to spinal cord injury, and also to propose alternative therapies to the treatment of spinal cord injury in humans.

In the axolotl, miR-125b expression in response to injury seems to be tightly regulated to properly create a permissive environment for regeneration. Therefore understanding the mechanisms that regulate the expression of this miRNA could shed light in our understanding of the differences between mammals and axolotls in the cellular response after injury. Though the activation of different signaling pathways has been described for different model systems in response to injury, how these pathways are activated still remains unclear. In the present work we showed that changes in the cell cytoskeleton can induce changes in the expression of miR-125b, and that the dynamic state of the same can alter the proper response of miRNA expression in response to injury.

To understand how changes in cellular cytoskeleton could induce changes in the expression of miR-125b we treated axolotls with drugs that alter the dynamics of the cytoskeleton, in the presence and in the absence of injury. Depolymerization of the actin cytoskeleton with in the absence of injury induced the same decrease in miR-125b expression levels observed in injured animals, while stabilization of the actin cytoskeleton seemed to stabilize the levels of miR-125b. Although depolymerization or stabilization of microtubules in the absence of injury did not induce changes in the expression of miR-125b, in the presence of injury the normal decrease of the expression of the microRNA was prevented. This suggests that injury-induced depolymerization of actin cytoskeleton could trigger transcription repression of miR-125b in a microtubule dynamic dependent manner. In other words, biomechanical regulation could be the key

pathway through which the cells are able to respond to spinal cord injury to create a permissive environment for regeneration in axolotls.

In recent years biomechanical regulation of gene expression has been shown to be an important mechanism through which cells can sense changes in their environment and adapt their cellular response in order to differentiate, proliferate or migrate. During spinal cord regeneration these three processes are key to ensure a proper regeneration of the spinal cord and other structures such as limbs in the axolotl. However the complete pathway through which mechanical cues are transduced into changes in gene expression is still not completely understood. Here we showed that a possible pathway might involve the activation of the AP1 transcription factor, in particular the c-Fos transcription factor that is one of the members of the AP1 transcription factors family. We also showed that the small GTPase RhoA might mediate the activation of c-Fos in response to changes in the actin cytoskeleton. Although there are still gaps in our model, such as showing the direct regulation of miR-125b expression by c-Fos or determining how the Rho pathway is activated by the actin cytoskeleton, the known interaction of RhoA with cellular cytoskeleton dynamics and RhoA with c-Fos, shows that our model could be in agreement to the current knowledge in the field of biomechanical regulation. It would be also important to study the role of myosin II and other important components of biomechanical sensing such as the Focal adhesion kinase. Also, it would be interesting to see whether other early cues of injury, such as increase in intracellular calcium, also play a role in the regulation of miR-125b in response to injury.

We used again a comparative analysis approach to try to determine whether biomechanical regulation of miR-125b in response to injury is a mechanism particular to the axolotl to promote spinal cord regeneration, or could be a conserved mechanism that is misregulated in non-regeneration competent mammals. We showed that, though injury can alter cellular cytoskeleton and that this changes can activate c-Fos in a RhoA dependent manner in primary rat astrocytes *in vitro*, we were not able to show that those changes lead consistently to a change in the transcription of miR-125b. This lack of consistency could have been caused by the intrinsic variability of primary cultures or the artificial environment created by *in vitro* cultures. Therefore, to better study the pathways through which the mechanical cues can influence regulation of miR-125b after injury in mammals cell behavior, the development of a better *in vitro* system to study seems to be a good strategy circumvent the afore mentioned problems.

We proposed to develop a 3D *in vitro* culture system to model the mammalian spinal cord. 3D culture systems have been shown to better mimic the *in vivo* environment in comparison to 2D cultures, while still maintaining the advantages of *in vitro* cultures. We showed that in the development of a 3D *in vitro* system, the selection of the proper material for the scaffold is a key step. While the chemical composition of the material can influence cell attachment and survival, the mechanical properties can influence gene expression and cell behavior as discussed above. We showed that from the materials tested, collagen type I scaffolds seemed to give the best environment for the cells to attaché, grow and behave in a *in vivo* like manner. In particular, we found that primary rat cortical astrocytes seeded on fibronectin-laminin coated collagen scaffolds can give a proper response to injury by proliferating and overexpressing GFAP, vimetin, collagen IV and CSPG. Though this model is still in its first stages of development, observing the landmarks of reactive gliosis after injury is an indication that the model can faithfully represent the *in vivo* environment of the cells to give the proper response to external stimuli.

To fully develop the model it is necessary to establish culture conditions for including other cell types such as neurons and oligodendrocytes. We showed that in the present conditions, we can co-culture primary rat astrocytes and neuroblastoma derived cell line B35 neuronal precursors on collagen coated scaffolds. We also show that in these conditions we can induce the B35 cells to extend neurites and differentiate into neurons. Though we were able to maintain the cultures up to a week, cell survival of the cells seems to be affected by the culture conditions. Once these co-cultures are established, it would be interesting to see if with the addition of neurons the astrocytes still respond in an *in vivo* manner to injury. Our goal is to have a model were we can keep using the comparative approach between axolotls and mammals to understand the cellular and molecular mechanism that make the response to injury between species so different.

In the present work we have shown that miR-125b is a key regulator of the response to spinal cord injury in mammals and in axolotls. In axolotl the expression of miR-125b is tightly regulated by changes in the actin cytoskeleton and the activation of the RhoA-c-Fos pathway to create a permissive environment for regeneration. By developing an *in vitro* model of the spinal cord we hope to establish how the regulation

of miR-125b can be modulated in mammals to provide alternative therapies for treatment in humans.

Chapter 6: Materials and Methods

Animals

Housing, natural breeding and experimental procedures carried on axolotls were done following the protocols established by the Max Plank Institute for Cell Biology (Dresden, Germany) and by the Research Animal Resources center (RAR) of the University of Minnesota (Minneapolis/Saint Paul, USA) under the IACUC protocol# 1201A0838. The animals were housed in a room with controlled temperature (15-18°C) and 12 hours light cycles. The animals used in this project were fed daily with Brine shrimp prepared from unhatched eggs. 48 hrs prior to feeding unhatched eggs are incubated in a 20% marine salt solution at 28°C with bubbling aeration and constant light. On the feeding day, the shrimp sludge was filtered and the precipitated was re-suspended in distilled water.

The water from the growing tanks or cups was changed daily. Animals were kept in filter-purified water or in a 40% Holtfrteter's Solution (59 mM NaCl, 0.67 mM KCl, 0.76 mM $CaCl_2$, 2.4 mM $NaHCO_3$). The thanks were scrubbed with granular NaCl during the water change. For all the experiments the animals were anesthetized by submersion in 0.01% p-amino benzocaine. After the procedure (injury or injection) the animals were put back into fresh water. 20 min after putting them back in water the animals were monitored to check for resuming of swimming. The animals were monitored for survival for three days after the procedure. For tissue collection, the animals were anesthetized as described and after the sample collection they were sacrificed by overdose with p-amino benzocaine (10% in ethanol). The carcasses were kept at -20°C until they were incinerated by the RAR.

Housing and surgeries carried on rats were done according the protocols approved by the animal care committee of the Ottawa Hospital Research Institute (Ottawa, Canada).

Cells

Rat primary cortical astrocytes

Rat primary cortical astrocytes were purchased from Invitrogen or Lonza. Cells were culture in DMEM (Gibco) + 15% Fetal calf serum (Sigma or Hyclone) + 1% Penicillin/Streptomycin (Gibco) at 37°C in a 5% CO_2 incubator. Media was changed

every third day and cells would be passaged once they were approx. 80% confluent. For passaging, cells were washed once with PBS and incubated 5-15 minutes with a enzymatic cocktail (StemPro Accutase, Live Technologies) at 37°C. The enzymatic reaction was stopped by adding fresh media to the flask and cells were washed off the surface of the flask. Cells were then split 1 to 2. The cells were passaged until passage 5 (P5). P5 cells were used for the experiments. The cells were characterized by immunostaing against Glial Fibrillary Acidic Protein (GFAP, 1:800 dilution, Millipore), beta-III tubulin (1:1000 dilution, Sigma), S100beta (1:50 dilution, AbD Serotec) and Sox 2 (1:500 dilution, Millipore).

Rat neuroblastoma cell line (B35 cells)

A rat neuroblastoma cell line (B35 cells) was purchased from ATCC. Cells were culture in DMEM + 10% Fetal calf serum + 1% Penicillin/Streptomycin at 37°C in a 5% CO_2 incubator. Media was changed every other day and cells would be passaged once they were approx. 80% confluent. For passaging, cells were washed once with PBS and incubated 5 minutes with 0.25% Trypsin-EDTA (Gibco) at 37°C. Trypsin was inactivated by adding fresh media to the flask and cells were washed off the surface of the flask. Cells were then split 1 to 5 or 8. The cells were characterized by immunostain against GFAP, beta-III tubulin, S100beta and Sox 2.

Neuronal differentiation was induced by culturing B35 cells on Fibronectin (2.5 µg/cm^2, Sigma) Laminin coated dishes (1.5 µg/cm^2, Sigma) with DMEM or OptiMEM+ 0.5-1% Fetal calf serum + 1%Penicillin/Streptomycin for 2 days. Differentiation was also induced by culturing the cells in DMEM + 1 mM Dibutiryl-cAMP (DbcAMP) + 1%Penicillin/Streptomycin for 2 days. Differentiated B35 cells were characterized by immunostain against GFAP, beta-III tubulin.

Rat Brain Oligodendrocyte Precursor Cells (Oli-19 OPCs)

Rat brain Oligodendrocyte Precursor Cells (Oli-19 OPCs) were kindly donated by Doctor Rick Cohen. The cells were culture in DMEM:F12 (1:1) + 15% B35 cells Serum Free Conditioned Media + 1% N2 Suplement (Gibco) + 1% Insuline-Transferrin-Selenium (Gibco) + 1% Penicillin/Streptomycin at 37°C in a 5% CO_2 incubator. 50% of media was changed every other day and cells would be passaged once they were approx. 50% confluent. For passaging, cells were washed once with cold PBS and

incubated 2 minutes with StemPro Accutase, Live Technologies at 37°C. The enzymatic reaction was stopped by adding fresh media to the flask, and cells were washed off the surface of the flask. The cell suspension was centrifuged at 1000 RPM at 4°C for 7 min. Cells were then re-suspended in 1ml of fresh media and split 1 to 2. The cells were characterized by immunostaining against GFAP, Oligodendocyte Marker (O4, 1:100 dilution, Sigma), NG2 (1:200 dilution, Invitrogen) and Myelin-Oligodendrocyte Specific Protein (MOSP, 1:1000 dilution, Millipore).

B35 cells Serum Free Conditioned Media was prepared by culturing 80% confluent B35 cells with DMEM:F12 (1:1) + 1% N2 Suplement (Gibco) + 1%Penicillin/Streptomycin for 4 days. Afterwards the media was withdraw, filter sterilized (0.2µm Millex-HV Filter, Millipore) and stored at -20°C.

Oligodendrocyte differentiation was induced by culturing 50% confluent OPCs with DMEM:F12 (1:1) + 1% N2 Suplement (Gibco) + 1% Insuline-Transferrin-Selenium (Gibco) + 1%Penicillin/Streptomycin for 2 days. Differentiated OPCs were characterized by immunostain against GFAP, Oligodendocyte Marker (O4, Sigma), NG2 (Invitrogen) and Myelin-Oligodendrocyte Specific Protein (MOSP, Millipore).

Human Embryonic Kidney cells (HEK 293T cells)

Human Embryonic Kidney cell line (HEK 293T cells) was kindly donated by Doctor Federico Calegari. Cells were culture in DMEM + 10% Fetal calf serum + 1% Penicillin/Streptomycin at 37°C in a 5% CO_2 incubator.. Media was changed every other day and cells would be passaged once they were confluent. For passaging, cells were washed once with PBS and incubated 5 minutes with 0.25% Trypsin-EDTA at 37°C. Trypsin was inactivated by adding fresh media to the flask and cells were washed off the surface of the flask. Cells were then split 1 to 5.

Axolotl Dermal Fibroblast cells (AL1 Cells)

Axolotl Dermal Fibroblast cells were culture in Leibovitz's L-15 Media + 10% Fetal calf serum + 1% L-Glutamine (Gibco) + 1% Insuline-Transferrin-Selenium + 1% Penicillin/Streptomycin at 26°C in an incubator. Media was changed every third day and cells would be passaged once they were approx. 80% confluent. For passaging, cells were washed once with PBS and incubated 5 minutes with 0.25% Trypsin-EDTA at

26°C. Trypsin was inactivated by adding fresh media to the flask and cells were washed off the surface of the flask. Cells were then split 1 to 2.

Comparative array assay

Generation of tissue Samples

Mature adult axolotls were used for these experiments. Animals were anesthetized using 0.1% p-aminobenzocaine (Sigma). Using surgical scissors an incision was made in the skin above the position of the hind limb, a portion of the skin and muscle was removed and then a laminectomy was performed. A 2mm portion of the exposed spinal cord was removed. The skin was replaced over the wounded site and the animals were placed back into water. In control animals only a laminectomy was performed.

At 1 and 7 days post injury a similar procedure was performed and the tissue of the injury site plus 1mm rostral and caudal to the injury site was collected and placed immediately into liquid nitrogen.

For this study adult female Sprague-Dawley rats (250-230g) were used. Before surgery, 3 ml of normal saline was injected subcutaneously. For the surgery rats were anesthetized with 2-5% Isoflurane, shaved, and the skin was treated with povidone iodine (Betadine). A midline incision was made in the skin and paraspinal muscles were dissected between the thoracic vertebrae T7 and T9, under a surgical microscope (Zeiss). To expose the spinal cord a laminectomy was performed at T7-T9 with a 6-mm serrated malleus nippers (Stortz). Complete transection of the spinal cord was done at T8 using microscissors. Complete tissue severing was confirmed by passing a glass hook around the ventral side of the injury and by careful inspection of the tissue. The bleeding in the area was stabilized with Surgifoam (Ethicon). In control animals only a laminectomy was performed. Tissue samples were collected 1 day and 7 days post injury from the ventral and caudal side of the injury. For each time point a total of 10 animals per group was used.

Comparative microRNA array analysis

Total RNA was extracted from the tissue samples using the Trizol ® protocol (Invitrogen). A MicroRNA array containing 3361 probes of miRNAs expressed in vertebrates (Vertebrata miRNA Array, MRA-1033C, LC Science) was run. The results were reported as average signal, and were filtered using as inferior cutoff an average signal of 500. Then the filtered data for each miRNA was expressed for each condition (Rostral or Caudal, 1 or 7 days post-injury) as a fold of change in a log2 scale:

$$F.C. = Log_2\left(\frac{Av.Exp.Cond}{Av.Control}\right) \qquad \text{[Eq. 1]}$$

where *F.C.* is fold of change, *Av.Exp.Cond* is the average signal of the experimental condition and *Av.Control* is the Average signal of the control condition.

To facilitate the analysis of the array data, identical miRNAs of different species (bta-miR-126 and hsa-miR-126 e.g.) were grouped along with miRNAs with the same precursor or close related mature sequences (mdo-miR-26, hsa-miR-26a e.g.) as long as the seed sequences were still conserved. Then, for each system (rat and axolotl) the number of miRNAs that change their expression in response to injury was quantified, and miRNAs that change their expression in both systems were identified. For this miRNAs that were differentially expressed that there expression differ between rat and axolotl at 1 or 7 d.p.i on the rostral or caudal site, in both systems (14 in total) the predicted targets were determined using open source bioinformatics software (TargetScan, PicTar, microRNA.org) and 7 miRNAs with targets related mainly to axonal outgrowth or glia scar formation were preselected for further analyses.

In vivo modulation of miR-125b levels in Axolotls

Injection set up

Microinjection needles were pulled from glass capillaries (Harvard Apparatus, Cat. No. GC120F-10) using a needle puller (Sutter Instruments, model P-97) set up at the specific conditions provided by the equipment to obtain microinjection needles. Injection needles were back filled with 2 µl of the injection solution (see below) using a microloader tip (Eppendorf). The needle was then placed into the nozzle of a pressure injector (World Precision Instruments, model PV 820) attached to the micromanipulator

(World Precision Instruments, model M3301R). The pressure injector was set at 20 psi ejection pressure and 100ms timed ejection.

Under the dissecting microscope (Leica, model M80) the very tip of the needle was gently broke off using forceps, to open the end of the needle.

Injection solution

The injection solution to increase the expression levels of miR-125b was prepared by diluting a stock solution of 20μM miR-125b mimic (miRIDIAN, Dharmacon) into PBS to reach a final concentration of 10 μM. To help visualize the injection solution in the injection needle, fast green (Sigma) was added to a final concentration of 0.2 mg/ml.

To decrease expression levels of miR-125b, a 20 μM miR-125b hairpin inhibitor (miRIDIAN, Dharmacon) injection solution was prepared by diluting a 40 μM stock solution in PBS + 0.2 mg/ml fast green.

Spinal cord Injection and injury

At day 0, 3 to 5 centimeters long axolotls were anesthetized by submersion in 0.01% p-amino benzocaine. Once the animals were motionless they were placed on a sylgard dish with the tail lying flat using the tweezers. The animals were hold in place by putting four insect pins through the tail fin into the sylgard. Under the dissecting microscope, the injection needle was inserted into the spinal cord, using the micromanipulator. The injection solution was then released by pressing the pedal of the injector. Green color running up and down the spinal cord was a positive indicative that the spinal cord had been targeted. The same spot was injected five more times.

To facilitate the Mimic or Inhibitor uptake, the injection site was electroporated. For the electroporation, axolotls were covered with PBS and custom-made electrodes were placed on both sides of the tail, opposite to each other. The electroporator (BTX, model ECM 830) was set up at 5 square pulses, 50 ms, 50 V. The animals were elcetroporaded a second time inverting the position of the electrodes.

Animals injected with 10μM Control Mimic (Dharmacon, ThermoScientific) or PBS + Fast Green solution were used as controls. 30 min to 1 hour after the injections an ablation injury was performed by removing a portion of the spinal cord. Under the dissection microscope, the skin and muscles above the spinal cord 7 to 10 muscles

bundles caudally from the hind limbs was removed using the tip of a hypodermic needle. Spinal cords were transected on the caudal and rostral edges of the skin-free muscle segment (approx. 300 µm) with the hypodermic needle. Putting the hypodermic needle between the notochord and the spinal cord pulled out the transected spinal cord portion. The remaining tissue was removed with the hypodermic needle.

After the injury, the animals were put back in water, and were re-injected at 2 and 4 days after the injury into the spinal cord at a distance of 5 muscles bundles rostral and caudal from the injury site.

Whole Mount Staining

7 days after injury, tissue samples were collected amputating the tail of anesthetized axolotls at the level of the hind limb. The tip and the fins of the tail were removed and the tissue samples were fixed in freshly made 4% Paraformaldehyde (PFA) (Sigma) in PBS for 1 hour. To improve tissue penetration of the antibody the samples were washed with 0.1% Tween-20 (Sigma) in PBS (PBST, 3 times for 5 min), digested with 20 µg/mL Proteinase K in PBS (30 min) and postfixed in 4% PFA (10 min). The samples were washed with in PBST (3 times for 5 min) and 0.2% Triton X-100 (Sigma) in PBS (PBSTX) 3 times for 10 min. To prevent non-specific binding of the antibodies, the samples were block in 10% Goat serum (Sigma) in PBSTX for 1 hour at room temperature. Mouse anti-β-III-tubulin (Sigma) primary antibody was diluted 1:1000 in blocking buffer and samples were incubated in the antibody solution overnight at 4° C. To eliminate the unbound antibody, the next day the tissue samples were washed in PBST (4 times for 30 min). The secondary antibody (Goat anti-mouse Alexa Fluor 568 , Invitrogen) and DAPI were diluted 1:200 in blocking buffer and the samples were incubated in the antibody 1 hour at RT. To eliminate the unbound antibody, samples were washed in PBST(4 times for 30 min).

Prior to imaging, samples were cleared with 1:2 Benzyl alcohol:benzyl benzoate (BABB) (Sigma). Tissue samples were dehydrated by incubating in 50:50 PBS:Methanol (10 min) and 100% Methanol (twice for 10 min). Then the samples were incubated in BABB (10 min) and mounted into a cover slip using BABB as mounting media.

Images were taken in an inverted Zeiss Apotome Microscope (Carl Zeiss) at 10X magnification.

All incubations and washes were carried out at room temperature unless indicated otherwise.

Acid Fuchsine Orang G (AFOG) Staining

7 days after injury, tissue samples were collected as described and fixed in freshly made 4% PFA, 0.01% Glutharaldehyde (Sigma) in PBS for 3 hours. After fixation, samples were washed in PBS (3 times for 5 min) and in PBST (3 times for 5 min). Tissue samples were incubated 10 min in 50:50 PBS:30% Sucrose in PBS and overnight in 30% Sucrose in PBS, before embedding the samples in Tissue Tek (Sakura). Frozen tissue samples were cut into 20 µm thick longitudinal sections. Tissue sections were post-fixed in Bouin's solution (Sigma) overnight and washed with running ddH_2O for 30 min. Then, the sections were stained by successive 5 min incubation in 1% Phosphomolybdic acid (Sigma), AFOG solution (0.5% Aniline Blue, Waldeck-Chroma; 1% Orange G, Fluka; 1.5% Acid Fuchsin, Sigma) and 0.5% acetic acid (the slides were washed with running ddH_2O for 5 min between each incubation). After the staining step, the slides were dehydrated by successive incubation in 96% Ethanol (2 min), 100% Ethanol (2 min) and Xylene (5 min), and mounted with Cytoseal 60 (Thermo Scientific)

Images were taken in a Zeiss Apotome Microscope (Carl Zeiss) at 20X magnification.

Role of Semaphorin 4D in spinal cord injury

Semaphorin 4D immuno Staining

3 and 7 days after injury, tissue samples were collected as described and fixed in freshly made 4% PFA, 0.01% Glutharaldehyde (Sigma) in PBS for 3 hours. After fixation, samples were washed in PBS (3 times for 5 min) and in PBST (3 times for 5 min). Tissue samples were incubated 10 min in 50:50 PBS:30% Sucrose in PBS and overnight in 30% Sucrose in PBS, before embedding the samples in Tissue Tek (Sakura). Frozen tissue samples were cut into 20 µm thick longitudinal sections.

Tissue sections were incubated in pre-warmed PBS at 70°C for 30 min. Afterwards tissue sections were washed with PBS 3 times for 5 min, and in PBSTX 3 times for 10 min. The sections were then block with PBSTX + 2% Goat serum + 2% BSA (Sigma) for 1 hour at room temperature. Mouse anti-β-III-tubulin (1:1000, Sigma) and

rabbit anti-Sema4D () primary antibodies were diluted in blocking buffer and samples were incubated in the antibody solution overnight at 4°C. The next day the tissue sections were washed in PBST (4 times for 10 min). Secondary antibodies (Goat anti-mouse Alexa Fluor 488 and Goat anti-mouse Alexa Fluor 568, Invitrogen) was diluted 1:200 in blocking buffer and the sections were incubated in the antibody for 1 hour at RT. For counter stain, the sections were incubated in a DAPI (1:10000, Invitrogen) solution in PBS for 10 min. Finally, tissue sections sections were washed in PBST(4 times for 30 min) and mounted in 80% glycerol.

Images were taken in a Zeiss Apotome Microscope (Carl Zeiss) at 20X magnification.

Sema4D cloning

For cloning the Sema4D of axolotl, primers were designed to target conserved regions in the sequence coding the SEMA domain in different species. The final sequence of the primers was established using ESTs of the Sema4D of axolotl:

S4D_472_fwd 5'TTCCACTCAGACATCAGCTTCC3'

S4D_1107_rev 5'CAAAAGTTGAATATACCCAAAGGG3'

RT-PCR (One-step RT-PCR kit, Qiagen) was performed using total RNA extracted from spinal cords of axolotls injected with 20μM miR-125b Inhibitor. The PCR product was cloned into a p-Gem-T®Easy vector for sequencing (pS4D). This plasmid was also used to prepare the probes for *in situ* hybridization.

To clone the 5' and 3' ends of Sema4D, new primers were designed using the sequence obtained with the previous primers:

S4DRACE_510_fwd 5'CTGAGACAGAATGCGGGAATGGCAATAT3'

S4DRACE_91_rev 5'GGTTAGCGGTACTGTCGGGGAAGCTGAT3'

RACE-PCR (Invitrogen) was performed using 5' and 3' RACE-cDNA synthetized from the total RNA previously extracted.

The in situ hybridization probes were prepared by linearization of the pS4D with NcoI or SpeI (New England Biolabs). 1μg of linearized plasmids were then mixed with the nucleotide mix containing digoxigenin-UTP (Roche), RNAse inhibitor (Roche),T7 or SP6 RNA polymerase(Promega) to prepare both sense and antisense probes, and transcription buffer. The reaction was incubated at 37° C for 2 hours. After checking the transcription in a 1% agarose gel, the probes were treated with DNAse at 37° C for 15

min, and cleaned using the RNA easy kit from Qiagen. The probes were eluted with 10 µl of RNAse-free water, diluted with 90µl of hybridization buffer and stored at -20 ° C.

In Situ Hybridizations

3 and 7 days after injury, tissue samples were collected, fixed, embedded and cryo-sectioned as described above. Tissue sections were hydrated with PBS (5 min), treated with denaturation buffer (2%SDS, 100mM DTT, in PBS for 20 min) and washed in PBST (3 times for 5 min). The slides were digested with 2 µg/mL Proteinase K in PBS (5 min) and postfixed in 4% PFA (10 min). Then, slides were washed with 0.1%Tween-20 in PBS (3 times for 5 min), treated with Triethanolamine buffer (100mM Triethanolamine, 0.25% acetic anhydride in water) and washed again with PBST (3 times for 5 min).

Prior to hybridization, slides were treated with Hybridization solution (65% Formamide, 5x SSC, 50µg/ml Heparin, 0.1% Tween-20, 0.5 mg/mL tRNA) at 70°C for 15 min. The probes were diluted in hybridization buffer (500ng/ml) and denaturated at 75°C for 10 min. Hybridization was carry out at 70°C for overnight. The next day, the slides were incubated in 70°C pre-warmed 5X SSC (5 minutes at room temperature) and in 0.2X SSC at 70°C for 1 hour. The slides were then treated with Solution B1 (0.1 M Tris pH 7.5, 0.15 M NaCl in water) for 10 min, and with blocking buffer (10% Fetal Calf Serum, Sigma; 0.05 % Tween-20 in Solution B1). Alkaline phosphatase associated Anti-digoxigenin antibody (Roche) was diluted 1:2000 in blocking buffer and slides were incubated in antibody solution at 4° C overnight.

The next day, slides were washed with PBST (3 times for 10 min and once for 5 min) and with freshly prepared Alkaline phosphatase (AP) buffer (100 mM TrisHCl pH 9.5, 50 mM MgCl2, 100 mM NaCl, 0.1% Tween-20 in water) 3 times for 5 min. Finally, slides were incubated with AP substrate (0.5% NBT, Roche; 0.375% BCIP, Roche; in AP buffer) in the dark until development of blue/purple color. Slides were rinsed with PBST several times and a drop of 0.5M EDTA was added on top of the slides to stop the reaction.

Slides were mounted with 80% glycerol and imaged in a Zeiss Apotome Microscope (Carl Zeiss) at 20X magnification.

Luciferase Assay

The 3'UTR region of the rat and axolotl's Semaphorin 4D containing the seeding sequence for miR-125b (CTCAGGGA) was subcloned into a luciferase expression reporter vector (pMIR-REPORT System, Applied Bioscence) using the following primers:

AxoS4D_3UTR_sacl_2	5'ACCGGAGCTCTTTGTGACCAATTTATGTTC3'
AxoS4D_3UTR_hind_1	5'ATTGAAGCTTCACACATCCCTCTTGCATA3'
RatS4DUTR_SpeI1_fwd	5'ACCGACTAGTTAACTTAATCTCCTGCCATCCG3'
RatS4DUTR_HindIII1_rev	5'ACCGAAGCTTATCTGCCCTCACTCAAAACG3'

On the day before to the transfection, HEK293T cells were seeded in a 96 well plate at a seeding density of $1x10^5$ cell/cm^2. On the day of the transfection the culture media was withdrew and replaced it with 50µl of media without antibiotics.

The luciferase plasmids containing the 3'UTR regions of Semaphorin 4D were diluted into 25µl of OptiMEM (Gibco) along with a b-galactosidase plasmid (pMIR-REPORT System, Applied Bioscence) as an internal control, and the mimic for miR-125b or a control mimic(Thermo Scientiofic). The total amount of plasmid DNA was 200 ng/well with a Luciferase plasmid:b-Galactosidase plasmid ratio of 1:1 and 25nM final concentration of mimic for the rat Semaphorin4D, and with a a Luciferase plasmid:b-Galactosidase plasmid ratio of 3:1 and 50nM final concentration of mimic for the axolotl Semaphorin4D. The DNA-mimic solution was mixed with 25 µl of a Lipofectamine solution in OptiMEM (0.5µl of lipofectamine per well, Invitrogen) and incubated at room temperature for 20 min. Afterwards the 50µl of mixture was added to the cells, and the cells were incubated at 37°C for 48 hours. The quantification of the luciferase expression was done using the Dual Light System (Applied Bioscience) following the manufactures instructions and a multilevel microtiter plate reader (Envision, Perkin Elmer)

Semaphorin 4D siRNA Assay

On the day before the transfection, P5 Astrocytes were seeded on 24 well plates at a seeding density of $5x10^5$ cell/cm^2. On the day of the transfection the culture media was withdrew and replaced it with 400µl of media without antibiotics.

Semaphorine 4D or a control siRNA (Ambion) was diluted in 50 µl of OptiMEM to reach a final amount of 15pmol per well. The diluted siRNA was mixed with 50µl of a Lipofectamine solution in OptiMEM (1µl of lipofectamine per well, Invitrogen) and

incubated at room temperature for 20 min. Afterwards the 100µl of mixture were added to the cells, and the cells were incubated at 37°C for 48 hours.

48 hours after transfection a vial of primary cortical neurons (Lonza) was thawed and seeded on top of the astrocytes at a seeding density of $1x10^5$ cell/cm^2. Co-cultures were incubated at 37°C in Neurobasal media (Lonza) suplemented with 2% NSF-1, 2mM L-glutamine and Gentamicin/Amphotericin (50µg/ml and 37ng/ml). The co-cultures were monitored daily to detect neurite outgrowth and 50% of the media was change 2 days after seeding the cells. 4 days after seeding, when neurite outgrowth was evident, the co-cultures were scratched with a P10 pipet tip.Phase contrast pictures of the scratched co-cultures were taken after 30 min, 6 hours and 24 hours after scratch. Scrtached co-cultures were fixed with 4% PFA 48 and 72 hours after scratch, and stained with a mouse anti-b-III-tubulin (1:1000 dilution) and a rabbit anti-GFAP (1:800 dilution) antibodies. Images of the scratched co-cultures were taken using a Leica microscope (DMI 6000B, Leica). Neurite lenght, and growth angle were meassured using the "Simple Neurite Tracer" tool from ImageJ. Neurites growing directly towards the scratch were considered to have a 90 degress angle, while neurites growing paralel to the scratch were considered to hae a 0 degrees angle. The angle distribution was ploted using the "Roseta Histogram" tool from Matlab, and the statistical significance of the data was analyzed using a c^2 test.

Biomechanical regulation of miR-125b expression in response to spinal cord injury

In vivo miRNA expression after SCI

3 groups of 4 axolotls (3 to 5 cm long) were injured as described above. 1 day after injury the animals were anesthetize and the tail was amputated at the hind limb level. The tail was pined down to a sylgard dish and the spinal cord was separated from the notochord with a 27 ½ G needle. Tissue was collected from 4 muscle-bundles rostral and caudal from the injury site. The tissue samples included the muscle and the skin lying above the spinal cord. The dissected tissue from the 4 animals of each group was pooled and flash-frozen by immersion in liquid nitrogen. Tissue was also dissected from 3 groups of 4 animals that were not injured as controls. Total RNA was extracted using Trizol. RNA concentration and purity was assessed using a Nanodrop. 1 µg or RNA was

treated with DNAse I and cDNA was synthetized using the miScript II RT kit from Quiagen. The cDNA was diluted 1:1 with ddH2O and stored at -20°C. Quantitative PCR (qPCR) was performed using the miScript SYBR Green PCR kit (Quiagen). The following qPCR primers were used for quantifications:

miR-125b :	Hs_miR-125b_1 (miScript Primer Assays, Quiagen)
pre-miR-125b:	Hs_mir-125b-1_1_PR (miScript Precursor Assays, Quiagen)
miR-29a:	Hs_miR-29a_1 (miScript Primer Assays, Quiagen)
snoRD25:	Hs_SNORD25_11(miScript Primer Assays, Quiagen)
Axo_c-Fos	Forward GCTGCTACTTCCATTTCGCA
	Reverse GCAAAGTAGGCGAACAGAGG
18S	Forward CGGCTTAATTTGACTCAACACG
	Reverse CGGCTTAATTTGACTCAACACG

For each sample, 4 measurements were done in parallel. The short nuclear RNA (snoRD25) was used as a normalization control for miRNA and pre-miRNA quantification, while ribosomal 18S RNA was used as a normalization control for c-Fos. Relative expression of miR-125b, pre-miR-125b, miR-29a and c-Fos was calculated as follows:

$$\boldsymbol{R.E.} = \frac{2^{Average\ Norm.Contr.C_T}}{2^{miR\ C_T}} \times 100 \qquad \text{[Eq. 2]}$$

where *R.E.* is Relative Expression, *Norm.Contr.* is the normalization control *and* C_T is the Threshold Cycle of PCR reaction. For each sample, out of the 4 C_T values measured, the 3 with a difference below 0.5 were used for calculating the R.E. Also, for each sample the average of the *R.E.* was normalized to the uninjured controls by dividing the *R.E.* by the average *R.E.* of uninjured control animals. The average of the normalized *R.E.* 3 groups of animal was plotted.

In vivo modulation of actin and microtubule cytoskeleton in Axolotls

3 groups of 4 axolotls (3 to 5 cm long) were injected, as described above, with Cytochalasin D (10 µm, Sigma) to induce actin cytoskeleton depolymerization, Jasplakinolione (900 nM, Santa Cruz) to stabilize actin filaments, Nocodazole (10 µm,

Sigma) to induce microtubule depolymerization and Taxol (500 nM, Sigma) to stabilize microtubules. After injection the animals were not electroporated. 1 day after injection, RNA extraction and qPCR quantification of miR-125b, pre-miR-125b, miR-29 and c-Fos was carried as described above.

Another set of animals were injected with the same drugs, left in anesthetic for 30-40 min and then injured as described before. After injury, animals were re-injected with the corresponding drug on both the rostral and the caudal sides of the injury (4 to 5 muscle bundles away from the injury). 1 day after injection and injury, RNA extraction and qPCR quantification of miR-125b, pre-miR-125b, miR-29 and c-Fos was carried as described above.

A set of 3 groups of 4 uninjured animals was used as controls.

Phalloidin and alpha-Tubulin staining

1 min, 10 min, 30 min, 1 hour, 4 hours and 24 hours after injury tissue samples were collected as described above and fixed in in freshly made 4% PFA, 1% Glutharaldehyde in PBS at 4°C overnight. For tubulin staining, samples were post-fixed in 100% methanol for 10 min at -20°C. After fixation, samples were embedded for cryosection as described above. Frozen tissue samples were cut into 10 µm thick longitudinal sections.

For alpha tubulin staining, tissue sections were incubated in pre-warmed PBS at 70°C for 30 min. Afterwards tissue sections were washed with PBS 3 times for 5 min, and in PBSTX 3 times for 10 min. The sections were then block with PBSTX + 2% Goat serum + 2% BSA (Sigma) for 1 hour at room temperature. Mouse anti-alpha-tubulin (Diagnostic BioSystems) primary antibody was diluted 1:500 in blocking buffer and samples were incubated in the antibody solution overnight at 4°C. The next day the tissue sections were washed in PBST (4 times for 10 min). Secondary antibody (Goat anti-mouse Alexa Fluor 647 , Invitrogen) was diluted 1:200 in blocking buffer and the sections were incubated in the antibody for 1 hour at RT. For counter stain, the sections were incubated in a DAPI (1:10000, Invitrogen) solution in PBS for 10 min. Finally, tissue sections sections were washed in PBST(4 times for 30 min) and mounted in 80% glycerol.

For phalloidin staining, tissue sections were incubated in pre-warmed PBS at 70°C for 30 min. Afterwards tissue sections were washed with PBS 2 times for 5 min,

and in PBSTX 3 times for 10 min. Rhodamine conjugated Phalloidin (Cytoskeleton) was diluted 1:200 in PBSTX and samples were incubated in the antibody solution 1 hour at room temperature. For counter stain, the sections were incubated in a DAPI (1:10000) solution in PBS for 10 min. Finally, tissue sections sections were washed in PBST(4 times for 30 min) and mounted in 80% glycerol.

Images of radioglial cells along the ependymal tube on the rostral and the caudal side of the injury were taken using a Leica microscope (DMI 6000B, Leica) at 20 and 40X magnifications.

The same procedure was carried on for samples collected 30 min and 24 hours after treatments with Cytochlasin D, Jasplakinoline, Nococdazole, Taxol and from uninjured animals.

In vivo imaging: Lifeact injection

3 groups of 10 axolotls (3 to 5 cm long) were injected as described above, with mCherry-lifeact construct (Riedl et al., 2008) at a final concentration of 250 ng/µl in solution. Animals were monitored 24 and 48 hrs after injection to check for mCherry expression in the spinal cord.

In vivo imaging: Epifluorescence microscope

On the day of imaging, one animal expressing mCherry-lifeact was anesthetized as previously described. Once immobilized, the animal was put on a cover sleep and using a Leica microscope (DMI 6000B, Leica) at 10X and 20X a region for injury was selected and imaged.

Spinal cord injury was performed as previously described using a fluorescence-dissecting microscope in the region previously selected. After injury the animal was lay on a glass bottom petri dish. The head of the animal was held in place by using a drop of sonogram gel (Aquasonic 100, Parker Labs). A small coverslip (22x22mm, Fisherfinest) was placed on top of the tail and the space between the two glasses was filled with 1% low melting point agarose prepared in anesthetic. The head of the animal and the body parts that were not embedded in agarose were covered with anesthetic and dish was closed. Using again the Leica scope the injury site was identified and time-lapse images (2 hrs at 5 min intervals) were taken. For fluorescence images the exposure time was

set at 200 ms and a gain of 5 and for Differential Interference Contrast (DIC) the exposure time was set at 100 ms and gain of 1.

After the time lapse the animals were put back into water and monitored on the following days for survival.

In vivo imaging: 2-photon microscope

On the day of imaging, one animal expressing mCherry-lifeact was anesthetized as previously described. Once immobilized, the animal was put on a petri dish with a glass bottom as previously described. Once the animal was prepared, an image was acquired using a Multiphoton microscope (Nikon A1RMP, Nikon) at the Imaging Center of the University of Minnesota. The laser power was set at 10% and the other acquisition parameters were adjusted accordingly to each animal or the region to image to get the better resolution possible.

Spinal cord injury was performed as previously described using a dissecting microscope without fluorescence. After injury the animal was lay again on the petri dish and re-embedded in the 1% low melting point agarose. Using again the Nikon scope the injury site was identified and time lapse images (2 hrs at 5 min intervals) were taken.

After the time lapse the animals were put back into water and monitored on the following days for survival.

In vivo imaging: Organotypic cultures

On the day of imaging, one animal expressing mCherry-lifeact was anesthetized as previously described. Once immobilized, the tail of the animal was amputated and embedded in 4% low melting point agarose prepared in aPBS (PBS + 20% water). The sample was set up in a Vibratome (Leica) set at 100 Hz, 0.125 mm/s to obtain 50 µm. Samples were section until the tissue would fall out of the agarose or would brake. The obtained sections were put in AL1 Cells media (described above). The sections were then mounted in media between 2 coverslips and using the Leica microscope at 10X and 20X a region for injury was selected and imaged.

Spinal cord injury was performed in the same way as for injuries in whole animals using a fluorescence-dissecting microscope in the region previously selected. After injury the section was mounted again between two coverslips. Using again the Leica scope the injury site was identified and time-lapse images (2 hrs at 5 min intervals) were taken. For

fluorescence images the exposure time was set at 200 ms and a gain of 5 and for Differential Interference Contrast (DIC) the exposure time image was set at 100 ms and gain of 1.

After the time lapse the sections were put back into media, incubated at 26°C and monitored on the following days for survival.

Prediction of transcription factors binding to miR-125b regulatory region

The sequence of miR-125b gene for different species was found in the National Center for Biotechnology Information (NCBI). For the different species, the sequence of 500 bp upstream the miR-125b gene was used as input for open source bioinformatics software that predict binding sites for different transcription factors within a sequence. The software used were PROMO (http://alggen.lsi.upc.es/cgi-bin/promo_v3/promo/promoinit.cgi?dirDB=TF_8.3) TFbind (http://tfbind.hgc.jp/) and TFSEARCH (http://www.cbrc.jp/research/db/TFSEARCH.html). The sequences of the following species were used:

Bos taurus	miR-125b-1 and miR-125b-2
Rattus norvegicus	miR-125b-1 and miR-125b-2
Macaca mulatta	miR-125b-1 and miR-125b-2
Gallus gallus	miR-125b
Homo sapiens	miR-125b-1 and miR-125b-2
Mus musculus	miR-125b-1
Danio rerio	miR-125b-1, miR-125b-2 and miR-125b-3

miR-125b gene cloning

For cloning the miR-125b gene of axolotl, forward primers were designed to target conserved regions in the sequence 500 bp upstream the miR-125b gene in different species. The reverse primer was designed based on the conserved sequence of the mature miRNA:

miR125b1_37_fwd	5’ AGATGCATATTTTCCTCTCCTC 3’
miR125b_reverse	5’ TCACAAGTTAGGGTCTCAGGG 3’

PCR (FastStart Taq DNA Polymeraze dNTPack, Roche) was performed using genomic DNA extracted from axolotl embryos. The PCR product was cloned into a p-Gem-T®Easy vector for sequencing. The sequence obtained was then used as input for the PROMO, TFbind and TFSEARCH software to confirm the predicted biding of transcription factors, in particular c-Fos, c-Jun and the AP-1 complex.

To quantify and amplify specifically the miR-125b gene in the axolotl, new forward primers were designed using the sequence obtained with the previous primers:

gmiR-125b_C11_fwd 5' ATTGAAGCCTGCCAGAGAAAG 3'.

Chromatin immunoprecipitation (ChIP) assay

To confirm the binding of c-Fos and/or c-Jun to the regulatory region of miR-125b a ChIP assay was performed. 7 3 to 5 cm long axolots were injured as described above. To increase the amount of tissue responding to the injury, each animal was injured twice along the spinal the spinal cord leaving a space of 4-5 muscle bundles between injuries. 24 hrs after injury, tissue samples were collected amputating the tail of anesthetized axolotls at the level of the hind limb. The fins of the tail were removed and the tissue samples were weighted. The collected tissue was minced on ice in 250 µl of ice cold PBS using a #10 scalpel and transferred to a 1.5 ml tube. The minced tissue was then homogenized using a tissue homogenizer (Argos Technologies) and passing the tissue through a 16G and a 20G needles. The homogenize tissue was spun down, the PBS was removed and the tissue was fixed in 1 ml of freshly made 1%PFA at 37°C for 10 min. Fixed tissue was spun down and washed twice with ice cold PBS. The tissue was then re-suspended in 800µl of 1%SDS (Sigma) + 10 mM EDTA (Sigma) + 50mM Tris (Sigma) pH 8.1 + Proteinase Inhibitors (Complete, Roche) lysis buffer. The sample was divided into 2 15 ml conical tubes and sonicated using a Fisher Price Sonicator model 500 set at an 25% amplitude, 30 sec on/30 sec off cycles and 6 min total of on cycles. After sonication the samples were centrifuged at top speed for 10 min and the supernatant was transferred to a new 1.5 ml tube. A 50µl aliquot was taken to check the degree of shearing of the chromatin. The rest of the sample was stored at -80°C.

Immuno-precipitation was done using the EZ ChIP Kit (Protein A agarose beads, Upstate) or the SimpleChIP Enzymatic Chromatin IP kit (Protein G magnetic beads, Cell Signaling). 500 µl of the sheared chromatin was diluted in 4.5 ml of ChIP dilution buffer (provided by the kit) and a 10 µl aliquot was saved as the 2% input. To clarify the DNA,

100 µl of Protein A beads or 150 µl of Protein G beads were added to the diluted chromatin. Each antibody used was diluted into 300 or 500 µl of ChIP dilution buffer containing 25 µl of Protein A beads or 30 µl Protein G beads. A tube containing ChIP dilution buffer and Protein A or G beads but no antibody was used as mock control. Diluted Chromatin and antibodies were incubated at 4°C for 2 hours on a rotatory shaker. The following antibodies were used:

Table 6-1. Antibodies and dilutions used for ChIP assays.

Antibody	Dilution
Mouse anti-Polymeraze II (Positive control, Sigma)	1:300
Rabbit ant-Histone 3 (Positive control, Cell Signaling)	1:50
Normal mouse IgG (Negative control, Sigma)	1:300
Normal rabbit IgG (Negative control, Cell Signaling)	1:500
Mouse anti-c-Fos (Santa Cruz)	1:150
Rabbit anti-c-Fos (Cell Signaling)	1:50
Rabbit anti-c-Fos (Millipore)	1:50
Rabbit anti-c-Jun (Cell Signaling)	1:100

After incubation, Protein A beads were spun down for 30 sec while Protein G beads were precipitated using a magnet. The supernatant from the antibody tubes was discarded and clarified chromatin was distributed equally into the antibody tubes (500-1300 µl/tube). Chromatine-antibody-beads complex were incubated at 4°C overnight on a rotatory shaker.

On the next day beads were washed once with a low salt washing solution (provided by the kit) and once with a high salt washing solution. Protein A beads were additionally washed with a LiCl solution (provided by the kit) and twice with TE buffer (10 mM Tris, 1 mM EDTA pH 8.0). DNA was eluted from the Protein A beads by incubating the beads in 150µl of 1%SDS + 0.1M $NaHCO_3$ for 15 min at room temperature. Protein A beads were spun down and the supernatant was saved into a tube containing 10µl of 5M NaCl. The elution was repeated once more and the pooled eluted was incubated at 65°C overnight. DNA was precipitated with Ammonium Acetate as it will be described bellow. DNA was eluted from the Protein G beads by incubating the beads in 150µl of Elution buffer (provided by the kit) for 30 min at 65°C. Protein G beads were precipitated and the supernatant was saved into a tube containing 6µl of 5M NaCl and 2µl of

proteinase K. The eluted DNA was incubated at 65°C for 2 hours DNA was precipitated using spin columns provided by the kit.

Immuno-precipitated DNA was used as template for PCR and qPCR amplification of the regulatory region of miR-125b using the miR125b1_37_fwd or gmiR-125b_C11_fwd primers and the miR125b_reverse primer.

The evaluation of the degree of shearing of the Chromatin was done as follow. To reverse crosslinking, 2µl of 5M NaCl were added to the 50µl aliquot and the sample was incubated at 65°C overnight. DNA was precipitated by adding 1 volume of 5M Ammonium Acetate and 2 volumes of chloroform to the chromatin. The sample was mixed, incubated on ice for 15 min and centrifuged at 14,000 rpm for 10 min at 4°C. The top layer was collected into a new tube and mixed with 3 µl of Glycogen (Sigma) and 200µl of 100% Ethanol and incubated on ice for extra 15 min. Samples were centrifuged as before and the precipitated DNA was washed once with 70% Ethanol. After air-drying, the DNA was re-suspended in 20 µl of ddH_2O. A 5µl and a 10µl aliquots were treated with 1µl of RNAse A (promega) for 10 min at room temperature and ran in a 1.5% agarose gel.

In vitro miRNA expression after injury

To assess whether biomechanical regulation of miRNA expression is a conserved mechanism across species, a scratch *in vitro* injury model on rat primary astrocytes was used. P5 astrocytes were seeded on 24 well plates at $1x10^5$ cells/cm^2 seeding density. Once the cells were confluent, they were scratched 8 times with a P10 pipette tip and and the culture media was replaced. RNA was extracted from scratched cells at 0, 6, 12, 24, 48 and 72 hours (4 wells per time point) after the injury. For RNA extraction, culture media was withdrawn and cells were washed once with PBS. In each well 200µl of Trizol were added and cells were incubated for 20 min on a shaker at room temperature. For each time point the cell lysate in Trizol was polled and the RNA extraction continued following the user manual's instructions and qPCR quantification of miR-125b was carried as described above. A set of untreated and unscratched cells was used as control.

After determining the dynamics of miR-125b expression after injury the following sets of experiment were set up:

Table 6-2. Experimental conditions used for scratch assays.

Number of cells plated	Substrate plated on	Composition of the media before and after the scratch	Time after plating the scratch was performed	Number of scratches per well.	Time cells were harvested after scratch
$1x10^5$ cell/cm^2	No coating	15% FBS + 1% Pen/Strep		8	0, 6, 12, and 24 hrs after scratch
$1x10^5$ cell/cm^2	No coating	15% FBS + 1% Pen/Strep		8	0, 6, 12, and 24 hrs after scratch
$5x10^4$ cell/cm^2	No coating	15% FBS + 1% Pen/Strep		8	0, 6, 12, 24 48 and 72 hrs after scratch
$5x10^4$ cell/cm^2	No coating	15% FBS + 1% Pen/Strep		8	24 hrs after scratch
$5x10^4$ cell/cm^2	No coating	15% FBS + 1% Pen/Strep		8	24 hrs after scratch
$5x10^4$ cell/cm^2	No coating	15% FBS + 1% Pen/Strep		8	24 hrs after scratch
$5x10^4$ cell/cm^2	No coating	15% FBS + 1% Pen/Strep (before) 2% FBS + 1% Pen/Strep (after)		8	10 min and hrs after scratch
$2.5x10^4$ cell/cm^2	No coating	15% FBS + 1% Pen/Strep	5 days after seeding	8	10 min, 1, 4 and 24 hrs after scratch
$2.5x10^4$ cell/cm^2	No coating	15% FBS + 1% Pen/Strep	2 days after seeding	8	24 hrs after scratch
$2.5x10^4$ cell/cm^2	No coating	15% FBS + 1% Pen/Strep	1 day after seeding	8	24 hrs after scratch
$2.5x10^4$ cell/cm^2	No coating	15% FBS + 1% Pen/Strep	1 day after seeding	8	24 hrs after scratch
$2.5x10^4$ cell/cm^2	No coating	15% FBS + 1% Pen/Strep	1 day after seeding	8	4 hrs after scratch
$2.5x10^4$ cell/cm^2	No coating	15% FBS + 1% Pen/Strep	2 days after seeding	8	4 hrs after scratch
$2.5x10^4$ cell/cm^2	No coating	15% FBS + 1% Pen/Strep	3 days after seeding	8	4 hrs after scratch
$2.5x10^4$ cell/cm^2	PLL coating	15% FBS + 1% Pen/Strep (before) 2% FBS + 1% Pen/Strep (after)	2 days after seeding	8	10 min and 4 hrs after scratch
$2.5x10^4$ cell/cm^2	PLL coating	15% FBS + 1% Pen/Strep (before) 2% FBS + 1% Pen/Strep (after)	3 days after seeding	8	10 min and 4 hrs after scratch
$2.5x10^4$ cell/cm^2	PLL coating	15% FBS + 1% Pen/Strep (before) 2% FBS + 1% Pen/Strep (after)	4 days after seeding	8	10 min and 4 hrs after scratch
$2.5x10^4$ cell/cm^2	PLL coating	15% FBS + 1% Pen/Strep (before) 2% FBS + 1% Pen/Strep (after)	2 days after seeding	8	10 min and 4 hrs after scratch

$1x10^4$ cell/cm^2	PLL coating	15% FBS + 1% Pen/Strep (before) 2% FBS + 1% Pen/Strep (after)	1 week after seeding	8	4hrs after scratch
$1x10^4$ cell/cm^2	PLL coating	15% FBS + 1% Pen/Strep (before) 2% FBS + 1% Pen/Strep (after)	1 week after seeding	8	4hrs after scratch
$1x10^4$ cell/cm^2	PLL coating	15% FBS + 1% Pen/Strep (before) 2% FBS + 1% Pen/Strep (after)	1 week after seeding	8	4hrs after scratch

The different conditions were tested to adjust the miRNA quantification to the conditions used for the immune stain and transferase assays (See below).

In vitro modulation of actin and microtubule cytoskeleton in rat astrocytes

P5 astrocytes were seeded on 24 well plates at $1x10^5$ cells/cm^2 seeding density. Once the cells were confluent, they were treated with Cytochalasin D (10 µm) Jasplakinolione (250 nM) Nocodazole (10 µm, Sigma) Taxol (50 nM, Sigma) Blebbistatin (20µM, Sigma) and Latrunculin B (200 nM, donated by the Ervasti Lab) for 30 min at 37°C. After treatment, the culture media was replaced and cells were incubated for 24hrs at 37°C. Afterwards the RNA extraction and miR-125b and pre-miR-125b quantification was carried on as described above.

Another set of cells were treated with the same drugs and scratched 8 times with a P10 pipette tip. After the scratch, in the cells treated with Cytochalasin D and Nocodazol fresh media was added, while in the cells treated with Jasplakinoline and Taxol the replacement media had the drugs in it. A set of untreated and unscratched cells was used as control.

C3 transferase assay

To block RhoA activity, P5 astrocytes were seeded on 24 well plates at $2.5x10^4$ cells/cm^2 seeding density. Once the cells were confluent, they were scratched 8 times (for RNa extraction) or 1 time (for staining). After scratch, fresh media (DMEM + 2% Fetal calf serum + 1% Penicillin/Streptomycin) with C3 transferase (3µg/ml) was added to the cultures. Cells were cultured in low serum C3 containing media for 30 min at 37°C.

After treatment, the culture media was replaced and cells were incubated for 4hrs at 37°C due to the short half-life of the enzyme. Afterwards the RNA extraction and miR-125b quantification and phosphor c-Fos staining were carried on as described above and below.

Another set of cells was treated with the C3 without scratching. A set of untreated and unscratched cells was used as control.

In vitro phalloidin, alpha-Tubulin and phospho-c-Fos staining

P5 astrocytes were seeded on Poly-L-Lysine coated (PLL, 0.5 µg/cm^2, Sigma) glass bottom dishes (In Vitro Scientific) at a seeding density of 2.5x10^4 cells/cm^2. Once the cells were confluent, they were scratched once with a P10 pipette tip. Cells were fixed at 1 min, 10 min, 30 min, 1 hour, 4 hours and 24 hours after scratch by directly adding freshly made 4% PFA and incubating at RT for 10 min. Afterwards cells were post-fixed in 4% PFA and incubating at RT for additional 15 min. After fixing, cells were washed 3 times with PBS for 5 min and once with PBSTX for 10 min. Cultures were then blocked by incubation in PBSTX + 10% Goat serum for 30 min at room temperature. To visualize the plasma membrane, mouse anti-beta-catenin primary (Sigma) antibody was diluted 1:800 in blocking buffer and cells were incubated in the antibody solution 1 hr at room temperature. Afterwards, the cultures were washed with PBS 3 times for 5 min. Secondary antibody (Goat anti-mouse Alexa Fluor 488) and Rhodamine phalloidin were diluted 1:200 in blocking buffer and cells were incubated in the antibodies for 1 hour at RT. Cells were counter stained with DAPI (1:10000) solution in PBS for 5 min. Finally, cells were washed in PBS 3 times for 5 min and left in PBS. Stained cultures were stored at 4°C.

For tubulin staining, once the cells were taken out from the incubator, media was withdrew and cells were fixed with in ice cold 100% methanol and incubated at -20°C for 3 min. After fixation, cells were rehydrated in PBST 3 times for 5 min and incubated in PBSTX for 10 min. Cultures were then blocked by incubation in PBSTX + 10% Goat serum for 30 min at room temperature. Mouse anti-beta-catenin primary antibody was diluted 1:800 in blocking buffer and cells were incubated in the antibody solution 1 hr at room temperature. Afterwards, the cultures were washed with PBS 3 times for 5 min. Secondary antibody (Goat anti-mouse Alexa Fluor 488) diluted 1:200 and Cy5 conjugated alpha-tubulin antibody was diluted 1:500 in blocking buffer and cells were

incubated in the antibodies for 1 hour at RT. Cells were counter stained with DAPI (1:10000) solution in PBS for 5 min. Finally, cells were washed in PBS 3 times for 5 min and left in PBS. Stained cultures were stored at 4°C.

For phospho-c-Fos staining, after treatments the cells were fixed by directly adding freshly made 4% PFA and incubating at RT for 10 min. Afterwards cells were post-fixed in 4% PFA and incubating at RT for additional 15 min. The staining procedure was followed as described before. Rabbit anti-phospho-c-Fos primary antibody was diluted 1:800 and secondary antibody, Goat anti-mouse Alexa Fluor 568, was diluted 1:200.

Development of a 3D in vitro model system

Agarose tubes and cultures

1.5% agarose tubes were fabricated by pouring agarose into a casting mold made of Polydimethylsoloxane (PDMS, Corning). The mold consisted of a base and a lid. The base was made by pouring uncured PDMS into plastic box (P1000 pipette box cap) and placing a plastic tube drying rack (13 mm diameter) upside down in to the PDMS solution. The PDMS was pre-cured at 42°C for 12 hrs and cured for extra 12 hrs at 55°C. The lid was made by pouring uncured PDMS into plastic box (P1000 pipette box cap) and placing a plastic tube drying rack upside down in to the PDMS solution. The PDMS was pre-cured at 42°C for 12 hrs. After pre-curing, the rack was removed and each of the wells in the PDMS mold was performed with an 18G needle, which will form the lumen of the agarose tube. After modifications, the pre-cured PDMS cured for extra 12 hrs at 55°C.

1.5% agarose casted into the PDMS mold was incubated at 4°C overnight. After solidification, agarose tubes were removed from the casting mold and sterilized by placing them under UV light for 1 hr in a culture hood. After sterilization, the tubes were coated twice with PLL (2 $\mu g/cm^2$ in PBS) at 4°C overnight. Afterwards the agarose tubes were coated once with type I Collagen (10 $\mu g/cm^2$ in PBS, Sigma) at 4°C overnight. After coating, the agarose tubes were washed with PBS + 2xPen/Strep at 4°C overnight with one change of washing solution. After washing the tubes were pre-incubated on B35 cells culture media for 24 hrs at 37°C.

B35 cells, between P7-P10, were seeded at a cell density of $1x10^4$ cells/cm^2. For each tube to be seeded, the cells were suspended in 1ml of media, and put on a 1.5 ml tube. The agarose tubes were then submerged in the cell suspension and incubated at 25°C for 7 hrs on a shaker. Afterwards the agarose tubes and the cell suspension were placed on culture dishes and incubated at 37°C. On the next day the media was changed and the tubes were incubated for 3 days. Four days after seeding, the tubes were change into media containing 1 mM Dibutiryl-cAMP (DbcAMP) to induce differentiation and neurite outgrowth. The media was changed daily for 4 days and then the tubes were fixed with 4%PFA at 4°C overnight for immunostaining. Tubes were immunostained for β-III-tubulin (dilution 1:1000) and counter stained with DAPI following the whole mount staining protocol described previously, without the proteinase K treatment. Other tubes were processed for cryosection as described before and only counter stained with DAPI.

1.5% agarose sheets were fabricated by pouring agarose into a western blot gel castin system (Biorad). After solidification, agarose sheets were removed from the casting mold and sterilized, coated with PLL (2 µg/cm^2 in water) and type I Collagen (10 µg/cm^2 in PBS) and washed as described for the tubes. After washing the tubes were pre-incubated on astrocytes culture media for 24 hrs at 37°C.

P5 astrocytes were seeded at a cell density of $1x10^4$ cells/cm^2 on top of the agarose sheets and incubated at 37°C. On the next day the media was changed and the tubes were incubated for 7 days. Afterwards the sheets were fixed with 4%PFA at 4°C overnight for staining. Sheets were only counter stained with DAPI following the whole mount staining protocol described previously, without the proteinase K treatment.

Images were taken in an inverted Zeiss Apotome Microscope (Carl Zeiss) at 10 and 20X magnification.

Cell Light-BacMan transfection

Astrocytes and B35 cells were transfected using the Cell light-BacMan system (Invitrogen). B35 cells were transfected to express GFP tagged Tubulin while astrocytes were transfected to express RFP tagged Histone 2B. On the day before the transcription the cells were seeded into 24 well plates at a cell density of $5x10^4$ cells/cm^2. When the cultures were between 50-80% confluent the culture media was change with media

containing 25 particles per cell of the Cell light-BacMan reagent. The cells were checked 24 hours after transfection to confirm the expression of GFP and RFP.

PCL tubes and cultures

PCL tubes were obtained from the NanoFibers Solutions company (Columbus, OH, USA). PCL tubes were sterilized by placing them under UV light overnight in a culture hood. After sterilization, the tubes were submerged on a PLL solution (10 µg/ml in water) or a Fibronectin solution (10 µg/ml in PBS, Sigma) and incubated on a rocking platform at 4°C overnight. Afterwards the coted PCL tubes were washed with PBS at 4°C overnight. After washing, the tubes were pre-incubated on astrocytes culture media for 24 hrs at 37°C. P5 astrocytes were seeded in the tubes at a density of $1x10^5$ cells/cm^2. For each tube to be seeded, the cells were suspended in 1ml of media, and put on a 1.5 ml tube. The PCL tubes were then submerged in the cell suspension and incubated at 37°C for 4 hrs on a shaker. Every hour the cell suspension was perfused through the tubes lumen using a $27^{1/2}$ G needle. Afterwards the PCL tubes and the cell suspension were placed culture dishes and incubated at 37°C. On the next day the media was changed and the tubes were incubated for 4 days with media change every other day. The tubes were then fixed with 4%PFA at 4°C overnight for immunostaining. Tubes were immunostained for GFAP (Dilution 1:800) and counter stained with DAPI following the whole mount staining protocol described above, without the proteinase K treatment. Stained tubes were imaged using the Leica microscope.

PCL tubes with three different wall thicknesses (200, 400 and 700µm) were sterilized coated with PLL or Fibronectin and washed as previously described. After washing, the tubes were pre-incubated on B35 cells culture media for 24 hrs at 37°C. Tubulin-GFP expressing B35 cells were seeded in the tubes at a density of $1x10^5$ cells/cm^2 as previously described. On the next day the media was changed and the tubes were incubated for 10 days with media change every other day. The cells were then serum starved (1% FBS) to induce differentiation and neurite outgrowth. The media was changed daily for 4 days and then the tubes were imaged using the Leica microscope at 10X and 20X. For each wall thickness and coating used, the length of the neurites was quantified using the Neurite Tracer feature from ImageJ.

For the Astrocytes-B35 co-cultures, PCL tubes with a wall thickness of 400µm were sterilized, coated with Fibronectin and washed as previously described. The tubes

were then incubated in astrocytes media at 37°C overnight. Histone-RFP expressing astrocytes were seeded in the tubes at a density of $5x10^4$ cells/cm^2 as previously described. On the next day the media was changed and the tubes were incubated for 4 days with media change every other day. The tubes were observed in the Leica microscope to confirm the presence of red nuclei in the tubes. Tubulin-GFP expressing B35 cells were seeded on astrocytes-seeded-PCL tubes at a density of $2x10^5$ cells/cm^2 as previously described. The next day the tubes were observed in the Leica microscope to confirm the presence of red nuclei and green neurites in the tubes. The cells were then serum starved (1% FBS) to induce differentiation and neurite outgrowth. The media was changed daily for 4 days and then the tubes were imaged using the Leica microscope (DMI 6000B, Leica) at 10X and 20X.

Collagen Hydrogels and cultures

Collagen type I hydrogels were prepared in collaboration with Yuping Li from the Laboratory of Conrado Aparicio in the Dentistry department at the University of Minnesota. Collagen hydrogels were prepared in a culture hood from collagen type I solution obtained by mixing 4.8 ml of 3mg/ml bovine type I collagen + 1.2 ml of 10X PBS + 0.8 ml of 0.1N NaOH. This solution yields a final concentration of collagen of 2 mg/ml at pH 8.0. Between 400-500 µl of the solution were poured into 10 wells of a 24 well plate, taking care not to add bubbles. The dish was incubated at 37°C for 3 days. To reduce the pH form 8 to 7 the hydrogels were washed once with sterile water for 3 hrs in a shaker and once for 2 hours. The gels were finally washed with PBS + 4X Pen/Strep for three hour on a shaker. After washings, the hydrogels were incubated with 1 ml of DMEM without phenol red + 10% FBS + 1% Pen/Strep to test the sterility. After confirming that there was not microbial growth the hydrogels were coated with Fibronectin and Laminin. The culture media was removed from the hydrogels and a Fibronectin-Laminin solution was layered on top of the gels. The Fibronectin-Laminin solution was prepared to yield a coating concentration of 2.5 µg/cm^2 of Fibronectin and 1.5µg/cm^2 for Laminin. The dish was incubated at 37°C on a rocking platform overnight. The hydrogels were washed once with PBS at 37°C overnight and incubated afterwards with B35 cells conditioned media (filtered-sterilized media collected from 2 days old B35 cells cultures).

Tubulin-GFP expressing B35 cells were seeded on the hydrogels at a density of $1x10^6$ cells/well, incubated for 4 hrs at 37°C on a rocking platform and then placed in the regular incubator. The next day the media was changed and hydrogels were cultured for 4 days with media change every other day. In half of the hydrogels the cells were then serum starved (1% FBS) to induce differentiation and neurite outgrowth. The media was changed daily for 4 days and then the hydrogels were imaged using the Leica microscope at 10X and 20X

Collagen Scaffolds and cultures

Collagen type I sheets and tubes were prepared by Yuping Li from the Laboratory of Conrado Aparicio in the Dentistry department at the University of Minnesota. The collagen sheets provided by Yuping were prepared from 2 mg/ml collagen solutions pH 7 without any crosslinking. For all the experiments described on forward the sheets were cut to fit into a well of a 96 well plates. The sheets were coated with Fibronectin and Laminin as it was described for the hydrogels. After coating with Fibronetin-Laminin the sheets were washed with PBS at room temperature 3 times for 30 min. Afterwards the sheets were incubated with B35 cells conditioned media. Tubulin-GFP expressing B35 cells were seeded on top of the sheets at a density of $2x10^5$ cells/well and incubated at 37°C. The next day the media was changed and the sheets were incubated for 4 days with media change every other day. The sheets were checked using the Leica microscope to confirm the presence of green bipolar cells. In half of the sheets seeded cells were then serum starved (1% FBS) to induce differentiation and neurite outgrowth. The media was changed daily for 4 days and then the sheets were imaged using the Leica microscope at 10X and 20X.

The sheets were coated with Fibronectin and Laminin as it was described for the hydrogels. After coating with Fibronetin-Laminin the sheets were washed with PBS at room temperature 3 times for 30 min. Afterwards the sheets were incubated with B35 cells conditioned media. Tubulin-GFP expressing B35 cells were seeded on top of the sheets at a density of $2x10^5$ cells/well and incubated at 37°C. The next day the media was changed and the sheets were incubated for 4 days with media change every other day. The sheets were checked using the Leica microscope to confirm the presence of green bipolar cells. In half of the sheets, seeded cells were then serum starved (1%

FBS) to induce differentiation and neurite outgrowth. The media was changed daily for 4 days and then the sheets were imaged using the Leica microscope at 10X and 20X.

P5 astrocytes were seeded on top of Fibronectin-Laminin sheets pre-incubated with astrocytes conditioned media (filtered-sterilized media collected from 4 days old astrocytes cultures) at a seeding density of $2.5x10^5$ cells/cm^2. The next day the culture media was changed for fresh media and the cells were cultured for 4 days. In half of the sheets compression injury was induced by holding the sheets between forceps for 30 seconds. The culture media was change after injury. In cultures were cell proliferation was going to be quantified the media contained 10 μM 5-ethylnyl-2'-deoxyuridine (EdU, Invitrogen). 48 hrs after injury, injured and uninjured cultures were fixed with 4% PFA at 4°C overnight for immunostaining. Staining against GFAP (dilution 1:800) Vimentin (dilution 1:100, Developmental Studies Hybridoma Centers) Collagen type IV (dilution 1:50, Abcam) and Chondroitin Sulfate Proteoglycan (CSPG, 1:50, Developmental Studies Hybridoma Centers) was carried out following the whole mount staining protocol without the proteinase K treatment. Detection of EdU incorporation was done following the instructions of the "Click-it-EdU" kit from Invitrogen. Images were taken using the Leica microscope at 10X and 20X.

Collagen tubes provided by Yuping were coated with Fibronectin and Laminin as it was described for collagen sheets. After coating with Fibronetin-Laminin the tubes were washed as it was described for the PCL tubes. The tubes were then incubated in astrocytes conditioned media at 37°C overnight. P5 astrocytes were seeded in the tubes at a density of $2.5x10^5$ cells/cm^2 using a hanging drop system made in PDMS (Doshi, 2009). On the next day the tubes were placed in culture dishes with fresh media the tubes were incubated for 4 days. B35 cells were seeded on astrocytes-seeded-collagen tubes at a density of $2.5x10^5$ cells/cm^2 using the hanging drop system. The next day the tubes were placed in culture dishes with fresh media the tubes were incubated for 4 days. The cells were then serum starved (1% FBS) to induce differentiation and neurite outgrowth. The media was changed daily for 6 days and then the tubes were fixed with 4% PFA at 4°C overnight for immunostaining. Staining against GFAP (dilution 1:800) and β-III-tubulin (dilution 1:1000) was carried out following the whole mount staining protocol without the proteinase K treatment. Images were taken using the Leica microscope at 10X and 20X.

References

Abou Neel, E.a., L. Bozec, J.C. Knowles, O. Syed, V. Mudera, R. Day, and J.K. Hyun. 2013. Collagen - Emerging collagen based therapies hit the patient. *Advanced Drug Delivery Reviews*. 65:429-456.

Abramov, A., L. Canevari, and M. Duchen. 2004. β-Amyloid Peptides Induce Mitochondrial Dysfunction and Oxidative Stress in Astrocytes and Death of Neurons through Activation of NADPH Oxidase. *The Journal of Neuroscience*. 24.

Abreu-Blanco, M.T., J.M. Verboon, and S.M. Parkhurst. 2014. Coordination of Rho family GTPase activities to orchestrate cytoskeleton responses during cell wound repair. *Current Biology*. 24:144-155.

Adams, D., A. Masi, and M. Levin. 2007. H+ pump-dependent changes in membrane voltage are an early mechanism necessary and sufficient to induce Xenopus tail regeneration. *Development (Cambridge, England)*. 134:1323-1335.

Agudelo-Garcia, P., J. Jesus, S. Williams, M. Nowicki, E. Chiocca, S. Liyanarachchi, P.-K. Li, J. Lannutti, J. Johnson, S. Lawler, M. Viapiano, P. Agudelo-Garcia, J. Jesus, S. Williams, M. Nowicki, E. Chiocca, S. Liyanarachchi, P.-K. Li, J. Lannutti, J. Johnson, S. Lawler, and M. Viapiano. 2011. Glioma Cell Migration on Three-dimensional Nanofiber Scaffolds Is Regulated by Substrate Topography and Abolished by Inhibition of STAT3 Signaling 12. *Neoplasia*. 13.

Akhmanova, A., and M. Steinmetz. 2008. Tracking the ends: a dynamic protein network controls the fate of microtubule tips. *Nature Reviews Molecular Cell Biology*. 9.

Aktories, K., C. Wilde, and M. Vogelsgesang. 2004. Rho-modifying C3-like ADP-ribosyltransferases. *Reviews of Physiology, Biochemistry and Pharmacology*. 152:1-22.

Alilain, W., K. Horn, H. Hu, T. Dick, and J. Silver. 2011. Functional regeneration of respiratory pathways after spinal cord injury. *Nature*. 475:196-200.

Ambros, V. 2004. The functions of animal microRNAs. *Nature*. 431:350-355.

Anand, S., and D.a. Cheresh. 2011. Emerging Role of Micro-RNAs in the Regulation of Angiogenesis. *Genes & cancer*. 2:1134-1138.

Archibald, S.J., C. Krarup, J. Shefner, S.T. Li, and R.D. Madison. 1991. A collagen-based nerve guide conduit for peripheral nerve repair: an electrophysiological study of nerve regeneration in rodents and nonhuman primates. *The Journal of comparative neurology*. 306.

Aristotle. 1910. Historia animalium. Oxford, The Clarendon Press, Oxford.

Baker, B., and C. Chen. 2012. Deconstructing the third dimension – how 3D culture microenvironments alter cellular cues. *Journal of Cell Science*. 125.

Balgude, A.P., X. Yu, A. Szymanski, and R.V. Bellamkonda. 2001. Agarose gel stiffness determines rate of DRG neurite extension in 3D cultures. *Biomaterials*. 22.

Banerjee, J., and P.B. Wedegaertner. 2004. Identification of a novel sequence in PDZ-RhoGEF that mediates interaction with the actin cytoskeleton. *Molecular biology of the cell*. 15:1760-1775.

Barnabé-Heider, F., C. Göritz, H. Sabelström, H. Takebayashi, F. Pfrieger, K. Meletis, and J. Frisén. 2010. Origin of new glial cells in intact and injured adult spinal cord. *Cell stem cell*. 7:470-482.

Bartel, D.P. 2004. MicroRNAs: genomics, biogenesis, mechanism, and function. *Cell*. 116:281-297.

Bartel, D.P. 2009. MicroRNAs: target recognition and regulatory functions. *Cell*. 136.

Bartsch, U., C. Bandtlow, L. Schnell, S. Bartsch, A. Spillmann, B. Rubin, R. Hillenbrand, D. Montag, M. Schwab, and M. Schachner. 1995. Lack of evidence that myelin-associated glycoprotein is a major inhibitor of axonal regeneration in the CNS. *Neuron*. 15:1375-1381.

Beattie, M., J. Bresnahan, and G. Lopate. 1990. Metamorphosis alters the response to spinal cord transection in Xenopus laevis frogs. *Journal of neurobiology*. 21:1108-1122.

Beck, C.W., B. Christen, and J.M.W. Slack. 2003. Molecular Pathways Needed for Regeneration of Spinal Cord and Muscle in a Vertebrate. *Developmental Cell*. 5:429-439.

Becker, C., and T. Becker. 2008. Adult zebrafish as a model for successful central nervous system regeneration. *Restorative neurology and neuroscience*. 26:71-80.

Bellamkonda, R., J.P. Ranieri, and P. Aebischer. 1995. Laminin oligopeptide derivatized agarose gels allow three-dimensional neurite extension in vitro. *Journal of neuroscience research*. 41.

Bellamkonda, R.V. 2006. Peripheral nerve regeneration: an opinion on channels, scaffolds and anisotropy. *Biomaterials*. 27:3515-3518.

Bely, A.E., and K.G. Nyberg. 2010. Evolution of animal regeneration: re-emergence of a field. *Trends in ecology & evolution*. 25:161-170.

Boido, M., D. Garbossa, and A. Vercelli. 2011. Early graft of neural precursors in spinal cord compression reduces glial cyst and improves function. *Journal of neurosurgery. Spine*. 15.

Boomkamp, S.D., M.a. McGrath, M.D. Houslay, and S.C. Barnett. 2014. Epac and the high affinity rolipram binding conformer of PDE4 modulate neurite outgrowth and myelination using an in vitro spinal cord injury model. *British journal of pharmacology*. 171:2385-2398.

Boomkamp, S.D., M.O. Riehle, J. Wood, M.F. Olson, and S.C. Barnett. 2012. The development of a rat in vitro model of spinal cord injury demonstrating the additive effects of rho and ROCK inhibitors on neurite outgrowth and myelination. *Glia*. 60:441-456.

Bozkurt, A., G.A. Brook, S. Moellers, F. Lassner, B. Sellhaus, J. Weis, M. Woeltje, J. Tank, C. Beckmann, P. Fuchs, L.O. Damink, F. Schügner, I. Heschel, and N. Pallua. 2007. In vitro assessment of axonal growth using dorsal root ganglia

explants in a novel three-dimensional collagen matrix. *Tissue engineering*. 13:2971-2979.

Bradbury, E., L. Moon, R. Popat, V. King, G. Bennett, P. Patel, J. Fawcett, and S. McMahon. 2002. Chondroitinase ABC promotes functional recovery after spinal cord injury. *Nature*. 416:636-640.

Bradke, F., J. Fawcett, and M. Spira. 2012. Assembly of a new growth cone after axotomy: the precursor to axon regeneration. *Nature reviews. Neuroscience*. 13:183-193.

Britt, J., J. Kane, C. Spaeth, A. Zuzek, G. Robinson, M. Gbanaglo, C. Estler, E. Boydston, T. Schallert, and G. Bittner. 2010. Polyethylene glycol rapidly restores axonal integrity and improves the rate of motor behavior recovery after sciatic nerve crush injury. *Journal of neurophysiology*. 104:695-703.

Brockes, J., and A. Kumar. 2008. Comparative aspects of animal regeneration. *Annual review of cell and developmental biology*. 24:525-549.

Brockes, J.P. 1997. Amphibian limb regeneration: rebuilding a complex structure. *Science (New York, N.Y.)*. 276.

Burda, J.E., and M.V. Sofroniew. 2014. Reactive gliosis and the multicellular response to CNS damage and disease. *Neuron*. 81:229-248.

Busch, S., K. Horn, F. Cuascut, A. Hawthorne, L. Bai, R. Miller, and J. Silver. 2010. Adult NG2+ cells are permissive to neurite outgrowth and stabilize sensory axons during macrophage-induced axonal dieback after spinal cord injury. *J Neurosci*. 30:255-265.

Butler, E., and M. Ward. 1965. Reconstitution of the spinal cord following ablation in urodele larvae. *The Journal of experimental zoology*. 160:47-65.

Butler, E., and M. Ward. 1967. Reconstitution of the spinal cord after ablation in adult Triturus. *Developmental biology*. 15:464-486.

Cafferty, W., P. Duffy, E. Huebner, and S. Strittmatter. 2010. MAG and OMgp synergize with Nogo-A to restrict axonal growth and neurological recovery after spinal cord trauma. *J Neurosci*. 30:6825-6837.

Carlson, M., Y. Komine, S. Bryant, and D. Gardiner. 2001. Expression of Hoxb13 and Hoxc10 in developing and regenerating Axolotl limbs and tails. *Developmental biology*. 229:396-406.

Caroni, P., and M. Schwab. 1988. Two membrane protein fractions from rat central myelin with inhibitory properties for neurite growth and fibroblast spreading. *The Journal of cell biology*. 106:1281-1288.

Caubit, X., S. Nicolas, and Y. Le Parco. 1997. Possible roles for Wnt genes in growth and axial patterning during regeneration of the tail in urodele amphibians. *Developmental dynamics : an official publication of the American Association of Anatomists*. 210:1-10.

Ceballos, D., X. Navarro, N. Dubey, G. Wendelschafer-Crabb, W.R. Kennedy, and R.T. Tranquillo. 1999. Magnetically aligned collagen gel filling a collagen nerve guide improves peripheral nerve regeneration. *Experimental neurology*. 158.

Chang, T.-C., D. Yu, Y.-S. Lee, E. Wentzel, D. Arking, K. West, C. Dang, A. Thomas-Tikhonenko, and J. Mendell. 2007. Widespread microRNA repression by Myc contributes to tumorigenesis. *Nature Genetics*. 40.

Chen, L., Z. Wang, A. Ghosh-Roy, T. Hubert, D. Yan, S. O'Rourke, B. Bowerman, Z. Wu, Y. Jin, and A. Chisholm. 2011. Axon regeneration pathways identified by systematic genetic screening in C. elegans. *Neuron*. 71:1043-1057.

Chen, M., A. Huber, M. van der Haar, M. Frank, L. Schnell, A. Spillmann, F. Christ, and M. Schwab. 2000. Nogo-A is a myelin-associated neurite outgrowth inhibitor and an antigen for monoclonal antibody IN-1. *Nature*. 403:434-439.

Chen, M., and X. Shen. 2007. Nuclear actin and actin-related proteins in chromatin dynamics. *In* Current Opinion in Cell Biology. Vol. 19. 326-330.

Chen, W.-H., S.-J. Cheng, J. Tzen, C.-M. Cheng, and Y.-W. Lin. 2013. Probing Relevant Molecules in Modulating the Neurite Outgrowth of Hippocampal Neurons on Substrates of Different Stiffness. *PLoS ONE*. 8.

Chernoff, E.A.G., D.L. Stocum, H.L.D. Nye, and J.A. Cameron. 2003. Urodele spinal cord regeneration and related processes. *In* Developmental Dynamics. Vol. 226. 295-307.

Chevallay, B., and D. Herbage. 1999. Collagen-based biomaterials as 3D scaffold for cell cultures: applications for tissue engineering and gene therapy. *Medical and Biological Engineering and Computing*. 38.

Chevallier, S., M. Landry, F. Nagy, and J.-M. Cabelguen. 2004. Recovery of bimodal locomotion in the spinal-transected salamander, Pleurodeles waltlii. *Eur J Neurosci*. 20:1995-2007.

Chihara, K., M. Amano, N. Nakamura, T. Yano, M. Shibata, T. Tokui, H. Ichikawa, R. Ikebe, M. Ikebe, and K. Kaibuchi. 1997. Cytoskeletal rearrangements and transcriptional activation of c-fos serum response element by Rho-kinase. *Journal of Biological Chemistry*. 272:25121-25127.

Chiu, H., A. Alqadah, C.-F. Chuang, and C. Chang. 2011. C. elegans as a genetic model to identify novel cellular and molecular mechanisms underlying nervous system regeneration. *Cell adhesion & migration*. 5:387-394.

Chou, R., and T. Langan. 2003. In vitro synchronization of mammalian astrocytic cultures by serum deprivation. *Brain Research Protocols*. 11.

Clarke, J., R. Alexander, and N. Holder. 1988. Regeneration of descending axons in the spinal cord of the axolotl. *Neurosci Lett*. 89:1-6.

Clarke, J.D.W., and P. Ferretti. 1998. CNS Regeneration in lower vertebrates. *In* Cellular and Molecular Basis of Regeneration. P.G.J. Ferretti, editor. Wiley and sons, New York. 255-269.

Costa, P., F.V. Almeida, and J.T. Connelly. 2012. Biophysical signals controlling cell fate decisions: how do stem cells really feel? *The international journal of biochemistry & cell biology*. 44.

Cronin, M., P.N. Anderson, J.E. Cook, C.R. Green, and D.L. Becker. 2008. Blocking connexin43 expression reduces inflammation and improves functional recovery after spinal cord injury. *Molecular and Cellular Neuroscience*. 39:152-160.

Cronin, M., P.N. Anderson, C.R. Green, and D.L. Becker. 2006. Antisense delivery and protein knockdown within the intact central nervous system. *Frontiers in bioscience : a journal and virtual library*. 11:2967-2975.

Daud, M.F., K.C. Pawar, F. Claeyssens, A.J. Ryan, and J.W. Haycock. 2012. An aligned 3D neuronal-glial co-culture model for peripheral nerve studies. *Biomaterials*. 33.

Davis, B., and A. Hata. 2009. Regulation of MicroRNA Biogenesis: A miRiad of mechanisms. *Cell Communication and Signaling*. 7.

Dawley, E.M., S. O.Samson, K.T. Woodard, and K.A. Matthias. 2012. Spinal cord regeneration in a tail autotomizing urodele. *Journal of Morphology*. 273:211-225.

De Winter, F., M. Oudega, A. Lankhorst, F. Hamers, B. Blits, M. Ruitenberg, R. Pasterkamp, W. Gispen, and J. Verhaagen. 2002. Injury-induced class 3 semaphorin expression in the rat spinal cord. *Experimental neurology*. 175:61-75.

Dent, E.W., S.L. Gupton, and F.B. Gertler. 2011. The growth cone cytoskeleton in axon outgrowth and guidance. *Cold Spring Harbor perspectives in biology*. 3.

Dergham, P., B. Ellezam, C. Essagian, H. Avedissian, W.D. Lubell, and L. McKerracher. 2002. Rho signaling pathway targeted to promote spinal cord repair. *The Journal of neuroscience : the official journal of the Society for Neuroscience*. 22:6570-6577.

Dias, T., Y.-J. Yang, K. Ogai, T. Becker, and C. Becker. 2012. Notch signaling controls generation of motor neurons in the lesioned spinal cord of adult zebrafish. *J Neurosci*. 32:3245-3252.

Diaz Quiroz, J.F., and K. Echeverri. 2012. In Vivo Modulation of MicroRNA Levels during Spinal Cord Regeneration. 112:235-246.

Diaz Quiroz, J.F., and K. Echeverri. 2013. Spinal cord regeneration: where fish, frogs and salamanders lead the way, can we follow? *The Biochemical journal*. 451.

Diaz Quiroz, J.F., E. Tsai, M. Coyle, T. Sehm, and K. Echeverri. 2014. Precise control of miR-125b levels is required to create a regeneration-permissive environment after spinal cord injury: a cross-species comparison between salamander and rat. *Disease Models & Mechanisms*. 7.

Dickson, B. 2001. Rho GTPases in growth cone guidance. *Current Opinion in Neurobiology*. 11.

Dimou, L., L. Schnell, L. Montani, C. Duncan, M. Simonen, R. Schneider, T. Liebscher, M. Gullo, and M. Schwab. 2006. Nogo-A-deficient mice reveal strain-dependent differences in axonal regeneration. *J Neurosci*. 26:5591-5603.

Doshi, K.J. 2009. Direct Cell Seeding on Collagen-Coated Silicone Mandrels to Generate Cell-Derived Tisuue tubes. *In* Department of Biomedical Engineering. Vol. Master in Sciences. Worcester Polytechnic Institute. 85.

Dubey, N., P.C. Letourneau, and R.T. Tranquillo. 1999. Guided neurite elongation and schwann cell invasion into magnetically aligned collagen in simulated peripheral nerve regeneration. *Experimental neurology*. 158.

Dubreuil, C.I., M.J. Winton, and L. McKerracher. 2003. Rho activation patterns after spinal cord injury and the role of activated Rho in apoptosis in the central nervous system. *The Journal of cell biology*. 162:233-243.

East, E., J. Golding, and J. Phillips. 2009. A versatile 3D culture model facilitates monitoring of astrocytes undergoing reactive gliosis. *Journal of Tissue Engineering and Regenerative Medicine*. 3.

Echeverri, K., and E. Tanaka. 2002. Ectoderm to mesoderm lineage switching during axolotl tail regeneration. *Science (New York, N.Y.)*. 298:1993-1996.

Echeverri, K., and E. Tanaka. 2003. Electroporation as a tool to study in vivo spinal cord regeneration. *Developmental dynamics : an official publication of the American Association of Anatomists*. 226:418-425.

Egar, M., and M. Singer. 1972. The role of ependyma in spinal cord regeneration in the urodele, Triturus. *Experimental neurology*. 37:422-430.

Ehlers, M. 2004. Deconstructing the axon: Wallerian degeneration and the ubiquitin-proteasome system. *Trends in neurosciences*. 27:3-6.

Ehrlich, D., and R. Mark. 1977. Fiber counts of regenerating peripheral nerves in axolotls and the effect of metamorphosis. *The Journal of comparative neurology*. 174:307-316.

Ertürk, A., F. Hellal, J. Enes, and F. Bradke. 2007. Disorganized microtubules underlie the formation of retraction bulbs and the failure of axonal regeneration. *The Journal of neuroscience : the official journal of the Society for Neuroscience*. 27:9169-9180.

Etienne-Manneville, S. 2004. Actin and microtubules in cell motility: Which one is in control? *Traffic*. 5:470-477.

Evans, A., S. Euteneuer, E. Chavez, L. Mullen, E. Hui, S. Bhatia, and A. Ryan. 2007. Laminin and fibronectin modulate inner ear spiral ganglion neurite outgrowth in an in vitro alternate choice assay. *Developmental Neurobiology*. 67.

Even-Ram, S., A. Doyle, M. Conti, K. Matsumoto, R. Adelstein, and K. Yamada. 2007. Myosin IIA regulates cell motility and actomyosin–microtubule crosstalk. *Nature Cell Biology*. 9.

Faulkner, J., J. Herrmann, M. Woo, K. Tansey, N. Doan, and M. Sofroniew. 2004. Reactive astrocytes protect tissue and preserve function after spinal cord injury. *J Neurosci*. 24:2143-2155.

Fawcett, J., and R. Asher. 1999. The glial scar and central nervous system repair. *Brain research bulletin*. 49:377-391.

Ferretti, P., F. Zhang, and P. O'Neill. 2003. Changes in spinal cord regenerative ability through phylogenesis and development: Lessons to be learnt. *In* Developmental Dynamics. Vol. 226. 245-256.

Filipowicz, W., S. Bhattacharyya, and N. Sonenberg. 2008. Mechanisms of post-transcriptional regulation by microRNAs: are the answers in sight? *Nature Reviews Genetics*. 9.

Fish, J.E., M.M. Santoro, S.U. Morton, S. Yu, R.F. Yeh, J.D. Wythe, K.N. Ivey, B.G. Bruneau, D.Y. Stainier, and D. Srivastava. 2008. miR-126 regulates angiogenic signaling and vascular integrity. *Dev Cell*. 15:272-284.

Fisher, D., B. Xing, J. Dill, H. Li, H.H. Hoang, Z. Zhao, X.L. Yang, R. Bachoo, S. Cannon, F.M. Longo, M. Sheng, J. Silver, and S. Li. 2011. Leukocyte common antigen-related phosphatase is a functional receptor for chondroitin sulfate proteoglycan axon growth inhibitors. *J Neurosci*. 31:14051-14066.

Fletcher, D., and D. Mullins. 2010. Cell mechanics and the cytoskeleton. *Nature*. 463.

Forgione, N., and M.G. Fehlings. 2013. Rho-ROCK Inhibition in the Treatment of Spinal Cord Injury. *World neurosurgery*:1-5.

Gaete, M., R. Muñoz, N. Sánchez, R. Tampe, M. Moreno, E. Contreras, D. Lee-Liu, and J. Larraín. 2012. Spinal cord regeneration in Xenopus tadpoles proceeds through activation of Sox2-positive cells. *Neural development*. 7:13.

García-Parra, P., M. Maroto, F. Cavaliere, N. Naldaiz-Gastesi, J. Álava, A. García, A. Munain, and A. Izeta. 2013. A neural extracellular matrix-based method for in vitro hippocampal neuron culture and dopaminergic differentiation of neural stem cells. *BMC Neuroscience*. 14.

Gargioli, C., and J. Slack. 2004. Cell lineage tracing during Xenopus tail regeneration. *Development (Cambridge, England)*. 131:2669-2679.

Gee, A., B. Baker, A. Silverstein, G. Montero, J. Esterhai, and R. Mauck. 2012. Fabrication and evaluation of biomimetic-synthetic nanofibrous composites for soft tissue regeneration. *Cell and tissue research*. 347.

Geiger, B., J.P. Spatz, and A.D. Bershadsky. 2009. Environmental sensing through focal adhesions. *Nature reviews. Molecular cell biology*. 10:21-33.

George, E., J. Glass, and J. Griffin. 1995. Axotomy-induced axonal degeneration is mediated by calcium influx through ion-specific channels. *The Journal of neuroscience : the official journal of the Society for Neuroscience*. 15:6445-6452.

Georges, P., W. Miller, D. Meaney, E. Sawyer, and P. Janmey. 2006. Matrices with Compliance Comparable to that of Brain Tissue Select Neuronal over Glial Growth in Mixed Cortical Cultures. *Biophysical Journal*. 90.

Géraudie, J., R. Nordlander, M. Singer, and J. Singer. 1988. Early stages of spinal ganglion formation during tail regeneration in the newt, Notophthalmus viridescens. *The American journal of anatomy*. 183:359-370.

Ghosh-Roy, A., A. Goncharov, Y. Jin, and A. Chisholm. 2012. Kinesin-13 and tubulin posttranslational modifications regulate microtubule growth in axon regeneration. *Developmental cell*. 23:716-728.

Ghosh-Roy, A., Z. Wu, A. Goncharov, Y. Jin, and A. Chisholm. 2010. Calcium and cyclic AMP promote axonal regeneration in Caenorhabditis elegans and require DLK-1 kinase. *The Journal of neuroscience : the official journal of the Society for Neuroscience*. 30:3175-3183.

Gibbs, K., S. Chittur, and B. Szaro. 2011. Metamorphosis and the regenerative capacity of spinal cord axons in Xenopus laevis. *Eur J Neuroscience*. 33:9-25.

Gibbs, K., and B. Szaro. 2006. Regeneration of descending projections in Xenopus laevis tadpole spinal cord demonstrated by retrograde double labeling. *Brain Res.* 1088:68-72.

Goldshmit, Y., T. Sztal, P. Jusuf, T. Hall, M. Nguyen-Chi, and P. Currie. 2012. Fgf-dependent glial cell bridges facilitate spinal cord regeneration in zebrafish. *J Neurosci*. 32:7477-7492.

Goss, R.J. 1969. Principles of Regeneration. Academic Press, New York. 287 pp.

Goss, R.J., and L. Russell. 1969. Principles of regeneration. *Academic Press New York:*.

GrandPré, T., S. Li, and S. Strittmatter. 2002. Nogo-66 receptor antagonist peptide promotes axonal regeneration. *Nature*. 417:547-551.

GrandPré, T., F. Nakamura, T. Vartanian, and S. Strittmatter. 2000. Identification of the Nogo inhibitor of axon regeneration as a Reticulon protein. *Nature*. 403:439-444.

Griffin, J., R. George, C. Lobato, W. Tyor, L. Yan, and J. Glass. 1992. Macrophage responses and myelin clearance during Wallerian degeneration: relevance to immune-mediated demyelination. *Journal of neuroimmunology*. 40:153-165.

Gu, X., F. Ding, and D. Williams. 2014. Neural tissue engineering options for peripheral nerve regeneration. *Biomaterials*. 35.

Gwak, Y., J. Kang, G. Unabia, and C. Hulsebosch. 2012. Spatial and temporal activation of spinal glial cells: role of gliopathy in central neuropathic pain following spinal cord injury in rats. *Exp Neurol*. 234:362-372.

Hagen, J.W., and E.C. Lai. 2008. MicroRNA control of cell-cell signaling during development and disease. *In* Cell Cycle. Vol. 7. 2327-2332.

Han, N., S.S. Rao, J. Johnson, K.S. Parikh, P.A. Bradley, J.J. Lannutti, and J.O. Winter. 2011. Hydrogel-electrospun fiber mat composite coatings for neural prostheses. *Frontiers in neuroengineering*. 4.

Han, Q., W. Jin, Z. Xiao, H. Ni, J. Wang, J. Kong, J. Wu, W. Liang, L. Chen, Y. Zhao, B. Chen, and J. Dai. 2010. The promotion of neural regeneration in an extreme rat spinal cord injury model using a collagen scaffold containing a collagen binding neuroprotective protein and an EGFR neutralizing antibody. *Biomaterials*. 31.

Han, Q., W. Sun, H. Lin, W. Zhao, Y. Gao, Y. Zhao, B. Chen, Z. Xiao, W. Hu, Y. Li, B. Yang, and J. Dai. 2009. Linear ordered collagen scaffolds loaded with collagen-binding brain-derived neurotrophic factor improve the recovery of spinal cord injury in rats. *Tissue engineering. Part A*. 15.

Han, S., B. Wang, W. Jin, Z. Xiao, X. Li, W. Ding, M. Kapur, B. Chen, B. Yuan, T. Zhu, H. Wang, J. Wang, Q. Dong, W. Liang, and J. Dai. 2015. The linear-ordered collagen scaffold-BDNF complex significantly promotes functional recovery after completely transected spinal cord injury in canine. *Biomaterials*. 41.

Hanson Shepherd, J.N., S.T. Parker, R.F. Shepherd, M.U. Gillette, J.A. Lewis, and R.G. Nuzzo. 2011. 3D Microperiodic Hydrogel Scaffolds for Robust Neuronal Cultures. *Advanced functional materials*. 21.

Harrison, R.G. 1898. The growth and regeneration of the tail of the frog larva. *Development Genes and Evolution*. 7:430-485.

Hayashi, M., T. Ueyama, K. Nemoto, T. Tamaki, and E. Senba. 2000. Sequential mRNA expression for immediate early genes, cytokines, and neurotrophins in spinal cord injury. *Journal of neurotrauma*. 17:203-218.

He, L., and G.J. Hannon. 2004. MicroRNAs: small RNAs with a big role in gene regulation. *Nature reviews. Genetics*. 5:522-531.

Hellal, F., A. Hurtado, J. Ruschel, K. Flynn, C. Laskowski, M. Umlauf, L. Kapitein, D. Strikis, V. Lemmon, J. Bixby, C. Hoogenraad, and F. Bradke. 2011. Microtubule stabilization reduces scarring and causes axon regeneration after spinal cord injury. *Science (New York, N.Y.)*. 331:928-931.

Hermanns, S., P. Reiprich, and H.W. Müller. 2001. A reliable method to reduce collagen scar formation in the lesioned rat spinal cord. *Journal of neuroscience methods*. 110.

Holtzer, H. 1951. Reconstitution of the urodele spinal cord following unilateral ablation. Part I. Chronology of neuron regulation. *Journal of Experimental Zoology*. 117:523-557.

Holtzer, H. 1952. An experimental analysis of the development of the spinal column. Part II. The dispensability of the notochord. *Journal of Experimental Zoology*. 121:573-591.

Holtzer, S.W. 1956. The inductive activity of the spinal cord in urodele amphibian regeneration. *J. Morphol.* 99:1-33.

Höpker, V., D. Shewan, M. Tessier-Lavigne, M.-m. Poo, and C. Holt. 1999. Growth-cone attraction to netrin-1 is converted to repulsion by laminin-1. *Nature*. 401.

Horn, K., S. Busch, A. Hawthorne, N. van Rooijen, and J. Silver. 2008. Another barrier to regeneration in the CNS: activated macrophages induce extensive retraction of dystrophic axons through direct physical interactions. *J Neurosci*. 28:9330-9341.

Hossain-Ibrahim, M.K., K. Rezajooi, W.B. Stallcup, A.R. Lieberman, and P.N. Anderson. 2007. Analysis of axonal regeneration in the central and peripheral nervous systems of the NG2-deficient mouse. *BMC Neurosci*. 8:80.

Houle, J. 1991. Demonstration of the potential for chronically injured neurons to regenerate axons into intraspinal peripheral nerve grafts. *Experimental neurology*. 113:1-9.

Howard, H. 1951. Reconstitution of the urodele spinal cord following unilateral ablation. Part I. Chronology of neuron regulation. *Journal of Experimental Zoology*. 117.

Hu, J., A. Ferreira, and L. Eldik. 1997. S100β Induces Neuronal Cell Death Through Nitric Oxide Release from Astrocytes. *Journal of Neurochemistry*. 69.

Huber, F., J. Schnauß, S. Rönicke, P. Rauch, K. Müller, C. Fütterer, and J. Käs. 2013. Emergent complexity of the cytoskeleton: from single filaments to tissue. *Advances in Physics*. 62.

Hui, S., A. Dutta, and S. Ghosh. 2010. Cellular response after crush injury in adult zebrafish spinal cord. *Developmental dynamics : an official publication of the American Association of Anatomists*. 239:2962-2979.

Hui, S.P., J.R. Monaghan, S.R. Voss, and S. Ghosh. 2013. Expression pattern of Nogo-A, MAG, and NgR in regenerating urodele spinal cord. *Developmental Dynamics*. 242:847-860.

Iten, L., and S. Bryant. 1976a. Regeneration from different levels along the tail of the newt, Notophthalmus viridescens. *The Journal of experimental zoology*. 196:293-306.

Iten, L., and S. Bryant. 1976b. Stages of tail regeneration in the adult newt, Notophthalmus viridescens. *The Journal of experimental zoology*. 196:283-292.

Janmey, P., and R. Miller. 2011. Mechanisms of mechanical signaling in development and disease. *Journal of Cell Science*. 124.

Ji, B., L. Case, K. Liu, Z. Shao, X. Lee, Z. Yang, J. Wang, T. Tian, S. Shulga-Morskaya, M. Scott, Z. He, J. Relton, and S. Mi. 2008. Assessment of functional recovery and axonal sprouting in oligodendrocyte-myelin glycoprotein (OMgp) null mice after spinal cord injury. *Mol Cell Neurosci*. 39:258-267.

Johansson, C., S. Momma, D. Clarke, M. Risling, U. Lendahl, and J. Frisén. 1999. Identification of a neural stem cell in the adult mammalian central nervous system. *Cell*. 96:25-34.

Johnson, J., A. Niehaus, S. Nichols, D. Lee, J. Koepsel, D. Anderson, and J. Lannutti. 2009. Electrospun PCL in vitro: a microstructural basis for mechanical property changes. *Journal of biomaterials science. Polymer edition*. 20.

Jones, L.L., D. Sajed, and M.H. Tuszynski. 2003. Axonal regeneration through regions of chondroitin sulfate proteoglycan deposition after spinal cord injury: a balance of permissiveness and inhibition. *J Neurosci*. 23:9276-9288.

Jones, L.L., Y. Yamaguchi, W.B. Stallcup, and M.H. Tuszynski. 2002. NG2 is a major chondroitin sulfate proteoglycan produced after spinal cord injury and is expressed by macrophages and oligodendrocyte progenitors. *The Journal of neuroscience : the official journal of the Society for Neuroscience*. 22:2792-2803.

Kemp, S.W., S. Syed, W. Walsh, D.W. Zochodne, and R. Midha. 2009. Collagen nerve conduits promote enhanced axonal regeneration, schwann cell association, and neovascularization compared to silicone conduits. *Tissue engineering. Part A*. 15.

Kerschensteiner, M., M.E. Schwab, J.W. Lichtman, and T. Misgeld. 2005. In vivo imaging of axonal degeneration and regeneration in the injured spinal cord. *Nat Med*. 11:572-577.

Kim, D.-H., E. Lipke, P. Kim, R. Cheong, S. Thompson, M. Delannoy, K.-Y. Suh, L. Tung, and A. Levchenko. 2010. Nanoscale cues regulate the structure and function of macroscopic cardiac tissue constructs. *Proceedings of the National Academy of Sciences*. 107.

Kim, J., S. Li, T. GrandPré, D. Qiu, and S. Strittmatter. 2003. Axon regeneration in young adult mice lacking Nogo-A/B. *Neuron*. 38:187-199.

Klapka, N., and H.W. Müller. 2006. Collagen matrix in spinal cord injury. *Journal of neurotrauma*. 23.

Kolega, J., L.W. Janson, and D.L. Taylor. 1991. The role of solation-contraction coupling in regulating stress fiber dynamics in nonmuscle cells. *Journal of Cell Biology*. 114:993-1003.

Kolodkin, A.L., D.J. Matthes, and C.S. Goodman. 1993. The semaphorin genes encode a family of transmembrane and secreted growth cone guidance molecules. *Cell*. 75:1389-1399.

Koopmans, G.C., R. Deumens, W.M. Honig, F.P. Hamers, H.W. Steinbusch, and E.A. Joosten. 2005. The assessment of locomotor function in spinal cord injured rats: the importance of objective analysis of coordination. *Journal of neurotrauma*. 22:214-225.

Kopp, M.A., B. Brommer, N. Gatzemeier, J.M. Schwab, and H. Prüss. 2010. Spinal cord injury induces differential expression of the profibrotic semaphorin 7A in the developing and mature glial scar. *Glia*. 58:1748-1756.

Környei, Z., A. Czirók, T. Vicsek, and E. Madarász. 2000. Proliferative and migratory responses of astrocytes to in vitro injury. *Journal of Neuroscience Research*. 61.

Kosik, K.S. 2006. The neuronal microRNA system. *Nature reviews. Neuroscience*. 7:911-920.

Krautstrunk, M., F. Scholtes, D. Martin, J. Schoenen, A.B. Schmitt, D. Plate, W. Nacimiento, J. Noth, and G.A. Brook. 2002. Increased expression of the putative axon growth-repulsive extracellular matrix molecule, keratan sulphate proteoglycan, following traumatic injury of the adult rat spinal cord. *Acta neuropathologica*. 104:592-600.

Krendel, M., F. Zenke, and G. Bokoch. 2002. Nucleotide exchange factor GEF-H1 mediates cross-talk between microtubules and the actin cytoskeleton. *Nature Cell Biology*. 4.

Krol, J., I. Loedige, and W. Filipowicz. 2010. The widespread regulation of microRNA biogenesis, function and decay. *Nature reviews. Genetics*. 11:597-610.

Kruger, R.P., J. Aurandt, and K.-L.L. Guan. 2005. Semaphorins command cells to move. *Nature reviews. Molecular cell biology*. 6:789-800.

Krylyshkina, O., I. Kaverina, W. Kranewitter, W. Steffen, M. Alonso, R. Cross, and J. Small. 2002. Modulation of substrate adhesion dynamics via microtubule targeting requires kinesin-1. *The Journal of cell biology*. 156.

Kumbar, S.G., R. James, S.P. Nukavarapu, and C.T. Laurencin. 2008. Electrospun nanofiber scaffolds: engineering soft tissues. *Biomedical materials (Bristol, England)*. 3.

Lee, H.J., N.X. Wang, D.L. Shi, and J.J. Zheng. 2009. Sulindac inhibits canonical Wnt signaling by blocking the PDZ domain of the protein Dishevelled. *Angew Chem Int Ed Engl*. 48:6448-6452.

Lee, J., R. Chow, F. Xie, S. Chow, K. Tolentino, and B. Zheng. 2010a. Combined genetic attenuation of myelin and semaphorin-mediated growth inhibition is insufficient to promote serotonergic axon regeneration. *The Journal of neuroscience : the official journal of the Society for Neuroscience*. 30:10899-10904.

Lee, J., C. Geoffroy, A. Chan, K. Tolentino, M. Crawford, M. Leal, B. Kang, and B. Zheng. 2010d. Assessing spinal axon regeneration and sprouting in Nogo-, MAG-, and OMgp-deficient mice. *Neuron*. 66:663-670.

Lee, R., R. Feinbaum, and V. Ambros. 1993. The C. elegans heterochronic gene lin-4 encodes small RNAs with antisense complementarity to lin-14. *Cell*. 75.

Lee, S., M. Leach, S. Redmond, S. Chong, S. Mellon, S. Tuck, Z.-Q. Feng, J. Corey, and J. Chan. 2012. A culture system to study oligodendrocyte myelination processes using engineered nanofibers. *Nature Methods*. 9.

Li, M., A. Shibata, C. Li, P. Braun, L. McKerracher, J. Roder, S. Kater, and S. David. 1996. Myelin-associated glycoprotein inhibits neurite/axon growth and causes growth cone collapse. *J Neurosci Res*. 46:404-414.

Li, X., Z. Xiao, J. Han, L. Chen, H. Xiao, F. Ma, X. Hou, X. Li, J. Sun, W. Ding, Y. Zhao, B. Chen, and J. Dai. 2013. Promotion of neuronal differentiation of neural progenitor cells by using EGFR antibody functionalized collagen scaffolds for spinal cord injury repair. *Biomaterials*. 34.

Li, Y., and C. Aparicio. 2013. Discerning the Subfibrillar Structure of Mineralized Collagen Fibrils: A Model for the Ultrastructure of Bone. *PLoS ONE*. 8.

Li, Y., T.T. Thula, S. Jee, S.L. Perkins, C. Aparicio, E.P. Douglas, and L.B. Gower. 2012. Biomimetic mineralization of woven bone-like nanocomposites: role of collagen cross-links. *Biomacromolecules*. 13.

Liesi, P., and T. Kauppila. 2002. Induction of type IV collagen and other basement-membrane-associated proteins after spinal cord injury of the adult rat may participate in formation of the glial scar. *Exp Neurol*. 173:31-45.

Lin, P.-W.W., C.-C.C. Wu, C.-H.H. Chen, H.-O.O. Ho, Y.-C.C. Chen, and M.-T.T. Sheu. 2005. Characterization of cortical neuron outgrowth in two- and three-dimensional culture systems. *Journal of biomedical materials research. Part B, Applied biomaterials*. 75.

Liu, J., J. Chen, B. Liu, C. Yang, D. Xie, X. Zheng, S. Xu, T. Chen, L. Wang, Z. Zhang, X. Bai, and D. Jin. 2013. Acellular spinal cord scaffold seeded with mesenchymal stem cells promotes long-distance axon regeneration and functional recovery in spinal cord injured rats. *Journal of the neurological sciences*.

Liu, T., J. Xu, B. Chan, and S. Chew. 2012. Sustained release of neurotrophin‐3 and chondroitinase ABC from electrospun collagen nanofiber scaffold for spinal cord injury repair. *Journal of Biomedical Materials Research Part A*. 100A.

Lore, A., J. Hubbell, and D. Bobb. 1999. Rapid induction of functional and morphological continuity between severed ends of mammalian or earthworm myelinated axons. *The Journal of …*.

Lubińska, L. 1982. Patterns of Wallerian degeneration of myelinated fibres in short and long peripheral stumps and in isolated segments of rat phrenic nerve. Interpretation of the role of axoplasmic flow of the trophic factor. *Brain research*. 233:227-240.

Ma, P.X. 2004. Scaffolds for tissue fabrication. *Materials Today*. 7:30-40.

Maden, M. 1982. Vitamin A and pattern formation in the regenerating limb. *Nature*. 295.

Madigan, N.N., S. McMahon, T. O'Brien, M.J. Yaszemski, and A.J. Windebank. 2009. Current tissue engineering and novel therapeutic approaches to axonal regeneration following spinal cord injury using polymer scaffolds. *Respiratory physiology & neurobiology*. 169.

Madura, T., T. Yamashita, T. Kubo, M. Fujitani, K. Hosokawa, and M. Tohyama. 2004. Activation of Rho in the injured axons following spinal cord injury. *EMBO reports*. 5:412-417.

Mandato, C., and W. Bement. 2003. Actomyosin Transports Microtubules and Microtubules Control Actomyosin Recruitment during Xenopus Oocyte Wound Healing. *Current Biology*. 13.

Mariani, F.V. 2010. Proximal to distal patterning during limb development and regeneration: a review of converging disciplines. *Regenerative medicine*. 5.

Marín-Pareja, N., E. Salvagni, J. Guillem-Marti, C. Aparicio, and M.-P. Ginebra. 2014. Collagen-functionalised titanium surfaces for biological sealing of dental implants: Effect of immobilisation process on fibroblasts response. *Colloids and Surfaces B: Biointerfaces*. 122.

Marinissen, M.J., M. Chiariello, T. Tanos, O. Bernard, S. Narumiya, and J.S. Gutkind. 2004. The small GTP-binding protein RhoA regulates c-jun by a ROCK-JNK signaling axis. *Molecular Cell*. 14:29-41.

Marson, A., S.S. Levine, M.F. Cole, G.M. Frampton, T. Brambrink, S. Johnstone, M.G. Guenther, W.K. Johnston, M. Wernig, J. Newman, J.M. Calabrese, L.M. Dennis, T.L. Volkert, S. Gupta, J. Love, N. Hannett, P.A. Sharp, D.P. Bartel, R. Jaenisch, and R.A. Young. 2008. Connecting microRNA Genes to the Core Transcriptional Regulatory Circuitry of Embryonic Stem Cells. *Cell*. 134:521-533.

Martinez, M., J.M. Brezun, L. Bonnier, and C. Xerri. 2009. A new rating scale for open-field evaluation of behavioral recovery after cervical spinal cord injury in rats. *J Neurotrauma*. 26:1043-1053.

Mather, J.P., and P.E. Roberts. 1998. Introduction to cell and tissue culture: theory and technique. *Cell*:241.

McHedlishvili, L., H. Epperlein, A. Telzerow, and E. Tanaka. 2007. A clonal analysis of neural progenitors during axolotl spinal cord regeneration reveals evidence for both spatially restricted and multipotent progenitors. *Development (Cambridge, England)*. 134:2083-2093.

McHedlishvili, L., V. Mazurov, and E. Tanaka. 2012. Reconstitution of the central nervous system during salamander tail regeneration from the implanted neurospheres. *Methods in molecular biology (Clifton, N.J.)*. 916:197-202.

Meletis, K., F. Barnabé-Heider, M. Carlén, E. Evergren, N. Tomilin, O. Shupliakov, and J. Frisén. 2008. Spinal cord injury reveals multilineage differentiation of ependymal cells. *PLoS biology*. 6.

Menet, V., M. Prieto, A. Privat, and M. Gimenez y Ribotta. 2003. Axonal plasticity and functional recovery after spinal cord injury in mice deficient in both glial fibrillary acidic protein and vimentin genes. *Proc Natl Acad Sci U S A*. 100:8999-9004.

Merkler, D., G. Metz, O. Raineteau, V. Dietz, M. Schwab, and K. Fouad. 2001. Locomotor recovery in spinal cord-injured rats treated with an antibody neutralizing the myelin-associated neurite growth inhibitor Nogo-A. *J Neurosci*. 21:3665-3673.

Miller, B., C. Press, R. Daniels, Y. Sasaki, J. Milbrandt, and A. DiAntonio. 2009. A dual leucine kinase-dependent axon self-destruction program promotes Wallerian degeneration. *Nature neuroscience*. 12:387-389.

Miralles, F., G. Posern, A.I. Zaromytidou, and R. Treisman. 2003. Actin dynamics control SRF activity by regulation of its coactivator MAL. *Cell*. 113:329-342.

Miyashita, T., M. Koda, K. Kitajo, M. Yamazaki, K. Takahashi, A. Kikuchi, and T. Yamashita. 2009. Wnt-Ryk signaling mediates axon growth inhibition and limits functional recovery after spinal cord injury. *Journal of neurotrauma*. 26:955-964.

Mofrad, M.R.K. 2009. Rheology of the Cytoskeleton. *The Annual Review of Fluid Mechanics*. 41.

Moftah, M., M. Landry, F. Nagy, and J.-M. Cabelguen. 2008. Fibroblast growth factor-2 mRNA expression in the brainstem and spinal cord of normal and chronic spinally transected urodeles. *J Neurosci Res*. 86:3348-3358.

Monaghan, J.R., J.A. Walker, R.B. Page, S. Putta, C.K. Beachy, and S.R. Voss. 2007. Early gene expression during natural spinal cord regeneration in the salamander Ambystoma mexicanum. *Journal of Neurochemistry*. 101:27-40.

Moore, D., M. Blackmore, Y. Hu, K. Kaestner, J. Bixby, V. Lemmon, and J. Goldberg. 2009. KLF family members regulate intrinsic axon regeneration ability. *Science (New York, N.Y.)*. 326:298-301.

Moreau-Fauvarque, C., A. Kumanogoh, E. Camand, C. Jaillard, G. Barbin, I. Boquet, C. Love, E. Jones, H. Kikutani, C. Lubetzki, I. Dusart, and A. Chédotal. 2003. The transmembrane semaphorin Sema4D/CD100, an inhibitor of axonal growth, is expressed on oligodendrocytes and upregulated after CNS lesion. *The Journal of neuroscience : the official journal of the Society for Neuroscience*. 23:9229-9239.

Mouw, J.K., Y. Yui, L. Damiano, R.O. Bainer, J.N. Lakins, I. Acerbi, G. Ou, A.C. Wijekoon, K.R. Levental, P.M. Gilbert, E.S. Hwang, Y.-Y. Chen, and V.M. Weaver. 2014. Tissue mechanics modulate microRNA-dependent PTEN expression to regulate malignant progression. *Nature medicine*. 20:360-367.

Muddashetty, R., V. Nalavadi, C. Gross, X. Yao, L. Xing, O. Laur, S. Warren, and G. Bassell. 2011. Reversible Inhibition of PSD-95 mRNA Translation by miR-125a, FMRP Phosphorylation, and mGluR Signaling. *Molecular Cell*. 42.

Nagai, M., D.B. Re, T. Nagata, A. Chalazonitis, T.M. Jessell, H. Wichterle, and S. Przedborski. 2007. Astrocytes expressing ALS-linked mutated SOD1 release factors selectively toxic to motor neurons. *Nature neuroscience*. 10.

Nam, J., J. Johnson, J. Lannutti, and S. Agarwal. 2011. Modulation of embryonic mesenchymal progenitor cell differentiation via control over pure mechanical modulus in electrospun nanofibers. *Acta biomaterialia*. 7.

Nam, J., B. Rath, T. Knobloch, J. Lannutti, and S. Agarwal. 2009. Novel Electrospun Scaffolds for the Molecular Analysis of Chondrocytes Under Dynamic Compression. *Tissue Engineering Part A*. 15.

Neumann, B., K. Nguyen, D. Hall, A. Ben-Yakar, and M. Hilliard. 2011. Axonal regeneration proceeds through specific axonal fusion in transected C. elegans neurons. *Developmental dynamics : an official publication of the American Association of Anatomists*. 240:1365-1372.

Ng, M.R., A. Besser, G. Danuser, and J.S. Brugge. 2012. Substrate stiffness regulates cadherin-dependent collective migration through myosin-II contractility. *Journal of Cell Biology*. 199:545-563.

Nguyen, T., N. Mehta, K. Conant, K.-J. Kim, M. Jones, P. Calabresi, G. Melli, A. Hoke, R. Schnaar, G.-L. Ming, H. Song, S. Keswani, and J. Griffin. 2009. Axonal protective effects of the myelin-associated glycoprotein. *J Neurosci*. 29:630-637.

Niclou, S.P., E.H. Franssen, E.M. Ehlert, M. Taniguchi, and J. Verhaagen. 2003. Meningeal cell-derived semaphorin 3A inhibits neurite outgrowth. *Molecular and cellular neurosciences*. 24:902-912.

Norman, L., K. Stroka, and H. Aranda-Espinoza. 2009. Guiding axons in the central nervous system: a tissue engineering approach. *Tissue engineering. Part B, Reviews*. 15:291-305.

Norton, W., D. Aquino, I. Hozumi, F. Chiu, and C. Brosnan. 1992. Quantitative aspects of reactive gliosis: a review. *Neurochem Res*. 17:877-885.

O'Connor, S.M., D.A. Stenger, K.M. Shaffer, and W. Ma. 2001. Survival and neurite outgrowth of rat cortical neurons in three-dimensional agarose and collagen gel matrices. *Neuroscience letters*. 304.

O'Malley, A.M., D.K. Shanley, A.T. Kelly, and D.S. Barry. 2014. Towards an understanding of semaphorin signalling in the spinal cord. *Gene*. 553:69-74.

Olson, E.N., and A. Nordheim. 2010. Linking actin dynamics and gene transcription to drive cellular motile functions. *Nature reviews. Molecular cell biology*. 11:353-365.

Ozsolak, F., L.L. Poling, Z. Wang, H. Liu, X.S. Liu, R.G. Roeder, X. Zhang, J.S. Song, and D.E. Fisher. 2008. Chromatin structure analyses identify miRNA promoters. *Genes and Development*. 22:3172-3183.

Pak, C., K. Flynn, and J. Bamburg. 2008. Actin-binding proteins take the reins in growth cones. *Nature Reviews Neuroscience*. 9.

Palazzo, A., and G. Gundersen. 2002. Microtubule-Actin Cross-talk at Focal Adhesions. *Science Signaling*. 2002.

Pasterkamp, R.J., and J. Verhaagen. 2006. Semaphorins in axon regeneration: developmental guidance molecules gone wrong? *Philosophical Transactions of the Royal Society of London B: Biological Sciences*. 361:1499-1511.

Pederson, T., and U. Aebi. 2002. Actin in the nucleus: What form and what for? *In* Journal of Structural Biology. Vol. 140. 3-9.

Pekny, M., and M. Nilsson. 2005. Astrocyte activation and reactive gliosis. *Glia*. 50.

Percipalle, P., N. Fomproix, K. Kylberg, F. Miralles, B. Bjorkroth, B. Daneholt, and N. Visa. 2003. An actin-ribonucleoprotein interaction is involved in transcription by RNA polymerase II. *Proceedings of the National Academy of Sciences of the United States of America*. 100:6475-6480.

Percipalle, P., A. Jonsson, D. Nashchekin, C. Karlsson, T. Bergman, A. Guialis, and B. Daneholt. 2002. Nuclear actin is associated with a specific subset of hnRNP A/B-type proteins. *Nucleic acids research*. 30:1725-1734.

Philimonenko, V.V., J. Zhao, S. Iben, H. Dingová, K. Kyselá, M. Kahle, H. Zentgraf, W.A. Hofmann, P. de Lanerolle, P. Hozák, and I. Grummt. 2004. Nuclear actin and myosin I are required for RNA polymerase I transcription. *Nature cell biology*. 6:1165-1172.

Poss, K. 2010. Advances in understanding tissue regenerative capacity and mechanisms in animals. *Nature Reviews Genetics*. 11.

Provenzano, P.P., and P.J. Keely. 2011. Mechanical signaling through the cytoskeleton regulates cell proliferation by coordinated focal adhesion and Rho GTPase signaling. *Journal of cell science*. 124:1195-1205.

Ragancokova, D., K. Jahn, A. Kotsiari, F. Schlesinger, K. Haastert, M. Stangel, S. Petri, and K. Krampfl. 2009. Analysis of neuroprotective effects of valproic acid on primary motor neurons in monoculture or co-cultures with astrocytes or Schwann cells. *Cellular and molecular neurobiology*. 29.

Ramón y Cajal, S. 1928. Degeneration & regeneration of the nervous system. Oxford University Press, Humphrey Milford.

Rando, O.J., K. Zhao, and G.R. Crabtree. 2000. Searching for a function for nuclear actin. *In* Trends in Cell Biology. Vol. 10. 92-97.

Rao, K.V., K.S. Panickar, A.R. Jayakumar, and M.D. Norenberg. 2005. Astrocytes protect neurons from ammonia toxicity. *Neurochemical research*. 30.

Ravi, M., V. Paramesh, S.R. Kaviya, E. Anuradha, and F.D. Solomon. 2015. 3D Cell Culture Systems: Advantages and Applications. *Journal of Cellular Physiology*. 230.

Reaumur, R. 1712. Sur les diverses reproductions qui se font dans les Ecrevisse, les Omars, les Crabes, etc. et entr'autres sur celles de leurs Jambes et de leurs Ecailles. *Mémoires de l'Académie Royale des Sciences*. 1712:223-241.

Ren, X.D., W. Kiosses, and M. Schwartz. 1999. Regulation of the small GTP‐binding protein Rho by cell adhesion and the cytoskeleton. *The EMBO Journal*. 18.

Ribeiro-Resende, V.T., B. Koenig, S. Nichterwitz, S. Oberhoffner, and B. Schlosshauer. 2009. Strategies for inducing the formation of bands of Büngner in peripheral nerve regeneration. *Biomaterials*. 30.

Riedl, J., A.H. Crevenna, K. Kessenbrock, J.H. Yu, D. Neukirchen, M. Bista, F. Bradke, D. Jenne, T.a. Holak, Z. Werb, M. Sixt, and R. Wedlich-Soldner. 2008. Lifeact: a versatile marker to visualize F-actin. *Nature methods*. 5:605-607.

Rodriguez, O.C., A.W. Schaefer, C.a. Mandato, P. Forscher, W.M. Bement, and C.M. Waterman-Storer. 2003. Conserved microtubule-actin interactions in cell movement and morphogenesis. *Nature cell biology*. 5:599-609.

Rose, G.H. 1907. Observations of the living developing nerve fiber. *The Anatomical Record*. 1.

Rosner, B.I., T. Hang, and R.T. Tranquillo. 2005. Schwann cell behavior in three-dimensional collagen gels: evidence for differential mechano-transduction and the influence of TGF-beta 1 in morphological polarization and differentiation. *Experimental neurology*. 195.

Sanchez Alvarado, A., and P.A. Tsonis. 2006. Bridging the regeneration gap: genetic insights from diverse animal models. *Nat Rev Genet.* 11:873-884.

Sandvig, A., M. Berry, L. Barrett, A. Butt, and A. Logan. 2004. Myelin-, reactive glia-, and scar-derived CNS axon growth inhibitors: expression, receptor signaling, and correlation with axon regeneration. *Glia*. 46:225-251.

Santos, E., R. Hernández, J. Pedraz, and G. Orive. 2012. Novel advances in the design of three-dimensional bio-scaffolds to control cell fate: translation from 2D to 3D. *Trends in Biotechnology*. 30.

Schanen, B.C., and X. Li. 2011. Transcriptional regulation of mammalian miRNA genes. *In* Genomics. Vol. 97. 1-6.

Schmidt, A., and M. Hall. 1998. SIGNALING TO THE ACTIN CYTOSKELETON. *Annual Review of Cell and Developmental Biology*. 14.

Schnapp, E., M. Kragl, L. Rubin, and E. Tanaka. 2005. Hedgehog signaling controls dorsoventral patterning, blastema cell proliferation and cartilage induction during axolotl tail regeneration. *Development (Cambridge, England)*. 132:3243-3253.

Schubert, D., S. Heinemann, W. Carlisle, H. Tarikas, B. Kimes, J. Patrick, J.H. Steinbach, W. Culp, and B.L. Brandt. 1974. Clonal cell lines from the rat central nervous system. *Nature*. Vol.249.

Schwab, M. 2004. Nogo and axon regeneration. *Current opinion in neurobiology*. 14:118-124.

Sehm, T., C. Sachse, C. Frenzel, and K. Echeverri. 2009. miR-196 is an essential early-stage regulator of tail regeneration, upstream of key spinal cord patterning events. *Developmental biology*. 334:468-480.

Seifert, A., J. Monaghan, S. Voss, and M. Maden. 2012. Skin regeneration in adult axolotls: a blueprint for scar-free healing in vertebrates. *PloS one*. 7.

Seifert, A.W., and S.R. Voss. 2012. Revisiting the relationship between regenerative ability and aging. *BMC biology*. 11:2.

Sharma, K., M.E. Selzer, and S. Li. 2012. Scar-mediated inhibition and CSPG receptors in the CNS. *Experimental neurology*. 237.

Shifman, M.I., and M.E. Selzer. 2007. Differential expression of class 3 and 4 semaphorins and netrin in the lamprey spinal cord during regeneration. *The Journal of comparative neurology*. 501:631-646.

Shim, S.-O., W. Cafferty, E. Schmidt, B. Kim, H. Fujisawa, and S. Strittmatter. 2012. PlexinA2 limits recovery from corticospinal axotomy by mediating oligodendrocyte-derived Sema6A growth inhibition. *Molecular and cellular neurosciences*. 50:193-200.

Silver, J., and J. Miller. 2004. Regeneration beyond the glial scar. *Nat Rev Neurosci*. 5:146-156.

Singer, M., R. Nordlander, and M. Egar. 1979. Axonal guidance during embryogenesis and regeneration in the spinal cord of the newt: the blueprint hypothesis of neuronal pathway patterning. *The Journal of comparative neurology*. 185:1-21.

Sit, S.-T., and E. Manser. 2011. Rho GTPases and their role in organizing the actin cytoskeleton. *Journal of Cell Science*. 124.

Slack, J.M.W., G. Lin, and Y. Chen. 2008. Molecular and cellular basis of regeneration and tissue repair: The Xenopus tadpole: A new model for regeneration research. *In* Cellular and Molecular Life Sciences. Vol. 65. 54-63.

Small, E., and E. Olson. 2011. Pervasive roles of microRNAs in cardiovascular biology. *Nature*. 469.

Sofroniew, M. 2009. Molecular dissection of reactive astrogliosis and glial scar formation. *Trends in neurosciences*. 32:638-647.

Spiering, D., and L. Hodgson. 2011. Dynamics of the rho-family small GTPases in actin regulation and motility. *In* Cell Adhesion and Migration. Vol. 5. 170-180.

Spira, M.E., R. Oren, A. Dormann, and D. Gitler. 2003. Critical calpain-dependent ultrastructural alterations underlie the transformation of an axonal segment into a growth cone after axotomy of cultured Aplysia neurons. *The Journal of comparative neurology*. 457.

Stang, F., H. Fansa, G. Wolf, M. Reppin, and G. Keilhoff. 2005. Structural parameters of collagen nerve grafts influence peripheral nerve regeneration. *Biomaterials*. 26.

Stewart, S., A. Rojas-Muñoz, and J.C. Izpisúa Belmonte. 2007. Bioelectricity and epimorphic regeneration. *BioEssays : news and reviews in molecular, cellular and developmental biology*. 29.

Stoick-Cooper, C.L., R.T. Moon, and G. Weidinger. 2007. Advances in signaling in vertebrate regeneration as a prelude to regenerative medicine. *Genes & development*. 21.

Stokols, S., J. Sakamoto, C. Breckon, T. Holt, J. Weiss, and M.H. Tuszynski. 2006. Templated agarose scaffolds support linear axonal regeneration. *Tissue engineering*. 12:2777-2787.

Stokols, S., and M.H. Tuszynski. 2004. The fabrication and characterization of linearly oriented nerve guidance scaffolds for spinal cord injury. *Biomaterials*. 25.

Streit, W., S. Walter, and N. Pennell. 1999. Reactive microgliosis. *Progress in neurobiology*. 57:563-581.

Subramanian, A., U.M. Krishnan, and S. Sethuraman. 2009. Development of biomaterial scaffold for nerve tissue engineering: Biomaterial mediated neural regeneration. *Journal of biomedical science*. 16.

Sybil, W.H. 1956. The inductive activity of the spinal cord in urodele tail regeneration. *Journal of Morphology*. 99.

Tanaka, E., and P. Ferretti. 2009. Considering the evolution of regeneration in the central nervous system. *Nat Rev Neurosci*. 10:713-723.

Tojkander, S., G. Gateva, and P. Lappalainen. 2012. Actin stress fibers--assembly, dynamics and biological roles. *Journal of cell science*. 125:1855-1864.

Tsao, J., M. Brown, M. Carden, W. McLean, and V. Perry. 1994. Loss of the compound action potential: an electrophysiological, biochemical and morphological study of early events in axonal degeneration in the C57BL/Ola mouse. *The European journal of neuroscience*. 6:516-524.

Tseng, A.-S., W.S. Beane, J.M. Lemire, A. Masi, and M. Levin. 2010. Induction of vertebrate regeneration by a transient sodium current. *The Journal of neuroscience : the official journal of the Society for Neuroscience*. 30:13192-13200.

Tseng, A.S., and M. Levin. 2012. Transducing Bioelectric Signals into Epigenetic Pathways During Tadpole Tail Regeneration. *In* Anatomical Record. Vol. 295. 1541-1551.

Vicente-Manzanares, M., X. Ma, R.S. Adelstein, and A.R. Horwitz. 2009. Non-muscle myosin II takes centre stage in cell adhesion and migration. *Nature reviews. Molecular cell biology*. 10.

Visvanathan, J., S. Lee, B. Lee, J. Lee, and S.-K. Lee. 2007. The microRNA miR-124 antagonizes the anti-neural REST/SCP1 pathway during embryonic CNS development. *Genes & Development*. 21.

Walder, S., F. Zhang, and P. Ferretti. 2003. Up-regulation of neural stem cell markers suggests the occurrence of dedifferentiation in regenerating spinal cord. *Development Genes and Evolution*. 213:625-630.

Wang, J.T., Z.A. Medress, and B.A. Barres. 2012. Axon degeneration: molecular mechanisms of a self-destruction pathway. *The Journal of cell biology*. 196:7-18.

Wang, K., V. Koprivica, J. Kim, R. Sivasankaran, Y. Guo, R. Neve, and Z. He. 2002. Oligodendrocyte-myelin glycoprotein is a Nogo receptor ligand that inhibits neurite outgrowth. *Nature*. 417:941-944.

White, J., E. Southgate, J. Thomson, and S. Brenner. 1986. The structure of the nervous system of the nematode Caenorhabditis elegans. *Philosophical transactions of the Royal Society of London. Series B, Biological sciences*. 314:1-340.

Whitmarsh, A.J., and R.J. Davis. 1996. Transcription factor AP-1 regulation by mitogen-activated protein kinase signal transduction pathways. *Journal of molecular medicine (Berlin, Germany)*. 74:589-607.

Winter, J., S. Jung, S. Keller, R.I. Gregory, and S. Diederichs. 2009. Many roads to maturity: microRNA biogenesis pathways and their regulation. *Nature cell biology*. 11:228-234.

Witte, H., D. Neukirchen, and F. Bradke. 2008. Microtubule stabilization specifies initial neuronal polarization. *The Journal of cell biology*. 180:619-632.

Wu, B., D. Matic, N. Djogo, E. Szpotowicz, M. Schachner, and I. Jakovcevski. 2012. Improved regeneration after spinal cord injury in mice lacking functional T- and B-lymphocytes. *Exp Neurol*. 237:274-285.

Xia, H.-F., T.-Z. He, C.-M. Liu, Y. Cui, P.-P. Song, X.-H. Jin, and X. Ma. 2009. MiR-125b expression affects the proliferation and apoptosis of human glioma cells by targeting Bmf. *Cellular physiology and biochemistry : international journal of experimental cellular physiology, biochemistry, and pharmacology*. 23:347-358.

Xiao, Z.D., L.T. Diao, J.H. Yang, H. Xu, M.B. Huang, Y.J. Deng, H. Zhou, and L.H. Qu. 2013. Deciphering the transcriptional regulation of microRNA genes in humans with ACTLocater. *Nucleic Acids Research*. 41:1-12.

Yang, H., X.-P. Cheng, J.-W. Li, Q. Yao, and G. Ju. 2009. De-differentiation response of cultured astrocytes to injury induced by scratch or conditioned culture medium of scratch-insulted astrocytes. *Cellular and molecular neurobiology*. 29:455-473.

Yanik, M.F., H. Cinar, H. Cinar, A.D. Chisholm, Y. Jin, and A. Ben-Yakar. 2004. Functional regeneration after laser axotomy. *Nature*. 432:822.

Yanik, M.F., H. Cinar, H.N. Cinar, A. Gibby, A.D. Chisholm, Y. Jin, and A. Ben-Yakar. 2006. Nerve Regeneration in Caenorhabditis elegans After Femtosecond Laser Axotomy. *IEEE Journal of Selected Topics in Quantum Electronics*. 12.

Yannas, I.V., D.S. Tzeranis, B.a. Harley, and P.T.C. So. 2010. Biologically active collagen-based scaffolds: advances in processing and characterization. *Philosophical transactions. Series A, Mathematical, physical, and engineering sciences*. 368:2123-2139.

Yin, Z., J. Albrecht, T. Syversen, H. Jiang, M. Summar, J.B. Rocha, M. Farina, and M. Aschner. 2009. Comparison of alterations in amino acids content in cultured astrocytes or neurons exposed to methylmercury separately or in co-culture. *Neurochemistry international*. 55.

Yukawa, K., T. Tanaka, N. Takeuchi, H. Iso, L. Li, A. Kohsaka, H. Waki, M. Miyajima, M. Maeda, H. Kikutani, and A. Kumanogoh. 2009. Sema4D/CD100 deficiency leads to superior performance in mouse motor behavior. *The Canadian journal of neurological sciences. Le journal canadien des sciences neurologiques*. 36:349-355.

Zambetti, G., a. Ramsey-Ewing, R. Bortell, G. Stein, and J. Stein. 1991. Disruption of the cytoskeleton with cytochalasin D induces c-fos gene expression. *Experimental cell research*. 192:93-101.

Zenz, R., R. Eferl, C. Scheinecker, K. Redlich, J. Smolen, H.B. Schonthaler, L. Kenner, E. Tschachler, and E.F. Wagner. 2008. Activator protein 1 (Fos/Jun) functions in inflammatory bone and skin disease. *Arthritis Research & Therapy*. 10:201-201.

Zhai, Q., J. Wang, A. Kim, Q. Liu, R. Watts, E. Hoopfer, T. Mitchison, L. Luo, and Z. He. 2003. Involvement of the ubiquitin-proteasome system in the early stages of wallerian degeneration. *Neuron*. 39:217-225.

Zhang, F., J. Clarke, and P. Ferretti. 2000. FGF-2 Up-regulation and proliferation of neural progenitors in the regenerating amphibian spinal cord in vivo. *Developmental biology*. 225:381-391.

Zhang, F., P. Ferretti, and J. Clarke. 2003. Recruitment of postmitotic neurons into the regenerating spinal cord of urodeles. *Developmental dynamics : an official publication of the American Association of Anatomists*. 226:341-348.

Zhang, H.L., J. Wang, and L. Tang. 2014a. Sema4D Knockdown in Oligodendrocytes Promotes Functional Recovery After Spinal Cord Injury. *Cell Biochemistry and Biophysics*. 68:489-496.

Zhang, L., S. Kaneko, K. Kikuchi, A. Sano, M. Maeda, A. Kishino, S. Shibata, M. Mukaino, Y. Toyama, M. Liu, T. Kimura, H. Okano, and M. Nakamura. 2014b. Rewiring of regenerated axons by combining treadmill training with semaphorin3A inhibition. *Molecular Brain*. 7:14.

Zhang, L., N. Stokes, L. Polak, and E. Fuchs. 2011. Specific microRNAs are preferentially expressed by skin stem cells to balance self-renewal and early lineage commitment. *Cell Stem Cell*. 8:294-308.

Zhao, Y., E. Samal, and D. Srivastava. 2005. Serum response factor regulates a muscle-specific microRNA that targets Hand2 during cardiogenesis. *Nature*. 436:214-220.

Zhu, Z., Q. Zhang, Z. Yu, L. Zhang, D. Tian, S. Zhu, B. Bu, M. Xie, and W. Wang. 2007. Inhibiting cell cycle progression reduces reactive astrogliosis initiated by scratch injury in vitro and by cerebral ischemia in vivo. *Glia*. 55:546-558.

Zukor, K., D. Kent, and S. Odelberg. 2011. Meningeal cells and glia establish a permissive environment for axon regeneration after spinal cord injury in newts. *Neural development*. 6:1.